

Hydrogen Research and Development Program

Neil P. Rossmeyl
U.S. Department of Energy
Office of Power Technologies
Washington, D.C. 20585

KEYWORDS: hydrogen, renewable energy, greenhouse gas emissions

INTRODUCTION

Over the last two decades, federal, state, and local institutions have been actively involved in developing technologies to reduce or eliminate air pollution. One technology that offers tremendous potential is hydrogen. Hydrogen can be a cost-effective energy carrier and fuel in reducing greenhouse gas emissions and other toxic emissions from end-use technologies. However, hydrogen is not found in the free state in nature but must be produced from primary energy sources. Producing hydrogen from renewable energy offers the potential for cooperative pre-proprietary research and development projects due to their long-term nature and high risk associated with these technologies.

Hydrogen can be produced directly from sunlight and water by biological organisms and using semiconductor-based systems similar to photovoltaics (PV), or indirectly, via thermal processing of biomass. These production technologies have the potential to produce essentially unlimited quantities of hydrogen in a sustainable manner. Hydrogen production using biological processes or advanced semiconductors is new, innovative and potentially more efficient in the direct conversion of solar energy and biomass to hydrogen. Such processes use, adapt or genetically engineer the biochemical mechanisms present in microalgae or bacteria for the production of hydrogen and use multijunction semiconductors engineered with specific bandgaps to split water, respectively. In order to achieve the goals of practical renewable hydrogen processes, advanced low cost bioreactors, systems with oxygen tolerant hydrogenase and lower cost semiconductor materials with high efficiencies (greater than 10% total solar conversion), need to be developed and engineered.

Storage of hydrogen is also a critical technology area when consideration of energy density is compared to conventional alternatives for the transportation market. Although compressed gas and liquid storage systems have been used in demonstrations worldwide, the issues of safety, capacity and reliability have not been fully addressed.

The U.S. Department of Energy (DOE) is funding an innovative research and development program focused on exploration of longer-term, higher-risk concepts to address hydrogen as an alternative energy form. The work is challenging, but provides an excellent opportunity for the community to work across political and ideology barriers to develop collaborations.

The DOE has considered the potential use of hydrogen as an energy carrier since the early 1970's following the OPEC oil embargo. At that time, the limitations included the ability to produce low-cost hydrogen and store it for transportation use. Concepts included using base loaded nuclear power to produce "clean" hydrogen with low cost electrical power and store and transport it as a liquid. Over the last 29 years, the Department is still faced with the challenge of producing low-cost hydrogen, storing the hydrogen with an acceptable energy density and converting the hydrogen to useful work with a device that has a high efficiency. In 1990 and 1996, legislation was passed by the Congress to authorize the DOE to conduct a comprehensive hydrogen research and development program to address the limitations that has prevented the introduction of hydrogen as an alternative energy form. This paper presents the Hydrogen Program that was developed and some of the results of the projects funded.

DIRECT HYDROGEN PRODUCTION TECHNOLOGIES

The use of solar energy to split water into oxygen and hydrogen is an attractive means to directly convert solar energy to chemical energy. Biological, chemical, and electrochemical systems are being investigated within DOE as long-term (>10 years), high-risk, high-payoff technologies for the sustainable production of hydrogen.

Biological Systems

In nature, algae absorb light and utilize water and CO₂ to produce cell mass and oxygen. A complex model referred to as the "Z-scheme" has been identified to describe the charge separation and electron transfer steps associated with this process that ultimately drives photosynthesis. A number of enzymatic side pathways that can also accept electrons have been identified. Of interest is a class

of enzymes known as hydrogenases that can combine protons and electrons obtained from the water oxidation process to release molecular hydrogen. These algal hydrogenases are quickly deactivated by oxygen. Researchers have identified mutant algal strains that evolve hydrogen at a rate that is 4 times that of the wild type, and are 3-4 times more oxygen tolerant [1,2].

Photosynthetic organisms also contain light harvesting, chlorophyll-protein complexes that effectively concentrate light and funnel energy for photosynthesis. These antenna complexes also dissipate excess incident sunlight as a protective mechanism. The amount of chlorophyll antennae in each cell is directly related to the amount of "shading" experienced by subsequent layers of microorganisms in a mass culture. In a recent set of experiments, researchers have observed that green alga grown under high light intensities exhibit lower pigment content and a highly truncated chlorophyll antennae size. These cells showed photosynthetic productivity (on a per chlorophyll basis) that was 6-7 times greater than the normally pigmented cells [3], a phenomenon that could lead to significant improvements in the efficiency of hydrogen production on a surface-area basis.

These technical challenges are being addressed by a team of scientists from Oak Ridge National Laboratory (ORNL), the University of California Berkeley, and the National Renewable Energy Laboratory (NREL). Various reactor designs are under development for photobiological hydrogen production processes (single-stage vs two-stage, single organism vs dual organism). At the University of Hawaii's Natural Energy Institute (HNEI), a new, potentially low cost, outdoor tubular photobioreactor is under development to test a sustainable system for the production of hydrogen [4].

In addition to the photosynthetic production of hydrogen from water, the Program supports the development of systems to convert CO (found in synthesis gas) to hydrogen via the so-called water-gas shift reaction ($\text{CO} + \text{H}_2\text{O} = \text{CO}_2 + \text{H}_2$). This reaction is essential to the widely-used commercial steam methane reforming process for the production of hydrogen. In the industrial process in use today, high-temperature (450°C) and low-temperature (230°C) shift reactors are required to increase the overall hydrogen production efficiency and to reduce the CO content to acceptable levels. In this project, microorganisms isolated from nature are used to reduce the level of CO to below detectable levels (0.1 ppm) at temperatures of around 25-50°C in a single reactor [5]. This process, under development at NREL, has significant potential to improve the economics of hydrogen production when combined with the thermal processing of biomass or other carbon-containing feeds.

Photochemical Systems

Among the technologies that have been investigated, photocatalytic water splitting systems using relatively inexpensive, durable, and nontoxic semiconductor photocatalysts show promise. Supported catalysts such as Pt-RuO₂/TiO₂ have sufficient band gaps for water splitting, although the current rate of hydrogen production from these systems is too low for commercial processes. Modifications to the system are required to address issues such as the narrow range of solar wavelengths absorbed by TiO₂, the efficiency of subsequent catalytic steps for formation of hydrogen and oxygen, and the need for high surface areas. Binding of catalyst complexes that absorb light in the visible range to the TiO₂ should improve the absorption characteristics. Aerogels of TiO₂ as a semiconductor support for the photocatalysts have potential for addressing reaction efficiency and surface area issues. The University of Oklahoma is investigating these systems.

The Florida Solar Energy Center (FSEC), in conjunction with the University of Geneva, is investigating tandem/dual bed photosystems using sol/gel-deposited WO₃ films as the oxygen-evolving photocatalyst, rather than TiO₂. In this configuration, the dispersion containing the wider band gap photocatalyst must have minimal light scattering losses so that the lower band gap photocatalyst behind it can also be illuminated.

Photoelectrochemical Systems

Multijunction cell technology developed by the PV industry is being used to develop photoelectrochemical (PEC) light harvesting systems that generate sufficient voltage to split water and are stable in a water/electrolyte environment. The cascade structure of these devices results in greater utilization of the solar spectrum, resulting in the highest theoretical efficiency for any photoconversion device. In order to develop cost effective systems, a number of technical challenges must be overcome. These include identification and characterization of semiconductors with appropriate band gaps; development of techniques for preparation and application of transparent catalytic coatings; evaluation of effects of pH, ionic strength, and solution composition on semiconductor energetics and stability, and on catalyst properties; and development of novel PV/PEC system designs. NREL's approach to solving these challenges is to use the most efficient semiconductor materials available, consistent with the energy requirements for a water splitting system that is stable in an aqueous environment. To date, a PV/PEC water splitting system with a

solar-to-hydrogen efficiency of 12.4% (lower heating value, LHV) using concentrated light, has operated for over 20 hours [6]. HNEI is pursuing a low-cost amorphous silicon-based tandem cell design with appropriate stability and performance, and is developing protective coatings and effective catalysts. An outdoor test of the a-Si cells resulted in a solar-to-hydrogen efficiency of 7.8% LHV under natural sunlight [7].

INDIRECT HYDROGEN PRODUCTION TECHNOLOGIES

These systems offer the opportunity to produce hydrogen from renewable resources in the mid-term (5-10 years). Using agricultural residues and wastes, or biomass specifically grown for energy uses, hydrogen can be produced using a variety of processes.

Biomass pyrolysis produces a bio-oil that, like petroleum, contains a wide spectrum of components. Unlike petroleum, bio-oil contains a significant number of highly reactive oxygenated components derived mainly from constitutive carbohydrates and lignin. These components can be transformed into hydrogen via catalytic steam reforming using Ni-based catalysts. By using high heat transfer rates and appropriate reactor configurations that facilitate contact with the catalyst, the formation of carbonaceous deposits (char) can be minimized. The resulting products from the thermal cracking of the bio-oils are steam reformed at temperatures ranging from 750-850°C. At these conditions, any char formed will also be gasified. At NREL and the Jet Propulsion Laboratory, research and modeling are underway to develop processing technologies that take advantage of the wide spectrum of components in the bio-oil, and address reactivity and reactor design issues [8,9]. Evaluation of co-product strategies indicates that high value chemicals, such as phenolic resins, can be economically produced in conjunction with hydrogen [10].

Biomass is typically 50 weight % (wt%) moisture (as received); biomass gasification and pyrolysis processes require drying of the feed to about 15 wt% moisture for efficient and sustained operation, in addition to requiring size reduction (particle size of ~1 cm). In supercritical gasification processes, feed drying is not required, although particle size reduction requirements are more severe. A slurry containing approximately 15 wt% biomass (required size reduction ~1 mm) is pumped at high pressure (>22 MPa, the critical pressure of water) into a reactor, where hydrothermolysis occurs, leading to extensive solubilization of the lignocellulosics at just above the supercritical conditions. If heat transfer rates to the slurry are sufficiently high, little char is formed, and the constituents of biomass are hydrolyzed and solubilized in the supercritical medium. Increasing the temperature to ~700°C in the presence of catalysts results in the reforming of the hydrolysis products. Catalysts have been identified that are suitable for the steam reforming operation [11]. HNEI and Combustion Systems Inc. are investigating appropriate slurry compositions, reactor configurations, and operating parameters for supercritical water gasification of wet biomass.

HYDROGEN STORAGE, TRANSPORT, AND DELIVERY

The storage, transport, and delivery of hydrogen are important elements in a hydrogen energy system. With keen interest in mobile applications of hydrogen systems, and as intermittent renewables penetration of the electric grid increases, storage becomes essential to a sustainable energy economy. Light weight and high energy density storage will enable the use of hydrogen as a transportation fuel. Efficient and cost effective stationary hydrogen storage will permit PV and wind to serve as base load power systems.

Compressed Gas Storage Tanks

Currently, compressed gas is the only commercially available method for ambient-temperature hydrogen storage on a vehicle. Compressed hydrogen stored at 24.8 MPa in a conventional fiberglass-wrapped aluminum cylinder results in a volumetric storage density of 12 kg of hydrogen per m³ of storage volume and a gravimetric density of 2 wt% (grams of hydrogen per gram of system weight). Carbon fiber-wrapped polymer cylinders achieve higher densities (15 kg/m³ and 5 wt%), but are significantly below target values required for hydrogen to make major inroads in the transportation sector (62 kg/m³ and 6.5 wt%). Advanced lightweight pressure vessels have been designed and fabricated by Lawrence Livermore National Laboratory [12]. These vessels use lightweight bladder liners that act as inflatable mandrels for composite overwrap and as permeation barriers for gas storage. These tank systems are expected to exceed 12 wt% hydrogen storage (at 33.8 MPa) when fully developed.

Carbon-based Storage Systems

Carbon-based hydrogen storage materials that can store significant amounts of hydrogen at room temperature are under investigation. Carbon nanostructures could provide the needed technological

breakthrough that makes hydrogen powered vehicles practical. Two carbon nanostructures are of interest: single-walled nanotubes and graphite nanofibers. Single-walled carbon nanotubes, elongated pores with diameters of molecular dimensions (12 Å), adsorb hydrogen by capillary action at non-cryogenic temperatures. Single-walled nanotubes have recently been produced and tested at NREL in high yields using a number of production techniques, and have demonstrated hydrogen uptake at 5-10 wt% at room temperature [13]. Graphite nanofibers are a set of materials that are generated from the metal catalyzed decomposition of hydrocarbon-containing mixtures. The structure of the nanofibers is controlled by the selection of catalytic species, reactant composition, and temperature. The solid consists of an ordered stack of nanocrystals that are evenly spaced at 0.34-0.37 nanometers (depending on preparation conditions). These are bonded together by van der Waals forces to form a "flexible wall" nanopore structure. Northeastern University estimates that excellent hydrogen storage capacities are possible in these structures.

Metal Hydride Storage and Delivery Systems

Conventional high capacity metal hydrides require high temperatures (300-350°C) to liberate hydrogen, but sufficient heat is not generally available in fuel cell transportation applications. Low temperature hydrides, however, suffer from low gravimetric energy densities and require too much space on board or add significant weight to the vehicle. Sandia National Laboratories (SNL) and Energy Conversion Devices (ECD) are developing low-temperature metal hydride systems that can store 3-5 wt% hydrogen. Alloying techniques have been developed by ECD that result in high-capacity, multi-component alloys with excellent kinetics, albeit at high temperatures. Additional research is required to identify alloys with appropriate kinetics at low temperatures.

A new approach for the production, transmission, and storage of hydrogen using a chemical hydride slurry as the hydrogen carrier and storage medium is under investigation by Thermo Power Corporation. The slurry protects the hydride from unanticipated contact with moisture and makes the hydride pumpable. At the point of storage and use, a chemical hydride/water reaction is used to produce high purity hydrogen. An essential feature of the process is recovery and reuse of spent hydride at a centralized processing plant. Research issues include the identification of safe, stable and pumpable slurries and the design of an appropriate high temperature reactor for regeneration of spent slurry.

END USE TECHNOLOGIES

Proton exchange membrane (PEM) fuel cells could provide low-cost, high-efficiency electric power, and be operated "in reverse" as electrolyzers to generate hydrogen. There has been a significant increase in industry activity for the development of PEM fuel cells for vehicular applications, with a number of active demonstration projects. Improvements in catalyst loading requirements, water management, and temperature control have helped move these power units from mere curiosities to legitimate market successes. In order to increase the market penetration in both the transportation and utility sectors, additional improvements are required. Los Alamos National Laboratory is developing non-machined stainless steel hardware and membrane electrode assemblies with low catalyst loadings to achieve cost reductions and efficiency improvements [14]. The most important barriers to implementation of low-cost PEM fuel cells are susceptibility of the metal or alloy to corrosion, water management using metal screens as flow fields, and effective stack sealing. Operating the PEM fuel cell "in reverse" as an electrolyzer is possible, but optimum operating conditions for the power production mode and for the hydrogen production mode are significantly different. Design issues for the reversible fuel cell system include thermal management, humidification, and catalyst type and loading.

In an effort to promote near-term use of hydrogen as a transportation fuel, the Program is investigating the development of cost effective, highly efficient, and ultra-low emission internal combustion engines (ICE) operating on pure hydrogen and hydrogen-blended fuels. Research at SNL is focused on the development of a hydrogen fueled ICE/generator set with an overall efficiency of >40% while maintaining near zero NO_x emissions [15].

SAFETY

Hydrogen leak detection is an essential element of safe systems. The development of low-cost fiber optic and thick film sensors by NREL and ORNL, respectively, will provide affordable and reliable options for hydrogen safety systems. NREL is using optical fibers with a thin film coating on the end that changes optic properties upon reversible reaction with hydrogen. Change in the reflected light signal is an indication of the presence of hydrogen. Sensitivity and selectivity are important research issues. ORNL is focused on the development of monolithic, resistive thick film sensors that

are inherently robust, selective to hydrogen, and easy to manufacture. Research issues include developing appropriate techniques for active (versus traditional passive) thick film applications.

Recognizing the importance of safe use of hydrogen, the DOE, in conjunction with Natural Resources Canada, has compiled a comprehensive document of prevailing practices and applicable codes, standards, guidelines, and regulations for the safe use of hydrogen. The *Sourcebook for Hydrogen Applications* is intended to be a "living document" that can be updated to reflect the current state of knowledge about, and experience with, safely using hydrogen in emerging applications. DOE also supports the development of codes and standards under the auspices of the International Standards Organization.

CONCLUSIONS

The DOE Hydrogen Program conducts R&D in the areas of production, storage, and utilization, for the purpose of making hydrogen a cost-effective energy carrier for utility, buildings, and transportation applications. Research is focused on the introduction of renewable-based options to produce hydrogen; development of hydrogen-based electricity storage and generation systems that enhance the use of distributed renewable-based utility systems; development of low-cost technologies that produce hydrogen directly from sunlight and water; and support of the introduction of safe and dependable hydrogen systems including the development of codes and standards for hydrogen technologies.

REFERENCES

- [1] Ghirardi, M.L., R.K. Togasaki, and M. Seibert, 1997, "Oxygen Sensitivity of Algal Hydrogen Production," *Appl. Biochem. Biotechnol.*, 63-65, 141-151.
- [2] Seibert, M., T. Flynn, D. Benson, E. Tracy, and M. Ghirardi, 1998, "Development of Selection/Screening Procedures for Rapid Identification of Hydrogen-Producing Algal Mutants with Increased Oxygen Tolerance," International Conference on Biological Hydrogen Production, Plenum, NY, 227-234.
- [3] Melis, A., J. Neidhardt, I. Baroli, and J.R. Benemann, 1998, "Maximizing Photosynthetic Productivity and Light Utilization in Microalgal by Minimizing the Light-Harvesting Chlorophyll Antenna Size of the Photosystems." International Conference on Biological Hydrogen Production, Plenum, NY, 41-52.
- [4] Szyper, J.P., B.A. Yoza, J.R. Benemann, M.R. Tredici, and O.R. Zaborsky, 1998, "Internal Gas Exchange Photobioreactor: Development and Testing in Hawaii," International Conference on Biological Hydrogen Production, Plenum, NY, 441-446.
- [5] Maness, P.-C. and P.F. Weaver, 1997, "Variant O₂-Resistant Hydrogenase from Photosynthetic Bacteria Oxidizing CO," Proceedings of the Fifth International Conference on the Molecular Biology of Hydrogenase, Albertville, France.
- [6] Khaselev, O. and J.A. Turner, 1998, "A Monolithic Photovoltaic-Photoelectrochemical Device for Hydrogen Production via Water Splitting," *Science*, 280, 425.
- [7] Rocheleau, R., 1998, "High Efficiency Photoelectrochemical H₂ Production using Multijunction Amorphous Silicon Photoelectrodes," *Energy & Fuels*, 12 (1), 3-10.
- [8] Wang, D., S. Czernik, and E. Chornet, 1998, "Production of Hydrogen from Biomass by Catalytic Steam Reforming of Fast Pyrolysis Oil," *Energy & Fuels*, 12 (1), 19-24.
- [9] Miller, R.S. and J. Bellan, 1997, "A Generalized Biomass Pyrolysis Model Based on Superimposed Cellulose, Hemicellulose and Lignin Kinetics," *Comb. Sci. and Techn.*, 126, 97-137.
- [10] Wang, D., S. Czernik, D. Montane, M.K. Mann, and E. Chornet, 1997, "Hydrogen Production via Catalytic Steam Reforming of Fast Pyrolysis Oil Fractions," Proceedings of the Third Biomass Conference of the Americas, Montreal, 845-854.
- [11] Matsunaga, Y., X. Xu, and M.J. Antal, 1997, "Gasification Characteristics of an Activated Carbon in Supercritical Water," *Carbon*, 35, 819-824.
- [12] Mitlitsky, F., and B. Myers, and A.H. Weisberg, 1998, "Regenerative Fuel Cell Systems," *Energy & Fuels*, 12 (1), 56-71.
- [13] Dillon, A.C., K.M. Jones, T.A. Bekkedahl, C.H. Kiang, D.S. Bethune, and M.J. Heben, 1997, "Storage of Hydrogen in Single-Walled Carbon Nanotubes," *Nature*, 386, 377-279.
- [14] Cleghorn, S., X. Ren, T. Springer, M. Wilson, C. Zawodzinski, T. Zawodzinski, and S. Gottesfeld, 1997, "PEM Fuel Cells for Transportation and Stationary Power Generation Applications," *Int. J. Hydrogen Energy*, 23, 1137-1144.
- [15] Cleghorn, S., X. Ren, T. Springer, M. Wilson, C. Zawodzinski, T. Zawodzinski, and S. Gottesfeld, 1997, "PEM Fuel Cells for Transportation and Stationary Power Generation Applications," *Int. J. Hydrogen Energy*, 23, 1137-1144.

ISOLATION OF *CHLAMYDOMONAS* MUTANTS WITH IMPROVED OXYGEN-TOLERANCE

Timothy Flynn, Maria L. Ghirardi, and Michael Seibert
National Renewable Energy Laboratory, Golden, CO 80401

ABSTRACT

The photoproduction of H₂ from water by anaerobically-induced algae is catalyzed by a bidirectional hydrogenase, an enzyme that is rapidly deactivated by exposure to low levels of O₂. We have developed two selective pressures, with which a mutant's survival depends on hydrogenase activity in the presence of O₂, and a chemochromic screening method to quickly identify and isolate desirable O₂-tolerant hydrogenase mutants. The clones that still produced H₂ after exposure to O₂ were further characterized by gas chromatography for maximal H₂-production rate and tolerance to O₂. The best mutant obtained by a single round of mutagenesis/selection/screening maintained up to 35% of its maximal H₂-production rate (measured with no exposure to O₂) following deactivation of the enzyme by 2% O₂ for 2 minutes, a condition that almost totally inactivates wild-type (WT) H₂ production. A mutant that underwent a second round of mutagenesis and selection exhibited 49% of its maximal activity following the deactivation treatment. This represents a 10-fold improvement over the WT strain and suggests that even better mutants will be forthcoming.

INTRODUCTION

Photobiological H₂-production by green algae is catalyzed by the reversible hydrogenase (1,2), a chloroplast stromal enzyme (3) that catalyzes both H₂ production and H₂ uptake in the organism. This nuclear-encoded protein (4) is induced by anaerobic incubation of algal cells in the dark but is inhibited by the presence of very low concentrations of O₂ (5). This problem has precluded the application of algae up to this point in applied H₂-producing systems.

Future development of a cost-effective, commercial H₂-production system using green algae will depend on the availability of strains that produce H₂ directly from water under aerobic conditions (6). One of our approaches to generate O₂-tolerant, H₂-producing algal mutants was based on a selection pressure involving the H₂-uptake activity of the reversible hydrogenase (7). Hydrogen uptake (or photoreductive) selection is applied to a population of mutagenized *Chlamydomonas reinhardtii* cells in an atmosphere of H₂, CO₂, and controlled concentrations of O₂, as well as in the presence of the herbicides 3-(3,4-dichlorophenyl)-1,1-dimethyl urea (DCMU) and atrazine. These herbicides blocks photosynthetic O₂ evolution and electron flow at the reducing side of photosystem II and prevent electrons from water from reaching the hydrogenase enzyme. The surviving organisms grow by fixing CO₂ with electrons obtained from the oxidation of H₂ catalyzed by the O₂-tolerant hydrogenase, and ATP generated by cyclic electron transport around photosystem I (5).

Since photoreductive selection only exploits the H₂ oxidation activity of the hydrogenase, we have also developed a new selective pressure designed to exploit the H₂-evolving function of the enzyme (8). This selection depends on the fact that, in the absence of CO₂, metronidazole (MNZ) will compete with the hydrogenase at the level of ferredoxin for electrons derived from the photosynthetic electron transport chain (9). Reduced MNZ generates a radical that is reoxidized by O₂ with the concomitant formation of superoxide radicals and H₂O₂, both of which are toxic to the algae. If the hydrogenase is still active following exposure to O₂, then some of the electrons from reduced ferredoxin can be used for H₂ production instead of MNZ reduction, and decreased toxicity can be observed (8).

The traditional assays (Clark electrode or gas chromatograph analysis) used to determine a clone's O₂-tolerance require many time-consuming steps and are a severely limiting factor for rapidly identifying useful mutants (10). This problem was solved by the development of a screening assay using a thin-film, multilayer chemochromic sensor (11) that permits the evaluation of hundreds of mutant clones in a single day. This sensor, when held in close contact to anaerobically induced algal colonies that can evolve H₂ after exposure to O₂, produces an easily visualized blue spot. These spots correspond to colonies that were able to withstand O₂ deactivation treatment, and allow for the rapid identification of desirable mutants clones (10). The combination of random mutagenesis, selection, and screening has yielded H₂-producing *Chlamydomonas* mutants with significantly improved O₂-tolerance.

MATERIALS AND METHODS

Cell Growth: Wild-type (WT) *C. reinhardtii* (137c⁺) was a gift from Prof. S. Dutcher, University of Colorado, Boulder. Algal cells were grown photoautotrophically in basal salts (BS), a modification of Sueoka's high salt medium (12) that includes citrate to prevent salt precipitation. This formulation contains the following salts: 10 mM NH₄Cl, 1 mM MgSO₄, 7.5 mM KH₂PO₄, 7.5 mM K₂HPO₄, 1.5 mM Na₃-citrate, 0.5 mM CaCl₂, 20 μM FeCl₃, and 1/2 x Hutner's trace elements (12). This medium can be solidified with 1.5% w/v agar and amended with 0.5 g/l yeast extract (Difco) for plates, and may be supplemented with 10 mM sodium acetate depending on the

experiment. Liquid cultures were grown under continuous cool white fluorescent lamp illumination ($70 \mu\text{E}\cdot\text{m}^{-2}\cdot\text{s}^{-1}$ PAR) at 25°C and agitated on a shaker. Cells were harvested by centrifugation at $2000 \times g$ for 10 min and resuspended in liquid BS medium.

Mutagenesis: Mid-log phase cultures were harvested and resuspended in liquid BS to yield a 10^8 ml suspension of 7×10^6 cells/ml. Ethylmethane sulfonate (EMS) was added to a final concentration of $5 \mu\text{l/ml}$ (46 mM), and the cells were incubated with gentle agitation for various periods of time. At the end of the incubation period the cells were washed and resuspended in 50 ml of the same medium lacking EMS. Liquid cultures were grown in the light as above for at least 7 days before being submitted to the selective pressures.

Photoreductive Selection (PR) Procedure: Liquid cultures of mutagenized algal cells (250 ml , 2.8×10^5 cells/ml) in BS were treated with $15 \mu\text{M}$ each of DCMU and atrazine, and the flasks were placed in anaerobic jars. The gas phase contained 16.5% H_2 , 2% CO_2 , 5% O_2 , balanced with Ar. The cultures were grown for a couple of weeks with stirring and illuminated with fluorescent light ($70 \mu\text{E}\cdot\text{m}^{-2}\cdot\text{s}^{-1}$ PAR). At the end of the selection period, the cells were washed with BS medium and revived in liquid BS medium plus 10 mM sodium acetate.

H_2 -Production Selection (MZ) Procedure: A suspension of anaerobically-induced algal cells was mixed with an anaerobic MNZ-Na azide solution to final concentrations of 40 mM MNZ and 1 mM sodium azide and 2.8×10^6 cells/ml. While maintaining darkness, O_2 was added to 5% in the gas phase, and the mixtures were shaken vigorously for 4 min. Immediately following the O_2 treatment, the cultures were exposed for 6 min to light ($320 \mu\text{E}\cdot\text{m}^{-2}\cdot\text{h}^{-1}$ PAR) filtered through a solution of 1% CuSO_4 with mixing. At the end of the selection period, the cells were washed with BS medium and either resuspended in the same medium or plated for cell counting.

Chemochromic screening: Individual colonies surviving mutagenesis and selection were transferred to square petri dishes that can easily accommodate an 8×8 colony matrix and the square chemochromic sensor. Following a 7-14 day growth period, the agar plates were made anaerobic overnight to induce the algal hydrogenase and then preexposed to 21% O_2 for different periods of time in the dark to deactivate the WT phenotype. The plates were immediately transferred to an anaerobic glove box, the sensor applied, and the colonies were illuminated for 3 minutes to photoevolve H_2 . At the end of the illumination period, the sensors were analyzed for the location of blue dots, corresponding to the algal colonies that still evolved H_2 following the O_2 pretreatment. The identified clones were transferred from the original plate to liquid BS + 10 mM acetate, and were cultivated for further characterization.

H_2 -Evolution Assay: Mid-log phase algal cultures were harvested and resuspended in phosphate buffer (8) supplemented with 15 mM glucose and 0.5% v/v ethanol and were then made anaerobic with Ar bubbling. Concurrently, 2 ml of an enzymatic O_2 -scrubbing system (13) that consisted of 1mg/ml glucose oxidase and 27720 units/ml catalase was dispensed into dialysis tubing (6-8 kD MW cutoff) and made anaerobic as above. The dialysis bags were added to the cell suspensions and the vials were sealed, covered with aluminum foil, and incubated at room temperature for 4 h. Following this induction treatment, the cell suspensions were kept at 4°C overnight. The assay reaction consists of exposing the cells to various levels of O_2 for two minutes, reestablishing anaerobiosis, and adding reduced methyl viologen to serve as the electron donor to the hydrogenase. The reactions mixtures were incubated in the dark for 15 minutes at 30°C in a shaking water bath, and the reaction was stopped by adding trichloroacetic acid. The presence of H_2 was detected by gas chromatography.

RESULTS

Figure 1 shows the dose response curve when WT cells were treated with the mutagen EMS (46 mM for various periods of time). The survivors from the 10, 15 and 20 minute cultures (corresponding to 66, 56, and 42% survival) were harvested (see methods) and used in future experiments.

Figure 2 shows the subsequent treatment histories of the various populations. Each of the three polygenic mutant populations were initially subjected to the PR selection, and individual surviving clones were subjected to the chemochromic screening. Screening and preliminary characterization of representative clones obtained from the populations PR8, PR9, PR10, failed to yield mutants with significantly improved O_2 -tolerance. The insufficient enrichment of desirable mutants by this particular experiment will be discussed later. The populations surviving the PR selection were maintained in liquid BS plus acetate and were then subjected to the MZ procedure. Figure 3 shows the killing kinetics of the MZ selections, where less than 3% of the initial population density survived in each case. The apparent decreased killing rate of the MZ14 population was probably caused by incomplete mixing of the gas and liquid phase during the dark deactivation treatment. Following resuspension in liquid BS, the resulting cultures were diluted and spread onto agar to obtain individual colonies derived from single cell clones.

Two hundred and forty clones from each of the three populations that survived the MZ selection pressure were isolated for the chemochromic screening assay. The colonies on agar plates were exposed to 21% O_2 for various periods of time for a maximum of 10 minutes before screening.

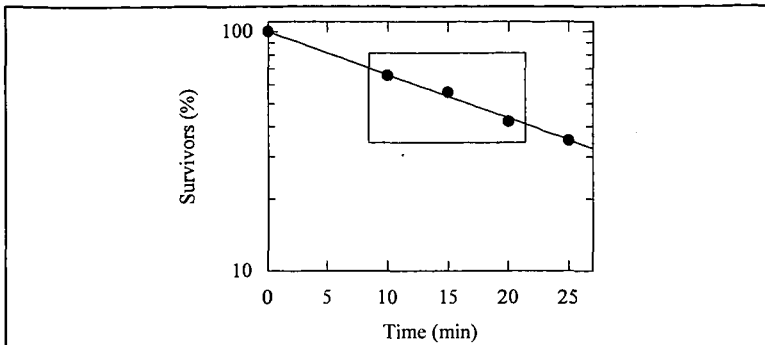


Figure 1: Ethylmethane sulfonate (EMS) mutagenesis of WT *C. reinhardtii* using 5 μl/ml (46 mM) EMS and a 10 ml suspension of 7×10^6 cells/ml. The harvested populations are indicated.

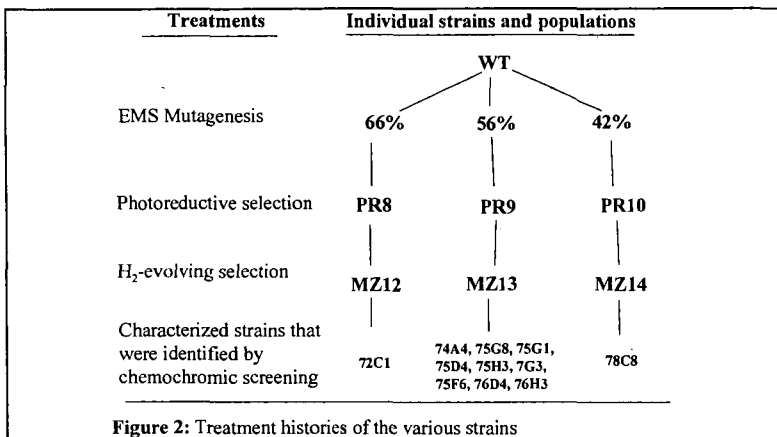


Figure 2: Treatment histories of the various strains

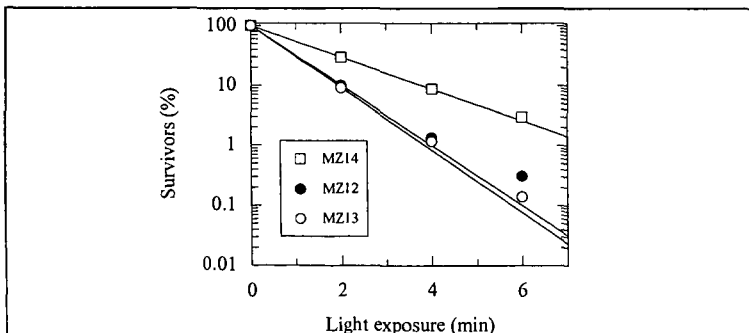


Figure 3: Metronidazole selection of the photoreductive selection survivors (PR8, PR9, and PR10), giving rise to MZ12, MZ13, and MZ14 respectively. The anaerobically induced cells were preexposed for 4 minutes to 5% O₂ before illumination.

The clones that produced the most H₂ under these conditions were further characterized using the methyl viologen assay. Table 1 summarizes the characteristics of the indicated selected clones. The parameters used to initially characterize the mutants included the maximum rate of H₂ evolution measured without any exposure to O₂ (V₀), and the amount of remaining H₂-evolution activity following an exposure to 2% O₂ for two minutes (% of V₀). The % of V₀ parameter was used to roughly compare the relative O₂-tolerance of the mutants compared to the WT strain. Four strains were more fully characterized by titrating the H₂-evolving activity following deactivation of the enzyme with increasing levels of O₂ for 2 minutes. The O₂ I₅₀ was estimated by fitting the data to a single exponential decay function. Inspection of Table 1 reveals that all of the mutants identified by the screening assay are improved with respect to V₀ and O₂-tolerance compared to their parental WT strain. The V₀'s were increased in all of the mutants, with a 2.3-fold increase in strain 75D4. The I₅₀'s, were increased by 3.7- and 4.4-fold in the strains 76D4 and 76H3. The least improved strain, 78C8, had only a 9% increase in O₂-tolerance compared to the WT strain, and may represent the minimum phenotype for surviving the conditions used in this H₂-evolving selection experiment.

The strain 76D4 was remutagenized with EMS (61% survival), selected using the MZ procedure with a selective pressure of 40% O₂ in the dark for 5 minutes, and finally screened following deactivation with 100% O₂ for 5 minutes. A resulting clone, 141F2, had over a 2-fold increase in I₅₀ compared to its parent (76D4) and almost a 10-fold improvement compared to the grandparent WT strain.

MZ population ^A	Strain	V ₀ ^B (μmoles H ₂ /(mg Chl x h))	% of V ₀ ^C	O ₂ I ₅₀
-----	WT	39	0.26%	0.22
MZ12	72C1	81	14%	-----
MZ13	76D4	78	18%	0.82
	76H3	72	35%	0.96
	74A4	64	15%	-----
	75G8	50	26%	-----
	75G1	82	17%	-----
	75D4	88	18%	-----
	75H3	67	27%	-----
MZ14	78C8	64	9%	-----
	141F2	86	49%	2.04

Table 1: Characteristics of selected strains. A: see Fig. 2. B: maximum rate of H₂ evolution without any exposure to O₂. C: rate of H₂ evolution following deactivation by pre-exposure of the cells to 2% O₂ for 2 minutes (expressed as % of V₀). D: The O₂ concentration (in %) that reduces V₀ by 1/2 (2 minute exposure).

DISCUSSION

Mutagenesis of *C. reinhardtii* cells was induced by exposure to EMS, an agent that alkylates the keto groups of guanines and thymine. This causes anomalous base-pairing upon the replication of DNA (14) and ultimately results in transition mutation (G≡C becomes A=T). The frequency of mutants among survivors increases with mutagen dose, but so does the damage to the genetic background (15). Therefore, killing rates of less than 60% were chosen to minimize damage to the remainder of the genome. The problem of decreased mutant frequencies among the survivors is normally solved by employing effective selection procedures.

However, upon finding little improvement in O₂-tolerance in the populations obtained from the first photoreductive selection, it appeared that either the hydrogenase was not mutated, or the conditions employed were not sufficiently specific for the enrichment of desirable O₂-tolerant mutants. Since improved mutants could be generated by MZ selection (Table 1), but were not recovered from the original PR populations, the PR procedure clearly needs improvement. We have reexamined the initial PR selection protocol (see Materials and Methods section) and have determined that the initial O₂ concentration in the anaerobic jar could have been significantly decreased by cellular respiration of the cultures during the application of the selective treatment. This could and apparently did reduce the effectiveness of the selective pressure. This problem was solved by replacing the gas mixture daily until the culture became chlorotic indicating that the

majority of the cells are dead. Preliminary results obtained from this modification appear promising and will be published elsewhere.

The results of this paper clearly demonstrate the utility of the chemochromic screening technique. It has not only allowed us to rapidly identify mutants with desired phenotypes but also permitted the rapid assessment of the effectiveness of the selection procedures themselves. It is also encouraging that all of the strains that were identified with the chemochromic sensor were improved compared to their parental strain upon further characterization.

The mutants identified with the chemochromic sensor were chosen for further characterization based on the intensity of the color change following an exposure to various pretreatment doses of O₂. The clones that demonstrated the best potential, based on the intensity of the color change, were obtained from the MZ13 population, and were most heavily sampled. Given the range of increased O₂-tolerance (% of V₀, Table 1) detected among the 10 sampled first round mutants, one could argue that there is more than one genotype that gives rise to the O₂-tolerant phenotype. Three obvious possibilities exist: (a) different amino acid substitutions at a single critical residue, (b) random substitutions distributed throughout the O₂-sensitive domain, or (c) mutations of genes other than the hydrogenase that cause a decrease in intracellular O₂ concentration, such as through increased rates of respiration.

The ultimate goal of our research is to create an organism that photo-oxidizes water to H₂ under aerobic conditions using solar energy. Our current results are encouraging, and validate the use of classical mutagenesis/selection to obtain the desirable organisms.

ACKNOWLEDGMENTS

This work was supported by the U.S. Department of Energy Hydrogen Program. We thank Dr. Se-Hee Lee for making the sensors.

REFERENCES

1. Weaver, P.F., Lien, S., and Seibert, M. (1980) in *Proceedings of the Fifth Joint US/USSR Conference of the Microbial Enzyme Reactions Project*, Jurmala, Latvia, USSR, pp. 461-479.
2. Adams, M.W.W., Mortenson, L.E., and Chen, J.-S. (1981) *Biochim. Biophys. Acta* **594**, 105-176.
3. Happe, T., Mosler, B., and Naber, D. (1994) *Eur. J. Biochem.* **222**, 769-774.
4. Roessler, P.G., and Lien, S. (1984) *Plant Physiol.* **75**, 1086-1089.
5. Maione, T.E., and Gibbs, M. (1986) *Plant Physiol.* **80**, 364-368.
6. Schulz, R. (1994) *J. Mar. Biotechnol.* **4**, 16-22.
7. McBride, A.C., Lien, S., Togaasaki, R.K., and San Pietro, A. (1977) in *Biological Solar Energy Conversion*, Mitsui, A., Miyachi, S., San Pietro, A., and Tamura, S. eds. Academic Press, New York, NY.
8. Ghirardi, M.L., Togaasaki, R.K., and Seibert, M. (1997) *Appl. Biochem. Biotechnol.* **63-65**, 141-151.
9. Schmidt, G.W., Matlin, K.S., and Chua, N.-H. (1977) *Proc. Natl. Acad. Sci. USA* **74**, 610-614.
10. Seibert, M., Flynn, T., Benson, D., Tracy, E., and Ghirardi, M. (1998) In *Biohydrogen* (Zaborsky, O.R., et al. eds), Plenum Publishing Corporation, New York, NY.
11. Benson, D.K., Tracy, C.E., and Bechinger, C. (1996) In *Proceedings of the 1996 U.S. DOE Hydrogen Program Review*, vol. II, 605-624, NREL/CP-21908430.
12. Harris, E.H. (1989) *The Chlamydomonas Sourcebook*, Academic Press, New York.
13. Packer, L., and Cullingford, W. (1978) *Z. Naturforsch.* **33c**, 113-115.
14. Klug, W.S., and Cummings, M.R. (1983) *Concepts in Genetics*, Charles E. Merrill Publishing Company, Columbus, Ohio.
15. Bos, C.J. (1987) *Curr. Genet.* **12**: 471-474.

PHOTOSYNTHETIC HYDROGEN AND OXYGEN PRODUCTION BY GREEN ALGAE

E. Greenbaum and J. W. Lee

Oak Ridge National Laboratory
P. O. Box 2008
Oak Ridge, TN 37831

Summary

Photosynthesis research at Oak Ridge National Laboratory is focused on hydrogen and oxygen production by green algae in the context of its potential as a renewable fuel and chemical feed stock. Beginning with its discovery by Gaffron and Rubin in 1942, motivated by curiosity-driven laboratory research, studies were initiated in the early 1970s that focused on photosynthetic hydrogen production from an applied perspective. From a scientific and technical point of view, current research is focused on optimizing net thermodynamic conversion efficiencies represented by the Gibbs Free Energy of molecular hydrogen. The key research questions of maximizing hydrogen and oxygen production by light-activated water splitting in green algae are (1) removing the oxygen sensitivity of algal hydrogenases; (2) linearizing the light saturation curves of photosynthesis throughout the entire range of terrestrial solar irradiance — including the role of bicarbonate and carbon dioxide in optimization of photosynthetic electron transport and (3) constructing real-world bioreactors, including the generation of hydrogen and oxygen against workable back pressures of the photoproducted gases.

Introduction

Photosynthetic hydrogen production by green algae was discovered in the pioneering experiments of Gaffron and Rubin (1942). This work was followed up by Gaffron and his colleagues in a series of seminal papers (Gaffron, 1960; Kaltwasser *et al.*, 1969; Stuart and Gaffron, 1971 & 1972;) as well as many others. From the point of view of renewable fuels and chemical feedstock production, it is light-activated simultaneous photoproduction of hydrogen and oxygen that is of primary interest. The pioneering experiments in this field were performed by Spruit (1958) who developed a novel two-electrode polarographic technique for the simultaneous measurement of hydrogen and oxygen transients by the green alga *Chlorella*. The principle conclusion he came to was that hydrogen and oxygen metabolisms are closely related and they derived from water splitting. Later work by Bishop and Gaffron (1963) indicated that light-dependent evolution of hydrogen appeared to require both photosystems.

Research on photosynthetic hydrogen production as a renewable energy source began in the 1970s (Gibbs, *et al.*, 1973; Lien and San Pietro, 1975; Mitsui *et al.*, 1977). Using the two-electrode technique Bishop *et al.* (1977) measured and interpreted hydrogen and oxygen production from a large group of green algae. However, due to the buildup of hydrogen and oxygen, with subsequent inhibition (*vide infra*) these reactions could be followed for only several minutes. Using a flow system that removed inhibitory oxygen, it was shown (Greenbaum, 1980) that sustained simultaneous photoproduction of hydrogen and oxygen could be observed for hours. In prior experiments using a glucose-glucose oxidase trap, Benemann *et al.* (1973) demonstrated hydrogen production from water by a chloroplast-ferredoxin-hydrogenase system. Measurement of the hydrogen analog of the Emerson and Arnold photosynthetic unit size (Greenbaum, 1977a, b) indicated that photogenerated reductant expressed as molecular hydrogen was derived from the mainstream of the photosynthetic electron transport chain. Direct measurement of the turnover time of photosynthetic hydrogen production (Greenbaum, 1979 and 1982) demonstrated that this parameter was comparable to the turnover time of oxygen production. It was also shown (Greenbaum, 1988) that net conversion efficiencies of 5-10% could be achieved in the linear low-intensity region of the light saturation curve.

Research Problems

The hydrogenase enzyme is synthesized *de novo* under anaerobic conditions. In normal

photosynthesis carbon dioxide is the preferred electron acceptor for photogenerated reductant from Photosystem I. However, direct kinetic competition between hydrogen evolution and the Calvin cycle can easily be observed (Graves et al. 1989; Cinco et al. 1993). The three scientific research problems associated with photosynthetic hydrogen and oxygen production are (1) oxygen sensitivity of hydrogenase; (2) antenna size, bicarbonate and the light saturation problem; and (3) the minimum number of light reactions required to split water to molecular hydrogen and oxygen.

Oxygen Sensitivity of Hydrogenase

In the application of intact unicellular green algae for hydrogen production one is confronted with the problem of oxygen sensitivity of the hydrogenase enzyme. Hydrogenase is synthesized under anaerobic conditions and, at present, must be kept that way in order to preserve its functionality. In one approach, oxygen and hydrogen by green algae are coproduced in the same volume. Therefore, a way must be found to prevent inhibition of hydrogenase activity by the photosynthetically produced oxygen. This challenging problem is the focus of research at the National Renewable Energy Laboratory (Ghirardi et al., 1997).

Antenna Size, Bicarbonate and the Light Saturation Problem

In full sunlight, $\approx 1000 \text{ W/m}^2$, there exists a kinetic imbalance between the rate of photon excitation of the reaction centers and the ability of the thermally-activated electron transport chains to process photogenerated electrons. Whereas the reaction centers can receive photoexcitations at the rate of $\approx 2000 \text{ sec}^{-1}$, movement through the electron transport chain is of the order of 200 sec^{-1} or less (Gibbs et al., 1973). Therefore, normal photosynthesis saturates at much less than full sunlight, typically $\approx 10\%$.

Since there is little opportunity to increase the rate of thermally-activated electrons through the photosynthetic electron transport chain, an alternate strategy is to reduce the antenna size. Kinetic balance between the rate of photon excitation and rate of photosynthetic electrons can, in principle, be balanced, even at full sunlight, by reducing the absolute antenna size per reaction center. If such a response could be achieved in a real-world system, photosynthetic productivity on a per chlorophyll basis would increase and high solar irradiances would be converted to useful biomass energy. Linearization of the light saturation curve of photosynthesis was demonstrated by Herron and Mauzerall (1972). Melis et al. (1998) have demonstrated linearization of the light saturation curve for high-light grown cultures of *Dunaliella*. These results indicate that the concept is technically correct.

An additional complication of the light saturation problem involves the requirement of bicarbonate to optimize electron transport through Photosystem II. Since carbon dioxide/bicarbonate are the exclusive sink for photosynthetically generated reductant they need to be removed so that the flow of electrons produces hydrogen rather than carbon dioxide fixation compounds. Complete removal of carbon dioxide, however, impairs electron transport in Photosystem II and further reduces the saturating light intensity for sustained simultaneous photoproduction of hydrogen and oxygen by about factor of 10. Qualitatively speaking, light saturation occurs at about 10 W/m^2 . One strategy to overcome this limitation is to take advantage of the differential affinity of $\text{CO}_2/\text{bicarbonate}$ between the Photosystem II binding site and the Calvin cycle. Such an approach has been explored by Cinco et al. (1993) in which light-activated hydrogen and oxygen evolution as a function of CO_2 concentration in helium were measured for the unicellular green alga *Chlamydomonas reinhardtii*. The concentrations were 58, 30, 0.8 and 0 ppm CO_2 . The objective of these experiments was to study the differential affinity of $\text{CO}_2/\text{HCO}_3^-$ for their respective Photosystem II and Calvin cycle binding sites vis-à-vis photoevolution of molecular oxygen and the competitive pathways of hydrogen photoevolution and CO_2 photoassimilation. The maximum rate of hydrogen evolution occurred at 0.8 ppm CO_2 . The key result of this work was that the rate of photosynthetic hydrogen evolution can be increased, at least partially, by satisfying the Photosystem II $\text{CO}_2/\text{HCO}_3^-$ binding site requirement without fully activating the Calvin-Benson CO_2 reduction pathway. These preliminary experiments suggest that mutants of *Chlamydomonas reinhardtii* that have a genetically engineered low CO_2 affinity for the

Calvin cycle and relatively higher affinity for the PS II $\text{CO}_2/\text{HCO}_3^-$ binding site may be good candidates to explore for relieving the CO_2 part of the light saturation constraint.

Thermodynamic Driving Pressure of Photosynthetic Hydrogen Production

We have shown that the thermodynamic driving pressure of hydrogen production in the green alga *Scenedesmus* D₃ is equal to or greater than one atmosphere. This was accomplished by measuring the rate of photosynthetic oxygen production by *Scenedesmus* in one-atmosphere of pure hydrogen. The practical significance of this work is that it helps to minimize the amount of pump work required to deliver hydrogen at a useable pressure. At a minimum, the amount of energy saved is $\Delta W = RT \ln(P_{\text{final}}/P_{\text{initial}})$. Since this is the reversible equilibrium thermodynamic value, the actual value for real gases, including irreversible processes, will be several times this. The amount of energy saved can be calculated to be in the range 68,500 - 114,200 J mol⁻¹. ΔG_p° for the reaction, $\text{H}_2\text{O} \rightarrow \text{H}_2 + \frac{1}{2}\text{O}_2$, is 237,200 J mol⁻¹. Another significant aspect of this result is that it demonstrates for the first time that the oxygen evolution enzyme is insensitive to the presence of high concentrations (*i.e.*, pure) hydrogen. That is to say, unlike the well-known sensitivity of the hydrogenase enzyme to even low concentrations of oxygen, the oxygen evolving complex of photosynthesis is unaffected by the presence of hydrogen. The indirect method of measuring oxygen was necessary because it is experimentally impossible to measure photosynthetically produced hydrogen against a background carrier gas of pure hydrogen since the gas sensitive semiconducting detectors that are used for the hydrogen analysis are saturated in pure hydrogen. Isotopic labeling experiments are currently under way for direct measurement of hydrogen production.

[Note: Much of the text of this abstract has been previously published. Please see E. Greenbaum and J. W. Lee, "Photosynthetic Hydrogen and Oxygen Production by Green Algae: An Overview," in *BioHydrogen*, O. Zaborsky, Ed. pp.235-242 (1998). [Copyright Plenum Press, New York, 1998]

References

- Bishop NI and Gaffron H (1963) On the interrelation of the mechanisms for oxygen and hydrogen evolution in adapted algae. In *Photosynthetic Mechanisms in Green Plants*, B. Kok and A. T. Jagendorf, Eds. (Natl. Acad. Sci.-Natl. Res. Council, Washington, DC), pp. 441-451
- Bishop NI, Fricke M, and Jones LW (1977) Photohydrogen production in green algae: water serves as the primary substrate for hydrogen and oxygen production. In *Biological Solar Energy Production*, A. Mitsui, S. Miyachi, A. San Pietro, and S. Tamura, Eds. (Academic Press, New York) pp. 1-22
- Cinco RM, MacInnis JM and Greenbaum E (1993) The Role of Carbon Dioxide in Light-Activated Hydrogen Production by *Chlamydomonas reinhardtii*. *Photosyn. Res.* 38: 27-33 (1993)
- Gaffron H (1960) Energy storage: photosynthesis. In *Plant Physiology* **1B**: 4-277
- Gaffron H and Rubin J (1942) Fermentative and photochemical production of hydrogen in algae. *J. Gen. Physiol.* 26: 219-240
- Ghirardi ML, Togasaki RK and Seibert M (1997) Oxygen sensitivity of algal hydrogen production. *Appl. Biochem. Biotech.*, in press
- Gibbs M, Hollaender A, Kok B, Krampitz, LO and San Pietro A (1973) Proceedings of the Workshop on Bio-Solar Conversion, September 5-6, 1973, Bethesda, MD, NSF RANN Grant GI 40253 to Indiana University
- Graves DA, Tevault CV and Greenbaum E (1989) Control of Photosynthetic Reductant: The Effect of Light and Temperature on Sustained Hydrogen Photoevolution in *Chlamydomonas* sp. in an Anoxic Carbon Dioxide Containing Atmosphere. *Photochem. Photobiol.* 50: 571-576
- Greenbaum E (1982) Photosynthetic hydrogen and oxygen production: kinetic studies. *Science* 215: 291-293
- Greenbaum E (1977a) The photosynthetic unit size of hydrogen evolution. *Science* 196: 878-879
- Greenbaum E (1977b) The molecular mechanisms of photosynthetic hydrogen and oxygen production. In *Biological Solar Energy Production*, A. Mitsui, S. Miyachi, A. San Pietro, and S. Tamura, Eds. (Academic Press, New York) pp. 101-107
- Greenbaum E (1979) The turnover times and pool sizes of photosynthetic hydrogen production by green algae. *Solar Energy* 23: 315-320
- Greenbaum E (1988) Energetic efficiency of hydrogen photoevolution by algal water splitting. *Biophys. J.* 54: 365-368

- Greenbaum E (1980) Simultaneous photoproduction of hydrogen and oxygen by photosynthesis. *Biotechnol. Bioengin. Symp.* 10, 1-13
- Greenbaum E, Lee JW, Blankinship SL and Tevault CV (1997b) Hydrogen and oxygen production in mutant Fud26 of *Chlamydomonas reinhardtii* Proceedings of the 1997 U.S. DOE Hydrogen Program Review. May 21-23, 1997, Herndon, VA, in press.
- Greenbaum E, Lee JW, Tevault CV, Blankinship SL, Mets LJ, and Owens TG (1997a) Photosystem I measurement in mutants B4 and F8 of *C. reinhardtii*. *Science* 277: 167-168, *Nature*, in press.
- Greenbaum E, Lee JW, Tevault CV, Blankinship SL and Mets LJ (1995) CO₂ Fixation and photoevolution of H₂ and O₂ in a mutant of *Chlamydomonas* lacking Photosystem I. *Nature* 376: 438-441
- Herron HA and Mauzerall D. (1972) The development of photosynthesis in a greening mutant of *Chlorella* and an analysis of the light saturation curve. *Plant Physiol.* 50: 141-148
- Kaltwasser H, Stuart TS and Gaffron H (1969) Light-Dependent Hydrogen Evolution by *Scenedesmus*. *Planta* (Berlin) 89: 309-322.
- Lee JW, Tevault CV, Owens TG and Greenbaum E (1996) Oxygenic photoautotrophic growth without Photosystem I. *Science* 273: 364-367
- Lien S and San Pietro A (1975) An Inquiry into Biophotolysis of Water to Produce Hydrogen, NSF RANN report under grant GI 40253 to Indiana University
- Melis A, Neidhardt J, Baroli I, and Benemann, JR (1998) Maximizing photosynthetic productivity and light utilization in microalgae by minimizing the light-harvesting chlorophyll antenna size of the photosystems. These proceedings, in press
- Mitsui A, Miyachi S, San Pietro A and Tamura S, Eds. (1977) *Biological Solar Energy Production* (Academic Press, New York)
- Spruit CJP (1958) Simultaneous photoproduction of hydrogen and oxygen by *Chlorella*. *Mededel. Landbouwhogeschool* (Wageningen/Nederland) 58:1-17
- Stuart TS and Gaffron H (1972) The mechanism of hydrogen photoproduction by several algae. *Planta* (Berlin) 106: 91-100
- Stuart TS and Gaffron H (1971) The kinetics of hydrogen photoproduction by adapted *Scenedesmus*. *Planta* (Berlin) 100: 228-243

PRODUCTION OF HYDROGEN FROM BIOMASS BY PYROLYSIS/STEAM REFORMING

S. CZERNIK, R. FRENCH, C. FEIK, AND E. CHORNET
National Renewable Energy Laboratory
1617 Cole Boulevard, Golden, CO 80401

Keywords: biomass pyrolysis, bio-oil, steam reforming

INTRODUCTION

Hydrogen is the most environmentally friendly fuel that can be efficiently used for power generation. While burning or oxidising it generates steam as the only emission. At present, however, hydrogen is produced almost entirely from fossil fuels such as natural gas, naphtha, and inexpensive coal. In such a case, the same amount of CO₂ as that formed from combustion of those fuels is released during hydrogen production stage. Renewable biomass is an attractive alternative to fossil feedstocks because of essentially zero net CO₂ impact. Unfortunately, hydrogen content in biomass is only 6-6.5% compared to almost 25% in natural gas. For this reason, on a cost basis, producing hydrogen by the biomass gasification/water-gas shift process cannot compete with the well-developed technology for steam reforming of natural gas. However, an integrated process, in which biomass is partly used to produce more valuable materials or chemicals with only residual fractions utilised for generation of hydrogen, can be an economically viable option.

The proposed method, which was described earlier¹, combines two stages: fast pyrolysis of biomass to generate bio-oil and catalytic steam reforming of the bio-oil to hydrogen and carbon dioxide. This concept has several advantages over the traditional gasification/water-gas shift technology. First, bio-oil is much easier to transport than solid biomass and therefore, pyrolysis and reforming can be carried out at different locations to improve the economics. A second advantage is the potential production and recovery of higher value added co-products from bio-oil that could significantly impact the economics of the entire process. In this concept, the lignin-derived fraction would be separated from bio-oil and used as a phenol substitute in phenol-formaldehyde adhesives while the carbohydrate-derived fraction would be catalytically steam reformed to produce hydrogen. Assuming that the phenolic fraction could be sold for \$0.44/kg (approximately half of the price of phenol), the estimated cost of hydrogen from this conceptual process would be \$7.7/GJ², which is at the low end of the current selling prices.

In previous years we demonstrated, initially through micro-scale tests then in the bench-scale fixed-bed reactor experiments³ that bio-oil model compounds as well as its carbohydrate-derived fraction can be efficiently converted to hydrogen. Using commercial nickel catalysts the hydrogen yields obtained approached or exceeded 90% of those possible for stoichiometric conversion. The carbohydrate-derived bio-oil fraction contains a substantial amount of non-volatile compounds (sugars, oligomers) which tend to decompose thermally and carbonize before contacting the steam reforming catalyst. Even with the large excess of steam used, the carbonaceous deposits on the catalyst and in the reactor freeboard limited the reforming time to 3-4 hours. For this reason we decided to employ fluidized bed reactor configuration that should overcome at least some limitations of the fixed-bed unit. Even if carbonization of the oil cannot be avoided, still the bulk of the fluidizing catalyst would be in contact with the oil droplets fed to the reactor. Catalyst regeneration can be done by steam or carbon dioxide gasification of carbonaceous residues in a second fluidized bed reactor providing additional amounts of hydrogen.

EXPERIMENTAL

The bio-oil was generated from poplar wood using the NREL fast pyrolysis vortex reactor system⁴. The oil was comprised of 46.8% carbon, 7.4% hydrogen, and 45.8% oxygen with water content of 19%. It was separated into aqueous (carbohydrate-derived) and organic (lignin-derived) fractions by adding water to the oil at a weight ratio of 2:1. The aqueous fraction (55%

of the whole oil) contained 22.9% organics ($\text{CH}_{1.34}\text{O}_{0.81}$) and 77.1% water.

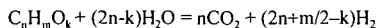
U91, a commercial nickel-based catalyst used for steam reforming of natural gas, was obtained from United Catalysts and ground to the particle size of 300-500 μ .

The aqueous solution was steam reformed using a bench-scale fluidized bed reactor shown in Figure 1. The two-inch-diameter inconel reactor supplied with a porous metal distribution plate was placed inside a three-zone electric furnace. The reactor contained 150-200g of commercial nickel-based catalyst from United Catalysts ground to the particle size of 300-500 μ . The catalyst was fluidized using superheated steam, which is also a reactant in the reforming process. Steam was generated in a boiler and superheated to 750 C before entering the reactor at a flow rate of 2-4 g/min. Liquids were fed at a rate of 4-5 g/min using a diaphragm pump. Specially designed injection nozzle supplied with a cooling jacket was used to spray liquids into the catalyst bed. The temperature in the injector was controlled by a coolant flow and maintained below the feed boiling point to prevent evaporation of volatile and deposition of nonvolatile components. The product collection line included a cyclone that captured fine catalyst particles and, possibly, char generated in the reactor and two heat exchangers to condense excess steam. The condensate was collected in a vessel whose weight was continuously monitored. The outlet gas flow rate was measured by a mass flow meter and by a dry test meter. The gas composition was analyzed every 5 minutes by a MTI gas chromatograph. The analysis provided concentrations of hydrogen, carbon monoxide, carbon dioxide, methane, ethylene, and nitrogen in the outlet gas stream as a function of time of the test. The temperatures in the system as well as the flows were recorded and controlled by the G2/OPTO data acquisition and control system.

The measurements allowed to determine total and elemental balances as well as to calculate the yield of hydrogen generated from the biomass-derived liquid feed.

RESULTS AND DISCUSSION

The overall steam reforming reaction of any oxygenated organic compound can be presented as follows:



Thus the maximum (stoichiometric) yield of hydrogen is $2+m/2n-k/n$ moles per mole of carbon in feed. The steam reforming experiments in the fluidized bed reactor were carried out at the temperature of 800°C and 850°C. The steam to carbon ratio was held at 7-9 while methane-equivalent gas hourly space velocity $G_{CH_4}HSV$ was in the range of 1200-1500 h^{-1} . At 800°C a slow decrease in the concentration of hydrogen and carbon dioxide and an increase of carbon monoxide and methane in the gas generated by steam reforming of the carbohydrate-derived oil fraction was observed. These changes resulted from a gradual loss of the catalyst activity, probably due to coke deposits. As a consequence of that, the yield of hydrogen produced from the oil fraction decreased from the initial value of 95% of stoichiometric (3.24 g of hydrogen from 100 g of feed) to 77% after 12 hours on stream. If a water-gas shift reactor followed the reformer the hydrogen yields would increase to 99% and 84% respectively. During eight hours of reforming at 850°C, the product gas composition remained constant, as presented in Figure 2. This indicates that no catalyst deactivation was observed throughout the run time. The yield of hydrogen produced from the bio-oil fraction was approximately 90% of that possible for stoichiometric conversion. It would be greater than 95% if carbon monoxide underwent the complete shift reaction with steam. Only small amounts of feed were collected as char in the cyclone and condensers, and little or no coke was deposited on the catalyst.

CONCLUSIONS

We successfully demonstrated that hydrogen could be efficiently produced by catalytic steam reforming carbohydrate-derived bio-oil fraction using a commercial nickel-based catalyst in a fluidized bed reactor. Greater steam excess than that used for natural gas reforming was necessary to minimize the formation of char and coke (or to gasify these carbonaceous solids) resulting from thermal decomposition of complex carbohydrate-derived compounds.

At 850°C with a steam to carbon ratio of 9 the hydrogen yield was 90% of that possible for stoichiometric conversion during eight hours of the catalyst on-stream time. This yield could be 5-7% greater if a secondary water-gas shift reactor followed the reformer.

Coke deposits were efficiently removed from the catalyst by steam and carbon dioxide gasification, which restored the initial catalytic activity.

ACKNOWLEDGMENTS

The authors are thankful to the U.S. Department of Energy Hydrogen Program, managed by Mr. Neil Rossmeyssl and Ms. Catherine Gregoire-Padró, for financial support of this work.

REFERENCES

1. D. Wang, S. Czernik, D. Montané, M. Mann, and E. Chornet, *I&EC Research*, 36 (1997) 1507.
2. M.K. Mann, P.L. Spath, K. Kadam, In *Proceedings of the 1996 U.S. DOE Hydrogen Program Review*, Miami, FL, May 1-2, 1996, NREL/CP-430-21968; pp. 249-272.
3. D. Wang, S. Czernik, and E. Chornet, *Energy&Fuels*, 12 (1998) 19.
4. J.W. Scahill, J. Diebold, C.J. Feik, In *Developments in Thermochemical Biomass Conversion*, A.V. Bridgwater and D.G.B. Boocock (eds.), Blackie Academic&Professional, London 1997, pp.253-266.

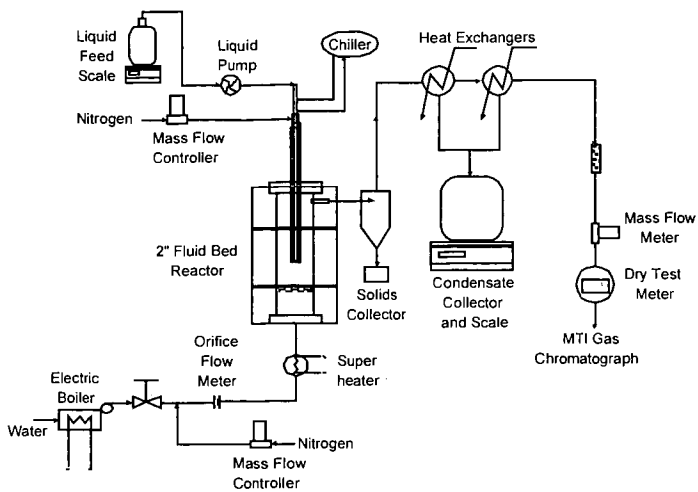


Figure 1. Schematic of the 2" fluidized bed reactor system

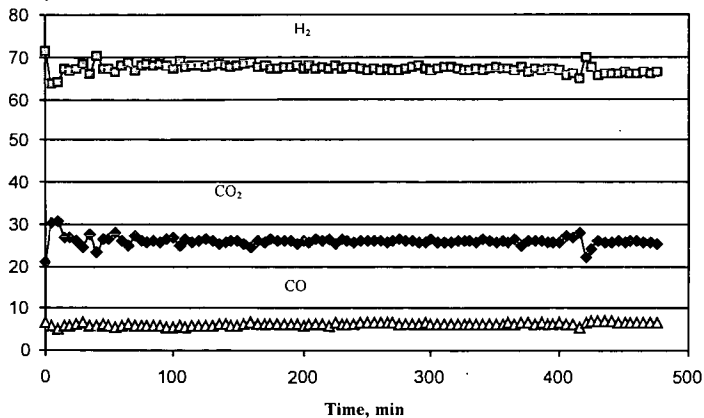


Figure 2. Reforming Gas Composition

DEVELOPMENT OF POROUS CERAMIC MEMBRANES FOR A SOLAR THERMAL WATER-SPLITTING REACTOR

Abraham Kogan

*Solar Research Facilities Unit, The Weizmann Institute of Science,
P.O. Box 26, Rehovot 76100, Israel*

The efficiency of hydrogen production by solar thermal water splitting (HSTWS) depends strongly on reactor temperature. The process must be conducted at least at about 2100 °C, in order to be of practical significance. Stabilized zirconia, with a maximum useful temperature of 2300 °C, is a suitable HSTWS reactor construction material. A crucial element in the solar thermal water-splitting reactor is the porous ceramic membrane that enables separation of hydrogen from the hot water splitting reaction products. Zirconia porous membranes are manufactured by powder sintering at about 1800 °C. When such a membrane is exposed in the solar reactor to a higher temperature, it loses its gas permeability due to pore closure by continued sintering. Efforts were made to inhibit the membrane sintering process and to postpone its fast occurrence to higher temperatures, by the use of special stabilized zirconia powders consisting of particles with a rounded shape. The fast sintering of membrane samples made of a homogeneous powder of relatively large spherical particles, prepared by the Sol-Gel method, occurred at some 200 °C above the normal zirconia sintering temperature. The overall picture gathered from our experiments suggests, however, that it will be hardly possible to bridge the temperature gap between the normal sintering temperature of stabilized zirconia and the HSTWS reactor temperature, by the use of stabilized zirconia powders of a particular morphology.

Keywords: solar hydrogen production; zirconia membranes; microspherical powder ceramics.

Introduction

Water vapor can be dissociated by exposure to a high temperature at reduced pressure. In the hydrogen production process by solar thermal water splitting (HSTWS), water vapor is heated by highly concentrated solar radiation and is partially dissociated. Hydrogen is separated from the hot mixture of water dissociation products by gas diffusion. Part of the gas mixture is extracted from the reactor cavity by diffusion through a porous ceramic membrane. It is enriched with hydrogen. The oxygen-enriched gas mixture leaves the reactor cavity bypassing the porous membrane (1).

The thermodynamic efficiency of a HSTWS reactor increases with increasing reactor temperature. The results of an extensive computer simulation study indicate that a temperature of at least 2100 °C must be maintained in the reactor, for the process to be of practical value (2). The inner structural components of the reactor can be manufactured from stabilized zirconia, a material that exhibits chemical, mechanical and thermal stability and fair thermal shock resistance up to 2300 °C. The porous ceramic membrane utilized for hydrogen separation by gas diffusion presents, however, a special problem. Porous ceramic membranes are obtained by sintering powders at a high temperature. Zirconia powders are sintered at 1700–1800 °C. When a porous zirconia membrane is subject to a temperature exceeding its normal sintering temperature, the sintering process continues resulting in loss of gas permeability, due to membrane densification and pore closure (1).

In an effort to develop zirconia porous membranes useful for our application, we tried to inhibit the sintering process and to postpone its fast occurrence to temperatures beyond the working temperature of the HSTWS reactor, by the use of special zirconia powders consisting of particles with a rounded shape. The results of this study are reported below.

Experimental Procedure and Results

Composition of Powders for Membrane Sample Preparation. The fast clogging of a porous zirconia membrane exposed to an elevated temperature is illustrated by the two SEM \times 500-magnification photographs of Figure 1. These photographs were taken after 2 h and 22 h of exposure to 1750 °C, respectively. The membrane sample shown in Figure 1 was made of a CaO-stabilized zirconia powder that was prepared by repeated pelletization, calcining at 1600 °C for 24 h, milling and collection of the relatively coarse particle powder.

Dr. R. Fischer, of the Israel Ceramics and Silicates Institute (ICSI), Haifa, Israel, suggested that the fast sintering of zirconia membranes, made of powders consisting of quasi-spherical or of spherical particles, would be hindered and delayed to higher temperatures. We solicited the collaboration of ICSI in the development of porous membranes characterized by improved stability with respect to pore closure at high temperature.

In order to determine the stabilized zirconia composition suitable for our purpose, ICSI prepared samples of zirconia powder doped with 5.6, 8 and 12% yttria. They were sintered at 1700 °C for 5 h. Subsequently, they were exposed in a solar furnace to 1900 °C for 1.5 h. The ZY-8 and ZY-12 ceramic samples preserved their original shape, whereas the ZY-5.6 sample disintegrated into powder. An XRD analysis of the heat-treated samples showed that the ZY-8 and ZY-12 ceramics were monophase tetragonal and cubic, respectively, while the ZY-5.6 ceramic underwent partial tetragonal-monoclinic phase transition. Obviously, phase transition is the cause of the sample destruction.

The ZY-8 composition was chosen as the basic material for the preparation of stabilized zirconia samples.

We obtained from ICSI two series of stabilized zirconia membranes for the experiment. One series consisted of samples made of spheroidal particle powders. The powders utilized in the preparation of the second series of samples consisted of homogeneous spherical particles obtained by the Sol-Gel method.

Membranes Made of Spheroidal Particle Powders. The particle-size range of powders used in the preparation of the first series of membrane samples is listed in Table 1. The samples were sintered at 1850 °C for 1 h. They were then fired at 1700 °C for 33.7 h in an electric furnace. All these samples were cracked after the firing.

The features of the membrane microstructure degradation, following the 1700 °C/33.7-h firing period, are depicted in Figures 2–4.

The SEM × 5000-magnification picture of a membrane particle (Figure 2a) was taken after a 1850 °C/1-h sintering. The particle consists of 1–5- μ m granules. After the additional firing at 1700 °C/33.7-h (Figure 2b), the big granules grew bigger by diffusion of material from smaller neighboring granules. The granule mean linear size grew more than twofold. Small cracks developed between adjacent granules. At the SEM × 500-magnification level (Figure 3a,b), it is observed that as a result of the prolonged additional firing, clusters of particles are formed by interparticle bridges. The clustering process implies apparently stress generation between neighboring clusters, which leads to initiation of fissures (Figure 3b). The SEM × 50-magnification picture (Figure 4) exhibits mature cracks across the sample.

Membranes Made of Spherical Particle Powders. The Sol-Gel process of ceramic powder production eliminates milling and granulation operations. This method enables production of free flowing powders consisting of homogeneous microspheres of a predetermined size. Low sinterability of these powders was expected, in view of their morphology.

In the second series of membrane samples, prepared at ICSI from 8% yttria-stabilized zirconia powders by the Sol-Gel method, the main variable was the diameter of the powder particle. Membrane samples were prepared from microspherical particle powders, the particle diameter varying at the range $25 \mu\text{m} \leq d \leq 50 \mu\text{m}$. The samples were sintered for 5 h at 1700–1750 °C. Then they were fired in the solar furnace at higher temperatures.

Table 1. Spheroidal Particle Powders

Powder designation	Particle morphology	Particle size (μm)
FZ1	Spheroidal	35–45 + submicron fines
FZ2	Spheroidal	95–110 (50%) + 15–30 (50%)
FZ3	Spheroidal	22–44 (no fines)
FZ4	Spheroidal	10–20 (no fines)
FZ1'	Spheroidal	As FZ1 – with a fraction at the 15–20 range
JZ1	Spheroidal – with improved sphericity	20–44
JZ3	Spheroidal – with improved sphericity	53–63
JZ2	Spheroidal – with improved sphericity	63–74
JZ2	Spheroidal – with improved sphericity	> 74
JZ4	Spheroidal – with improved sphericity	< 20
A3	Non-spherical	3

Figure 5a is a SEM $\times 500$ -magnification picture of a sample made of a powder of $d \leq 25\text{-}\mu\text{m}$ particles sintered at $1750\text{ }^\circ\text{C}$ for 5 h. After an additional treatment at $1900\text{ }^\circ\text{C}/1.5\text{ h} + 1980\text{ }^\circ\text{C}/1.5\text{ h}$, the porous structure of the sample was completely destroyed (Figure 5b). By contrast, another sample made from a $d \geq 50\text{-}\mu\text{m}$ powder emerged from the same heat treatment sequence with almost unchanged open porosity ($OP \approx 35\%$) (Figure 5c). A similar heat treatment "surviving" sample made of a $d = 35\text{-}\mu\text{m}$ powder was exposed to an additional $1750\text{ }^\circ\text{C}/33.7\text{-h}$ firing in an electric furnace. It still preserved its porous structure, but some of the microspherical particles were split (Figure 6).

Conclusions

Our attempts to develop porous membranes from stabilized zirconia that undergo fast sintering at temperatures much higher than the normal zirconia sintering temperature met only with partial success. With membrane samples made of a homogeneous powder of relatively large spherical particles, prepared by the Sol-Gel method, we were able to demonstrate considerable retardation ($\sim 200\text{ }^\circ\text{C}$) of membrane blocking up by sintering.

The overall picture gathered from our experience suggests, however, that it will be hardly possible to bridge the ca. $500\text{ }^\circ\text{C}$ gap between the normal sintering temperature of stabilized zirconia and the reactor operating temperature by powder doping or by the use of powders of special particle morphology.

Besides metal oxides, there are other refractory materials that melt and sinter at extremely high temperatures, as seen in Table 2. We were reluctant to consider the utilization of membranes made from these materials, because we foresaw that they would undergo chemical attack in the presence of the water splitting reaction products. When this issue was brought up during a discussion with Dr. P. Bardham, Head of the Cellular Ceramics Division at Corning Corporation, he observed that some of the above-mentioned materials, when exposed to HSTWS working conditions, might develop a thin protective layer that would prevent their disintegration by chemical attack.

Efforts will be made to obtain samples of such materials and test them at HSTWS reactor working conditions.

Table 2. Some High Melting Point Ceramics

Carbides	Melting point ($^\circ\text{C}$)	Borides	Melting point ($^\circ\text{C}$)	Nitrides	Melting point ($^\circ$)
TiC	3160	TiB	2980	TiN	2930
ZrC	3030	ZrB	3040	ZrN	2980
HfC	3890	HfB	3100	HfN	3310

Acknowledgment. This study was supported by the Heineman Foundation for Research, Education, Charitable and Scientific Purposes, Inc., Rochester, NY. The author gratefully acknowledges the generous support of the Foundation. Thanks are expressed to the staff of ICSI, who supplied the ceramic samples for the experiments.

References

- (1) Kogan, A. Direct solar thermal splitting of water and on-site separation of the products. II. Experimental feasibility study. *Int. J. Hydrogen Energy* **1998**, *23*, 89-98.
- (2) Kogan, A. Direct solar thermal splitting of water and on-site separation of the products. I. Theoretical evaluation of hydrogen yield. *Int. J. Hydrogen Energy* **1997**, *22*, 481-486.

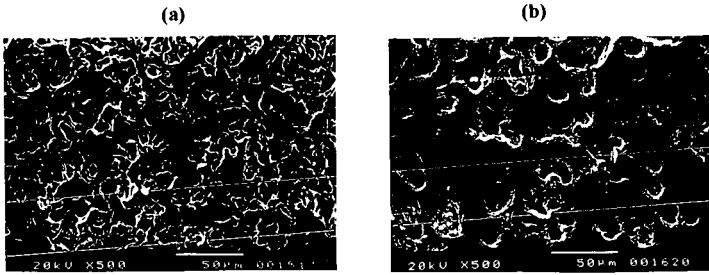


Figure 1. ZY-8-stabilized zirconia porous membrane from (-100/+325) powder. (a) After 1750 °C/2 h. (b) After 1750 °C/22 h.

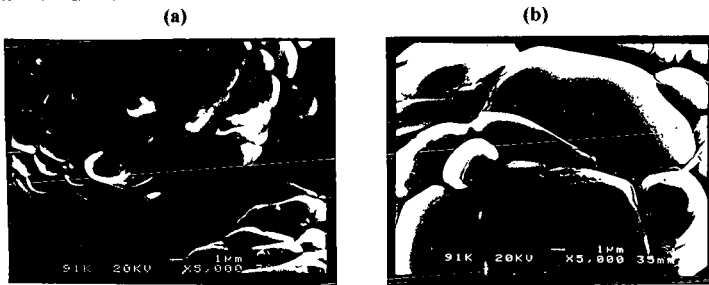


Figure 2. FZ1 + A3 membrane – SEM \times 5000. (a) After 1850 °C/1 h. (b) After 1850 °C/1 h + 1700 °C/33.7 h.

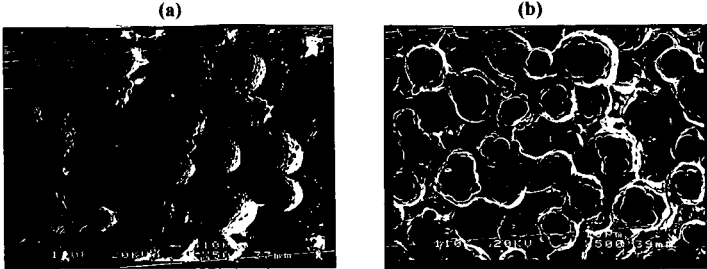


Figure 3. FZ1 + A3 membrane – SEM \times 500. (a) After 1850 °C/1 h. (b) After 1850 °C/1 h + 1700 °C/33.7 h.

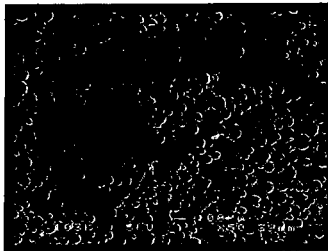


Figure 4. FZ2 + A3 membrane – SEM \times 50. After 1850 °C/1 h + 1700 °C/33.7 h.

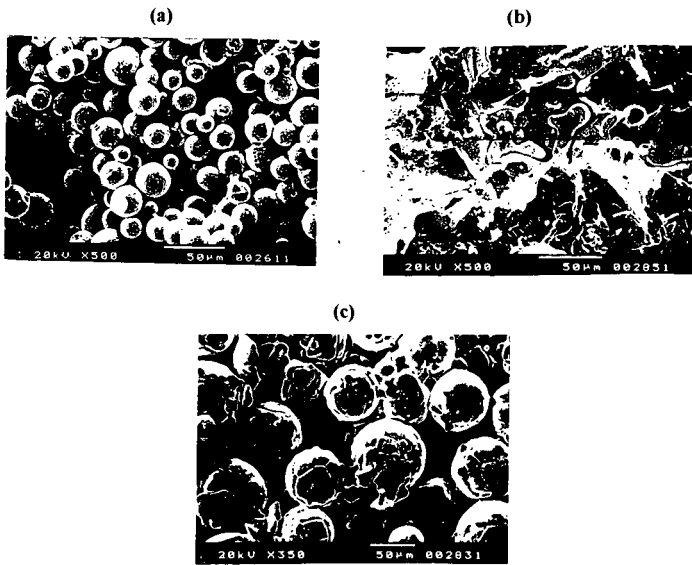


Figure 5. Membrane from Sol-Gel powder. (a) $d \leq 25 \mu\text{m}$ particles, 1750 °C/5 h. (b) $d \leq 25 \mu\text{m}$, 1750 °C/5h + 1900 °C/1.5 h + 1980 °C/1.5 h. (c) $d \geq 50 \mu\text{m}$, 1750 °C/5h + 1900 °C/1.5 h + 1980 °C/1.5 h.

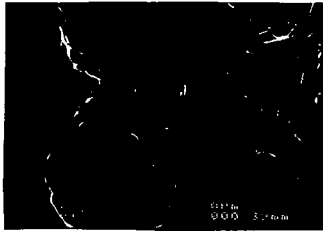


Figure 6. Membrane from Sol-Gel powder – $d = 35 \mu\text{m}$, 1750 °C/5 h + 1900 °C/1.5 h + 1980 °C/1.5 h + 1750 °C/33.7 h.

AN ULTRASAFE HYDROGEN GENERATOR:
AQUEOUS, ALKALINE BOROHYDRIDE SOLUTIONS AND Ru CATALYST

Steven C. Amendola, Stefanie L. Sharp-Goldman, M. Saleem Janjua,
Michael T. Kelly, Phillip J. Petillo, and Michael Binder

MILLENNIUM CELL LLC
8 Cedar Brook Drive
Cranbury NJ 08512
(732) 249-3250 ext 230
e-mail: steven @ amendola.com

ABSTRACT

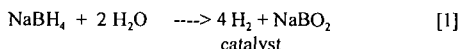
A novel, simple, convenient, and safe, chemical process generates high purity hydrogen gas on demand from stable, aqueous solutions of sodium borohydride, NaBH₄, and ruthenium based (Ru), catalyst. When NaBH₄ solution contacts Ru catalyst, it spontaneously hydrolyzes to form H₂ gas and sodium borate, a water-soluble, inert salt. When H₂ is no longer required, Ru is removed from the solution and H₂ generation stops. Since this H₂ generator is safer, has quicker response to H₂ demand, and is more efficient, than commonly used H₂ generators, it is ideal for portable applications.

INTRODUCTION

PEM fuel cells are attractive power sources for providing clean energy for transportation and personal electronics applications where low system weight and portability are important. For powering these systems, H₂ gas is the environmentally desirable anodic fuel of choice since only water is formed as a discharge product. A major hurdle is how to generate/store controlled amounts of H₂ fuel directly without resorting to high temperature reformers with significant heat signatures or bulky, pressurized cylinders.

Background of the Borohydride H₂ Generator

Our safe, portable H₂ generator overcomes these problems by using aqueous, alkaline, sodium borohydride (NaBH₄, tetrahydroborate) solutions which are extremely stable. However, as found by Schlesinger et al. (1), in the presence of selected metal (or metal boride) catalysts, this solution hydrolyzes to yield H₂ gas and water-soluble, sodium metaborate, NaBO₂.



This hydrolysis reaction occurs at different rates depending on the catalyst used and its preparation method. Levy et al. (2) and Kaufman and Sen (3) investigated cobalt and nickel borides as catalysts for practical, controlled generation of H₂ from NaBH₄ solutions. We studied ruthenium (Ru) based catalyst supported on ion exchange resin beads. Using Ru is based on the work of Brown and Brown (4), who investigated various metal salts and found that ruthenium and rhodium salts liberated H₂ most rapidly from borohydride solutions. We chose Ru because of its lower cost. Ru catalysts are not consumed during hydrolysis and are reusable. We have designed our system so that reaction [1] is either self-regulating or carefully controllable. To generate H₂, NaBH₄ solution is allowed to flow onto a Ru catalyst, or NaBH₄ solution is injected onto Ru catalyst. This ensures fast response to H₂ demand i.e. H₂ is generated only when NaBH₄ solution contacts Ru catalyst. When H₂ is no longer needed, NaBH₄ solution is removed from Ru catalyst and H₂ production ceases. With molecular weights of NaBH₄ (38) and 2 H₂O (36), forming 4H₂ (8), reaction [1] has a H₂ storage efficiency of 8/74 = 10.8%.

In addition to H₂, the other discharge product, NaBO₂, commonly found in laundry detergents, is safe. Unlike phosphates, borates are not environmentally hazardous in water supplies. Table 1 compares operational and safety features of generating H₂ via base-stabilized NaBH₄ solutions and via reactive chemical hydrides. Our generator is considerably safer/more efficient than producing H₂ via other reactive chemicals. The heat generated by our system (75 kJ/mole H₂ formed), is less than what is produced by other hydrides (>125 kJ/mole H₂), and ensures a safe, controllable chemical reaction.

The total amount of H₂ produced by reaction [1] depends on NaBH₄ solution volume and concentration. H₂ generation rates are primarily a function of Ru catalyst active surface area. H₂ pressure/flow rates can be accurately controlled and made self-regulating by numerous feedback

mechanisms. An added attribute of our generator is that generated H₂ gas also contains water vapor. Since prehumidified H₂ is needed in PEM fuel cells, NaBH₄ based H₂ generators should increase PEM fuel cell performance.

Experimental

Ru catalyst supported/dispersed on anionic exchange resin beads was prepared by ion exchange. Appropriate amounts of RuCl₃·3H₂O were dissolved in deionized water and acidified with HCl to convert RuCl₃ into [RuCl₄]⁻³. This H₃RuCl₆ solution was added to a weighed amount of anionic and cationic exchange resin beads which had been previously washed and dried at 50°C. The resulting slurry was allowed to stand at ambient temperature for 24 hours while stirring at regular intervals to maintain uniformity. The slurry was then dried by evaporation at 50°C. After drying, H₃RuCl₆, now impregnated in the resin, was reduced by addition of 20% NaBH₄, 15% NaOH, 65% H₂O solution. As prepared, our catalyst may be either metallic Ru or Ru boride of the form Ru₂B. The black, Ru coated resin beads were washed, dried, and separated with a 40 mesh sieve. Ru loadings were ~5% by weight.

In typical H₂ generation experiments ~30 ml of 20%NaBH₄ solution containing 10% NaOH was thermostated in a sealed flask fitted with an outlet tube for collecting evolved H₂ gas. Ru coated resin beads, were placed in a stainless steel screen container and dropped into the solution to begin H₂ generation. NaBH₄ solution could contact Ru catalyst through the screen, H₂ could exit, while lightweight resin beads were prevented from floating to the top of the solution. Although solutions were thermostated, temperatures near the catalyst were certainly higher due to the exothermic reaction. The outlet tube exhaust was placed under an inverted, water filled, graduated cylinder situated in a water-filled tank. Generated H₂ was measured by monitoring water displaced from the graduated cylinder as the reaction proceeded.

Results and Discussions

We evaluated anionic and cationic exchange resin beads as catalyst supports for Ru catalyst. Table 2. lists normalized H₂ generation rates for various ion exchange resin beads. Catalyst supports were evaluated based on their H₂ generation rates in liters H₂ generated/sec.-gram catalyst. This convenient standard meaningfully compares catalyst supports in our system because Ru catalyst performances are normalized with respect to catalyst weight. Table 2 illustrates that for catalytically generating H₂ from NaBH₄ solutions with ~5% Ru supported on ion exchange resins, anionic resins are better than cationic resins. A-26 and IRA-400 (Rohm and Haas) anion exchange resins when used as supports for Ru gave the highest H₂ generation rates.

Figure 1 plots H₂ volumes generated as a function of time for ~0.25 grams combined weight of Ru supported on IRA 400 anion exchange resin beads immersed in 20% NaBH₄, 10% NaOH, and 70% H₂O (wt %) solution at various temperatures. Volumes of H₂ generated by Ru catalyzed NaBH₄ hydrolysis increased linearly with time:

$$-4d[\text{NaBH}_4]/dt = d[\text{H}_2]/dt = k \quad [2]$$

Under our experimental conditions of relatively high [BH₄⁻] and low catalyst weights (and surface area), k is constant for a given temperature. This example of zero order kinetics implies that the first step in reaction [1] involves a surface reaction, most likely BH₄⁻ adsorption on Ru catalyst. We have observed zero order kinetics for NaBH₄ hydrolysis even at [NaBH₄] as low as 0.1%. Catalyzed NaBH₄ hydrolysis ultimately depends on NaBH₄. It would therefore not be surprising if diffusion controlled, first order kinetics dominates at very low [NaBH₄] and/or high catalyst weights where catalyst sites are not totally occupied. From the data in Fig. 1., an activation energy for Ru catalyzed hydrolysis of NaBH₄ (obtained by plotting log [H₂ generation rate] vs. reciprocal absolute temperature, 1/T), was computed to be 47 kJ mole⁻¹. This value compares with activation energies found (3) for NaBH₄ hydrolysis catalyzed with other metals: 75 kJ mole⁻¹ for Co, 71 kJ mole⁻¹ for Ni, and 63 kJ mole⁻¹ for Raney Ni.

As reaction [1] proceeds, NaBO₂ eventually exceeds its solubility limit and precipitates out of solution. We were concerned that this solid may block catalyst sites thereby affecting subsequent H₂ generation rates. To test this, 5 ml. of NaBH₄ solution was catalytically hydrolyzed to completion and the total generated H₂ measured. Although H₂ generation rates slowed as the reaction proceeded, nevertheless, >70% of the stoichiometric amount of H₂ was generated based on the amount of NaBH₄ in solution. This indicated that reaction [1] is quite efficient and that NaBO₂ precipitation at these concentrations/conditions does not seriously interfere with catalyst operation. If water generated by PEM fuel cells could be returned to NaBH₄ solutions, additional H₂ could be generated because NaBO₂ would remain in solution.

We can estimate achievable power levels from our H₂ generator. Assuming a standard PEM fuel cell operates at ~0.7V, generating 1 gram H₂/min is equivalent to 26.8 A-hr X 60 min/hr X 0.7V X 1/min = 1125 watts, i.e. 1liter H₂/minute can power a 100W fuel cell. Since ~5% of the 0.25 grams of our total catalyst weight was active Ru, Figure 1 illustrates that our H₂ generator produced the equivalent of ~ 0.3kW per gram Ru catalyst at 25°C and ~ 2kW/gram Ru catalyst at 55°C! Greater H₂ generation rates (and power levels) are expected for higher Ru loadings.

Prototypes of our H₂ generator have been used to power a commercial 35 watt H₂/air PEM fuel cell. For applications requiring long-term operation, H₂/air PEM fuel cells together with a NaBH₄ H₂ generator is considerably more advantageous than using rechargeable batteries. Our NaBH₄ generator can be quickly refueled by simply filling the reservoir with fresh NaBH₄ solution (the Ru catalyst is reusable).

Conclusions

Stabilized NaBH₄ solutions are an effective source for producing H₂. Due to system simplicity (NaBH₄ solution simply contacts Ru to produce H₂), it can be used for numerous applications where H₂ gas is used e.g. PEM fuel cells. High H₂ generation rates have been achieved from NaBH₄ solutions with tiny amounts of Ru supported on anion exchange resins. Optimizing catalyst loading, supports, and [NaBH₄], will lead to greater H₂ generation rates.

Acknowledgements

We thank Mike Strizki of the NJ Department of Transportation for constant encouragement and many enlightening technical suggestions. Kudos to Martin M. Pollak and Jerome I. Feldman of GP Strategies Inc. for their unfailing enthusiasm and constant support throughout this effort. We are grateful to Andersen-Weinroth for their interest and continued support. This research was partially funded by the State of New Jersey Commission on Science and Technology.

References

1. H.I.Schlesinger, H.C.Brown, A.E.Finholt, J.R.Gilbreath, H.R.Hockstra and E.K. Hyde, "New Developments in the Chemistry of Diborane and the Borohydrides", Journal of the American Chemical Society, 75, 215 (1953).
2. A. Levy, J.B. Brown, and C.J. Lyons, "Catalyzed Hydrolysis of Sodium Borohydride", Industrial and Engineering Chemistry 52, 211(1960).
3. C.M. Kaufman and B. Sen, "Hydrogen Generation by Hydrolysis of Sodium Tetrahydroborate: Effects of Acids and Transition Metals and Their Salts", Journal of the Chemical Society, Dalton Trans. 307 (1985).
4. H.C. Brown and C.A. Brown, "New, Highly Active Metal Catalysts for the Hydrolysis of Borohydride", Journal of the American Chemical Society, 84,1493(1962).

Table 1. Comparison between generating H₂ by chemical hydrides and by aqueous borohydride solutions.

PARAMETERS	CONVENTIONAL CHEMICAL HYDRIDE	BOROHYDRIDE
System	Water dripping on solid hydride	Borohydride solution contacting catalyst
Theoretical H ₂ Storage	<10%	10.8%
H ₂ contaminants	Possibly CO and CO ₂ (from binders) Possibly SO ₂ or NO (from acids)	None expected
Heat generated	Excessive	Moderate
Components carried	Water and dry hydride	Borohydride solution and catalyst
What limits H ₂ generation rate?	Rate at which water drips on solid hydride	Surface area of catalyst
What determines total H ₂ produced?	Amount of solid hydride	Amount of borohydride solution
H ₂ source	Water +Solid	Solution + Catalyst
Is reactant moisture sensitive?	Yes	No
Technical roadblocks	Solids tend to cake. Binders are needed to hold solids together	?
If too much liquid enters cell	Violent reaction	Reaction rate is limited by catalyst surface area.

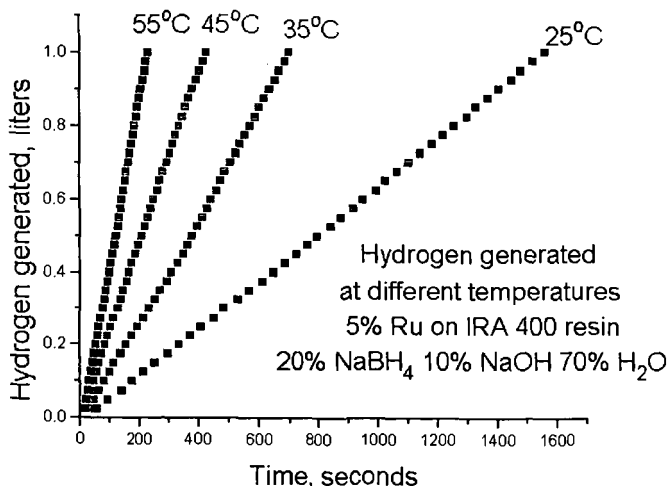
Table 2. Rate of H₂ generated catalytically per gram of catalyst (Ru + support resin) for various anionic and cationic support resins in 20% NaBH₄, 10% NaOH, 70% H₂O solution at 25°C. All catalysts had ~5% Ru loading.

Ru Resin Support	Time to generate 1 liter H ₂ gas (seconds)	Weight of Ru + support (grams)	Liters H ₂ /sec. per gram catalyst X 10 ³
ANIONIC RESINS			
A-26	1161	0.2563	336
A-26	633	0.5039	313
IRA-400	1173	0.2565	332
IRA-400	773	0.4116	314
IRA-900	1983	0.2555	197
Dowex 550A	672	0.7692	193
Dowex MSA-1	791	0.7691	164
Dowex MSA-2	1028	0.7691	126
A-36	1415	0.2550	111

CATIONIC RESINS

MSC-1B	2351	0.2592	164
Dowex HCR-W2	895	0.7631	146
MSC-1A	1382	0.5054	143
Amberlyst 15	2871	0.2563	136
Amberlyst 15	1324	0.5054	149
Dowex 22	1818	0.7678	72
Dowex 88	6163	0.2556	63

Figure 1. Volume of H₂ generated as a function of time by 5% Ru supported on IRA 400 anion exchange resin in 20% NaBH₄, 10% NaOH, 70% H₂O solution at various temperatures.



SUSTAINABLE HYDROGEN FOR THE HYDROGEN ECONOMY

Ronald W. Breault, Andrew W. M^cClaine,
Jonathan Rolfe, and Christopher Larsen
Thermo Power Corporation
Waltham, MA 02454-9046

INTRODUCTION

Hydrogen has immense potential as an efficient and environmentally-friendly energy carrier of the future. It can be used directly by fuel cells to produce electricity very efficiently (> 50%) and with zero emissions. Ultra-low emissions are also achievable when hydrogen is combusted with air to power an engine or to provide process heat, since the only pollutant produced, NO_x, is then more easily controlled. To realize this potential, however, cost-effective methods for producing, transporting, and storing hydrogen must be developed.

Thermo Power Corporation has developed a new approach for the production, transmission, and storage of hydrogen. In this approach, a chemical hydride slurry is used as the hydrogen carrier and storage media. The slurry protects the hydride from unanticipated contact with moisture in the air and makes the hydride pumpable. At the point of storage and use, a chemical hydride/water reaction is used to produce high-purity hydrogen. An essential feature of this approach is the recovery and recycle of the spent hydride at centralized processing plants, resulting in an overall low cost for hydrogen. This approach has two clear benefits: it greatly improves energy transmission and storage characteristics of hydrogen as a fuel, and it produces the hydrogen carrier efficiently and economically from a low-cost carbon source.

Our preliminary economic analysis of the process indicates that hydrogen can be produced for \$3.85 per million Btu, based on a carbon cost of \$1.42 per million Btu and a plant sized to serve a million cars per day. This compares to current costs of approximately \$9.00 per million Btu to produce hydrogen from \$3.00 per million Btu natural gas, and \$25 per million Btu to produce hydrogen by electrolysis from \$0.05 per Kwh electricity. The present standard for production of hydrogen from renewable energy is photovoltaic-electrolysis at \$100 to \$150 per million Btu.

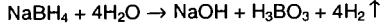
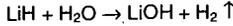
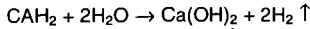
The overall objective of the current project is to investigate the technical feasibility and economic viability of the chemical hydride (CaH₂ or LiH) organic slurry approach for transmission and storage of hydrogen with analysis and laboratory-scale experiments, and to demonstrate the critical steps in the process with bench-scale equipment. Specific questions which have been addressed in work to date include:

- What is the formulation and physical properties of slurries that meet the energy density criteria?
- What are the organics that can be used to form the slurry?
- What are the conditions required for hydrogen generation?
- What are the properties of the slurry after hydrogen generation?
- What is the projected efficiency and cost of hydrogen production?

DISCUSSION

The way in which the metal hydride/water reaction would be used in a closed loop system for the storage and transmission of hydrogen is illustrated in Figure 1. The process consists of the following major steps: (1) slurring the metal hydride with a liquid carrier and transporting it to the point(s) of use, (2) generating hydrogen on demand from the metal hydride/liquid carrier slurry at the point of use by adding water and then transporting the resulting metal hydroxide/liquid slurry back to the hydride recycle plant, and (3) drying, separating, and recycling the metal hydroxide to the metal hydride at the centralized recycle plant and returning the liquid carrier for reuse.

A variety of metal hydrides react with water at ambient temperature to produce high purity hydrogen. Examples of reactions are:



The hydrogen generation capability of these hydrides when reacted with water is outstanding. For example, the volume of H_2 (STP) produced by complete hydrolysis of 1 kg (2.2 lb) of lithium hydride is 2800 liters (99 ft^3), and by 1 kg (2.2 lb) of lithium borohydride is 4100 liters (145 ft^3).

In Table 1, the energy density of these hydrides when reacted with water is presented and compared to gasoline, as well as the storage of H_2 as a liquid, gas, and a reversible hydride. The energy densities of the reactive hydrides are given on the basis of the initial hydride mass. The energy densities of the hydride/water reaction are respectable when compared to gasoline or methanol, with LiBH_4 having the highest energy densities on both a mass and volume basis. The heat of reaction must be removed during the H_2 generation.

The comparison is based on the energy densities of the initial hydride as a 50% slurry and the mass and volume of the storage container assuming a 20% void fraction in the container when the hydride is completely spent. The LiH , LiBH_4 , and NaBH_4 hydrides exceed the volumetric energy density goal by moderate factors (1.09 to 1.64). LiH and LiBH_4 exceed the gravimetric energy density goal by moderate factors (1.03 to 1.41), with CaH_2 slightly lower than the goal. It should be noted that energy density is not the only criterion that needs to be compared. Other factors such as cost and ease of handling must also be considered. In summary, several hydride/water reactions exceed the performance goals for both the volumetric and gravimetric energy densities. An additional feature is the ability to generate H_2 on demand and to control the rate of reaction by regulating the rate of water addition to the hydride bed. If desired, H_2 can also be generated at a high pressure for direct use in pressurized fuel cells without compression.

PRELIMINARY DESIGN OF HYDROXIDE REGENERATION SYSTEM

A preliminary design of the hydroxide to hydride regeneration system was conducted to identify process stream conditions and to allow the major equipment components to be sized such that a capital equipment cost could be developed. The system is shown in Figure 2. The analysis was conducted for both lithium hydroxide and calcium hydroxide regeneration.

The material and energy balances for the two metals were conducted for a plant supplying hydrogen to 250,000 cars. Such a plant would produce enough slurry to produce 13 tons of H_2 /hr. It would be small relative to typical chemical engineering projects, however. The first Fluid Catalytic Cracking (FCC) plant was three times larger and today's FCC plants are 25 times larger.

Lithium hydroxide is combined with carbon for the reduction and fuel, streams 1, 2a and 2b, to form stream 3, and is fed to the top of an indirect vertical heat exchanger, which preheats the incoming reactants while cooling the stream containing the lithium hydroxide, streams 5 and 6. The possibility for removing heat from the indirect fired process heater is also provided, streams 7 and 8. The hot preheated and partially reacted reactants, stream 4, enter the reduction reactor in which they are heated indirectly to the reaction temperature by combustion of the recycled carbon monoxide, stream 10, and additional fuel, stream 12, with preheated air, stream 11. The possibility of adding direct heat to the reactor is accomplished by adding oxygen to the reduction reactor by stream 9. The products of reduction leave the reduction reactor through stream 5. Within the reactant preheater, the lithium hydride is formed through the non-equilibrium kinetics as the mixture of lithium, hydrogen, and carbon monoxide is cooled. Additional heat is taken out of the product stream for the generation of electrical energy, which is added back into the reduction reactor to reduce the additional fuel.

The product, lithium hydride, is separated from the carbon monoxide in the hot cyclone, stream 16. This is further cooled to produce additional power, which is also added to the reduction reactor. The hot carbon monoxide, stream 15, is passed through a self recuperator to get a cold stream of CO, which could have a barrier filter installed to remove all the lithium hydride and a blower to circulate the CO, stream 18. This stream is reheated with the incoming CO and fed into the indirect process heater as discussed above. The hot combustion products leaving the solids preheater, stream 8, are used to preheat the combustion air and produce power, which is fed back into the reduction reactor. The energy efficiency of the hydrogen storage is obtained by dividing the heat of combustion of the hydrogen in the metal hydride by the heat of combustion of the carbon used for the reduction and the additional fuel. The results are: lithium (52.1%) and calcium (22.9%).

ECONOMICS OF THE APPROACH

The preliminary economics for the process are obtained by first developing a capital cost for the process equipment and then estimating the operating cost to define the needed sales price of the metal hydride for the required after tax return on the investment.

The capital equipment costs for the process are shown in Table 2 for the lithium process. These estimates, as well as the operating cost estimates, were obtained using standard chemical engineering practice. The operating cost assumptions are shown in Table 3.

The sensitivity of the cost of the hydride and the rate of return as a function of plant size and carbon cost is shown in Figures 3 and 4 for lithium. In Figure 3, the cost of hydrogen is plotted versus the plant size for four values of the cost of carbon. For a 250,000 car-per-day plant, the cost of hydrogen is on the order of \$3.61 per million Btu at a carbon cost of one-cent per pound and a fixed return on the investment of 15 percent. In Figure 4, the effect of plant size and carbon cost for a fixed hydrogen cost on the rate of return is shown. In this case, if the hydrogen can be sold for a value of \$4.57 per million Btu, the return to the investors can range from 15 to 65 percent, depending on plant size and carbon price. The same trends are seen for calcium.

SUMMARY AND FOLLOW ON ACTIVITIES

The results of the work to date are:

- Best Organic - Light Mineral Oil
- Best Hydrides -LiH & CaH₂
- +95% Hydrogen Release/Recovery
- Reaction rate controllable
- pH/Pressure Control
- Stable slurry
- Polymeric dispersants sterically stabilize the suspension
- Cost of Hydrogen \$2.75 to \$6.00 per 10⁶ Btu

REFERENCES

1. Block, D. and Melody, I, "Plans For A U.S. Renewable Hydrogen Program," Florida Solar Energy Center, Proceedings of 10th World Hydrogen Energy Conference, Cocoa Beach, FL, June 20-24, 1994.
2. Ulrich, "A Guide To Chemical Engineering Process Design And Economics," John Wiley & Sons, 1984.
3. Breault, Ronald W., Rolfe, J., and McClaine, A., "Hydrogen For The Hydrogen Economy," 24th Coal Utilization and Fuel Systems Conference, Clearwater, FL, March 8-11, 1999.

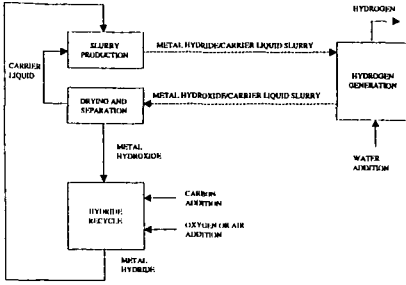


FIGURE 1. Simplified Process Diagram for Hydrogen Transmission/Storage With a Metal Hydride

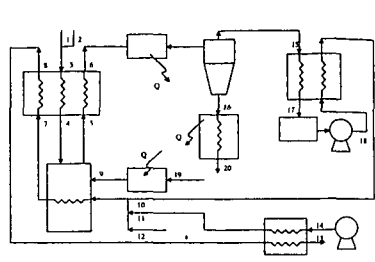


FIGURE 2. Hydroxide Regeneration System

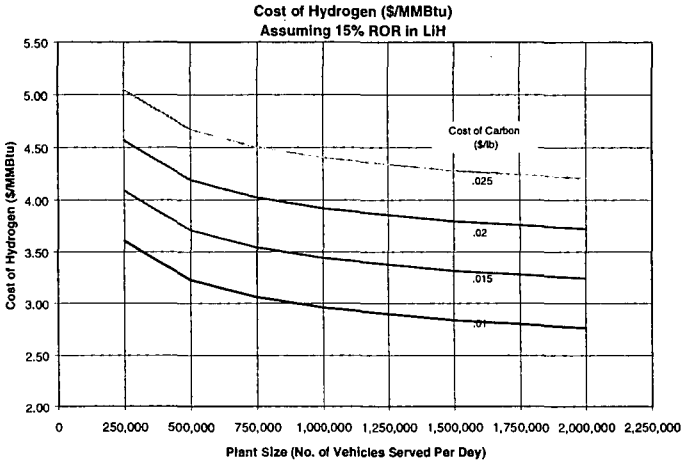


FIGURE 3. Sensitivity of Hydrogen Cost to Carbon Cost and Plant Size for Lithium Hydride

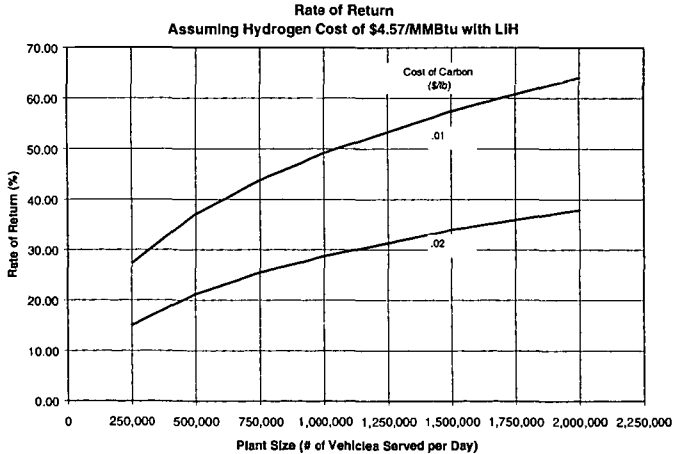


FIGURE 4. Sensitivity of Rate of Return to Carbon Cost and Plant Size for Lithium Hydride

TABLE 1. Comparison of Metal Hydrides to Other Hydrogen Storage Methods and Gasoline

Hydride	H ₂ Volume Per Mass Hydride (STP ft ³ /lb)	Energy Density		Water Reaction Enthalpy/HHV	Fraction Hydrolysis H ₂ (lb H ₂ per lb Hydride)	Hydride Density (gm/cm ³)
		HHV/Mass, Btu/lb	HHV/Bulk Volume (Btu/gallon)			
Ca H ₂ ⁽¹⁾	17.1	5,850	92,800	0.396	0.0958	1.90
Li H(1)	45.2	15,500	99,600	0.388	0.254	0.77
Li B H ₄ (1)	65.9	22,600	124,500	0.212	0.370	0.66
Na B H ₄ (1)	38.0	13,000	116,700	0.157	0.213	1.074
Fe Ti H(1.6)(2)	2.7	935	42,900	0.122(4)	0.0153	5.5
Liquid Hydrogen ⁽³⁾	—	61,100	35,650	—	—	0.07
Gaseous Hydrogen (5000 psia, 300 K)	—	61,100	15,574	—	—	0.03058
Gasoline	—	20,600	130,000	—	—	—

⁽¹⁾ Reaction with Water

⁽²⁾ Dissociation by Heating

⁽³⁾ Liquid Fuel

⁽⁴⁾ Based on Dissociation Energy

TABLE 2. Capital Cost - Lithium Hydride Regeneration

		Total cost
1	Furnace Cost, base 70m3	9,236,116
2	Solids preheater, 70 m3	9,236,116
3	Condensor, base 100MW	
4	Hydride Reactor, Base 35m3	720,417
5	Blower, H2 from sep.base, 75m3/s	270,254
6	Steam Turbine Generator	25,693,663
7	Cent Sturry sep.	189,413
8	Hydride cooler, base 70 m3	9,236,116
9	Heat Exch/recuperator, base 20e9J/s	2,814,328
10	Hydrocarbon Decomp, base 100MW	-
	Sum, Total Cost	57,396,424

TABLE 3. Operating Cost Assumptions

Carbon	Variable, \$0.67 to 1.67/10 ⁶ Btu
Fuel	\$2.5/10 ⁶ Btu
Labor	
-Operators	25 at \$35,000/yr
-Supervision & Clerical	15% of Operators
Operators	
Supervision & Clerical	
Maintenance & Repairs	5% of Capital
Overhead	50% of Total Labor and Maintenance
Local Tax	2% of Capital
Insurance	1% of Capital
G&A	25% of Overhead
Federal and State Tax	38% of Net Profit

NOVEL TECHNIQUE FOR THE PRODUCTION OF HYDROGEN USING PLASMA REACTORS

Christopher L. Gordon, Philip J. Howard, Lance L. Lobban, and Richard G. Mallinson
School of Chemical Engineering and Materials Science,
University of Oklahoma, Norman, OK 73019

ABSTRACT

Natural gas is one of the major sources of hydrogen via steam reforming. Alternate routes for the conversion of methane to more valuable products, such as higher hydrocarbons and hydrogen, have also drawn a lot of interest from researchers. Plasma reactors have been found to be an effective technique for the activation of methane at low temperatures. Cold plasmas can be generated by pulse streamer discharges (corona discharges) or by micro-discharges on the dielectric surface (silent discharges). The electron discharges are capable of exciting and decomposing the feed gas molecules. The corona reactor consists of dc current, a point to plane geometry, and zeolite catalyst in the reaction zone. The feed gases consist of methane, hydrogen, and oxygen. Methane conversion and hydrogen selectivities of 55% and 75%, respectively, have been found over X zeolite, and 20% and 70%, respectively, at high throughputs over Y zeolite with residence times on the order of seconds. Power consumption as low as 20 eV/converted CH₄ molecule has been achieved.

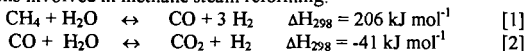
INTRODUCTION

With large increases in proven natural gas reserves worldwide, it can be expected that natural gas will play an increasingly important role in energy and chemicals supplies in the 21st century. The production of hydrogen from natural gas has also received more attention. Catalytic steam or CO₂ reforming of methane, the principal component of natural gas, is the principal process for the hydrogen production. About 50% of all hydrogen is produced from natural gas, and 40% of this is produced by steam reforming (1). A recent review by Armor (2) presents an excellent summary of the issues of hydrogen production by both conventional and potential technologies. While hydrogen production from fossil sources produce CO₂, methane has a significantly lower CO₂ impact than other fossil sources, see Table 1.

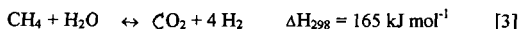
Table 1. CO₂ co-production with fossil hydrogen sources (3).

CO ₂ /H ₂	Hydrogen Source Technology
0.25	Methane steam reforming
0.31	Pentane steam reforming
0.33	Partial oxidation of methane
0.59	Partial oxidation of heavy oil
1.0	Partial oxidation of coal

Hydrogen is an important feedstock for the synthesis of ammonia, methanol, hydrochloric acid and so on. Hydrogen should become the ultimate non-polluting fuel, although it appears that it will be produced initially from fossil sources, and methane is the best source. There are two reversible reactions involved in methane steam reforming:



The overall reaction is:



Methane steam reforming is thermodynamically favorable at high temperatures (the operating temperature is usually higher than 800°C) and low pressure. An intensive energy input is required due to the high temperature operation, and the endothermic nature of the reaction requires extremely large heat fluxes. While this is the primary commercial process, the

constraints make the process relatively expensive and economically attractive only on a very large scale (a characteristic of all processes which operate at extreme temperatures due in significant part to the over-riding need to maximize energy efficiency).

To drive these reactions at much lower gas temperatures, a cold or non-equilibrium plasma can be used (4). The cold plasma is characterized by high electron temperatures and low bulk gas temperatures (as low as room temperature). Therefore, gas heating is not a significant energy sink with cold plasmas. For an electrically driven system, the energy converted to heat should be minimized since this is a relatively inefficient heating method. Additionally, the advantage of small thermal masses and small temperature gradients directly impact the economy of scale of the process. While the low temperature system may not significantly increase efficiency with increases in scale size, it may potentially operate economically at much smaller scales than for high temperature systems. We have previously reported the methane conversion to higher hydrocarbons via corona discharge (5,6) and plasma catalytic conversion (7-9). We have found that the corona discharge is an efficient and effective technique for the low gas temperature (as low as 40°C) methane conversion.

These systems exhibit non-equilibrium behavior, allowing production of substantial yields of C₂ hydrocarbons at very low temperatures. Hydrogen is a substantial co-product formed from both methane coupling and product dehydrogenation. Water is formed in only small quantities. Oxidative conditions, in both the dc system and also in ac systems, also produce substantial hydrogen yields with significant CO formation. CO₂ formation can vary, but generally CO₂ is a minor product. C₂ products may still be formed, but in lower quantities. Work to this point in time has focused on the production of hydrocarbon or oxygenate products and not on maximization of hydrogen production.

EXPERIMENTAL

The experimental apparatus will be essentially the same as has been previously described (5-9). The reactor is a quartz tube or quartz lined stainless tube. The reactor is heated (when needed) by a cylindrical furnace placed around the reactor. An Omega K-type thermocouple is attached to the outside wall of the reactor to monitor and control the gas reaction temperature. The temperature measured in this way has been calibrated against the internal temperature, and has been discussed elsewhere (5,6). When a low gas temperature is employed for the gas discharge reactions, the reactor is cooled outside by flowing room air. For the low temperature reactions (less than 100°C), the gas discharge is usually initiated at room temperature. Then the gas will be self-heated by the plasma. The gas temperature can be controlled by adjusting the flow rate of the flowing room air outside the reactor. The flow rates of feed gases methane, hydrogen, oxygen and helium are regulated by mass flow controllers (Porter Instrument Co. model 201). The gas from the reactor flows through a condenser to remove condensable liquid and is then analyzed by the chromatograph. A CARLE series 400 AGC (EG&G) was used for the detection of products. In some cases, a MKS mass spectrometer is used for on line analysis and for temperature programmed oxidation of carbon deposited on catalytic materials. Recovered liquids are analyzed off-line using a Varian GC with appropriate columns.

In the present reactor design, the plasma is generated in a gap between two stainless steel electrodes as diagrammed in Figure 1. The upper electrode, which may be a wire (generally dc) or a circular plate (generally ac) is centered axially within the reactor tube, while the lower electrode is a circular plate with holes for gas to flow through and positioned perpendicular to the reactor axis and a fixed distance below the top electrode. Catalyst beds (when used) are generally placed on the lower electrode, but placement below the lower electrode, outside of the discharge zone, is possible. The dc corona discharge is created using a high voltage power supply (Model 210-50R, Bertan Associates Inc.). The lower plate electrode is always held at a potential of zero volts (i.e., grounded). The ac power source consists of a primary AC power supply, transformer, wave generator, and an energy analyzer. An Elgar Model 251B power source supplies the primary AC power. A Wavetek Model 182A wave generator sends a sinusoidal wave signal at the selected frequency to the primary power supply. A midpoint grounded Magnetec Jefferson high voltage transformer supplies the secondary power to the reactor system. The secondary voltage is generally varied from 3.75 to 8.75 kV. An Elcontrol Microvip MK 1.2 energy analyzer measures primary power usage. The catalysts which will be used in some experiments is a NaY or NaX zeolite in a powder form (<80 mesh). The preparation and characterization of these zeolites has been discussed elsewhere (4-6). Other materials may be tried as well.

RESULTS

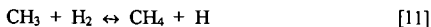
The previous investigations on oxidative conversion of methane by gas discharges in the absence (5,10) and/or presence (6-9) of heterogeneous catalysts have confirmed that cold plasma methane conversion proceeds via a free radical mechanism, where the formation of methyl radicals is the rate-controlling step. The oxygen used under those conditions will induce significant oxidation of methane and hydrocarbon products to produce carbon oxides (mostly carbon monoxide). The selectivity of higher hydrocarbons is thereby reduced. Methyl radicals also may be generated from reaction of methane with hydrogen radicals (10):



Hydrogen radicals are produced relatively easily within cold plasmas (11). One may supply hydrogen instead of oxygen for initiating higher hydrocarbon formation. It can be expected that a 100% selectivity of higher hydrocarbons will be achieved from methane and hydrogen plasma reactions except for possible carbon formation. In general, methyl radical formation is thought to be responsible for the initiation of radical reactions leading to higher hydrocarbon production. The methyl radical also can be formed by reaction of methane with other radicals (e.g., CH_3 , O, OH, and so on). In addition to the formation from radical reactions (e.g., reaction [8]), methyl radicals can be produced by electron-methane collisions (10). The hydrogen radical may also be an essential ingredient for the removal of undesired carbon deposition, which has a negative effect on gas discharges:



However, it has also been found that hydrogen appears to inhibit methane conversion in a discharge in the absence of a catalyst (12). The reason for this inhibition by hydrogen may be explained by the following reaction (5):



The inhibition was also observed during the plasma catalytic methane conversion over NaY zeolite.

The effects of hydrogen in the feed on methane conversion, Figure 2, and product selectivities, Figure 3, shows that the C_2 yield is higher than that achieved with plasma oxidative conversion of methane (7,8). The oxygen concentration is held constant at 2.5% while the ratio of methane and hydrogen is changed to achieve different partial pressures. It is also shown that the C_2 yield and methane conversion do not change significantly with the increasing hydrogen feed concentration. Most of the C_2 product is acetylene (more than 85%). Hydrogen yield is reduced and higher CO selectivity is observed with increasing hydrogen feed concentration in the presence of oxygen. This suggests that CO formation is not favored under conditions of higher hydrogen yield, and the higher hydrogen feed concentrations enhance CO formation.

Small amounts of oxygen added to the feed improve C_2 hydrocarbon production. The oxygen enrichment, Figure 4, in the gas feed reduces the C_2 selectivity but causes significant increases in methane conversion that more than offsets the loss of selectivities up to a maximum at about 2 percent oxygen. However, with very small amounts of oxygen, carbon deposition can cause deactivation of the reactions, Figure 4. The reason for the increase in the methane conversion with increasing oxygen partial pressure is that other active species are generated in addition to hydrogen radicals when oxygen is present in CH_4/H_2 plasmas. These new active species include O, oxygen anion and OH radicals. All of these strongly abstract hydrogen from methane. Hydrogen yield under the influence of added oxygen generally increases with increased oxygen in the feed.

Recent results from one experiment with a methane and oxygen (4/1) mixture and no diluent has shown that hydrogen, acetylene and CO are the major products in the dc system with catalyst. These results are shown in Figure 5.

CONCLUSIONS

Substantial hydrogen production has been observed as a by-product to methane conversion in low temperature plasmas. Various configurations and operating conditions have been used, including ac and dc power, with and without catalysts, under oxidative and non-oxidative conditions and at elevated pressures. The ability of a low temperature, and elevated pressure, process to efficiently produce hydrogen from methane holds significant promise for providing substantial increases in hydrogen utilization on shorter time frames and, perhaps most significantly, on smaller scales than may be achievable with thermal systems.

REFERENCES

1. Barbieri, G., and Di Maio, F.P., *Ind. Eng. Chem. Res.* **36**, 2121(1997).
2. Armor, J. N., *Applied Catalysis A: General*, **176**, 159(1999).
3. Scholz, W. H., *Gas Sep. Purif.*, **7**, 131 (1993).
4. Venugopalan, M., and Veprek, S., in "Topic in Current Chemistry: Plasma Chemistry IV." (Boschke, F.L. Ed.), p.1, Springer-Verlag, New York, 1983.
5. Liu, C-J., Marafee, A., Hill, B., Xu, G.-H., Mallinson, R., and Lobban, L., *Ind. Eng. Chem. Res.* **35**, 3295(1996).
6. Marafee, A., Liu, C-J., Hill, B., Xu, G-H., Mallinson, R., and Lobban, L., *Ind. Eng. Chem. Res.*, **36**, 632(1997).
7. Marafee, A., Liu, C., Xu, G., Mallinson, R. and Lobban, L., *Applied Catalysis A: General*, **164**, 21 (1997).
8. Liu, C-J, Mallinson, R. G. and L. L. Lobban, *Journal of Catalysis*, **179**, 326(1998).
9. Lobban, L., Liu, C.-J., and Mallinson, R., *Applied Catalysis A: General*, **178**, 17(1999).
10. Oumghar, A., Legrand, J.C., Diamy, A.M., and Turillon, N., *Plasma Chem. and Plasma Proc.* **15**, 87 (1995).
11. Hollahan, J.R., and Bell, A.T., "Techniques and Applications of Plasma Chemistry", John Wiley & Sons, New York, 1974.
12. Meshkova, G.I. and Eremin, E.N., *Russ. J. Phys. Chem.* **44**, 255(1970).

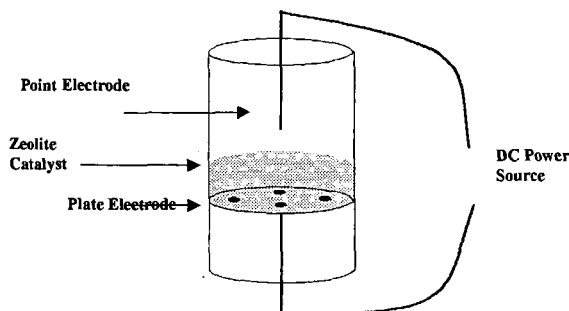


Figure 1. Point-plate dc Reactor Configuration with Catalyst Bed.

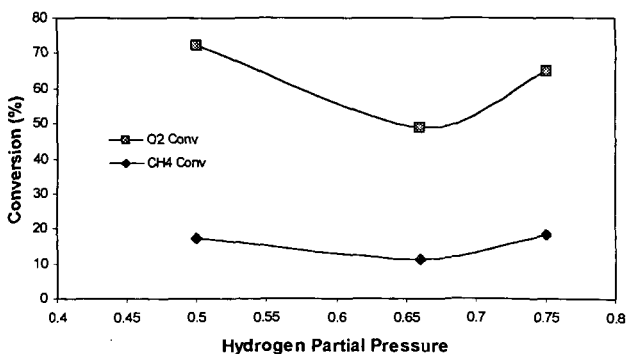


Figure 2. Methane Conversion at varying hydrogen partial pressures with constant oxygen concentration (2.5%) and balance methane, dc power over NaY Zeolite at 2 Bar.

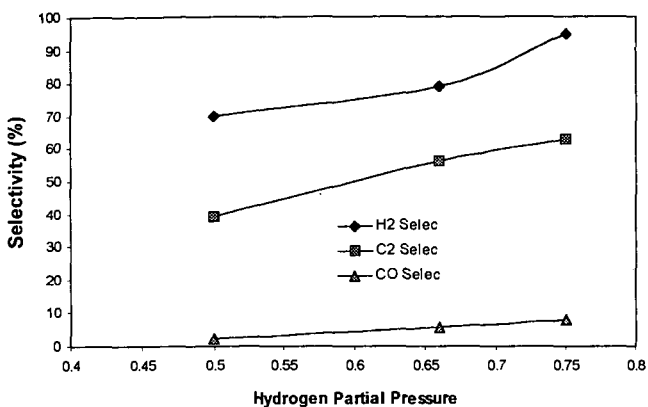


Figure 3. Product Selectivities at varying hydrogen partial pressures, dc Power over NaY Zeolite at 2 Bar.

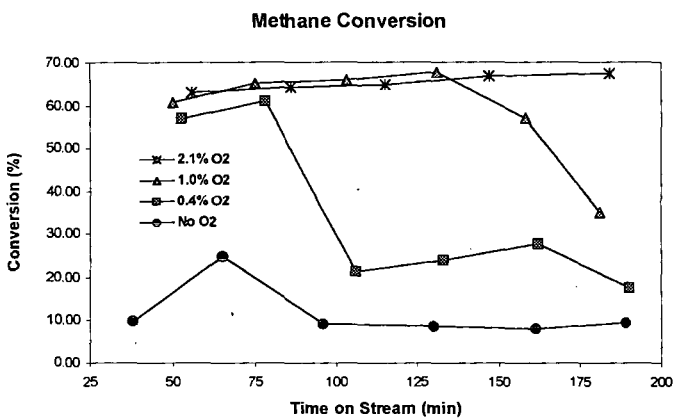


Figure 4. Methane Conversion vs. Reaction Time for Different O₂ Amounts.

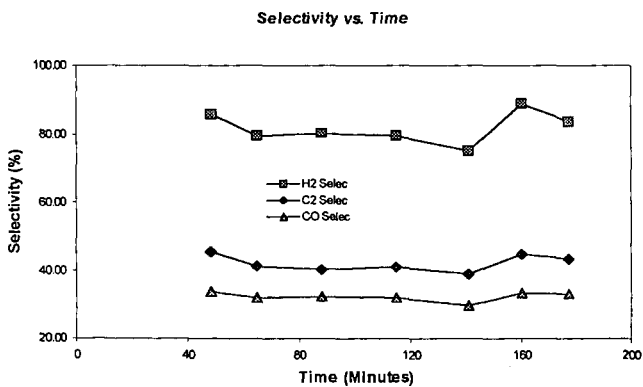


Figure 5. Product Selectivities for CH₄/O₂ = 4/1

TECHNOECONOMIC ANALYSIS OF HYDROGEN PRODUCTION FROM WESTERN COAL AUGMENTED WITH CO₂ SEQUESTRATION AND COALBED METHANE RECOVERY

Pamela Spath, Wade Amos
National Renewable Energy Laboratory
1617 Cole Blvd.
Golden, CO 80401
Harold Chambers, Diane Revay Madden, Denny Smith
Federal Energy Technology Center
P.O. Box 10940
Pittsburgh, PA 15236
Walter Shelton
EG&G Technical Services of West Virginia
3604 Collins Ferry Rd.
Morgantown, WV 26065

KEYWORDS: Hydrogen production, coal gasification, CO₂ sequestration

ABSTRACT

Hydrogen production via gasification of low sulfur western coal is being evaluated in a joint effort between the National Renewable Energy Laboratory (NREL) and the Federal Energy Technology Center (FETC). This work differs from past evaluations because it focuses on sequestering CO₂ and recovering coalbed methane. The off-gas stream, containing primarily CO₂, which is produced during hydrogen purification is used to displace methane from unmineable coalbeds. This methane is then utilized within the gasification-to-hydrogen system. Several processing schemes are being evaluated for maximizing hydrogen production or co-producing hydrogen and electricity. A combination of the following process steps are being used in these analyses: coal gasification, gas clean-up, shift conversion, hydrogen purification, hydrocarbon reforming, power generation, and hydrogen storage and transportation. The lowest cost storage and delivery method will be determined based on several factors including production rate, transport distance, and end use. A discussion of the cases being studied is presented.

INTRODUCTION

A collaborative effort to study the feasibility of producing hydrogen from low Btu western coal with an emphasis on CO₂ sequestration and coal bed methane recovery is being undertaken. The researchers at FETC are using their expertise in the field of coal gasification along with their existing models to examine coal gasification and gas clean-up. Because of extensive past technoeconomic analysis in the areas of hydrogen production, storage, and utilization NREL is examining the process steps associated with these operations using their previously developed models. Both parties are working to analyze CO₂ sequestration and coalbed methane recovery along with the possibility of power co-production. The models are being updated and integrated to incorporate the details of each system design as well as to account for the heat integration of the overall system.

COAL ANALYSIS

Wyodak coal was selected as a suitable coal that meets the needs of this study. This is a low rank Western coal that is inexpensive to produce and is available in an abundant supply. Additionally, the state regulations in Wyoming permit the extraction of coalbed methane making this site attractive for CO₂ sequestration and coalbed methane recovery. The elemental analysis and heating value of the Wyodak coal used in this work can be seen in the following table (EIA, 1995).

Table 1: Wyodak Coal Analysis

<u>Ultimate Analysis</u>	<u>(Weight %, dry basis)</u>
Carbon	67.6
Oxygen	17.7
Hydrogen	4.8
Nitrogen	1.2
Sulfur	0.8
Ash	7.9
Moisture, as-received (wt%)	26.6
Heat of combustion, HHV, as-received	20,073 J/g (8,630 Btu/lb)

GASIFIER TECHNOLOGY

The Destec gasifier which is a two-stage entrained, upflow gasifier is being used for this analysis. The gasifier is currently being demonstrated under FETC's Clean Coal Technology Program at the Wabash River Coal Gasification Repowering Project in West Terre Haute, Indiana. The gasifier operates at a temperature of 1,038 °C (1,900 °F) and a pressure of 2,841 k Pa (412 psia). For hydrogen production the gasifier must be oxygen blown in order to minimize the amount of nitrogen in the syngas. Nitrogen is a strongly adsorbed component in the pressure swing adsorption (PSA) unit and will reduce the hydrogen recovery rate even at low levels. The feed is a coal/water slurry containing 53 wt% solids. The following is the syngas composition exiting the gasifier:

Table 2: Syngas Composition

Component	N ₂	Ar	H ₂	CO	CO ₂	H ₂ O	CH ₄	H ₂ S	NH ₃	COS
mol %	0.6	0.7	27.7	27.4	16.5	26.6	0.0939	0.1399	0.2	0.0061
Heat of combustion, HHV, = 419 J/g (180 Btu/lb)										

From the composition listed in Table 2 it is apparent that reforming of the syngas for hydrogen production is not necessary because the gasifier produces only a trace amount of hydrocarbons. However, in order to maximize hydrogen production, one or more shift reactors will be needed to convert the carbon monoxide to hydrogen.

HYDROGEN PRODUCTION OPTIONS

Two options are currently being evaluated: Option 1 is maximum hydrogen production and Option 2 is co-production of hydrogen and power with the hydrogen being produced from the syngas and the power from recovered methane. See the simple block flow diagrams shown in Figures 1 and 2. The shaded blocks are the process steps that differ between the two options. Time permitting, other options for co-production of hydrogen and power will be tested in the future. In order to compare the economics as well as the overall CO₂ emissions from each option, the base case analysis will include only the process steps associated with coal gasification, shift, and hydrogen purification (i.e., none of the steps associated with CO₂ sequestration or coalbed methane recovery will be included in the base case). All of the options studied in this joint venture will be compared to this base case.

Figure 1: Option (1) - General block flow of maximum H₂ production

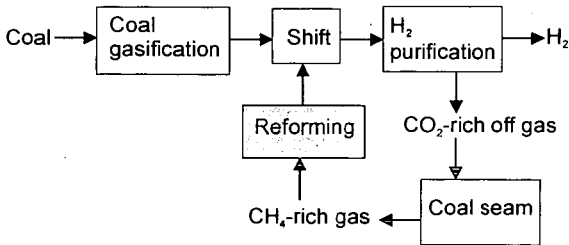
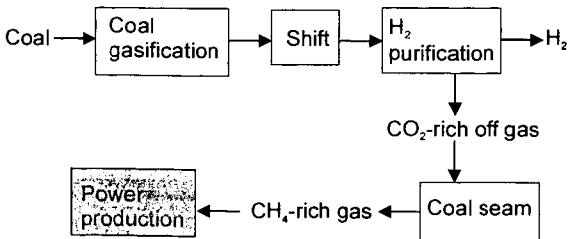


Figure 2: Option (2) - General block flow of H₂ Production from Syngas and Power Production from Recovered CH₄



HANDLING SULFUR IN THE SYNGAS

Because the syngas from the gasifier contains approximately 1,400 ppm of H_2S several schemes for handling the large sulfur concentration are being examined to determine which will be the most economical. Four potential schemes have been configured and are depicted in the drawings below (Figures 3 - 6). The dashed boxes contain the process steps which are different between the four schemes. Overall heat integration is not shown in these figures.

For the ZnO bed, the inlet H_2S concentration needs to be in the 10-20 ppm range. The high temperature shift (HTS) catalyst can tolerate concentrations up to 200 ppm but typically operates at lower levels whereas sulfur is a poison for the low temperature shift (LTS) catalyst and thus the H_2S needs to be reduced to a level below 0.1 ppm. Shift catalyst manufacturers produce a "dirty" shift catalyst which requires a sulfur concentration of at least 200 ppm in the inlet gas. Depending on the regulations for injecting sulfur into the ground, scheme 3 which does not remove the sulfur from the syngas, may not be a possibility. Also, note that there is not a scheme which incorporates the dirty shift catalyst with sulfur recovery via HGCU because HGCU would always be used prior to the shift reactors.

Figure 3: Sulfur scheme (1) - regular shift catalyst with hot gas clean up (HGCU)

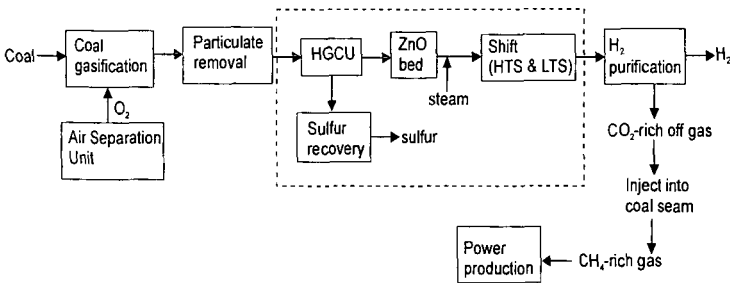


Figure 4: Sulfur scheme (2) - regular shift catalyst with cold gas clean up

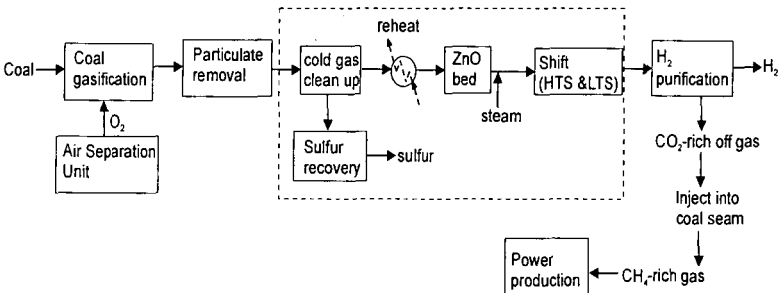


Figure 5: Sulfur scheme (3) - dirty shift catalyst with no sulfur recovery

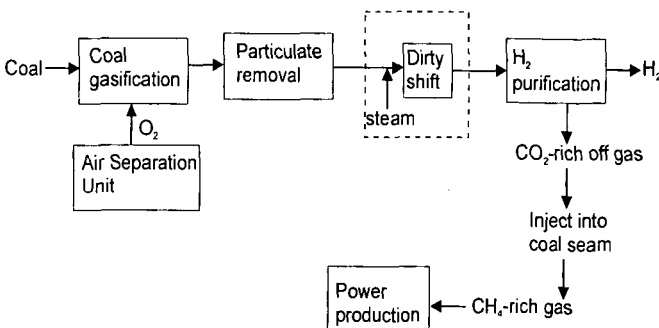
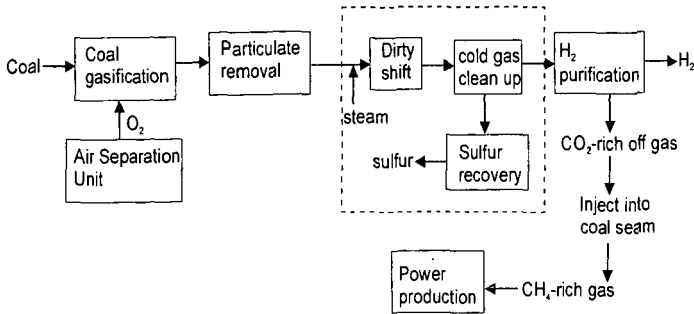


Figure 6: Sulfur scheme (4) - dirty shift catalyst with sulfur recovery via cold gas clean up



The coal gas leaving the gasifier contains entrained particles of char and ash. Particulate removal will be performed through cyclone separators and ceramic candle type hot-gas filters. Hydrogen purification will be done using a PSA unit. Because this unit operates at a pressure considerably lower than the coal seam, the off-gas must be compressed prior to injection.

CO₂ SEQUESTRATION AND CH₄ RECOVERY

Based on data from previous studies (Gunter *et al*, and Hendriks, 1994) this analysis assumes that two molecules of CO₂ are being injected for every one molecule of CH₄ released from the coalbed. This is based on worldwide data which shows that on average a little more than twice as much CO₂ can be stored in a methane field, on a volumetric basis, than the amount of CH₄ extracted. The off-gas from the hydrogen purification unit which contains primarily CO₂ (about 68 mol%) must be compressed from 2.7 MPa (392 psi) to a pressure of 3 - 14 MPa (500- 2,000 psi) which is the pressure range generally found in coalbed methane reservoirs (The American Association of Petroleum Geologists, 1994). Compressing the off-gas will require a significant amount of electricity. To adequately determine the overall reduction in CO₂ emissions for each option studied, the CO₂ emissions associated with electricity production must be added to the overall CO₂ balance of the system. Therefore, the net reduction in CO₂ will actually be less than the amount of CO₂ captured in the off-gas from the PSA unit. Additionally in the case of co-production of power, any CO₂ emitted during this process step must be included in the overall CO₂ balance to get a complete picture of the reduction in CO₂ emissions.

STORAGE AND TRANSPORTATION

In order to determine the effect of hydrogen storage and transport on the delivered cost of hydrogen, the following scenarios are being examined and incorporated into the analysis:

- (1) bulk delivery:
 - 16 km (10 mi) one-way
 - 160 km (100 mi) one-way
 - 1,610 km (1,000 mi) one-way
- (2) on site consumption: 12 hours of storage; no transport.
- (3) gas station supply: weekly hydrogen delivery; driving distance of 160 km (100 mi) round trip; supplying multiple stations along the way; hydrogen use of 263 kg/day (580 lb/day) per gas station.
- (4) pipeline: 3 km (5 mi) to the nearest pipeline infrastructure; no storage; an additional 160 km (100 mi) pipeline for hydrogen delivery to end user for which the cost is shared by 5 companies.

The cost of storing and transporting hydrogen depends on the amount of hydrogen the customer needs and how far their site is from the production facility. The most economical mode of storage and delivery (i.e., liquid, compressed gas, metal hydride or pipeline delivery) will also vary depending on production rate and distance. For example, while liquid hydrogen delivery is one of the cheapest methods of transporting hydrogen long distances, it requires a large capital investment for a liquefaction facility and there can be significant transfer losses during loading and unloading. This large capital investment at the production site, along with product losses, can make another method of delivery more cost effective.

The above cases represent four likely scenarios for hydrogen use. In each case, the cheapest delivery and storage method will be identified, along with the associated incremental cost that must be added to the production cost to get the total delivered cost of hydrogen. The technoeconomic analysis for this work will be completed this fall.

REFERENCES

1. Gunter, W.D; Gentzis, T.; Rottenfusser, B.A.; Richardson, R.J.H. (September 1996) "Deep Coalbed Methane in Alberta, Canada: A Fuel Resource with the Potential of Zero Greenhouse Gas Emissions." Proceedings of the Third International Conference on Carbon Dioxide Removal. Cambridge, Massachusetts.
2. Hendriks, C. (1994). *Carbon Dioxide Removal from Coal-Fired Power Plants*. Kluwer Academic Publishers. Dordrecht, Netherlands.
3. The American Association of Petroleum Geologists. (1994). Hydrocarbons from Coal. AAPG Studies in Geology #38. Tulsa, Oklahoma. Edited by Ben Lae and Dudley D. Rice.
4. Energy Information Administration. (February 1995) "Coal Data: A Reference." DOE/EIA-0064 (93).

ON PERSPECTIVES OF CO₂-FREE PRODUCTION OF HYDROGEN FROM HYDROCARBON FUELS FOR SMALL SCALE APPLICATIONS

Nazim Muradov
Florida Solar Energy Center,
1679 Clearlake Road, Cocoa, FL 32922

KEYWORDS: Hydrogen, Hydrocarbon, Pyrolysis

ABSTRACT

All conventional options of hydrogen production from fossil fuels, primarily, natural gas (e.g. steam reforming, partial oxidation) are complex, multi-stage processes that produce large quantities of CO₂. In general, there are two ways to solve CO₂ emissions problem:

a) sequestration of CO₂ produced by the conventional methods of hydrogen production, and
b) decomposition (thermal, thermocatalytic, plasmochemical) of hydrocarbon fuels into hydrogen and carbon. The capture of CO₂ from the process streams and its sequestration (underground or ocean disposal) is costly, energy intensive, and poses uncertain ecological consequences. The main objective of this work is to develop a viable process for CO₂-free production of hydrogen via one-step thermocatalytic decomposition of hydrocarbon fuels into hydrogen and carbon. This process could be the basis for the development of compact units for on-site production of hydrogen from hydrocarbon fuels (e.g. natural gas and gasoline) at gas refueling stations. The concept can also be used for a CO₂-free production of hydrogen for fuel cell applications (mobile and stationary).

INTRODUCTION

In the near- to medium-term future hydrogen production will continue to rely on fossil fuels, primarily, natural gas (NG). For decades, steam reforming (SR) of NG has been the most efficient and widely used process for the production of hydrogen. Other conventional processes for hydrogen production from fossil fuels: partial oxidation (PO), autothermal reforming (AR), steam-oxygen gasification of residual oil and coal) are more expensive than SR. The SR of NG process basically represents a catalytic conversion of methane (a major component of the hydrocarbon feedstock) and water (steam) to hydrogen and carbon oxides, and consists of three main steps: a) a synthesis gas generation, b) water-gas shift reaction, and c) gas purification (CO₂ removal). Four moles of hydrogen are produced in the reaction with half of it coming from the methane and another half from water. The energy requirement per mole of hydrogen produced for the overall process is equal to 40.8 kJ/mole H₂. To ensure a maximum conversion of CH₄ into the products, the process generally employs a steam/carbon ratio of 3-5, the process temperature of 800-900°C and pressure of 35 atm. A steam reformer fuel usage is a significant part (up to 30-40%) of the total NG usage of a typical hydrogen plant. There is no by-product credit (except for steam) for the process and, in the final analysis, it does not look environmentally benign due to large CO₂ emissions. The total CO₂ emission from SR process reaches up to 0.4 m³ per each m³ of hydrogen produced. Heavy residual oil and coal based hydrogen production processes result in the emission of enormous volumes of CO₂ (up to 0.8 m³ per m³ of H₂). Therefore, the problem of large scale production of hydrogen from fossil fuels and its utilization as a major energy carrier in the near future will be tied up with the development of effective, economical and environmentally acceptable ways of managing CO₂ emissions. In general, there are two ways to solve the problem of CO₂ emissions:

- Sequestration of CO₂ produced by the conventional methods of hydrogen production from fossil fuels, and
- Decomposition (thermal, thermocatalytic, plasmochemical) of hydrocarbon fuels into hydrogen and carbon

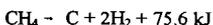
CARBON SEQUESTRATION

The main purpose of carbon sequestration is to keep CO₂ emissions from reaching the atmosphere by capturing and diverting them to secure storage. The perspectives of CO₂ capture and sequestration (ocean or underground disposal) is actively discussed in the literature [1-3]. The commercially available processes for CO₂ separation and capture include: physical and chemical absorption, physical and chemical adsorption, low temperature distillation and gas-separation membranes. It should be noted, however, that the capture, transportation and sequestration of CO₂ are energy intensive and costly processes. Thus, according to [3], the capture and disposal of CO₂ add about 25-30% to the cost of hydrogen produced by the SR of NG. The total electric energy consumption to pressurize CO₂ to 80 bar, transport it 100-500 km and inject it to the underground disposal site is estimated at approximately 2000 kJ/kg CO₂. World average for CO₂

emission associated with the electricity production is 0.153 kg of CO₂ per each kWh produced [2]. Thus, the amount of CO₂ produced as a result of the capture of CO₂ from the concentrated streams (after pressure swing adsorption, PSA, unit) of SR process and its sequestration reaches up to 0.1 kg per kg of sequestered CO₂. In principle, CO₂ can also be captured from the stack gases of the hydrogen plant (where it is presented in a highly diluted form) and sequestered, however, the energy cost of this operation would be very high. For example, it was estimated that the cost of eliminating CO₂ emissions from stack gases of advanced power generation plants range from \$35 to 264 per ton of CO₂ [4]. It was also estimated that the costs of CO₂ separation, capture, and compression to the required pressure would make up about three fourths of the total cost of ocean or geologic sequestration [5]. According to [6], the energy consumption associated with CO₂ recovery from the stack gases by hot K₂CO₃ solutions amounts to 3000 kJ/kg CO₂. In consequence, the total CO₂ emissions from CO₂ capture, transportation, and underground disposal could easily reach 0.25 kg CO₂ per kg of sequestered CO₂. Thus, CO₂ sequestration is an energy intensive process and, in the final analysis, does not completely eliminate CO₂ emission. In addition to this problem, some uncertainties remain regarding the duration and extent of CO₂ retention (underground or under the ocean) and its possible environmental effect.

THERMOCATALYTIC PYROLYSIS OF HYDROCARBON FUELS

Thermal (thermocatalytic) decomposition (pyrolysis) is the most radical way for a CO₂-free production of hydrogen from hydrocarbons, particularly, NG:



The energy requirement per mole of hydrogen produced from methane (37.8 kJ/mole H₂) is somewhat less than that for the SR process. The process is slightly endothermic so that less than 10% of the heat of methane combustion is needed to drive the process. The process is environmentally compatible, as it produces relatively small amounts of CO₂ (approximately 0.05 m³ per m³ of H₂ produced, if CH₄ is used as a fuel). It should be noted, however, that the process could potentially be completely CO₂-free if a relatively small part of hydrogen produced (approximately 14%) is used as a process fuel. In addition to hydrogen as a major product, the process produces a very important by-product: clean carbon. Currently, the total world production of carbon black is close to 6 mln tons per year, with prices varying in the range of hundreds to thousands dollars per ton, depending on the carbon quality [7]. The carbon black has a great market potential both in traditional (rubber industry, plastics, inks, etc.) and new areas.

Low pressure and high temperatures (up to 1400°C) are favorable for the complete thermal decomposition of methane. Attempts have been made to use catalysts to reduce the maximum temperature of the decomposition of various hydrocarbon fuels. In [8], for example, the authors used alumina, silica-alumina, silica-magnesia and other contacts at 800-1000°C for decomposition of NG and light hydrocarbons. The data on the catalytic decomposition of methane using Co, Cr, Ni, Fe, Pt, Pd and Rh-based catalysts have also been reported in the literature [9, 10]. In all cases, carbon produced was burned off the catalyst surface to regenerate its initial activity. In this regard, these processes display no significant advantages over the conventional processes (for example, SR) because of large CO₂ emissions.

The main objective of our work is to develop a thermocatalytic process for the simultaneous production of hydrogen and carbon from different hydrocarbon fuels (NG, liquid hydrocarbons) [11-13]. The use of carbon-based catalysts offers significant advantages over metal catalysts since there is no need for the separation of carbon from the catalyst surface: carbon produced builds up on the surface of the original carbon catalyst and can be continuously removed from the reactor (for example, using a fluidized bed reactor). There is a lack of information in the literature on the catalytic properties of various forms and modifications of carbon in methane decomposition reaction. We determined the catalytic activity of various carbon materials (graphite, carbon black, different types of activated carbon) for methane decomposition reaction over the range of temperatures from 700 to 900°C. It was found that the activated carbon produced from coconut shells displayed the highest initial activity among other forms of carbon, producing gas with hydrogen concentration up to 70-75%v at 850°C. In all cases, there were no methane decomposition products other than hydrogen and carbon and traces of ethane and ethylene detected in the effluent gas. Poor performance of the graphite and carbon black catalysts can be explained by the structure and size of carbon crystallites.

From the thermodynamic point of view the pyrolysis of liquid hydrocarbons is more favorable than the decomposition of methane, as almost 1.5-2 times less energy is required to produce a unit volume of hydrogen. We studied catalytic pyrolysis of a wide range of liquid hydrocarbons (pentane, hexane, octane, gasoline and diesel fuel) using different carbon-based catalysts. In the presence of activated carbon (coconut) the steady state pyrolysis of liquid hydrocarbons was achieved over period of approximately one hour. For example, gasoline pyrolysis over activated carbon (coconut) at 750°C produced gas consisting mainly of hydrogen (45-50 v.%) and methane (40-45 v.%) with relatively small fraction of C₂+ hydrocarbons (<10 v.%). The gas production rate reached 650 mL/min per mL/min of gasoline. In the case of diesel fuel the concentrations of hydrogen and methane in the effluent gas were in the range of 25-30 and 35-40 v.%, respectively (balance: C₂+ hydrocarbons).

COMPARATIVE ASSESSMENT OF DIFFERENT HYDROGEN PRODUCTION PROCESSES

Thermocatalytic pyrolysis (TP) of NG is a technologically simple one-step process without energy and material intensive gas separation stages, while SR is a multi-step and complex process. The techno-economic assessment showed that the cost of hydrogen produced by thermal decomposition of NG (\$58/1000 m³ H₂, with carbon credit), is somewhat lower than that for the SR process (\$67/1000 m³ H₂) [14].

The decomposition of methane can also be carried out plasmochemically. In a paper [7], the authors advocated a plasma-assisted decomposition of methane into hydrogen and carbon. It was estimated that up to 1.9 kWh of electrical energy is consumed per one normal cubic meter of hydrogen produced. Since almost 80% of the total world energy supply is based on fossil fuels [1], one can expect the electricity-driven hydrogen production processes to be among major CO₂ producers. A comparative assessment of the hydrogen production by SR, without and with CO₂ (after PSA unit) sequestration, electrolysis, plasmochemical decomposition (PD) and TP (with CH₄ and H₂ as a process fuel options) of NG is depicted on Figure. The comparison is based on two very important parameters, which reflect the energetic and ecological features of the processes. The first parameter (*En*) is equal to the total volume of NG consumed (both as a feedstock and a fuel) for the production of a unit volume of H₂ ($En = NG/H_2, m^3/m^3$). The second parameter (*Ec*) is equal to the total volume of CO₂ produced from both the feedstock and fuel usage of NG per a unit volume of H₂ produced ($Ec = CO_2/H_2, m^3/m^3$). Evidently, the lesser are both *En* and *Ec* parameters, the better is a hydrogen production process. For the sake of simplicity and comparability, it was assumed that NG was the primary fuel (at the power plant) for the water electrolysis and PD of NG. In fact, this assumption leads to rather conservative value for *Ec* parameter since NG share in total energy supply is only 19% and, what is more, NG produces 1.9 and 1.7 times less CO₂ (per kWh produced) than oil and coal, respectively [1]. The following conclusions can be extracted from Figure.

1. The processes with the large consumption of electric energy (water electrolysis, PD of NG) are characterized with the highest NG consumption and CO₂ emission per unit of hydrogen produced. It should be noted, however, that this conclusion is based on the world average energy production scenario, therefore, in countries with a large non-fossil fuel energy sector (hydroelectric, nuclear energy) both *En* and *Ec* parameters could be much lower.
2. SR with CO₂ capture (after PSA unit) and sequestration produces 30% less CO₂ emission than SR without CO₂ sequestration.
3. SR with CO₂ sequestration consumes 33% less NG than TP process, however, it produces 5 times more CO₂ emission.
4. TP of NG is the only fossil fuel based process which shows a real potential to be a completely CO₂-free hydrogen production process

SMALL SCALE HYDROGEN PRODUCTION UNITS

TP process does not include many material and energy intensive technological steps required by the conventional processes (SR, PO and AR), such as a two step water gas shift reaction, preferential oxidation, CO₂ removal, steam generation, etc. This is a significant advantage that TP holds over conventional processes, because it may potentially result in more simple, compact, and cost effective hydrogen production units. Based on our preliminary experimental data on gasoline pyrolysis, we project the volumetric power density of the TP-processor at approximately 0.8-1.0 kW_{th}/L. A comparative assessment of small scale hydrocarbon fuel processors based on SR, PO, PD and TP processes is presented in the Table.

There are several potential uses for the TP-based fuel processor (TPP):

1. The TPP can be used for on-site production of hydrogen at gas filling stations. TPP directly converts natural gas (or other hydrocarbon fuels) into methane-hydrogen blends, e.g. HYTHANE™ ($H_2:CH_4 = 30:70$ v.%(v.%) which can be used by ICE vehicles. Due to the flexibility of the TPP, it can produce different H_2-CH_4 mixtures in a single step, whereas, the conventional processes require 2 steps: initial production of hydrogen and then blending it with methane.
2. The TPP can be used in combination with fuel cells, for example, polymer electrolyte fuel cells (PEFC) for stationary applications (e.g. buildings, resort areas, etc.). It is known that PEFCs impose very stringent limitations on the level of CO impurity in the hydrogen feedstock ($[CO] < 100$ ppmv). TPP perfectly fits these requirements for it produces hydrogen that is completely free of carbon oxides.
3. The TPP can be combined with a PEFC for transportation applications. The TP process does not include bulky gas separation stages, and, therefore, leads to a compact fuel processor perfectly suited for on-board applications. On the other hand, mobile application of TPP is associated with the necessity for storing solid carbon on-board of a vehicle (approximately 3-8 kg per refueling, depending on feedstock).
4. Special CO_2 -sensitive applications (space, mines, medicine, etc.).

One of the major issues associated with the proposed technology is related to a byproduct carbon. The amount of carbon produced at average gas filling station is estimated at approximately 250 kg per day (based on HYTHANE™ production from NG). A 10 kW TPP/PEFC power system is expected to produce approximately 0.7 kg/h of clean carbon. Carbon produced can be conveniently collected by special trucks, stored at the central collector and sold at reasonable prices.

ACKNOWLEDGEMENTS

This work was supported by the U.S. Department of Energy and the Florida Solar Energy Center (University of Central Florida).

REFERENCES

1. Nakicenovic, N. *Energy Gases: The Methane Age and Beyond*; IIASA, Working Paper-93-033; Laxenburg, Austria, 1993; pp 1-23
2. Blok, K; Williams, R.; Katofsky, R.; Hendriks, C. *Energy* 1997, 22, 161-168
3. Audus, H.; Kaarstad, O.; Kowal, M. *Proceedings of 11th World Hydrogen Energy Conference*; Stuttgart, Germany, 1996; pp 525-534
4. International Energy Agency, *Carbon Dioxide Capture from Power Stations*, IEA, 1998
5. Herzog, H. *IV Intern. Conf. Greenhouse Gas Control Technologies*, Switzerland, 1998
6. Gritsenko, A. *Cleaning of Gases from Sulfurous Compounds*; Nedra: Moscow, 1985
7. Fulcheri, L.; Schwob, Y. *Int. J. Hydrogen Energy* 1995, 20, 197-202
8. Pohleny, J; Scott, N. *U. S. Patent No 3,284,161* (UOP), 1966.
9. Callahan, M. *Proc. 26th Power Sources Symposium*; Red Bank, N.J, 1974; 181
10. Pourier, M; Sapundzhiev, C. *Int. J. Hydrogen Energy* 1997, 22, 429-433
11. Muradov, N. *Int. J. Hydrogen Energy* 1993, 18, 211-215
12. Muradov, N. *Proceedings of 11th World Hydrogen Energy Conference*; Stuttgart, Germany, 1996; pp 697-702
13. Muradov, N. *Energy & Fuel* 1998, 12, 41-48
14. Steinberg, M.; Cheng, H. *Proceedings of the 7th World Hydrogen Energy Conference*; Moscow, USSR, 1988; p.699
15. Ogden, J.; Steinbugler, M.; Kreutz, T. *8th Annual U.S. Hydrogen Meeting*, Alexandria, VA, 1997, 469

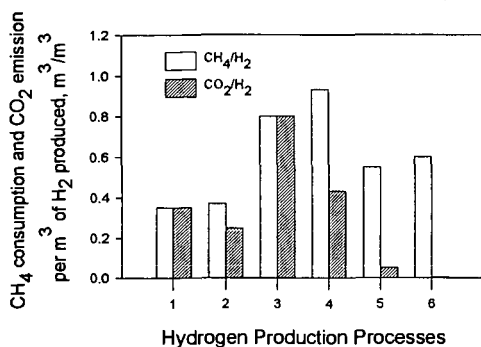


FIGURE. COMPARATIVE ASSESSMENT OF DIFFERENT HYDROGEN PRODUCTION PROCESSES:

1- SR, 2- SR with CO₂ sequestration, 3- electrolysis, 4- PD, 5- TP (CH₄- fuel), 6- TP (H₂- fuel)

TABLE. COMPARATIVE ASSESSMENT OF HYDROGEN PRODUCTION PROCESSES FOR SMALL SCALE APPLICATIONS

Process characteristics	Steam Reforming	Partial Oxidation	Plasmochem. Decompos.	Thermocatal. Pyrolysis
Capacity of small scale units, 10 ³ m ³ /h	0.1-5.9	0.02-4.0	2.0	N/A
Commercial availability	Yes	Yes	Yes	No
Number of steps	3	3	1	1
Maximum temperature, °C	850-900	1400	Plasma	800-900
Need for WGS and CO ₂ removal units	Yes	Yes	No	No
Special process requirements	Steam	Oxygen/Air	Electricity 1- 2 kWh per m ³ H ₂	None
Need for catalyst	Yes	No/Yes	No	Yes
Fuel flexibility	Low	High	Moderate	High
Tolerance to sulfur in a feedstock	Very low	High	Moderate	High
Useful byproduct	None	None	Carbon	Carbon
Efficiency, %	78.5	80	95	92.8 ¹⁾
Process CO ₂ emission ²⁾	High	High	None	None ³⁾
Power density, kW/L (kW/kg)	0.9 kW/kg ⁴⁾	0.9 kW/kg ⁵⁾	4 kW/L	0.8-1 kW/L ⁶⁾

- 1) - total efficiency with carbon as a byproduct;
 2) - does not include CO₂ generated at power plants
 3) - part of H₂ is used as a fuel
 4) - methanol steam reformer, [15]
 5) - PO of gasoline, [15]
 6) - based on our experimental data on TP of gasoline

FUEL PROCESSING OPTIONS FOR PROTON EXCHANGE MEMBRANE FUEL CELL SYSTEMS FOR MOBILE APPLICATIONS

R.A.J. Dams, P.R. Hayter, S.C. Moore
Wellman CJB Ltd.
Airport Service Road
Portsmouth
Hampshire PO 3 5 PG
United Kingdom

Keywords: Fuel Processing
Proton Exchange Membrane Fuel Cells
Mobile Transport Applications

INTRODUCTION

A fuel cell converts the chemical energy of a fuel directly to DC electricity and will do so continuously as long as a fuel (typically hydrogen or a hydrogen-rich gas) and oxidant (oxygen in air) are fed to it. Hydrogen can be provided in elemental form as a liquid or gas or can be derived by a chemical process from a suitable liquid feedstock such as an alcohol, liquid hydrocarbon or ether. Oxygen is normally available from ambient air or stored in elemental form in specialised applications.

Fuel cells are generally divided into two categories: low and high temperature. Low temperature fuel cells have as an electrolyte, either an acid (Phosphoric Acid - PAFC) or alkaline solution (Potassium Hydroxide - AFC) or a proton conducting membrane which is solid (PEMFC). In high temperature fuel cells, the electrolytes can be molten salts (Molten Carbonate - MCFC) or ion conducting ceramics (Solid Oxide - SOFC).

Of the fuel cell types, PEMFCs are most suitable for transport applications. Although PAFCs are closer to commercialisation, there is little room for major improvements in performance. Efforts are mainly concentrated on cost reduction through mass production. PEMFCs are still in the development phase and offer the possibility of improved performance and reduced costs in the near to middle future. High temperature fuel cells are still in the research and development phase and it will be some considerable time before they become a commercial proposition.

OPTIONS FOR SUPPLY OF HYDROGEN

Hydrogen can be supplied to a PEMFC stack in elemental form using a storage system or as a constituent of a gas stream resulting from the processing of a feedstock such as an alcohol, liquid hydrocarbon or ether. Whilst pure hydrogen produces a better performance from the fuel cell and eliminates the problems of poisoning, hydrogen storage techniques result in physically large systems and introduce logistic problems for refuelling. A number of techniques have been considered including compressed gas, liquid, hydride, glass microspheres, activated carbon and carbon nanofibres. All these techniques have drawbacks which prevent them from being an ideal solution, although the claims for carbon nanofibres, if substantiated could change this assessment.

As a consequence of this situation, much work has been done on fuel processing of alcohols, liquid hydrocarbons or ethers for transport applications. A fuel processor converts a suitable feedstock into a hydrogen-rich gas. The percentage of hydrogen is determined by the technique used. A number of fuel processing techniques have been evaluated for fuel cell applications. These include steam reforming, partial oxidation and autothermal reforming.

PROCESSING OF ALCOHOLS, HYDROCARBONS AND ETHERS

The fuel processor extracts hydrogen from a suitable feedstock. Much work has been done using alcohols such as methanol for transport applications. The

lack of a methanol infrastructure has caused a shift in the direction of liquid hydrocarbons such as gasoline, diesel RFG & LPG. Ethers, such as dimethylether have also been considered.

Carbon monoxide in the reformat feed to a PEMFC decreases the performance dramatically, but reversibly. The typical exit gas from a steam reforming fuel processor contains carbon monoxide at a concentration of 0.3% in approximately 75% hydrogen/25% carbon dioxide. A carbon monoxide concentration of less than 10 ppm is desirable and a concentration less than 2 ppm shows no effect on the performance of a PEMFC at all. Carbon dioxide acts mainly as an inert diluent. However, there is evidence that a certain amount of carbon dioxide is converted *in situ* to carbon monoxide with the consequent affect on performance. Much work has been done on combating the deleterious effect of carbon monoxide on the performance of PEMFC systems. A number of methods have emerged to achieve this:

1. the introduction of a bleed of air/oxygen into the reformat stream;
2. the introduction of a gas clean-up stage between the fuel processor and the anode side of the PEMFC stack;
3. the development of anode electrocatalysts containing ruthenium in addition to platinum to increase carbon monoxide tolerance.

These solutions, both singly and in combination, restore cell performance.

STEAM REFORMING

A hydrogen rich stream can be produced by the steam reforming of hydrocarbons, alcohols or ethers with or without the presence of a catalyst. The use of a catalyst results in lower temperatures and shorter reaction times. The objective of a catalytic steam reforming process is to liberate the maximum quantity of a hydrogen held in the water and feedstock fuel. Carbon in the feedstock is converted into carbon monoxide by oxidation with oxygen supplied in the steam. Hydrogen in the fuel, together with hydrogen in the steam, is released as free hydrogen. The reaction is endothermic. Practically, the reformed gas contains a large percentage of hydrogen, with carbon dioxide, carbon monoxide, methane and unreacted steam. In addition, prior to the reforming stage, it is necessary to remove traces of any components which will poison and deactivate the steam reforming catalyst or the fuel cell anode electrocatalyst. Therefore, as well as the reforming stage, the following steps may be required:

1. feed pre-treatment/desulphurisation;
2. pre-reforming (depending on the feedstock);
3. carbon monoxide conversion to carbon dioxide;
4. preferential oxidation or some other gas clean-up

In situations where low carbon monoxide levels are required, such as for fuel cells, carbon monoxide conversion is often achieved in two stages. The first step takes place as a high temperature shift stage (300-450°C) and the second as a low temperature shift stage (180 - 270°C). Because of the thermodynamics, gas leaving the low temperature shift will still contain a level of carbon monoxide greater than that acceptable for use in the fuel cell. A further stage of catalytic treatment is required to reduce the carbon monoxide level to less than 10 ppm

As an alternative to direct steam reforming, another process configuration which may be adopted is to include a stage of pre-reforming. This system consists of an adiabatic reactor containing a high activity catalyst. The outlet gas from this stage would have a high percentage of methane with other

negligible hydrocarbons present. Such a system operates at a lower temperature (400 - 500°C) than the direct reforming route and enables a lower overall steam to feed ratio to be used. Furthermore, as the gas leaving the pre-reformer is rich in methane, higher levels of preheat can be applied to the reformer feed without risk of cracking and carbon laydown.

PARTIAL OXIDATION REFORMING

Partial oxidation systems rely on the reaction of a hydrocarbon feedstock in a limited supply of oxygen or air to prevent complete oxidation. Traditionally it is carried out without the presence of a catalyst, although catalytic partial oxidation systems are being developed for fuel cell applications. The oxygen is supplied in air. Carbon in the fuel is converted into carbon monoxide whilst the hydrogen in the fuel is released as free hydrogen. The product gas now contains the residual nitrogen from air. Partial oxidation is an exothermic reaction and 17% of the (lower) heat of combustion of the gasoline is released. This raises the temperature of the product gases to approximately 870°C so no external heat source is required. Catalytic partial oxidation attempts to bring about the desired reaction with oxygen using a catalyst. This will enable a lower operating temperature to be used and hence reduce the oxygen consumption. The main difficulty in this area is the development of a durable catalyst which can promote the desired partial oxidation reaction whilst preventing other undesirable reactions from taking place.

AUTOTHERMAL REFORMING

Partial oxidation and steam reforming processes can be combined such that the exothermic partial oxidation reaction heat can be utilised by the endothermic steam reforming reaction. This system is known as autothermal reforming. The partial oxidation and steam reforming reactions can be carried out with or without a catalyst. The use of a catalyst is always accompanied by a potential catalyst poisoning problem by sulphur or lead components in the hydrocarbon or by carbon formation. There is little information in the literature about autothermal reforming of higher hydrocarbons. However, the Johnson-Matthey 'Hot-Spot™' technology has been developed to allow autothermal reforming of methanol. Unlike other autothermal reactors, which require complex heat exchange mechanisms between the exo and endothermic stages, the Hot-Spot™ reactor functions by catalysing steam reforming and partial oxidation on the same catalyst.

'CLEAN-UP' OF FUEL PROCESSING EXIT GAS

The more favoured methods of fuel processing, ie steam reforming, partial oxidation and autothermal reforming, require a further stage of gas processing or 'clean-up' due to the significant quantities of carbon monoxide produced during the processing reactions. The presence of carbon monoxide acts as a severe poison towards the platinum electrocatalyst in the PEMFC at its typical operating temperature of 80°C. Carbon monoxide preferentially adsorbs onto the catalyst surface and thus prevents the hydrogen adsorption necessary for the electrochemical reaction. Carbon monoxide concentrations above 10 ppm are known to cause substantial degradation in PEMFC performance. Ideally the concentration should be no more than 2 ppm. Therefore, it is necessary to include a further stage of gas clean-up prior to the fuel cell to reduce the carbon monoxide concentration to acceptable levels for introduction of the reformato into the cell. A number of processes are available for the removal of carbon monoxide from a gas stream:

1. chemical reduction;
2. membrane separation;
3. water gas shift;

4. chemical oxidation

Chemical reduction of carbon monoxide, ie methanation, is effected over a heterogeneous catalyst such as nickel on alumina at approximately 600°C. However, if large concentrations of carbon monoxide are present then due to the stoichiometry of the reaction there can be a substantial reduction in the hydrogen concentration of the fuel gas.

The use of silver palladium alloy membranes at the fuel processor exit can be used to produce ultra pure hydrogen for the fuel cell. The membrane allows the hydrogen to diffuse through its metallic crystal structure whilst remaining impermeable to the remaining gases produced by the reformation process. Although proven, the technology is at present expensive due to material costs. In addition, the thickness of the membranes (150 microns) necessitates the use of high pressure differentials for the production of acceptable hydrogen flow rates. High parasitic losses are, therefore, placed on the overall system. Research presently underway is focused on developing much thinner membranes (5-25 microns) supported on ceramics. Reductions in cost and operating pressures are, therefore expected without compromising the membrane strength.

The use of a heterogeneous catalyst such as copper/zinc oxide can be used to effect the water gas shift reaction. Since the catalysed reaction is carried out at approximately 200°C, thermal integration with the fuel processor may be possible. The utilisation of the reaction is advantageous since it can increase the hydrogen content of the processed fuel by 30-40%. However, reductions in carbon monoxide concentrations below 20 ppm are not practically possible and, as such, a further stage of gas clean-up is still required.

Finally, carbon monoxide may be selectively oxidised in the presence of hydrogen by air injection into the reformat over a suitable heterogeneous catalyst. Catalytic reactors to date have been used on either packed bed or monolithic designs. Noble metals such as platinum and rhodium (or mixtures of) are particularly active whilst copper based catalysts also show good activity for carbon monoxide oxidation. The reactor operating temperature for the selective oxidation is determined by the catalyst composition, with the reactors showing optimum activity and selectivity within a relatively small temperature range. Close thermal control of the exothermic reaction is therefore necessary to maximise the reaction efficiency.

PRACTICAL FUEL PROCESSING ON BOARD A VEHICLE

Major technical challenges for an integrated fuel processor and fuel cell for a vehicle are as follows:

- Start-up time
- Response to transients
- Methanol quality
- Catalyst deactivation
- Emissions
- Conversion efficiency
- Size
- Cost

It is perceived that for a fuel cell vehicle to be successful in the market place, it will have to perform at least as well as an internal combustion engine vehicle. This means that start up time and response to transient power demands are critical features. At the present time, fuel processors fall short of these goals. The lowest start up times from cold reported are typically several minutes. The quality of the feedstock has an effect on the rate of deactivation of the copper/zinc catalysts traditionally used for steam reforming. The emissions from a fuel cell vehicle with an onboard reformer will not be zero. However, nitrogen oxides and carbon monoxide emissions should be close to zero.

Hydrocarbons and particulate matter should be substantially reduced. There will be no sulphur emission. The emission goal for a fuel cell vehicle with an on-board fuel processor is the Super Ultra Low Emission Vehicle Limit set by California. Conversion efficiency of the feedstock should be as close to 100% as possible. Carryover of unreacted feedstock into a carbon monoxide selective oxidation system affects the performance resulting in an increase in carbon monoxide content of the exit gas. The system efficiency of a PEMFC system incorporating a reformer is predicted to be around 33%. Such a figure should be obtainable over a wide operating range. A reformer for use on-board a vehicle should be as small and light as possible, easy to manufacture using a simple design and cheap materials. The eventual cost target suggested by the motor industry is between \$30/45 per kW.

UNMIXED REFORMING: AN ADVANCED STEAM REFORMING PROCESS

Ravi V. Kumar, Jerald A. Cole and Richard K. Lyon
Energy and Environmental Research Corporation
18 Mason
Irvine, California 92618

ABSTRACT

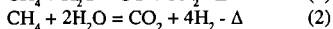
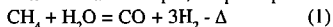
Unmixed Reforming is a novel steam reforming process to convert fossil fuels to hydrogen. It has been developed mainly for small scale generation of hydrogen. The target application is electric power generation in buildings and automobiles using fuel cells. The Unmixed Reforming process has been demonstrated in a packed bed reactor using diesel fuel and natural gas as the feedstock. The average purity of hydrogen in the product stream was around 70%, with the balance being primarily methane, carbon monoxide and carbon dioxide. In Unmixed Reforming, the catalyst is not deactivated by coke or sulfur. The coke is burnt off during a regeneration step. A significant portion of the sulfur is rejected as sulfur dioxide. The process has been simulated by performing chemical equilibrium calculations in different zones of the catalyst bed.

INTRODUCTION

There has been considerable increase in interest in fuel cells due to their higher efficiencies and environmental friendliness. Low temperature fuel cells are being considered for electric power generation in commercial and residential buildings and automobile applications. The low temperature fuel cells require a continuous supply of high-purity hydrogen.

Steam reforming is the most economical means of converting fossil fuels to hydrogen at large scales. Natural gas is principally used as the fossil fuel.

Using methane as an example, the principal reactions in the steam reformer are as follows:



The reforming reactions are highly endothermic and hence require that additional fuel be combusted to supply heat. Both the reforming reactions are equilibrium limited. The methane conversion is maximized by carrying out the reforming reactions at temperatures between 750 to 850°C. In the conventional steam reforming processor long tubes packed with catalyst are used to heat the reactants up to the required temperature. The tubes are contained in a gas-fired furnace.

The limitations of conventional steam reforming at small scales are two-fold—cost of reformer and efficiency (Adris et al., 1996). First consider the cost. The metal tubes are heated in a fired furnace. The metal wall of the tubes reaches temperatures of 900°C and the flue-gas reaches temperatures in excess of 1000°C. The tubes are made of high alloy nickel-chromium steel. The tubes are expensive and account for a large portion of the reformer cost. Second, the efficiency of reformer decreases at small scales due to heat transfer limitations and parasitic heat losses. The transfer of heat from the combustion products to the reactants is an inherently inefficient process, and in any practical system, especially for smaller scales, it is not possible to transfer all of the energy released by combustion into the process being heated.

If small scale hydrogen production is to be practical, the issues of cost and efficiency should be addressed. The Unmixed Reforming (UMR) process was developed to address these issues. UMR, like conventional reforming, can be used to generate hydrogen from a variety of liquid and gaseous fuels such as natural gas, landfill gas, propane, methanol, gasoline, diesel fuel, JP-8, etc.

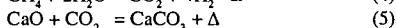
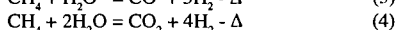
PROCESS DESCRIPTION

UMR relies on an EER-patented process (Lyon, 1996) known as Unmixed Combustion (UMC) to heat the packed bed. In the UMC process the combustion is carried out by alternately cycling air and fuel over a metal, in this case nickel, placed in a packed bed reactor. The metal is dispersed on a high surface area catalyst support. When air is passing over the bed, the nickel oxidizes to form nickel oxide in an highly exothermic reaction. Most of the heat is deposited on the ceramic matrix since there are no gaseous products for this oxidation reaction. The subsequent and separate introduction of a fuel will release additional energy while reducing the nickel oxide back to metallic nickel. The heat thus generated in-situ is then available for the endothermic steam reforming reactions. Nickel was chosen as the metal for UMC, since it is the most common catalyst for the steam reforming reactions. The UMR process was improved by introducing a carbon dioxide acceptor (e.g. calcium oxide) into the catalyst bed.

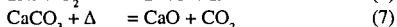
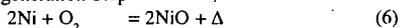
The three steps of the UMR process are shown in Figure 1. The figure portrays the progress of the reaction starting at the left of the figure and moving toward the right. The three steps are referred to as the reforming step, the air regeneration step and the fuel regeneration step. During the reforming step, fuel and steam react over the catalyst to produce hydrogen through conventional steam reforming chemistry. The calcium oxide is converted to calcium carbonate as it captures some of the carbon dioxide formed during the reforming reactions. This shifts the reforming reactions to higher conversions, thus improving the purity of the hydrogen product stream. During the next process step, air is passed through the packed-bed reactor to oxidize the catalyst. The heat released by the oxidation reaction raises the temperature of the bed. This decomposes the calcium carbonate to produce calcium oxide, while releasing carbon dioxide into a vent gas stream. In the final process step, fuel is introduced to the packed bed, reducing the oxide form of the catalyst back to its elemental form and further increasing the temperature.

The primary reactions that are occurring in the reactor are as follows:

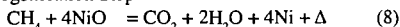
Reforming Step



Air Regeneration Step



Fuel Regeneration Step



The carbon dioxide acceptor material, calcium oxide, serves three functions in the process. First it provides additional "thermal mass" to transfer sensible heat from the regeneration step to the reforming step of the process. Second, the adsorption of carbon dioxide by the calcium oxide to produce calcium carbonate is an exothermic chemical reaction that also delivers energy to the reforming reactions in the form of chemical potential energy. During the air regeneration step, heat released by oxidation of nickel is largely absorbed by the process of decomposing the calcium carbonate to calcium oxide, and this substantially moderates the temperature rise of the packed bed. Much of the enthalpy of nickel oxidation is thereby stored as chemical potential energy in the calcium oxide. That chemical potential energy is subsequently released during the reforming process when calcium oxide is converted back to calcium carbonate. This method of using the interconversion between calcium oxide and calcium carbonate to supply heat to the reforming process, is a far more efficient means of transferring energy to the reforming process even than relying solely on the sensible heat stored in the ceramic catalyst support matrix. Furthermore, reducing the temperature rise during regeneration reduces parasitic heat losses from the reactor and promotes process efficiency. Finally, the presence of the solid-phase acceptor material improves the reaction equilibrium for reactions (1) and (2). By removing carbon dioxide from the products of the steam reforming process, equilibrium is shifted toward greater hydrogen production, reduced carbon monoxide and carbon dioxide concentrations, and increased fuel conversion.

Catalyst poisoning by carbon formation during reforming is not a problem, since any carbon formed is burnt off during the air regeneration step. UMR is also tolerant of fuel sulfur, which makes it a more robust process than conventional steam reforming. In conventional steam reforming sulfur must be removed from the feedstock fuel before it sees the catalyst, otherwise the catalyst is deactivated by the formation of nickel sulfide. In UMR, on the other hand, sulfur reacts with both nickel and calcium oxide during the reforming step, but is rejected as sulfur dioxide during the air regeneration step.

MATERIALS AND METHODS

The UMR process was studied in pilot scale and bench scale experimental systems. A simple schematic of the pilot scale system that was used to perform the experiments is shown in Figure 2. The pilot scale system consists of a dual packed bed reactor system. Switching valves are used to deliver steam and fuel, air and finally fuel to the packed bed for the three steps of the UMR process. The reactors are packed with a blended mixture of the catalyst and the carbon dioxide sorbent. The catalyst is Nickel supported on calcium aluminate and the carbon dioxide sorbent is dolomite. The particle sizes for the catalyst and dolomite are around 1 to 7 mm. A back pressure regulator is used to set the pressure in the reactor which in the reforming step is to 2-7 bar. The pressure during the regeneration step is around 1-2 bar. The reformat (reformer product) stream was analyzed using online infrared gas analyzers. The readings from the online analyzers were verified using gas chro-

matography with a thermal conductivity detector. The system was designed to produce 100 standard liters per minute of hydrogen, which is sufficient to generate 10kW of electricity using a Proton Exchange Membrane fuel cell. The bench scale system consisted of a single packed bed reactor.

The UMR process was simulated by modeling the packed bed reactor as a series of equilibrium reactors. The packed bed was divided into five zones. The reforming, air regeneration and fuel regeneration steps were subdivided into twenty, fifteen and five sub-steps respectively. The feed gas stream during each sub-step enters the first zone and reaches thermodynamic chemical equilibrium with the solid phase in the first zone. The gas leaving the first zone enters the second zone and reaches equilibrium with the solid phase in the second zone, and so forth. The equilibrium calculations were performed using a NASA Chemical equilibrium code (McBride and Gordon, 1996). The steam to fuel molar ratio during the reforming step was set to be three. The length of the time steps for the reforming, air regeneration and fuel regeneration steps were assumed to be 300, 225 and 75 seconds respectively. The model adjusts the fuel and steam flow rate during the reforming step to stabilize the maximum temperature during the UMR process to a preset value. A PID algorithm was used to adjust the fuel and steam flow rate. The flow rates for air and fuel during the regeneration steps were kept constant. The model was run for multiple cycles until steady state conditions were obtained.

RESULTS & DISCUSSION

Pilot plant experiments, using diesel fuel, have demonstrated product gas hydrogen concentrations typically averaging 70+ percent and as high as 85 percent under certain conditions, with the balance primarily CH_4 , CO and CO_2 . Figure 3 shows data collected over a one hour period of the pilot plant operation during which the average purity of hydrogen in the reformat stream was maintained at 70%. The reforming step was conducted for 300 seconds. The variation in the gas composition is a result of the cyclic UMR process. At the beginning of the reforming step the hydrogen concentration is low since the NiO in the bed is still being reduced to Ni by fuel. As the reforming step progresses the temperature of the packed bed decreases and as a result the methane concentration in the reformat stream increases and the carbon monoxide concentration decreases.

For low temperature fuel cells the concentration of CO needs to be reduced to 50 ppm, and hence a high H_2 to CO ratio is preferable in the reformat stream. The UMR process was able to generate a hydrogen product gas with an average H_2 to CO molar ratio in excess of 10. Competing technologies such as partial oxidation produce a reformat stream with H_2 to CO molar ratios ranging from less than 2 to about 3, while conventional steam reforming attains a ratio of about 5.

Bench scale experiments using diesel fuel have shown that for typical fuel sulfur concentrations there is no detectable sulfur in the product gases to at least the sub-ppm level. In the bench scale experiments, when sulfur was added to diesel fuel at a concentration of 2000 ppm by weight only 5 ppm H_2S was detected in the product gases. In pilot scale experiments using diesel fuel the sulfur concentration in the reformat stream was around 12 ppm.

Due to the manner in which fuel is oxidized in UMR, the byproduct exhaust gases contain no oxides of nitrogen, and the emissions of carbon monoxide are typically less than 10 ppm. Therefore, relative to conventional reforming, and when compared with most alternative hydrogen production processes, UMR is nearly pollution free.

The predicted UMR dry gas product composition using the theoretical model is shown in Figure 4, when methane is used as the fuel. The figure shows that the temperature of the gas leaving the bed decreases during the reforming step. The carbon monoxide concentration decreases as the temperature decreases. The model predicts that the methane concentration in the product gas is low (< 3%) and that the concentration of hydrogen in the product gas increases during the reforming step.

ACKNOWLEDGEMENTS

The authors would like to acknowledge the support of U.S. Defense Advanced Research Project Agency (contract #DAAH01-95-C-R162) and U.S. Department of Energy and Edison Technology Solutions (contract #DE-FC02-97EE50488).

REFERENCES

Adris, A.M., Pruden, B.B., Lim, C. J. and Grace, J.R., 1996, On the Reported Attempts to Radically Improve the Performance of the Steam Methane Reforming Reactor, Canadian J. Chem. Eng., 74, p177.

Lyon, R.K., 1996, Method and Apparatus for Unmixed Combustion as an Alternative to Fire. U.S. Patent No. 5,509,362.

McBride and Gordon, 1996, Computer Program for Calculation of Complex Chemical Equilibrium Compositions and Applications, NASA Reference Publication 1311.

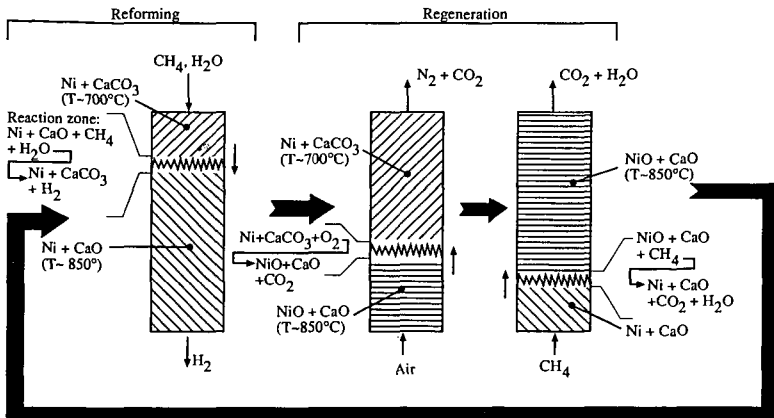


Figure 1. Illustration of the Unmixed Reforming process. The steam reforming of methane (left) produces hydrogen in an endothermic reaction which absorbs some of the sensible heat of the packed bed. Carbon dioxide, produced by the reforming reaction is absorbed by calcium oxide to form calcium carbonate. Once the calcium oxide is all consumed, the reactor must be both chemically and thermally regenerated using the unmixed combustion process as shown in the middle and right-side portions of the figure.

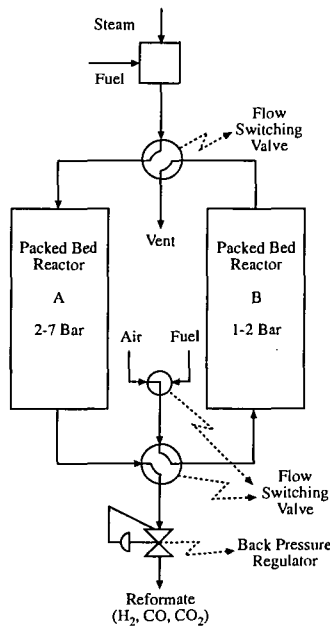


Figure 2. Schematic of experimental system.

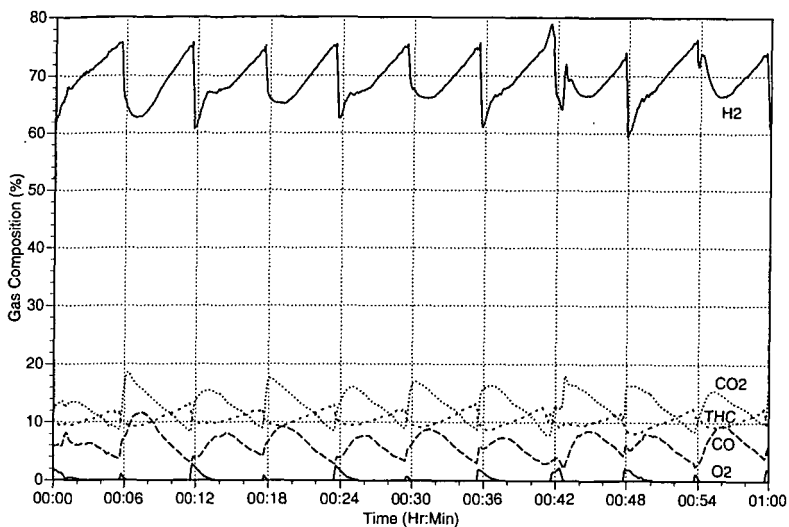


Figure 3. Experimental gas composition data from the Unmixed Reformer (THC - Total Hydro Carbon).

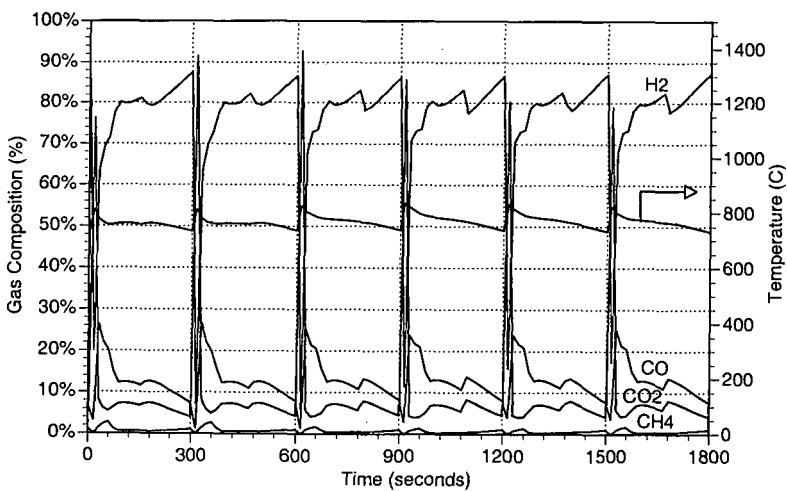


Figure 4. Predicted Unmixed Reformer gas composition using model.

FUEL-FLEXIBLE PARTIAL OXIDATION REFORMING OF HYDROCARBONS FOR AUTOMOTIVE APPLICATIONS

J. P. Kopasz, R. Wilkenhoener, S. Ahmed, J. D. Carter, and M. Krumpelt
Chemical Technology Division
Argonne National Laboratory
9700 South Cass Ave
Argonne, IL 60439

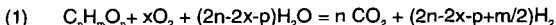
KEYWORDS partial oxidation, fuel-flexible reforming, hydrogen production

INTRODUCTION

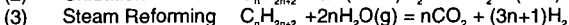
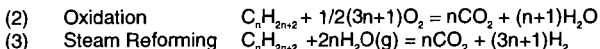
Research is underway to develop fuel cells for ultra-low-emission vehicles. However, automotive and petroleum companies have pointed out that the successful commercialization of fuel-cell-powered electric vehicles in the near future will depend, to a large extent, on the availability of a refueling infrastructure.¹ This infrastructure is completely lacking for hydrogen. To tap into the existing fuel infrastructure, fuel processors capable of converting liquid hydrocarbon fuels into hydrogen are required. Fuels of interest include gasoline, diesel, methanol, ethanol, and natural gas.

There is some debate about which hydrocarbon fuel is optimal for fuel cell systems. Methanol and ethanol are widely available commodity chemicals and have numerous advantages as fuel (easy to reform, water soluble, renewable, etc.). Gasoline and diesel have the advantage over the alcohols of existing refueling infrastructures and higher energy density. However, they are blends of different kinds of hydrocarbons and are believed to be more difficult to reform. Kumar et al., at Argonne National Laboratory, have developed a partial oxidation catalyst that can convert a broad range of alcohols and hydrocarbon fuels into a hydrogen-rich product gas.^{2,3} Tests in micro-reactors have shown high conversion and hydrogen yields from methane, methanol, ethanol, 2-pentene, cyclohexane, i-octane, hexadecane, gasoline, and diesel.

The overall partial oxidation reaction can be written as:



This can be thought of as an exothermic oxidation reaction combined with an endothermic steam-reforming reaction.



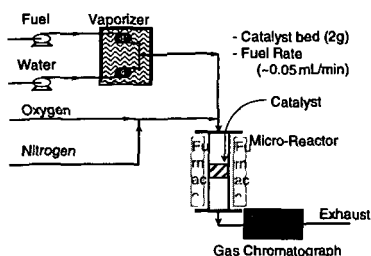
The overall partial oxidation or autothermal catalytic reforming can be exothermic or endothermic. The main factor determining the heat balance for the reaction is the oxygen-to-carbon ratio. The thermal neutral point (where enthalpy of the reaction is zero) varies from an x/n ratio of 0.23 for methanol to 0.37 for iso-octane. For autothermal reforming, it is advantageous to run in the exothermic region, but at a low x/n ratio to maximize the yield of H₂. The experiments reported here were performed with an x/n ratio of 0.5, except for methanol and ethanol experiments, which were performed at a lower x/n (0.32 and 0.25) to compensate for the oxygen already present in the alcohol.

EXPERIMENTAL APPROACH

The catalytic partial oxidation reforming of hydrocarbon fuels was demonstrated in a series of experimental activities, beginning with micro-reactor studies and progressing up to bench-reactor-scale investigations. Since gasoline and diesel fuels are blends of different types of hydrocarbons, the studies were initially carried out with representatives of the different types of hydrocarbons present in these fuels, e.g., iso-octane for paraffins and toluene for aromatics. A schematic of the micro-reactor apparatus is shown in Fig. 1. The liquid fuel and water are pumped through separate vaporizer coils. The vapors then combine with oxygen to form the reactant mix that flows into the micro-reactor. The reactor is a 10.6 mm-ID tube packed with ~2 g of catalyst. The temperature is controlled by a surrounding furnace. Samples are drawn from the product stream and analyzed with a gas chromatograph or gas chromatograph-mass spectrometer. Temperatures and pressures are measured above and below the catalyst bed. In order to facilitate comparisons between the

various fuels, micro-reactor tests were generally run with a fixed carbon-to-oxygen ratio and a slight excess of water with respect to equation 1 [$H_2O > (2n - 2x - p)$].

Fig. 1
Schematic of Experimental



RESULTS AND DISCUSSION

Hydrogen production from the partial oxidation reforming of several of the fuels tested is shown in Table I. The table lists the hydrocarbon feed, the reactor temperature at which complete conversion of the hydrocarbon was achieved and the percentages of hydrogen, carbon monoxide, and carbon dioxide measured in the product gas. The last three columns list the calculated percentages of the gases that would exist at equilibrium at the different temperatures. Using the Argonne catalyst, we were able to convert these hydrocarbons at less than 700°C. Comparison between the experimental and equilibrium gas compositions indicates that the use of the catalyst allows for lower carbon monoxide and slightly higher hydrogen concentrations than what might be achieved at equilibrium at these temperatures.

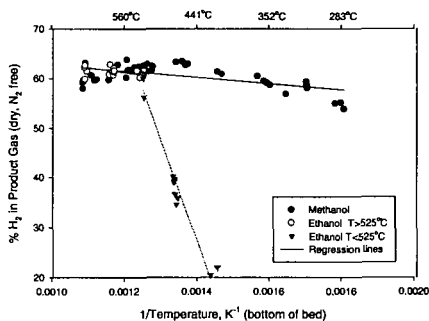
Table 1. Experimental Product Gas Composition Compared with Equilibrium Compositions Calculated for the Given Feed Mixture and Experimental Temperature

Fuel	Temperature for complete conversion, °C	Experimental (% dry N ₂ free)			Equilibrium (% dry N ₂ free)		
		H ₂	CO	CO ₂	H ₂	CO	CO ₂
Iso-octane	630	60	16	20	57	20	19
Toluene	655	50	8	39	49	23	26
2-Pentene	670	60	18	22	56	21	21
Ethanol	580	62	15	18	62	18	16
Methanol	450	60	18	20	60	19	17

Table I also indicates that the two alcohols (methanol and ethanol) are reformed at substantially lower temperatures than the other species. Of the fuels considered for partial oxidation reforming, alcohols should be considerably easier to reform since they are already partially oxidized.

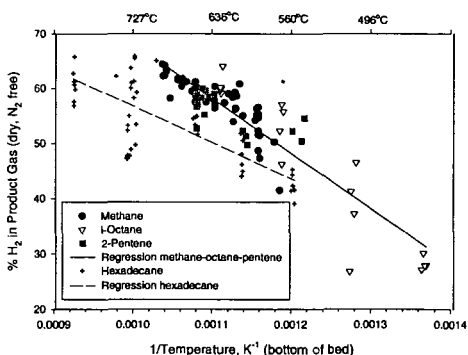
There is a substantial difference in the temperature at which complete conversion of the hydrocarbons was achieved, even between the two alcohols studied. Figure 2 illustrates the temperature dependence of hydrogen production from the partial oxidation reforming of methanol and ethanol using the Argonne partial oxidation. The two alcohols behave quite differently.

Fig. 2
Hydrogen Production from Partial Oxidation Reforming
of Alcohol Fuels



Methanol was easily reformed throughout the temperature range investigated. This fuel yielded a product gas that had hydrogen concentrations in the 55 to 65% range (on a dry N_2 free basis), with the product gas varying only slightly in composition with changes in temperature. The temperature dependence of ethanol reforming was quite different, with the product composition varying strongly with temperature in the range of 410 to 525°C. At 470°C, the product gas from ethanol reforming contained only about 35% hydrogen, compared to about 60% hydrogen for methanol reforming at the same temperature. For temperatures greater than 525°C, hydrogen production from ethanol was almost identical to that from methanol. However, the maximum hydrogen yield for the reactant mix with methanol was 70.2%, while that for ethanol was 71%. Defining hydrogen selectivity as the measured hydrogen yield divided by the maximum, we find slightly lower hydrogen selectivity for ethanol in the high temperature region (88% than for methanol (91%). This was due to the formation of methane in the ethanol reforming. The ethanol reformat contained substantial amounts of methane over the entire temperature range investigated, with the reformat containing about 5% methane at 640°C, while the methanol reformat contained an order of magnitude less methane at this temperature.

Fig. 3
Hydrogen Production from Partial Oxidation Reforming
of Alkanes and Alkenes



The effect of temperature on hydrogen production from reforming of methane, iso-octane, and 2-pentene is shown in Fig. 3. These hydrocarbons were more difficult to reform autothermally than the alcohols, as expected. Temperatures of nearly 650°C were needed to approach 60% hydrogen in the product gas. Hydrogen selectivities of 90% for methane and 88% for iso-octane and 2-pentene were obtained. The hydrogen concentration at a given temperature was similar regardless of the hydrocarbon. The data for methane, iso-octane, and 2-pentene all fall on the same regression line (see

Fig. 3). Hydrocarbon length over the range of C1 to C8 and the presence of unsaturation appear to have little affect on the product composition.

Increasing the hydrocarbon length to C16 (hexadecane) was observed to lead to lower hydrogen content in the product gas. Hexadecane reforming showed a temperature dependence similar to that observed for methane, iso-octane, and 2-pentene (i.e., similar slope in Fig.3). However, higher temperatures were needed to reach comparable hydrogen content in the product gas. This appears to be due to increased methane formation from hexadecane. At 650°C, the product gas from hexadecane reforming contained 6% methane (dry, nitrogen free), while that from iso-octane reforming contained only about 2% methane.

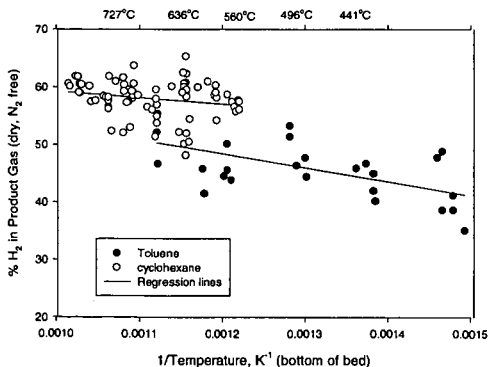
The iso-octane and hexadecane experiments also pointed out some potential difficulties in reforming longer hydrocarbons. The product gas from iso-octane and hexadecane reforming contained small amounts of benzene. This is illustrated in Table II, which compares the output from thermal reforming (no catalyst present) and catalytic reforming (catalyst present) of iso-octane. Benzene was present in the product gas at concentrations of about 0.1-0.2% for temperatures from 600 to 725°C when the catalyst was present; however, no benzene was detected in the product gas when the catalyst was absent. This suggests that benzene is formed as a side product during the reforming of C8 hydrocarbons. Studies on the formation of aromatics from C8 hydrocarbons have indicated that the most likely mechanism for benzene production involves formation of xylenes, which then form benzene by trans alkylation reactions.⁴

Table 2. Effect of Catalyst on Product Composition

	Product Composition at 725°C, % (dry, N ₂ free)					
	H ₂	O ₂	CH ₄	CO	CO ₂	C ₆ H ₆
No Catalyst	0.0	10.2	17.7	39.6	26.1	0.0
Catalyst	57.9	0.0	4.3	19.2	18.1	0.2

We have also investigated the reforming of cyclohexane, a possible benzene precursor, and toluene, a benzene derivative. The hydrogen production from partial oxidation reforming of cyclohexane and toluene did not exhibit the same temperature dependence as did that from reforming the alkanes and the alkene discussed previously. The product composition was much less sensitive to temperature for these cyclic compounds (see Fig. 4). Hydrogen selectivity was still high, but slightly lower for toluene (82%) than for cyclohexane (91%) and the non-cyclic alkanes (88%). The lower temperature dependence suggests that a different mechanism may be controlling the reforming of cyclohexane and toluene.

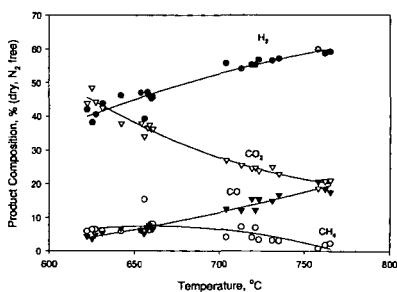
Fig. 4
Hydrogen Production from Partial Oxidation Reforming of Cyclohexane and Toluene



The results from reforming toluene suggest that if benzene, xylene, or other aromatics are formed at low levels as side products in the reforming of branched hydrocarbons they can be reformed. Increasing the temperature will increase the conversion of these aromatics to hydrogen, but not as effectively as it increases the rate of conversion of alkanes to hydrogen.

The ability of the Argonne catalyst to reform several types of hydrocarbons suggested that this catalyst would be able to reform commercial petroleum fuels. Therefore, we proceeded with tests of commercial gasoline and diesel fuel. The product composition from autothermal reforming of a commercial premium gasoline is shown in Fig. 5. Hydrogen concentrations in the product gas approaching 60% on a dry N_2 free basis were obtained at temperatures $\geq 700^\circ\text{C}$. The slope of the plot of inverse temperature versus hydrogen content in the product gas is similar to that found for the reforming of methane, iso-octane, and 2-pentene, suggesting a similar mechanism. However, methane concentrations in the product gas are higher than what we have seen from reforming the simple hydrocarbons. Commercial gasoline contains sulfur, a known catalyst poison, at levels of over 100 ppm. However, no change was observed in the product composition after 40 h of intermittent gasoline reforming, indicating it has some

Fig. 5
Product Distribution from Partial Oxidation Reforming of Premium Gasoline



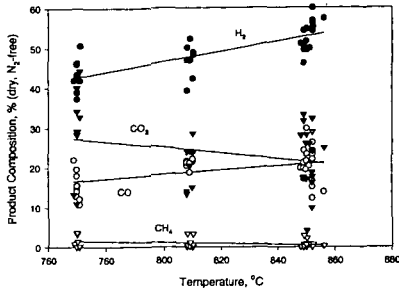
resistance to sulfur poisoning.

Reforming of diesel fuel proved slightly more difficult. Methane was observed in higher concentrations in the product gas from diesel reforming than in the product from gasoline reforming. Higher reforming temperatures were needed to decrease the methane and increase the hydrogen in the product gas. At 850°C we were able to obtain a product gas with hydrogen concentrations $>50\%$ on a dry N_2 free basis (see Fig. 6).

CONCLUSIONS

Micro-reactor tests indicate that our partial oxidation catalyst is fuel-flexible and can reform conventional (gasoline and diesel) and alternative (ethanol, methanol, natural gas) fuels to hydrogen rich product gases with high hydrogen selectivity. Alcohols are reformed at lower temperatures ($< 600^\circ\text{C}$) while alkanes and unsaturated hydrocarbons require slightly higher temperatures. Cyclic hydrocarbons and aromatics have also been reformed at relatively low temperatures, however, a different mechanism appears to be responsible for their reforming. Complex fuels like gasoline and diesel, which are

Fig. 6
Product Distribution from Partial Oxidation Reforming of Diesel Type 2



mixtures of a broad range of hydrocarbons, require temperatures of $> 700^{\circ}\text{C}$ for maximum hydrogen production.

ACKNOWLEDGMENTS

This work was supported by the U.S. Department of Energy, Office of Advanced Automotive Technologies, in the Office of Automotive Technologies, under contract No. W-31-109-ENG-38.

REFERENCES

1. R. L. Espino, "Fuels Processing for PEM Fuel Cells - Fuel Industry Perspective," Annual Automotive Technology Development Contractor's Coordination Meeting-PNGV Workshop on Fuel Processing for PEM Fuel Cells, Dearborn, MI, 23-27 October 1995.
2. R. Kumar, S. Ahmed and M. Krumpelt, *Electric and Hybrid Vehicle Technology* 96, 1996.
3. S. Ahmed, R. Doshi, R. Kumar, and M. Krumpelt, *Electric and Hybrid Vehicle Technology '97*, p. 77, 1997.
4. C. Marshall, Argonne National Laboratory, private communication, 1999.

Hydrogen Production via Methanol – Steam Reforming using Catalysts containing a Hydrotalcite Phase Structure

L.M. Kearns, J.C. Amphlett, E. Haliop, H.M. Jenkins, R.F. Mann and B.A. Peppley

Department of Chemistry and Chemical Engineering
Royal Military College of Canada
Kingston, Canada.

Abstract

Steam reformation of methanol is an actively studied process for supplying hydrogen rich fuel gas to proton-exchange membrane (PEM) fuel cells. The purpose of the present investigation is to improve activity and thermal stability of our optimized Cu/Zn/Al formulation. Cu/Zn/Cr, Cu/Zn/Cr/Al, Cu/Zn/Ce, Cu/Zn/Ce/Al, Cu/Zn/La and Cu/Zn/La/Al were prepared at different calcination temperatures. The catalysts were thoroughly characterized and activity studies were run at 250°C with 1:1 methanol/steam using a pulse reformer. Characterization results indicate that the hydrotalcite skeletal structure is still intact in catalysts calcined up to 300°C. The activity of the Cu/Zn/Cr catalyst calcined at 300°C of the calcination series was significantly higher than for any other catalyst series in the study with very little deactivation during the duration of the run. Activity studies using a high pressure reactor also showed superior activity for the Cu/Zn/Cr catalyst with analysis of the spent catalyst indicating very little structural damage.

1. Introduction

With growing support for environmental issues, there is incentive to develop an efficient, clean electric power system to operate stationary power plants and vehicles such as cars, buses and submarines. The increased interest is caused both by a search for an alternative energy source for the decreasing supply of fossil fuels and the increasingly stringent regulations for emission levels that are coming into effect in many parts of the world. A promising system actively being developed is the hydrogen fed Proton Exchange Membrane (PEM) fuel cell. The many benefits include a significant increase in energy efficiency and reduction of emissions by as much as 90%; specifically reducing CO₂ emissions by 40%[1]. A liquid fuel is the desirable form for transport and storage of hydrogen. Steam reformation of methanol is the most widely studied system for production of hydrogen rich gas to be utilized at the anode of a PEM fuel cell as compared to hydrocarbon reformation and steam reformation of ethanol[2,3]. Methanol, as a reactant in steam reformation, is a relatively inexpensive renewable fuel that produces less environmentally harmful products than the internal combustion of conventional petroleum fuel. We have developed an improved CuO/ZnO/Al₂O₃ catalyst for methanol steam reforming. Our latest formulation gives higher activities than commercial catalysts for the range of temperatures and time on line investigated [4,5].

Experience with our optimal catalyst showed that enhanced activity was correlated with the presence of hydrotalcite structure, therefore other elements that can be incorporated in a hydrotalcite structure may also show high activity and possibly higher thermal stability. Also, structures that resisted sintering would lower the rate of deactivation of a proposed catalyst. Cerium, Chromium and Lanthanum were incorporated in some catalyst formulations. These elements have potential to form hydrotalcite structures with Cu and Zn with or without Al present. Lanthanum has also been used to improve thermal stability of catalysts. The principle is that the small sized La atoms fit between the atoms in the phase structure and act as a physical block to inhibit sintering. Modified catalysts of Cu/Zn/Ce, Cu/Zn/Ce/Al, Cu/Zn/Cr, Cu/Zn/Cr/Al, Cu/Zn/La and Cu/Zn/La/Al were prepared at different calcination temperatures.

2. Experimental

2.1 Catalyst Preparation

The catalyst was prepared by a coprecipitation method using a dilute mixed Cu, Zn, X (X=Al,Ce,Cr,La) - nitrate solution and a solution of Na₂CO₃. The two solutions were simultaneously added to distilled water with vigorous stirring, using pumps whose flow rates were adjusted to keep the pH of the resulting mixture precisely at 7.0. The precipitate was filtered, washed, reslurried, then filtered again before drying at 110°C for 16 hrs. The precursor was crushed into smaller particles, then calcined in air at the specified temperature (300, 400, 550 or 650°C) for 6 hrs.

2.2 Catalyst Characterization

The catalyst series were characterized using thermal gravimetric analysis (TGA), x-ray powder diffraction (XRD) for phase structure analysis, N₂ adsorption for total surface area and CO chemisorption for copper surface area. Copper dispersion was calculated from the results of copper content and copper surface area. Surface studies were carried out using diffuse reflectance infrared fourier transform spectroscopy (DRIFTS).

TGA analyses were done using a TA Instruments Thermograph Model 2050 controlled by a Thermal Analyst 3000 computer. The He flow rate was 100 ml/min. The temperature was increased at 10°C/min. The first derivatives of the TGA curves (%Mass vs. Temperature) were calculated and used to determine the decomposition profile for the precursor phase structure.

XRD powder patterns were obtained using a Scintag diffractometer. Scans were taken at a 2θ step size of 0.03° between 10 and 60° using Cu-Kα₁ (nickel filtered) radiation. Cu and Zn crystallite sizes were calculated from the line broadening of the CuO(111) and ZnO(101) lines respectively using the Debye-Scherrer Method.

2.3 Study of Catalyst deactivation

The high pressure test reactor used for part of the activity studies was a fully automated tubular fixed-bed reactor. The catalyst was pelletized and screened to obtain a particle size distribution of 20-25 mesh. A

samples of the desorbing gases were analysed by mass spectrometry for each range of temperature, confirmed the assignment of the peaks from the 1st derivative of the TGA curves.

For these catalyst series, the precursors were XRD amorphous. A broad peak was observed between 34° and 36° 2θ for the catalysts calcined at 300°C which became more intense for the catalysts calcined at 400°C. Peaks for CuO and ZnO were observed for catalysts calcined at 550°C and 650°C. The activities of the Cu/Zn/La and Cu/Zn/Ce series were similar to the Cu/Zn/Al series as were the rates of deactivation. The precursor and catalysts calcined at 300°C and 400°C had the highest activities.

3.3 Chromium-Containing Catalysts

From TGA and TPD results the presence of a hydrotalcite structure was confirmed in precursors for both the Cu/Zn/Cr and Cu/Zn/Cr/Al formulations. The broad overlapping decomposition temperature range for the intralayer OH and interlayer CO₃²⁻ was shifted to a lower temperature centred at 210°C for the Cu/Zn/Cr/Al precursor and 190°C for the Cu/Zn/Cr precursor. Upon placing samples calcined at 300°C in water, reconstitution of the hydrotalcite was observed as with the other formulations. Very little surface carbon oxide species were present on the Cr catalyst series compared to any other catalysts studied. Also, the decomposition temperature for the surface carbon oxide species was shifted to a lower temperature of 440°C for the Cu/Zn/Cr precursor compared to 540°C for the Cu/Zn/Cr/Al precursor. In the XRD profiles,

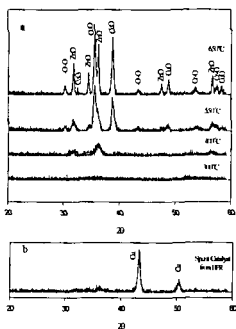


Figure 3. XRD profiles for a) Cu/Zn/Cr series calcined at various temperatures; b) spent Cu/Zn/Cr catalyst calcined at 300°C. The catalyst was removed from the high pressure reactor after 7 days at 280°C.

shown in Figure 3, the catalyst calcined at 300°C was XRD amorphous, as well as the precursor whose XRD profile is not shown. Very broad peaks attributed to zincite (ZnO) were observed for the catalyst calcined at 400°C. The ZnO crystallites were much smaller in the Cu/Zn/Cr catalyst than in the Cu/Zn/Cr/Al catalyst. Tenorite (CuO) was not observed until 550°C. CuO appears to be highly disperse (XRD amorphous). Chromium oxide appeared only in the catalysts calcined at 550°C and 650°C.

The low quantity of surface carbon oxides observed by FTIR indicates that Cr containing catalyst formulations are less basic than the other catalysts studied. Bands due to OH groups and hydrogen bonding between the interlayer hydroxy groups and carbonates of hydrotalcite were present.

The activity of the Cu/Zn/Cr catalyst calcined at 300°C was higher than the Cu/Zn/Al catalyst with very little deactivation during the duration of the run. The activity study of the Cr series is shown in Figure 4. The activities of the Cu/Zn/Cr/Al series was similar to that of the Cu/Zn/Al series except that the catalyst calcined at 550°C also had a high activity as the same series of catalysts calcined at lower temperatures.

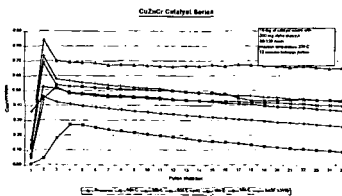
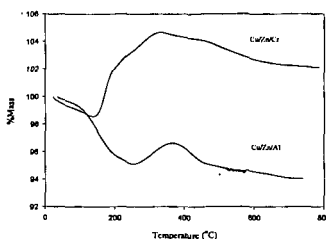


Figure 4. Deactivation study of the Cu/Zn/Cr series using a pulse reformer. Reaction was carried out at 250°C With 1:1 methanol/steam and pulses every 12 minutes.

4. Characterization of Spent Catalysts

4.1 Cu/Zn/Al

Characterization of the spent Cu/Zn/Al catalyst was carried out on the catalyst calcined at 300°C since it was the catalyst in the series with the highest activity. The XRD profile showed the presence of relatively large crystallites of zincite. No tenorite was observed, so if any CuO was present it was



amorphous or XRD invisible. Metallic Cu was observed in the XRD profiles and was evidently stable to air at room temperature. The very low weight loss of the spent catalysts in comparison to the fresh catalysts, observed in the TGA, indicated that very little hydroxycarbonate phases had remained intact after

Figure 5. TGA curves for the spent Cu/Zn/Cr and Cu/Zn/Al catalysts calcined at 300°C. The Cu/Zn/Cr catalyst was run at 280°C for 170 hours while the Cu/Zn/Al catalyst was run at 240°C in a high pressure reactor. The reactant feed was 1:1 methanol steam.

completion of the reaction run. A weight loss of 7% was observed compared to 18% for the fresh catalyst. The initial decrease in the TGA scan of the spent catalyst coincided with those found for the precursor hydroxalcalite representing decomposition of interlayer H₂O and intralayer OH/interlayer CO₃²⁻. The structure of the spent catalysts was considerably changed compared to the fresh catalyst. A gain in mass was observed beginning at 230°C (Figure 5) in the TGA curve. The mass increase was the result of formation of CuO from Cu metal during heating in air.

4.2. Cu/Zn/Cr

The Cu/Zn/Cr spent catalyst that was characterized was calcined at 300°C and run in the high pressure reactor for 170 hours at 280°C in a 1:1 ratio of methanol/steam reactant flow. The XRD profile of the spent Cu/Zn/Cr catalyst is shown in Figure 3b. Cu metal was the only phase observed. Crystallite size was determined using the Debye-Scherrer method and was found to be 19 nm. ZnO was not observed in the spent Cu/Zn/Cr. TGA analysis, shown in Figure 5, indicated that stable Cu metal began oxidizing at 190°C. A mass increase of more than 5% was observed.

5. Conclusions

The most active catalyst formulation was Cu/Zn/Cr. The catalyst calcined at 300°C gave the highest activity of any catalyst. In all cases, the catalyst calcined at 300°C gave higher activities than catalysts in the same calcination series. The Cu/Zn/Cr catalyst calcined at 300°C showed very little deactivation in the activity studies for reactions run in the pulse reformer and the high pressure reactor. Analyses of the spent catalysts gave very interesting results. For the Cu/Zn/Al catalyst, relatively large ZnO and Cu metal crystallites were observed by XRD. Whereas with the Cu/Zn/Cr spent catalyst, only crystallites of Cu metal were observed. The ZnO remained well dispersed during the test reaction using the high pressure reactor. Also, the Cu metal appeared to be more active in the Cu/Zn/Cr spent catalyst as observed in Figure 5 where oxidation of Cu metal during the TGA run occurred at a much lower temperature and in much greater abundance than for the Cu/Zn/Al spent catalyst. These findings help to identify the differences in the Cu/Zn/Cr catalyst, calcined at 300°C and may indicate why this catalyst has significantly higher activity and thermal stability.

References

1. P. Patil, P. Zegers, J. Power Sources 49 (1994) 169.
2. B.A. Peppley, J.C. Amphlett, L.M. Kearns, R.F. Mann, Methanol-Steam Reforming on Cu/ZnO/Al₂O₃, Part I: The Reaction Network, Appl. Catal., submitted for publication.
3. B.A. Peppley, J.C. Amphlett, L.M. Kearns, R.F. Mann, Methanol-Steam Reforming on Cu/ZnO/Al₂O₃, Part 2: A Comprehensive Kinetic Model, Appl. Catal., submitted for publication.
4. B.A. Peppley, "A Comprehensive Kinetic Model of Methanol-Steam Reforming on Cu/ZnO/Al₂O₃ catalyst". Ph.D. Thesis, Royal Military College of Canada, Kingston, Ontario, Canada, (1997).
5. R.O. Idem and N.N. Bakhshi, Chem. Eng. Sci. 51 (1996) 3697.

SYSTEM OPTIMIZATION AND COST ANALYSIS OF PLASMA CATALYTIC REFORMING OF HYDROCARBONS

L. Bromberg, D.R. Cohn, A. Rabinovich, N. Alexeev, A. Samokhin
MIT Plasma Science and Fusion Center
Cambridge MA 02139

and

R. Ramprasad, S. Tamhankar
BOC Gases
New Brunswick NJ 84501

Abstract

Thermal plasma reforming offers advantages in hydrocarbon reforming specially in small to medium scale plants and in plants with fast transients. The combination of a thermal plasma reformer operating in the range between partial oxidation to steam reforming with a catalyst bed will be described. Reduced concentrations of CO (1-3% vol) can be achieved, with high hydrogen yields and minimal plasmatron electrical power requirements. A model for the cost of hydrogen production by this method, including hydrogen cleanup, has been developed. The model uses experimentally determined conversion yields and operational parameters. The conditions that result in system optimization and cost minimization have been determined.

1 Introduction

Manufacturing of hydrogen from natural gas, biofuels and other hydrocarbons, is needed for a variety of applications. Plasma technology could provide important improvements in reforming hydrocarbon fuels for the production of hydrogen-rich gas for fuel cells and other applications. The plasma conditions (high temperatures and a high degree of ionization) can be used to accelerate thermodynamically favorable chemical reactions or provide the energy required for endothermic reforming processes. Plasma reformers can provide a number of advantages:

- economically attractive operation in small scale hydrogen production applications
- operation with a broad range of fuels, including natural gas and biofuels
- decreased problems of catalyst sensitivity and deterioration
- compactness and low weight (due to high power density)
- fast response time (fraction of a second)
- minimal cost
- high conversion efficiencies

Hydrogen-rich gas could be efficiently produced in compact plasma reformers with a variety of hydrocarbon fuels including natural gas, biomass, and others. The technology could be used to manufacture hydrogen for a variety of stationary applications (e.g., distributed, low pollution electricity generation from fuel cells or hydrogen-refueling gas stations for fuel cell driven cars). It could also be used for mobile applications (e.g., on-board generation of hydrogen for fuel cell powered vehicles).

In this paper, the cost issues of a plant that incorporate a plasma reformer are investigated. It is assumed that the plant operates on natural gas, although the plasmatron is capable of operating in a wide range of fuels. The experimental results of plasma reforming of natural gas are quickly reviewed in section 2. A model of a process plant is developed, and a model for determining the hydrogen cost is described in section 3. The sensitivity of the cost to capital cost, cost of natural gas and to manpower requirements are then presented in section 4. The tradeoff between higher conversion and increased electrically energy consumption in the plasmatron is described in section 5. Finally, the conclusions and direction of additional work is described in section 6.

2 Plasma reforming

Plasma devices referred to as plasmatrons can generate very high temperatures (>2000 C) with a high degree of control, using electricity [1]. The heat generation is independent of reaction chemistry, and optimal operating conditions can be maintained over a wide range of feed rates and gas composition. Compactness of the plasma reformer is ensured by high energy density associated with the plasma itself and by the reduced reaction times, resulting in short residence time. Hydrogen-rich gas can be efficiently produced in plasma reformers with a variety of hydrocarbon fuels (gasoline, diesel, oil, biomass, natural gas, jet fuel, etc.) with conversion efficiencies into hydrogen-rich gas close to 100% [2,3].

The plasma conditions (high temperatures, high degree of dissociation and substantial degree of ionization) can be used to accelerate thermodynamically favorable chemical reactions without a catalyst or provide the energy required for endothermic reforming processes.

The technology could be used to manufacture hydrogen for a variety of stationary applications e.g., distributed, low pollution electricity generation from fuel cells [4]. It could also be used for mobile

applications (e.g., on-board generation of hydrogen for fuel cell powered vehicles) and for refueling applications (stationary sources of hydrogen for vehicles).

A previous paper [5] presented results of plasma catalytic conversion of methane, using partial oxidation. In this section, more recent results are very briefly described. Figure 1 shows the hydrogen yield as a function of the specific energy consumption (electrical power required for a given hydrogen throughput). The best results are 95% yield at a specific energy consumption of 13 MJ/kg H₂. These results were obtained without the use of a heat exchanger. It is estimated that with a heat exchanger and with improved thermal management, the specific energy consumption can be decreased to 7 MJ/kg H₂ (0.18 kWh/m³ H₂) at slightly higher yield (97%). These numbers will be assumed in the calculations below.

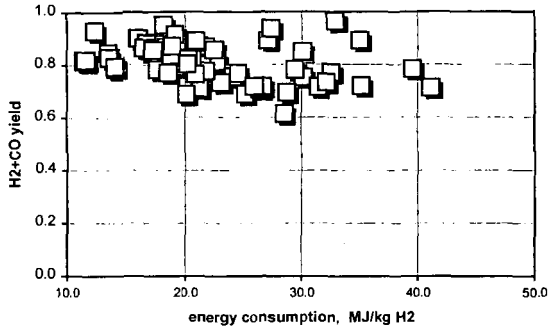


Figure 1. Hydrogen yield as a function of specific energy consumption for plasma catalytic reforming of methane.

3 Costing model

The cost of the hydrogen produced through a plasmatron process is investigated in this section. It is assumed that the hydrogen rich gas is produced at pressure so that it is not necessary to pressurize the hydrogen rich gas prior to the pressure swing absorption section. Air, not oxygen, is used as the oxidizer, which means that the synthesis gas contains a large amount of nitrogen. It is also assumed that methane is the hydrocarbon used, although other hydrocarbons can also be utilized. Further assumptions are that the system has good thermal management, and the power consumed by the plasmatron as well as the exothermic energy released by the partial oxidation process are used to produce the steam required for the system. Steam is required mainly in the water-shift reaction. There is an excess of steam for the steam shifter of 200%.

The capital costs of the system, for a 8570 m³/hr (3000 scfm) are shown in Table 1. The syngas is at pressure, and there is no need for boiler to produce steam since it can be produced by the syngas itself prior to the water shift reaction, which occurs at relatively low temperatures. If the plant is amortized over 10 years, then the amortized capital cost is on the order of \$500k per year.

Table 1. Capital costs for system with 8570 m³/hr

NG compressor	\$250,000
Air compressor	\$250,000
Reforming Reactor	\$50,000
plasmatron	\$500,000
converter (power supply)	\$300,000
spares	\$50,000
Shift Reactor	\$500,000
Syngas compressor	\$0
H ₂ PSA	\$1,500,000
Waste-to-Steam Boiler	\$0
Air Blower for Boiler	\$0
Incinerator	\$0
Cap cost total	\$3,400,000
Installation	\$680,000
Plant Cost (Installed)	\$4,080,000

The operational costs depend on the number of personnel operating the plant. Since the high power plasmatron is a well-established technology, it is assumed that the system is automated and needs minimal supervision. Maintenance to the plasmatron, consisting in replacing the electrodes, needs to be performed every 1000 hours of operation, and lasts only a few minutes. During plasmatron maintenance, the system can continue to operate at reduced level. Several plasmatrons are used in the system, and electrode replacement is carried out one by one.

The power requirements are shown in Table 2. The syngas is at pressure when leaving the plasmatron reactor. Air compression requires more power than the corresponding oxygen compression. The power requirements are dominated by the plasmatron power requirements of 1500 kW.

Table 2. Power consumption in 8570 m³/hr plant

NG Comp. power, kW	100
Air Comp. power, kW	200
Syngas Comp., kW	0
Plasmatron power, kW	1500
Total Power, kW	1800

The cost of the natural gas is assumed to be \$2.5/MMBTU, and the electricity cost is \$0.05/kWhr. Assuming that 8 full time people (all shifts) are required in the plant (at a cost of \$70000/person-year), then the annual costs are given in Table 3, for 8570 m³/hr.

Table 3. Annualized costs for a 8570 m³/hr hydrogen plant

Labor	\$560,000
Catalyst	\$100,000
Power	\$600,000
Other	\$1,801,237
Total Op. + Util.	\$3,061,237
Total cost Op+util+cap	\$3,571,237

With an annual hydrogen production of 720K MMBTU, then the cost of the hydrogen is about \$5/MMBTU. This is a very preliminary look at the cost, and more detailed calculations will be presented at a later time.

The model can be used to determine the cost of the hydrogen as a function of the plant capacity. Figure 2 shows the results from this calculations, assuming that the cost of the equipment (capital cost) scale linearly with plant capacity.

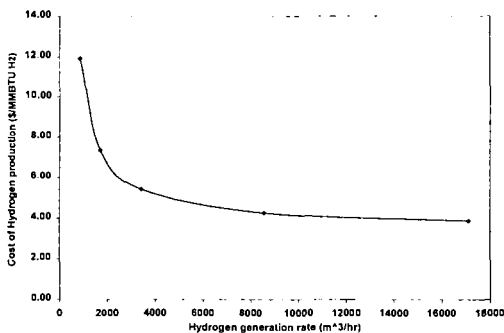


Figure 2 Cost of hydrogen as a function of the plant capacity.

4 Sensitivity of hydrogen cost

The dependence of the hydrogen costs on the capital cost, the methane cost and the required personnel is described in this section.

The sensitivity of the cost of hydrogen to the cost of natural gas is shown in Figure 3. The cost of the hydrogen is about \$3.5/MMBTU more expensive than the cost of the natural gas. For free natural gas, the cost of the hydrogen is about \$4/MMBTU.

From Table 3, it can be seen that the bulk of the cost is due to the natural gas, with the electrical power about 1/3 of the natural gas cost. Increasing the cost of the capital equipment by a factor of 2.5 increases the hydrogen cost from \$6.1/MMBTU to \$7.2/MMBTU, for 3430 m³/hr plant capacity. Increasing the cost of electricity to \$0.10/kWhr increases the cost of hydrogen to \$6.9/MMBTU.

The effect of the automation can be seen in Figure 4. 8 people per year corresponds to 2 persons attending the plant at all times, both at the control room and in maintenance operations. If plasma operation can decrease the required supervision, then the hydrogen cost can be decreased substantially. If only 2 personnel are required, for light supervision, transients and maintenance, then the hydrogen cost can be decreased to about \$4/MMBTU, which is about just 75% higher than the cost of the natural gas feedstock.

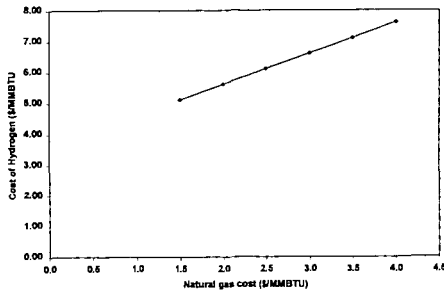


Figure 3. Hydrogen cost as a function of natural gas cost, for a 3430 m³/hr plant capacity

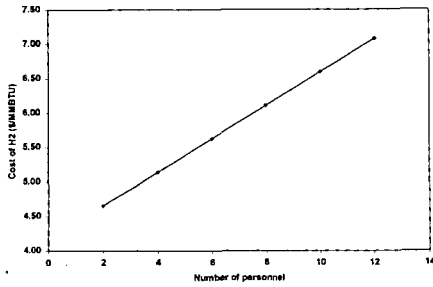


Figure 4. Hydrogen cost as a function of number of plant attendants, for a 3430 m³/hr plant capacity

5 Tradeoff between methane conversion and specific energy requirement

As mentioned in the sections above, there is a tradeoff between the methane conversion and the hydrogen yield. A simplified curve illustrating this tradeoff is shown in Figure 4. For a specific energy consumption less than about 0.17 kWhr/m³ there is a sharp drop in the methane conversion. At the higher specific energy consumption, the methane conversion does not increase much.

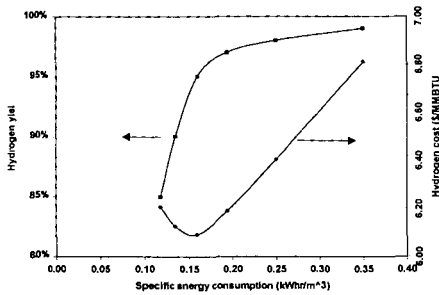


Figure 5. Methane yield and cost of hydrogen as a function of the specific energy, for 3430 m³/hr plant capacity

Figure 5 also shows the hydrogen cost as a function of the specific energy consumption. All the other parameters are the same as in the previous sections. There is a well-defined minimum in the cost. To the left of the minimum, the hydrogen yield is decreasing because of not enough conversion of methane, and to the right of the minimum the electrical cost is increasing faster than the hydrogen yield. It is important to determine experimentally the minimum cost.

6 Discussion and conclusions

Plasma reforming of natural gas has been briefly described. A process involving plasma reforming of natural gas for the production of hydrogen is then modeled to determine the cost and the cost-sensitivity of hydrogen produced by the process. Although preliminary, the costs indicate that there may be methods of producing hydrogen at competitive costs, specially important for small capacity hydrogen generating units.

Several assumptions need to be demonstrated experimentally. It is necessary to demonstrate the lower specific energy consumption assumed in the paper, by the use of better thermal management and heat recovery. It is necessary to operate the plasmatron at high pressure, to minimize the required pumping power. This could have substantial effect in the case of liquid feedstock, since it requires little power to pressurize the liquid but substantial power to pressurize the reformat. If electrode life or other effects limit the plasma reformer operation at high pressure, then a reformat compressor needs to be included in the system. Heat recovery requires a heat exchanger that was not included in the cost calculations.

The lifetime of the catalyst is another unknown. Sulfur in the feedstock is readily transformed into H_2S which needs to be removed from the system but which does not affect the catalyst.

The costing model is continuously being improved.

Acknowledgements

This work was supported by US Department of Energy, Grant No DE-FG04-95AL88002.

References

- [1]. For recent reviews of plasma technology, see: MacRae, D.R., *Plasm. Chem and Plasm. Processing*, 9 85S (1989); also see: Fauchais, P. and Armelle Vardelle, *Thermal Plasmas, IEEE Transactions on Plasma Science* 25 6 1258-1280 (1997).
- [2] Kaske, G., L. Kerke, and R. Muller, *Hydrogen Production in the Huls Plasma-Reforming Process*, *Hydrogen Energy Progress* VI, 1 (1986).
- [3] Muller, R., *The Use of Hydrogen Plasma Processes in the Petrochemical and Iron-Smelting Industries*, in: *Hydrogen Energy Progress* IV, 3 885 (1982).
- [4] L. Bromberg, D.R. Cohn, A. Rabinovich and N. Alexeev, *Plasma Catalytic Reforming of Methane* accepted for publication in *Int. J. of Hydrogen Energy*.
- [5] L. Bromberg, .R. Cohn, A. Rabinovich and N. Alexeev, presented at the 1999 Annual Peer Review of the Hydrogen Program, Denver CO 1999 (to be published)

PERFORMANCE TESTING OF HYDROGEN TRANSPORT MEMBRANES AT ELEVATED TEMPERATURES AND PRESSURES

K. S. Rothenberger, A. V. Cugini, R. V. Siriwardane, D. V. Martello, J. A. Poston, E. P. Fisher,
U.S. Department of Energy - Federal Energy Technology Center
Pittsburgh, PA 15236 and Morgantown, WV 26507.

W. J. Graham,
Parsons Infrastructure and Technology Group - Federal Energy Technology Center
Library, PA 15129.

U. Balachandran and S. E. Dorris,
Argonne National Laboratory, Argonne, IL 60439.

Keywords: Membranes, Hydrogen, Gas separation

ABSTRACT

The development of hydrogen transport ceramic membranes offers increased opportunities for hydrogen gas separation and utilization. Commercial application of such membranes will most likely take place under conditions of elevated temperature and pressure, where industrial processes producing and/or utilizing hydrogen occur, and where such membranes are theoretically expected to have the greatest permeability. Hydrogen separation membrane performance data at elevated temperature is quite limited, and data at elevated pressures is conspicuously lacking. This paper will describe the design, construction, and recent experimental results obtained from a membrane testing unit located at the U.S. Department of Energy's Federal Energy Technology Center (FETC). The membrane testing unit is capable of operating at temperatures up to 900°C and pressures up to 500 psi. Mixed-oxide ceramic ion-transport membranes, fabricated at Argonne National Laboratory (ANL), were evaluated for hydrogen permeability and characterized for surface changes and structural integrity using scanning electron microscopy/ X-ray microanalysis (SEM/EDS), X-ray photoelectron spectroscopy (XPS) and atomic force microscopy (AFM), as a function of temperature, pressure, and hydrogen exposure.

INTRODUCTION

The demand for hydrogen is expected to rise in coming years with increases in its use both directly as a fuel and indirectly in the synthesis or upgrading of fuels required to meet increasingly more demanding environmental standards. However, inexpensive and abundant sources of hydrogen, such as coal gasification, natural gas reforming, and off-gas streams from various process industries, usually contain hydrogen mixed with other gases. Recovery of hydrogen from these dilute streams would increase hydrogen supplies, improve overall process efficiencies, and provide a key component in the development of Integrated Gasification Combined Cycle (IGCC) power systems, fuel cells, advanced transportation fuel technology development, and "Vision 21" combination power and fuel production facilities. Advances in the area of membrane technology may provide the basis for improved methods of hydrogen recovery and thus reduce the cost associated with hydrogen production. Properly designed hydrogen membranes could be used to tailor syngas feed composition to optimize reactions producing fuel and/or chemical products.¹

Currently, several research organizations are engaged in the development of hydrogen transport membranes or their precursor materials.² Membrane materials range from organic polymers to metals to ceramics. Non-porous ceramic membranes are particularly desirable because they can be made exclusively selective to hydrogen and are durable enough to withstand the harsh conditions of temperature, pressure, and chemical exposure that would probably be encountered in commercial application. Practical application of these membranes would likely employ a high total pressure on the retentate (inlet) side coupled with reduced pressures on the permeate (outlet) side to enhance the flux. Hydrogen flux through these membranes is expected to be optimal in the range of 700-900°C and increase with increasing hydrogen partial pressure gradient across the membrane. However, obtaining characterization information at these conditions is difficult, and data at elevated pressures (and pressure drops) is particularly scarce. The goal of the current work is to measure and characterize membrane performance at these elevated-temperature and pressure conditions.

EXPERIMENTAL SECTION

Non-porous ceramic disk membranes were fabricated by a process developed at Argonne National Laboratory (ANL). Membranes used in this study were of composition $\text{BaCe}_{0.80}\text{Y}_{0.20}\text{O}_3$ (BCY), prepared by mixing appropriate amounts of BaCO_3 , CeO_2 , and Y_2O_3 , then calcining the mixture at

1000°C for 12 h in air. This powder was then ball-milled and calcined again at 1200°C for 10 h in air. After obtaining phase-pure powder (by x-ray diffraction), the BCY powder was mixed with 40 vol.% metallic nickel powder to increase its electronic conductivity. The powder mixture was then uniaxially pressed and sintered for 5 h at 1400-1450°C in an atmosphere of 4% hydrogen/balance argon.

Membranes for pressure and flux testing were mounted using a brazing process developed at ANL, in 0.75" O.D. Inconel 600 tubing that had been drilled out to form a small seat to accommodate the membrane. Unmounted membranes of the same composition were also supplied for characterization studies. Because the pressure tested membranes had to be pre-mounted, the before-and-after characterization studies refer to membranes of the same composition and fabrication, but *not* the same physical membranes.

Membrane pressure and flux testing was performed on the Hydrogen Technology Research (HTR) facility, currently under construction at FETC. The facility makes use of high pressure hydrogen handling infrastructure previously put in place for the study of high pressure hydrogenation reactions.³ For membrane testing, the unit has an operating range to 900°C temperature and 500 psig pressure (and pressure drop). The Inconel tubing containing the pre-mounted membrane from ANL was welded to an additional length of 0.75" O.D. Inconel 600 tubing. The membrane was hung in an inverted configuration and attached to a second piece of 0.75" OD Inconel tubing by means of a 0.75" I.D. x 1.125" O.D. x 3.125" long Inconel 600 sleeve. A ceramic fiber heater was positioned around the sleeve. The entire assembly was suspended within a 2 gallon stainless steel autoclave under nitrogen gas. A simplified drawing of the test assembly is shown in Figure 1. Inert gas pressure tests were performed using static pressure by pressurizing the portion of the tubing and sleeve below the membrane, i.e., forcing the membrane *onto* the seat of the tubing. For inert gas testing only, the upper (permeate) side of the membrane was left exposed to air and monitored for leaks by means of a bubbler. Pressure was stepped in approximately 50 psi increments with hold times of approximately 0.5 h between increments. For hot tests, heat up and cool down was performed at the rate of 120°C per hour while at a slight inert gas over pressure. Pressure was increased only after the unit had obtained target temperature. When the unit is completed, hydrogen flux measurements will be performed in a similar configuration, except that air will be totally excluded from the system and the reactor casing will be actively purged with nitrogen gas. The permeate side of the membrane will be swept with argon gas, and the effluent will be monitored with a gas chromatograph for hydrogen concentration.

Atomic Force Microscopic (AFM) images of the membrane were obtained using a Quesant Instrument Corporation AFM (Model-Resolver). X-ray photoelectron spectroscopy (XPS) spectra were recorded with a Physical Electronics model 548 XPS system. The binding energies were referenced to the C(1s) level at 284.6 eV for adventitious carbon. XPS data were obtained at various temperatures ranging from room temperature to 650°C. X-ray microanalysis was performed at room temperature and 575°C using a JOEL 840-A scanning electron microscopy equipped with a Noran Instruments Micro-Z energy dispersive spectrometer, which was interfaced to a Noran Instruments Voyager-4. Detector resolution, as referenced to the Manganese K α spectra line, was 148 eV.

RESULTS AND DISCUSSION

Cold membrane pressure tests were conducted using nitrogen and helium gases (separately) in the HTR unit. In each test, the ANL-1 disk membrane was pressurized in steps to 400 psig at ambient temperature. The membrane was held for approximately 0.5 h at each pressure and for 2 h at 400 psig. No leakage could be detected, either via a bubbler on the outlet side of the membrane, or via monitoring the pressure on the inlet side of the membrane. The pressure tests demonstrated that the membrane itself, as well as the ceramic-to-metal seal, was gas tight to 400 psig.

A hot membrane pressure test was conducted using nitrogen gas in the HTR unit. In this test, the ANL-1 disk membrane was heated to 800°C under a slight over pressure of nitrogen and held under these conditions for 17 h before pressure testing. During pressurization, no leakage could be detected up to and including 400 psig. At 450 psig, a small loss of pressure was observed together with bubble formation on the outlet side of the membrane. The leakage rate was measured at 1.6 mL/min at 450 psig. The leak persisted as the pressure was decreased in the same step wise fashion, although it slowly diminished in rate to 0.6 mL/min at 350 psig, and was undetectable at pressures below 200 psig. After decreasing to ambient pressure, the membrane was repressurized to 250 psig in the same step wise fashion and the leakage rate was confirmed. The membrane was again depressurized and cooled to ambient temperature. After cooling, the membrane was repressurized to 250 psig with cold nitrogen and the leakage rate was reconfirmed.

Following the hot membrane pressure test, visual inspection of the membrane revealed a powdery whitish coating on and around the membrane. Small areas of green discoloration were observed around the surface of the normally gray membrane. Some of the brazing material appeared to have migrated from around the edge of the membrane toward the center, moving a distance of approximately 0.5 mm. The braze migration had previously been observed during hot temperature-ambient pressure flux testing at ANL. Visual inspection under an optical microscope revealed cracks in the membrane surface along the perimeter of the disk, as well as cracks in the brazing material itself.

SEM/X-ray microanalysis was conducted to determine the changes in morphology, elemental distribution and compositional changes that occur to a fresh membrane upon heating. No major morphological changes were observed after heating the membrane from room temperature to 575°C. Elemental distribution was uniform and remained uniform following heating and hydrogen exposures at 575°C.

SEM examination of the membrane before testing showed an apparent two phase structure of mixed Ba-Ce-Y oxides (spinodal decomposition appearance in the back scattered electron images) decorated with 2 - 20 μm diameter sized nickel-rich nodules (Figure 2, left image). A similar image from the membrane after pressure testing is shown in Figure 2 (right image). The nickel rich nodules seem to have grown in size during exposure to the test conditions. The membrane surface also appeared to be covered by a film of some material on the side exposed to 450 psi nitrogen.

AFM was also utilized to determine both the surface morphology and the surface roughness. AFM images of the fresh membrane and the membrane after the pressure test with nitrogen are shown in Figure 3. The fresh membrane had structure containing nodules with an average surface height of 1.34 μm . The surface morphology changed after the pressure test. The original structure with nodules was not present after the pressure test and the average surface height was 1.89 μm . This change in the surface roughness and morphology could be due to the deposition of carbon and other materials during mounting of the membrane, the nitrogen pressure test, or other associated handling.

XPS was utilized to determine the elemental composition and oxidation states of elements at approximately the top 50 \AA of the surface of a fresh membrane upon heating. Ni 2p spectra of the fresh membrane at room temperature and 650°C are shown in Figure 4. At room temperature nickel was in the oxidized form and the intensity of the nickel peak was low. When the surface was heated up to 650°C, the intensity of the nickel peak increased substantially and the oxidation state of nickel changed to the metallic state. The ratios of Ni/Ba, Ni/Ce, and Ni/Y at the surface increased when the temperature was increased, but they decreased again when the surface was cooled back to room temperature. Thus, the nickel migrates to the surface and preferentially resides at the surface relative to the other elements at higher temperature. When the XPS analysis was performed at room temperature with the membrane after the pressure test, it was not possible to detect Ni, Ba, Ce, and Y on the surface. The intensity of the carbon peak was very high indicating that carbon may have been deposited on the surface during the pressure test. When the surface was heated to 300°C, the intensity of the carbon signal decreased by 33% and a small amount of yttrium was detected on the surface. When the surface was heated to 650°C, there was a 60% decrease in the amount of carbon, and it was possible to detect all the elements on the surface. The amounts of Ni and Y were higher on the surface relative to the other elements at 650°C. This differs from the observations made with the fresh membrane at 650°C in which the concentrations of barium and nickel were higher than those of the other elements.

CONCLUSION

The membrane and sealing methodology are impermeable to the inert test gases nitrogen and helium. In addition, both membrane and seal are structurally capable of withstanding a pressure differential of 400 psig, at least for the limited hold times employed in these tests. However, at 800°C, the membrane and seal would not withstand a pressure of 450 psig nitrogen and developed a leak. At this time, it is not known whether the failure was strictly a pressure effect, or if the elevated temperature and possible migration of some of the brazing material was involved. It is likely that exposing the membrane to atmospheric oxygen on the permeate side contributed to its demise. At high temperature, the membrane will also transfer oxygen, and the presence of what is probably oxide contamination around the membrane after the hot pressure test indicates that some degradation of the membrane and/or sealing materials may have occurred during the test. Both SEM and AFM indicated that the pressure tested membrane surface was coated with an impurity material, although it cannot be determined whether this occurred as a direct result of the pressure test or from other handling or exposure. XPS analysis indicates that significant elemental and oxidative changes occurred on the membrane surface upon heating. In particular, pools of metallic nickel migrated to the membrane surface at elevated temperature. The nickel "islands" may very well contribute to the

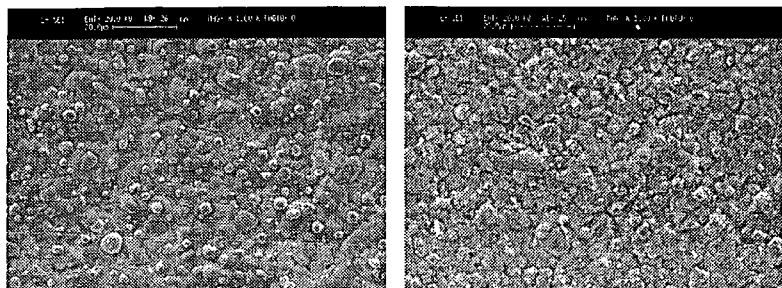
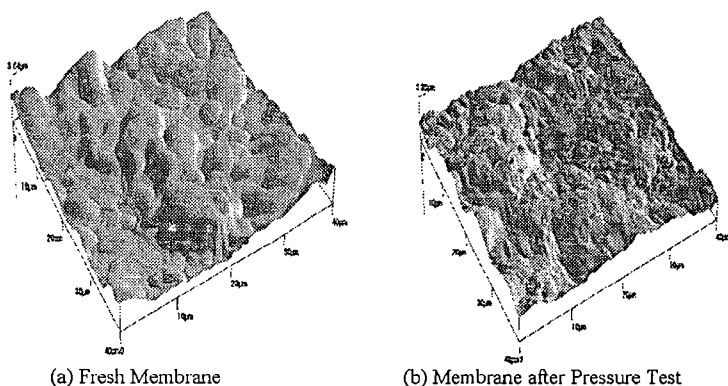


Figure 2: SEM images of the fresh membrane surface (left) and after exposure to 450 psig nitrogen at 800 °C. (right)

AFM Images of Fresh Membrane and after Nitrogen Pressure Test



(a) Fresh Membrane

(b) Membrane after Pressure Test

Figure 3: AFM Images of fresh membrane (left) and membrane after test (right)

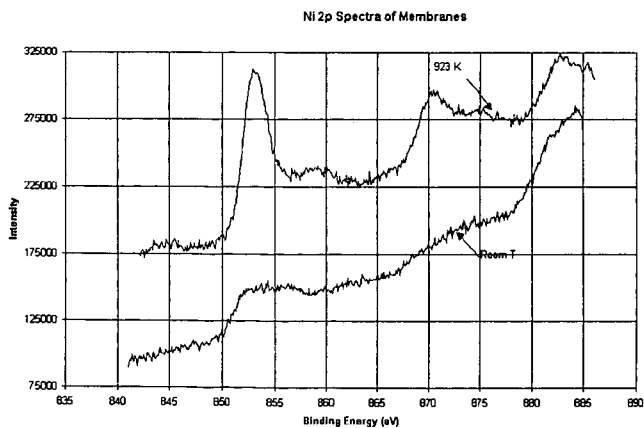


Figure 4: Ni 2p spectra of the fresh membrane at 650 C (top) and room temperature (bottom)

A MODEL OF A HIGH TEMPERATURE, HIGH PRESSURE WATER-GAS SHIFT TUBULAR MEMBRANE REACTOR

R.M. Enick and J. Hill

Department of Chemical and Petroleum Engineering, University of Pittsburgh
1249 Benedum Hall, Pittsburgh, PA, 15261

A. V. Cugini and K. S. Rothenberger (DOE); H.G. McIlvried (Burns and Roe Services)
Federal Energy Technology Center, U.S. Department of Energy
P.O. Box 10940, Pittsburgh, PA 15236-0940

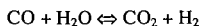
Keywords: membrane, hydrogen, water-gas shift

ABSTRACT

The reversible water-gas shift reaction is characterized by a very low equilibrium constant at elevated temperatures (>800°C). CO conversion at these temperatures is typically less than 40%. Higher conversions of CO can be achieved under these conditions only if one of the products, H₂ or CO₂, is removed from the reactor mixture. Several novel membranes are being developed for rapid H₂ diffusion/permeation and high H₂ selectivity at these high-temperature conditions. Therefore a model of a non-catalyzed tubular membrane reactor has been developed to evaluate the feasibility of achieving high levels of CO conversion at elevated temperatures via removal of H₂ from the reaction-side gas mixture along the length of a plug flow reactor. The model can provide membrane permeability values that must be achieved to attain desired levels of conversion in specified reactor geometry.

INTRODUCTION

The water-gas-shift reaction has been studied extensively as a basis for the production of hydrogen. In many applications, including ammonia synthesis or fuel reforming for fuel cells, the maximum acceptable level of CO in hydrogen is in the parts per million range. The water-gas shift reaction can also take place in other processes where CO and H₂O are present, such as methanol synthesis and supercritical water oxidation of organic compounds.



1

This reaction has no change in the number of moles (or the volume) as the reaction proceeds, therefore the equilibrium conversion is not affected by pressure. Side reactions associated with the water-gas-shift reaction are usually not significant. The equilibrium constant for this exothermic reaction (K, which can be expressed in terms of the concentrations of the reactants and products, Eq. 2) decreases with temperature. For example, the value of K decreases from 4523 at 366.5 K (93.3°C, 200°F) to 0.47 at 1366.5 K (1093.3°C, 2000°F).

$$K = \frac{([\text{CO}_2][\text{H}_2])}{([\text{CO}][\text{H}_2\text{O}]})$$

2

Therefore, conversion of CO to CO₂ (low concentrations of CO and H₂O, high concentrations of CO₂ and H₂, high values of K) is favored at low temperature⁽¹⁾. Most heterogeneous catalysis studies of the water-gas shift reaction have been conducted at temperatures less than 450°C. Examples of commercial water-gas shift catalysts include Fe₃O₄-Cr₂O₃ and CuZnO/Al₂O₃⁽²⁾. The kinetics associated with these catalysts can be adequately described with pseudo-first order or power law kinetics⁽²⁾. Another study of the stationary and transient kinetics of this reaction⁽³⁾ indicates that various mechanisms and kinetic expressions have been proposed for the water-gas shift, and that Langmuir-Hinshelwood and power-law kinetic models are adequate. The water-gas shift reaction also occurs in some processes that do not employ catalysts. For example, the supercritical water oxidation of organic wastes (typically conducted at 400-550°C, 200-300 bar) typically does not employ a catalyst because of the rapid destruction rates that are achieved. The very high rate of the water-gas shift reaction observed in this system^(4,5,6) is attributed to the formation of "cages" of water about the reactants under supercritical conditions and very high water concentrations.

There is relatively little information on the kinetics of the water-gas shift reaction at elevated temperatures (>600°C). This can be primarily attributed to the diminished value of K, which would limit CO conversion to unacceptably low levels. Catalysts are typically not used at elevated temperatures because of the rapid rate of the non-catalyzed reaction and the difficulty of identifying a catalyst that would be stable at these extreme conditions. A study of the opposing reactions of the water-gas shift reaction was conducted at extremely high temperatures and low pressure⁽⁷⁾ (800-1100°C, 1 bar). No catalyst was employed. Power-law kinetic expressions

developed for the forward and reverse reactions were substantially in agreement with a homogeneous chain mechanism. Despite the rapid attainment of equilibrium conversions without a catalyst, the ability to convert high temperature (800-1000° C) CO-rich combustion gases into hydrogen fuel via the water-gas shift reaction is limited by the low equilibrium conversions of CO.

It has long been recognized that high levels of conversion in equilibrium-limited reactions can be achieved only if one or more of the products can be simultaneously extracted during the reaction. (For a given value of K in Eq. 2, if the concentration of either CO_2 or H_2 is reduced, the concentrations of CO and H_2O must also decrease, thereby increasing conversion.) For example, a method for producing H_2 via the water-gas shift reaction with carbon dioxide removal was recently demonstrated⁽⁸⁾. In this study, a calcium-based sorbent was introduced to a non-catalyzed reactor operating in the 500-600°C temperature range. The CO_2 product reacted with the sorbent and formed calcium carbonate, diminishing the gas phase concentration of CO_2 and increasing CO conversion. Several research groups have recently developed hydrogen-permeable membranes that might also be used in a different approach to increasing CO conversion. The use of these membranes in a plug flow reactor would result in the removal of hydrogen from the reaction mixture, leading to an increase in CO conversion. Several types of membranes are now under development. Los Alamos National Laboratory has fabricated composite Pd/Ta membranes using vapor deposition techniques⁽⁹⁾. Measurements in the 300-400°C range indicate that the pressure-dependence of the gas flux is not proportional to $\Delta(P_{\text{H}_2})^{0.5}$ as in the case with membranes that are rate-limited by bulk diffusion. This implies that surface effects are significant in the determination of hydrogen flux. Argonne National Laboratory is developing proton-conducting ceramic membranes. These dense ceramic membranes are fabricated from mixed protonic/electronic conductors and have been tested at 800°C. Their hydrogen selectivity is very high because they do not have interconnected pores, and the only species that pass through them are those that participate in proton conduction⁽¹⁰⁾ (e.g. hydrogen). Inorganic membranes, composed of ceramics developed by Oak Ridge National Laboratory⁽¹²⁾, have interstitial pores with diameters as small as 5 angstroms and act as molecular sieves, have been tested at temperatures less than 600°C. An assessment of a conceptual plant that produces hydrogen from coal using these inorganic membranes⁽¹¹⁾ was recently completed.

OBJECTIVE

The goal of this investigation is to develop a model of a tubular, plug-flow, non-catalyzed, membrane reactor for the high temperature, high pressure water-gas shift reactor. This model will be used to assess the viability of obtaining a high purity hydrogen product from synthesis gas. Specifically, it will be used to estimate the surface area of the membrane required to achieve a desired level of CO conversion or hydrogen recovery. Alternately, it can be used to provide estimates of the hydrogen permeability a membrane must exhibit to attain a specified CO conversion or H_2 recovery in a reactor with a specified membrane area. This information, in conjunction with cost data for the membranes, can then be used to evaluate the economic feasibility of the process. A model of a reactor with hydrogen-permeable membranes has been previously developed⁽¹³⁾ for CO_2 control in IGCC systems using water-gas shift integrated with H_2/CO_2 separation. This system employed microporous ceramic membranes, Fe-Cr and Pt/ZrO₂ catalysts, maximum pressure of 70 bar, maximum pressure drop across the wall of the membrane of 25 bar, and temperatures up to 400°C. Another water-gas shift membrane reactor model was developed for a Fe-Cr catalyzed reactor operating at 400°C and low pressures with a Pd membrane⁽¹⁴⁾. The model developed in this work will focus on a higher temperature (>800°C), high pressure (25-50 bar), high pressure drop (up to 50 bar), non-catalyzed tubular membrane reactor with either Pd/Ta composite membranes, proton conducting dense ceramic membranes, or microporous ceramic diffusion membranes.

MODEL DESCRIPTION

The basis of the model is a tubular membrane located within a coaxial cylindrical shell. The feed gases are introduced on the shell-side (reaction-side, annular-side, retentate-side, raffinate-side) of the reactor. As the reaction proceeds, hydrogen will permeate the membrane if the concentration of the hydrogen on the reaction-side (shell-side) exceeds the concentration on the tube-side (permeate-side). As the reaction gases proceed down the length of the reactor, hydrogen will continue to permeate the membrane if the partial pressure of hydrogen on the reaction side exceeds the permeate hydrogen partial pressure, increasing the conversion of the CO . The CO_2 -rich retentate exits the reactor on the shell-side. A low-pressure, high-purity hydrogen permeate stream is recovered from the tube-side. It is desirable not use a sweep gas to avoid the need to for a subsequent hydrogen-sweep gas separation unit. This will result in a substantial pressure drop across the wall of the membrane, however. The basic design equations for a tubular, plug flow reactor were incorporated into the model⁽¹⁵⁾. The model predicts the

performance of the reactor under steady-state isothermal or adiabatic conditions. The adiabatic model accounts for the heat of reaction being transferred to the reaction gases and the permeate. The reactants and products are assumed to behave as ideal gases. The pressure drop along the length of the reactor is assumed to be negligible for both the retentate-side and the permeate-side of the reactor. Published correlations for $K^{(1,13)}$ can be used for pseudo-first order or power-law kinetic expressions that may include the equilibrium constant. The low pressure, high temperature (800-1100°C) results of Graven and Long⁽⁷⁾ are used to model the reaction kinetics. (During this investigation, more accurate rate expressions for the water-gas shift reaction at elevated temperature *and* pressure will be determined.) The appropriate expressions for the permeation of hydrogen in the dense, proton-conducting ceramic membrane or expressions for permeability of H₂, CO, and CO₂ (i.e. membrane selectivity) in the microporous metal or ceramic membranes^(9,12) are incorporated to account for the flow of gases through the membrane. The flux of hydrogen through these membranes, R_{H_2} , is proportional to the "permeability" of the membrane, k_{H_2} and inversely proportional to the membrane thickness, t_m . The driving force for the hydrogen flux is related to the hydrogen partial pressure or molar concentration of hydrogen, C_{H_2} , raised to the exponent n (the units of k are dependent upon the value of n).

$$R_{H_2} = A_m k_{H_2} (C_{H_2,retentate}^n - C_{H_2,permeate}^n) / t_m \quad 3$$

If transport through a membrane with surface reaction and ionic transport is limited by surface reactions, $n = 1$. If flux through the membrane is diffusion-limited, $n = 0.5$. Intermediate values of n ($0.5 < n < 1$) have also been reported⁽¹⁴⁾. During this investigation, values of n at elevated temperature and pressure will be determined for each membrane.

RESULTS

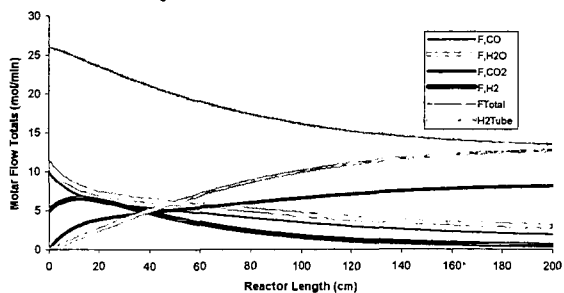
The following conditions are associated with a conceptual coal processing plant for producing hydrogen while recovering carbon dioxide⁽¹⁶⁾. Because membrane parameters have not yet been established at these conditions, a high value of permeability was selected to clearly illustrate the effect of hydrogen removal on conversion.

Catalyst	No catalyst used at this high temperature
Mode of Operation	Isothermal
Temperature	850°C
Reaction-Side	Annular-side, Shell-side
Pressure on reaction-side	27.572 bar
Pressure on tube-side	0.9869 bar
Reactor length	200 cm
Reactor (shell) diameter	4.0 cm
Tube-side sweep gas	None
Membrane	Proton Transport
Membrane diameter	2.0 cm
Permeable gases	Hydrogen Only
Membrane thickness	0.1 cm (1 mm)
Membrane driving force	$C_{H_2,retentate}^{0.5} - C_{H_2,permeate}^{0.5}$
Membrane permeability	$10 \text{ cm}^2 / (\text{min}(\text{mol}/\text{liter}))^{0.5}$
CO inlet flow rate	10 gmol/min
Steam inlet flow rate	11 gmol/min
Hydrogen inlet flow rate	5.0 gmol/min
Reaction kinetics	Reference 7

Table 1. Model Conditions and Assumptions Used in the Example Problem

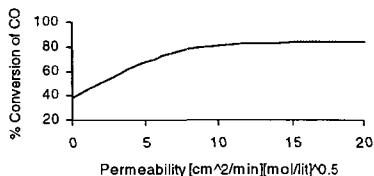
Conversion of CO *in the absence of a membrane* is 38.2% at 850° C, which is 99% of the equilibrium value. The *membrane reactor* profiles of molar flow rates of the components are illustrated in Figure 1. As the CO and H₂O react near the inlet, their molar flow rates decrease as the hydrogen flow rate on the reactor-side increases. The CO and H₂O continue to decrease as the CO₂ concentration increases along the length of the reactor. The hydrogen also begins to permeate the membrane because the concentration on the annular-side is greater than the hydrogen concentration on the tube side. Because the rate of hydrogen generation is initially greater than the rate of permeation, the hydrogen flow rate on the annular-side increases from 5 to 7 mol/min along the length of the reactor between 0 - 15 cm.

Figure 1. Flow Rate Profiles within the Membrane Reactor



After 15 cm, the rate of permeation exceeds the generation due to reaction and the flow rate of hydrogen on the annular-side decreases. As the end of the reactor is approached, the permeate flow rate of hydrogen approaches a limiting value because the concentration of the hydrogen on the annular-side (raffinate), 0.013 mol H₂/liter is approximately equal to the concentration on the tube-side (permeate), 0.011 mol H₂/liter. CO conversion has increased to 81%. The permeability of the membrane has a significant effect on the performance of the reactor. Figure 2 illustrates the conversion of CO that can be achieved in this particular membrane reactor as a function of the membrane permeability. For a permeability of 0 (impermeable membrane), the conversion is 38.5%. As the permeability increases beyond 10 (cm²/min)(mol/liter)^{0.5}, the limiting conversion of 84% is attained. To achieve comparable conversions with membranes of lower permeability, the length of the membrane tube must increase to provide more area for the hydrogen removal, increasing the membrane reactor size and cost.

Figure 2. Effect of Membrane Permeability on CO Conversion



CONCLUSIONS

A model of a tubular, plug flow membrane reactor has been developed for evaluating the effect of hydrogen permeable membranes on the conversion of CO in the water-gas shift reaction. The model has been developed for very high temperature systems (>800°C) that do not employ a catalyst. The model can incorporate hydrogen permeation/diffusion models that are appropriate for novel membranes currently being developed at several national laboratories. This tool will be used to assess the levels of CO conversion, H₂ purity and recovery, and CO₂-rich retentate flow rate and recovery that can be realized in a reactor of specified geometry if these novel membranes are incorporated. The model can also be used to provide "targets" for hydrogen permeability that would be required to make this technology economically feasible.

REFERENCES

1. Benson, H. E.; Processing of Gasification Products; Ch. 25 in *Chemistry of Coal Utilization*, Elliot, M., ed.; John Wiley and Sons; New York, NY, 1981.
2. Keiski, R.I.; Desponds, O.; Chang, Y.; Somorjai, G.A.; Kinetics of the Water-Gas Shift Reaction Over Several Alkane Activation and Water-Gas Shift Catalysts; *Applied Catalysis A: General*, 101 (1993) 317-338.
3. Keiski, R.; Salmi, T.; Niemisto, P.; Ainassaari, J.; Pohjola, V.J.; Stationary and Transient Kinetics of the High Temperature Water-Gas Shift Reaction; *Applied Catalysis A: General*, 137 (1996) 349-370.
4. Helling, R.K.; Tester, J.W.; Oxidation Kinetics of Carbon Monoxide in Supercritical Water; *Energy and Fuels*, 1 (1987) 417-423.

5. Holgate, H.R.; Webley, P.A.; Tester, J.W.; CO in Supercritical Water: The Effects of Heat Transfer and the Water-Gas Shift Reaction on Observed Kinetics; *Energy & Fuels*, 6 (1992) 586-597.
6. Rice, S.F., Steeper, R. R.; Aiken, J. D.; Water Density Effects on Homogeneous Water-Gas Shift Reaction Kinetics; *J. Phys. Chem. A*, 102(16) (1998), 2673-2678.
7. Graven, W. M.; Long, F. J.; Kinetics and Mechanisms of the Two Opposing Reactions of the Equilibrium $\text{CO} + \text{H}_2\text{O} = \text{CO}_2 + \text{H}_2$; *J. Amer. Chem. Soc.* 76 (1954) 2602.
8. Han, C.; Harrison, D.P.; Simultaneous Shift Reaction and Carbon Dioxide Separation for the Direct production of Hydrogen; *Chemical Eng. Sc.* 49(24B) (1994) 5875-5883.
9. Peachey, N. M.; Snow, R. C.; Dye, R. C.; Composite Pd/Ta Metal membranes for Hydrogen Separation; *Journal of Membrane Sciences* (in print).
10. Balachandran, U.; Guan, J.; Dorris, S. E.; Liu, M.; Development of Proton-Conducting Membranes for Separating hydrogen from Gas Mixtures; extended abstract of presentation at the AIChE 1998 Spring Meeting, New Orleans, LA, March 8-12, 1998.
11. Parsons Infrastructure and Technology Group; Decarbonized Fuel Plants Utilizing Inorganic Membranes for Hydrogen Separation; presented at the 12th Annual Conference of Fossil Energy Materials, May 12-14, 1998, Knoxville, Tennessee.
12. Fain, D. E.; Roetger, G. E.; Coal Gas Cleaning and Purification with Inorganic Membranes; *Trans. of the ASME Journal of Engineering for Gas Turbines and Power*, 115 (July 1993) 628-633.
13. Netherlands Energy Research Foundation; Combined Cycle Project – IGCC with CO₂ Removal Project Area – An Attractive Option for CO₂ Control in IGCC Systems: Water Gas Shift with Integrated Hydrogen/Carbon Dioxide Separation (WIHYS) Process – Phase 1 Proof of Principle; Alderliesten, P. T. and Bracht, M., eds.; Contract JOU2-CT92-0158, Final Report (1995).
14. Uemiya, S.; Sato, N.; Ando, H.; Kikuchi, E.; The Water Gas Shift Reaction Assisted by a Palladium Membrane Reactor; *Ind. Eng. Chem. Res.* 30 (1991) 585-589.
15. Fogler, H. S.; *Elements of Chemical Reaction Engineering*, Second Edition; Prentice Hall, Englewood Cliffs, NJ (1992).
16. Parsons Infrastructure and Technology Group; Decarbonized Fuel Plants for Vision 21 Applications, WYODAK Coal Substitution; DOE/FETC Report, April 13, 1999.

A FIRST-PRINCIPLES STUDY OF HYDROGEN-METAL INTERACTION IN VARIOUS METALS

Yasuharu Yokoi, Tsutomu Seki and Isamu Yasuda
Fundamental Technology Research Laboratory, Tokyo Gas Co., Ltd.
Tokyo, 105-0023, Japan

KEYWORDS: Hydrogen Separation Membrane, Hydrogen Dissolution, First-Principles Calculations

INTRODUCTION

Hydrogen-metal systems have been the subject of numerous investigations because of their potential applications such as hydrogen separation membranes and hydrogen storage alloys. As for the hydrogen separation membranes, palladium membranes are principally 100% selective for hydrogen separation [1]. Steam reformers equipped with the Pd membranes were developed and have been tested in Japan to produce pure hydrogen from city gas [2]. The performance of this type of membrane reformer directly depends on hydrogen permeability of the membranes. This has led us to develop the membranes with higher hydrogen permeability.

One of the effective approaches to increase the hydrogen permeability of the membranes is alloying. The alloying of Pd with silver is effective to enhance the hydrogen dissolution and thereby to increase the hydrogen permeability of the membrane [1]. The Ag-alloying is also effective to depress the α - β miscibility gap to well below room temperature, although it lies below 300°C and pressures below 20 atmosphere in Pd-H system without Ag-alloying. The β phase has a considerably expanded lattice compared with the α phase; for example, a H/Pd ratio of 0.5 results in an expansion of about 10% by volume, which should cause mechanical damages to the membranes after dissolution/evolution cycles during the operation of the reformer.

In the present work, we have applied first-principles calculations to the study of hydrogen-metal interactions in various metals and alloys. Our goal is to develop the membranes with higher hydrogen permeability than the conventional Pd/Ag alloys and mechanical reliability under the practical operating conditions. Our computations have focused on the heat of hydrogen dissolution and the hydrogen-induced lattice expansion that should be correlated with the hydrogen permeability and the mechanical reliability.

MATERIALS AND METHODS

All calculations in this study were implemented with the code CASTEP [3]. In the calculations, the valence electron orbitals are expanded in plane waves, whereas the core electrons are described by ultrasoft pseudopotentials. In the present investigation we selected an energy cut-off of 380 eV. The energy functional consists of the gradient-corrected local density approximation. Figure 1 illustrates the periodic supercell models for hydrogen occupation at interstitial sites in bcc (V, Nb, Ta, Cr, Mo and W) and fcc (Ni, Pd, Pt, Cu, Ag and Au) metals. The models consist of four metal atoms and one hydrogen atom. The initial positions of metal atoms and the initial values of lattice constants were those from experimental values of pure metals. The initial position of the hydrogen atom was either the octahedral site (O-site) or the tetrahedral site (T-site). The final geometry was obtained when the calculated forces acting on the atoms and stress on the supercell became smaller than the threshold values. To evaluate the relative expansion of the lattice induced by the interstitial hydrogen, geometry optimizations of the pure metals were also employed. The heat of hydrogen dissolution was calculated according to the following expression: $E_{\text{diss}} = E_{\text{(H,M+H)}} - E_{\text{H,M}} - 1/2 E_{\text{H}_2}$, where $E_{\text{(H,M+H)}}$ is the total energy of the optimized model for the hydrogen-metal system, $E_{\text{H,M}}$ is of the pure metal, and E_{H_2} is of the hydrogen molecule. The optimized bond length of H-H bond of the hydrogen molecule was confirmed to be nearly equal to the experimental value.

RESULTS

From the geometry optimization for the pure metals, all optimized fcc and bcc cells were nearly cubic. The lattice constants of the optimized cells are plotted versus the experimental values in Figure 2.

The O-site occupation for the bcc metals was confirmed not to be a stationary point on the potential energy surface (PES) except for V and Mo, whereas the T-site occupation was found to be the stationary point. As for the fcc metals, both interstitial sites were confirmed as the stationary point.

All optimized supercells for the hydrogen-metal systems were found to expand in comparison with pure metals. The optimized fcc cells for both the O- and T-site occupation maintained cubic. The average percentage of the lattice expansion for the O- and T-site occupation was 1.5% and 2.5%, respectively. The optimized bcc cells, on the other hand, were distorted. The average percentage for the O- and T-site occupation was 1.5% and 1.7%, respectively. Figure 3 shows the changes in the lattice constants for Pd and V as the representative of the fcc and bcc metals. The hydrogen occupation at the O-site in V was found to induce the lattice expansion of about 4.7% in the direction of the c-axis, in spite of small contraction of the lattice in the directions of the a- and b-axis. In the case of Pd, the relationship between the lattice expansion and the hydrogen concentration was also examined. The models used in this examination were constructed by adding hydrogen atoms 'one by one' to the original supercell model. The volume of the optimized fcc cells (in Å³) was 59.82, 62.17, 64.29, 66.04 and 67.82 for H/Pd ratio of 0, 0.25, 0.5, 0.75 and 1, respectively.

Figure 4 shows E_{int} for the fcc metals. As for Ni and Pd, the O-site occupation was found to be more stable than the T-site occupation, whereas the T-site occupation was found to be more stable for Pt, Cu, Ag and Au. Figure 5 shows E_{int} for the bcc metals. The T-site was suggested to be the stable interstitial hydrogen site for all bcc metals evaluated in this study.

To study the effects of alloying of Pd with Ag on the hydrogen solubility, E_{int} for Pd/Ag alloy was evaluated in the same manner. Figure 6(a) illustrates the supercells for the Pd/Ag alloy. These models consist of three Pd atoms, one Ag atom and one hydrogen atom. There are two distinguishable O-sites in these models; one is the center of the octahedron consisting of four Pd atoms and two Ag atoms (O_{c} -site), and the other is the center of the octahedron consisting of six Pd atoms (O_{p} -site). The calculated E_{int} is shown in Figure 6(b) in comparison with that of the O-site occupation for the pure Pd. The value of $|1 - E_{\text{int}}|$ of the O_{p} -site occupation was larger, whereas that of the O_{c} -site occupation was smaller, than that of the O-site occupation for the pure Pd.

DISCUSSION

As for the optimized lattice constants for the pure metals and the optimized bond length of H-H bond of hydrogen molecule, the agreement between the calculations and the experiments is quite satisfactory. This suggests that the calculated value of the lattice constants of the hydrogen-metal systems and the calculated relative expansion induced by the interstitial hydrogen are reliable. In this study we have estimated the lattice expansion of pure Pd induced by the hydrogen occupation at the interstitial sites; for example, a H/Pd ratio of 0.5 results in an expansion of 7.5% by volume. An experimental value corresponding to this estimation has been reported to be about 10% in the literature [1]. We have also evaluated the lattice expansion of V. From the result shown in Figure 3, the O-site occupation in V was found to induce the lattice expansion of 4.7% in the direction of the c-axis. This is qualitatively in line with the experimental fact that the lattice is expanded in the direction of the c-axis about 10% [4].

Figure 4 shows that the hydrogen occupation at both interstitial sites was found to be stable for the fcc metals. The O-site occupation is more stable than the T-site occupation for Ni and Pd. This suggests that the O-site occupation should be observed experimentally. As has been expected from the results, the O-site occupation for Ni and Pd has been experimentally observed [4,5]. As for the other fcc metals: Pt, Cu, Ag and Au, the T-site occupation is more stable than the O-site occupation. This suggests that the T-site occupation in these fcc metals should be experimentally observed, although this has not been reported yet to the best of our knowledge. On the other hand, the T-site occupation is stable for the bcc metals shown in Figure 5. As has been expected from the results, the preference of T-site occupation has already been reported for these bcc metals [4,5]. As for V, the O-site occupation, which occurred with the expansion of about 10% in the direction of the c-axis, has been also reported [6]. This also agrees with the present calculation result that the O-site occupation in V is stable as well as the T-site occupation shown in Figure 5 and the O-site occupation induces the lattice expansion with the distortion shown in Figure 3.

As the experimental heat of hydrogen dissolution (ΔH_1) plotted on Figure 4 and Figure 5 were estimated by applying Sieverts's law, the values may have large errors in high hydrogen concentration (far from $H/M = 0$) ranges [7]. Nevertheless the calculated E_{abs} qualitatively correlated with the experimental ΔH_1 . Before turning to a closer examination of the alloying of Pd with Ag, it is desirable to discuss the deviation of the calculated E_{abs} from the experimental ΔH_1 for Pd. The deviation for Pd shown in Figure 4 is somewhat larger than that of V, Nb and Ta, which are exothermic for the hydrogen dissolution as well as Pd. The dependence of ΔH_1 for Pd on hydrogen concentration has been experimentally studied in the previous literature [4]. In this literature, the experimental heat of hydrogen dissolution for Pd at $H/Pd = 0.25$, which is equal to the H/M ratio of the calculated model shown in Figure 1, have been reported as about -20 kJ/mol. The deviation of E_{abs} from the experimental value reduced by the correction for the hydrogen concentration. The calculated E_{abs} is believed to be reliable enough to discuss the qualitative difference in the heat of hydrogen dissolution.

The hydrogen permeability of metals is proportional to their solubility and diffusion coefficient of hydrogen. Since the hydrogen solubility increases with $-\Delta H_1$, increasing of $-\Delta H_1$ is effective to improve the hydrogen permeability. It has been reported that the high hydrogen solubility in Pd/Ag alloys leads to high permeability in the 20 to 25% Ag range [1]. According to this literature [1], about 150 mg of hydrogen can dissolve in 100g of the Pd/Ag alloys at 1 atmosphere and 183°C. This H/M ratio is below 0.25. As the hydrogen dissolution in Pd/Ag alloys is exothermic, the H/M ratio decreases with the increase in temperature. The steam reformers are usually operated above 500°C [2], then the hydrogen diffusion membranes made of the Pd/Ag alloys have hydrogen of the H/M ratio below 0.25. The simple calculation models for 25% Ag - Pd shown in Figure 6(a) have three O_{c} -sites and one O_{p} -site. Since the O_{p} -site occupation has been found to be more stable than the O_{c} -site occupation in the present study, hydrogen is suggested to occupy only the O_{p} -sites below 0.25 of the H/M ratio. As shown in Figure 6(b), the $-\Delta H_1$ for the O_{p} -site occupation is larger than that for the O_{c} -site occupation for in pure Pd. In this way, it suggests that the $-\Delta H_1$ of the Pd/Ag alloys is greater than that of the pure Pd in the low hydrogen concentration ranges. This is the reason for the high hydrogen solubility in the Pd/Ag alloys in the higher temperatures and contributes to high permeability. Hydrogen begins to occupy the O_{c} -sites with the increase in the H/M ratio. As shown in Figure 6(b), the $-\Delta H_1$ for the O_{c} -site occupation is smaller than that for the O_{p} -site occupation as well as for the O -site occupation for in pure Pd. This is the mechanism for the depression of the hydrogen dissolution at lower temperatures.

CONCLUSIONS

Interactions between various metals and hydrogen have been studied by using a periodic density functional theory at a generalized gradient approximation. Geometry optimizations were carried out for lattice constants of various metal-hydrogen systems as well as for stable sites of interstitial hydrogen. Both tetrahedral site (4-coordinated sites) hydrogen and octahedral site (6-coordinated sites) hydrogen was found to be stable and to induce lattice expansion. Reported experimental heat of hydrogen dissolution has been well reproduced from the calculated total energies. Similar estimations were carried out for Pd/Ag alloys that are used as hydrogen permeable membranes in hydrogen production. The theoretical calculations suggested that Ag-alloying enhance hydrogen dissolution in Pd. These can explain fairly well the increased hydrogen permeability by alloying Ag into Pd.

REFERENCES

1. A. G. Knapton, *Platinum Metals Review*, 21 (1977) 44.
2. Y. Ohta, M. Gondaira, K. Kobayashi, Y. Fujimoto and K. Kuroda, in *Extended Abstracts of AIChE Annual Meeting*, 1994, San Francisco.
3. The CASTEP code, originally written by M. C. Payne, is marketed by Molecular Simulations, Inc.
4. Y. Fukai, "*The Metal Hydrogen System*", Springer, Series in Materials Science Vol. 21 (1993) Chap. 4.
5. D. Richter, R. Hempelmann and R.C. Bowman "*Hydrogen in Intermetallic Compounds II : Surface and Dynamic Properties.Applications*", Springer, Topics in Applied Physics, Vol. 67 (1992) Chap. 3.
6. I. Okuda, H. Asano and M. Hirabayashi, *Trans. JIM*, 21 (1980) 89.
7. H.M. Lee, *Metall. Trans.*, 7A (1976) 431.

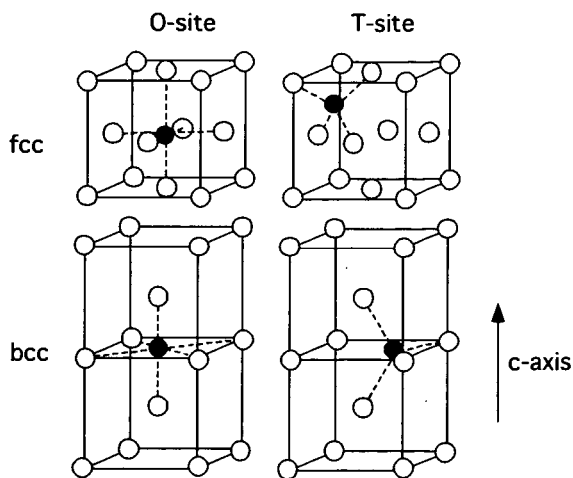


Figure 1. Periodic supercell models for hydrogen occupation at interstitial sites in bcc and fcc metals. Closed circles: Hydrogen; Open circles: Metal.

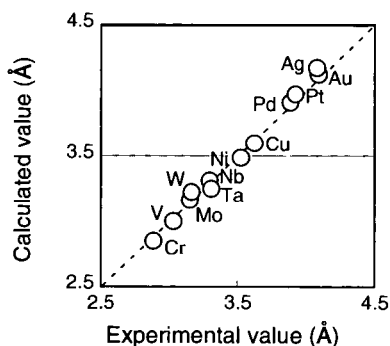


Figure 2. Correlation between calculations and experiments for lattice constants of various metals.

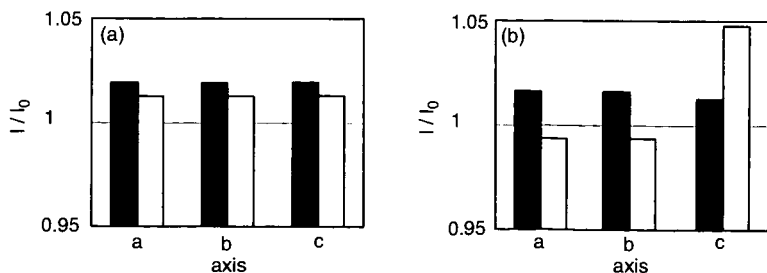


Figure 3. Relative expansion of the lattice constants by the interstitial hydrogen. (a) Pd, (b) V, Closed bars: T-site occupation; Open bars: O-site occupation.

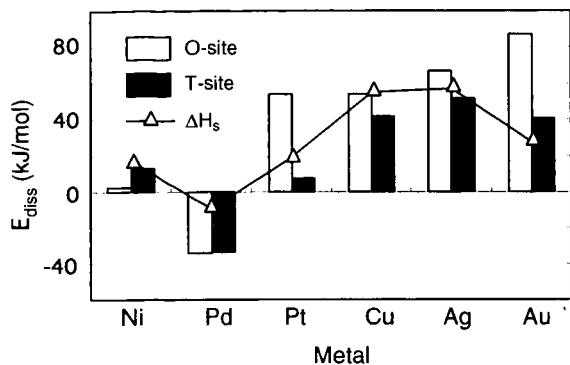


Figure 4. Calculated E_{diss} for various fcc metals in comparison with experimental ΔH_s .

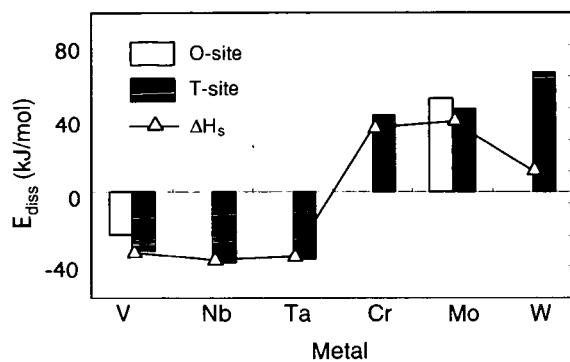


Figure 5. Calculated E_{diss} for various bcc metals in comparison with experimental ΔH_s . The O-site occupation is not stable for Nb, Ta, Cr and W.

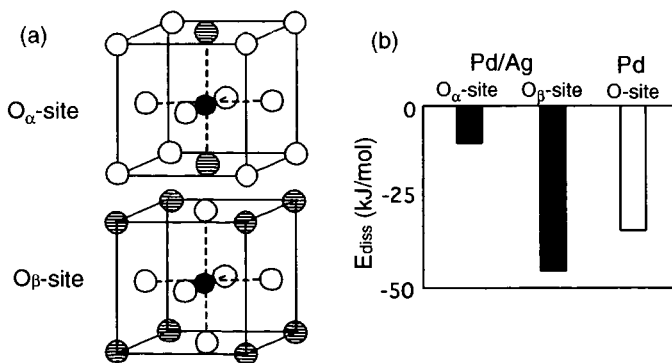


Figure 6. Relative expansion of the lattice constants by the interstitial hydrogen. (a) Interstitial O-sites in the Pd/Ag alloy model, shaded circles: Ag, (b) calculated E_{diss} .

Hydrogen Separation using Ternary Polymer Blend Compared with the Inorganic High Surface Area Zeolite Materials

Kal R. Sharma Ph.D. PE

Center for Computational Statistics, MS 4A7, Department of Applied and Engineering Statistics, George Mason University, Fairfax, VA 22030-4444

The gas separation of hydrogen by semi-permeable membrane technology can be achieved by the use of ternary, miscible polymer blend of tetramethylhexafluorobisphenol-A-polycarbonate, polyamide and aromatic polyether ketone. Simultaneous increases in permeability and permselectivity can be achieved. Mesoscopic simulations were performed to understand the permselectivity in porous inorganic high surface area materials such as zeolite. This was compared with the polymeric membrane technology. The inorganic materials has well controlled and tailored porosity. In situ separation of hydrogen can be used in fuel cells, underwater gill applications, chemical and biological sensing, neutralization devices, encapsulation applications, encryption of acoustic signature of structures. The permselectivity issues in zeolite material is discussed. Permeability as a function of pore size distribution and tortuosity, is presented for the inorganic high surface area material.

A robust design for membrane using polymeric system that acts as semipermeable membrane for purification of Hydrogen, Methane, Nitrogen and Carbon dioxide from process stream subsequent to cooling the gases was developed. The performance of the process for the purification using the membrane technology was appraised. A mathematical model is proposed for the permeability and permselectivity in polymeric membrane.

Systematic variations of the chemical structure can be used to achieve simultaneous increases in permeability and permselectivity. Systematic variations in the chemical structure and its effect on gas permeability and chain packing in substituted polycarbonates, for example, are proposed in the design of the membrane technology for separating hydrogen from a process stream. This process stream subsequent to cooling, may contain Hydrogen, Carbon Monoxide, Carbon Dioxide and Hydrocarbons. The membrane is proposed to be formulated from a ternary blend of miscible polymers or polymeric alloy. The permeability of Hydrogen can be written as a simple product of an average diffusivity, D , and an effective solubility, S , of the penetrant in the polymer matrix:

$$P = D * S \quad (1)$$

For conditions of negligible downstream pressure, the solubility coefficient, S , is equivalent to the secant slope of the gas sorption isotherm evaluated at upstream conditions. The average diffusivity, D , provides a measure of the effective mobility of the penetrant in the polymer matrix between the conditions at the upstream and downstream side of the film. The second key index of the performance of the membrane material is the separation factor, or permselectivity,

$$\alpha_{A/B...D} = P_A / \Sigma P_{A...D} \quad (2)$$

The ideal separation factor, by combining the two equations is,

$$\alpha_{A/B...D} = \{D_A S_A / \Sigma D_{A...D} S_{A...D}\} \quad (3)$$

where $D_A / \Sigma D_{A...D}$ is the diffusivity selectivity, and $S_A / S_{A...D}$ is the solubility selectivity. The solubility selectivity is determined by the differences in condensibility of the 5 penetrants and by their interactions with the membrane material. The diffusivity selectivity is based on the inherent ability of polymer matrices to function as size and shape selective media through segmental mobility and intersegmental packing factors. The glassy state of the polymeric system can have an influence on the porosity of the macrostructure. Typically there is a tradeoff between permeability and permselectivity. Exceptions are the polyimides, sulfonated aromatic polyether ketones, polyamides etc. Certain structural variations can substantially increase the permeability and permselectivity. Some of the design factors in material selection for the membrane technology include substitutions which inhibit chain packing, rotational mobility, miscibility, compatibility and compatibilizability.

Ternary miscible blends can increase the permeability and the glassy state can improve permselectivity. Chain packing inhibition can increase the permeability and decrease in permselectivity. Incompatibility can decrease the permselectivity and increase the permeability. An optimal can be found by simultaneously inhibiting chain packing and rotational mobility about flexible linkages which can lead to increases in both permeability and permselectivity. Decrease of mobile linkages can increase the permselectivity without decrease in permeability. Compatibilized alloy can improve the chemical stability of the membrane. Hydrophobicity can be increased to prevent the damage from condensibles by configurational manipulation of the polymer backbone. For example, Tetramethylhexafluorobisphenol-A polycarbonate blended with polyamide or with aromatic polyether ketone is an interesting system for the membrane material. When selecting a blend vs copolymer the commercial availability and molecular weight ranges of the products are to be considered carefully. Reversible sorption of the gas can be effected by alloying a salt into the system.

The morphologies of the miscible, immiscible and partially miscible polymer blends are another consideration in the membrane material selection. In a immiscible blend, two phases are present: 1) discrete phase (domain) which is lower in concentration and 2) continuous phase, which is higher in concentration. The miscible polymer blends exhibit single phase morphology. Partially miscible polymer blends may form completely miscible blend at a different concentration. The two phases in partially miscible blends may not have well-defined boundary. Each component of the blend penetrates the other phase at a molecular level. The molecular mixing that occurs at the interface of a partially miscible two-phase blend can stabilize the domains and improve interfacial adhesion.

A multicolumn membrane separator system is proposed for the separation and recovery of all of Hydrogen, Methane, Nitrogen and Carbon dioxide gases from process stream. A cooling stage is proposed to get the gases to temperatures where the polymeric membrane can withstand prior to the separation steps. Multiple sets of membrane separators are selected. For example six of them can be in parallel and may contain a membrane with a high permselectivity for Hydrogen and designated as A beds, B beds three in parallel that in a similar manner can remove the Methane, C beds, three in parallel to remove the Nitrogen and D beds, 2 in parallel to remove the Carbon di-oxide. Each bed of each set goes through a cyclic sequence of diffusion and concentration, adsorption/desorption and other complementary steps. Pressure and Temperature of these reactor systems are interesting variables and as a first approximation not considered as variables in the study.

The process performance was evaluated using design packages such as ECLIPSE and ASPEN. Different process scenarios were evaluated in this manner. The purity level, recovery (%), secondary product in each cycle are the parameters of interest. The waste gases generated has to be accounted for. Purge requirements is another process consideration. The optimization variable is cost. Flexibility of operation is also another salient consideration in this analysis. The number of beds in A, B, C and D were varied in the different scenarios.

The membrane can be formed by dissolution in dipolar aprotic solvents such N-Methyl-2-Pyrrolidone, Dimethyl Sulfoxide, Tetramethyl urea, Hexamethylphospharimide at elevated temperature. These solutions prepared at dilute concentrations of the polymers (about 5%) can be centrifuged and degassed and then the membranes cast onto glass plates. The membranes can be vacuum devolatilized and to remove the residual stress and defects. Thin membranes can be achieved by careful preparation. The permeability and permselectivity of the gases needs to be determined experimentally.

A model for the dependence of polymer structure on the permeability and permselectivity of the membrane is proposed. The different mechanisms such as substitution, miscibility, compatibility, morphology are modeled and the effects delineated. The models for miscibility in ternary blends are improved. The compositions of miscibility and conditions of phase separation can be calculated using the binary interaction model, and Equation of State such as the lattice fluid theory mentioned above. The interrelationships between permeability, permselectivity and polymer phase behavior is proposed to be captured in the model. The role of the morphology of the membrane in general and the glassy state, crystallinity and composition is proposed to be quantified.

The permeability in the inorganic high surface area material such as zeolite can be estimated from the diffusivity calculations. The diffusion through the solids with the macroporous microporous mesoporous distribution is given by;

$$D_{A, \text{tot}, \text{eff}} = D_{A, \text{tot}} \epsilon''/\tau \quad (4)$$

where the tortuosity factor is given by;

$$\tau = s'/\cos 2\phi \quad (5)$$

For example the tortuosity is 2 when $\phi = 45^\circ$, $s' = 1$. The experimental range for tortuosity is 1.5-7. The ϕ is the angle of the pores whereby the cylindrical molecules travel a $\sec\phi$ greater distance. The shape factor s' is used to correct for the non-cylindrical pores. The average pore radius can be determined from the pores sized distribution. The Kelvin equation relates the capillary radius to vapor pressure at which condensation occurs:

$$P(r)/P_{sat} = \exp(-2\sigma\cos\theta/V_m/RT) \quad (6)$$

where θ is the wetting angle

$$r = t + 2\sigma\cos\theta/(RT \ln(P_{sat}/P)) \quad (7)$$

The average pore radius can be determined from the PSD (Pore Size Distribution).

$$r_{psd} = \int r V(r) dr / \int V(r) dr \quad (8)$$

The number of saddle points in the pores size distribution is a measure of the presence of the macro pore, meso pore and micro pores. For pores of uniform size;

$$D_{A,tot,eff} = D_{g,tot} \epsilon^{1/\tau} \quad (9)$$

The total diffusion coefficient (bulk & Knudsen) in fluid phase and the porosity and tortuosity are the key parameters that affect the effective diffusivity. The porosity takes into account the fact that all of the material between the two faces of the solid is not entirely fluid phase. The zeolite material with tailored porosity can be used as a molecular sieve and thus be used in the process to separate the Hydrogen from the process stream. The tortuosity accounts for the case when the distance traveled by the fluid molecule in pore is much greater than distance between the two solid faces. For the trimodal distribution of macropores, mesopores and micropores;

$$D_{A,tot,eff} = \begin{aligned} & (\theta_{macro}^2/1/D_{AB} + 1/D_{A,K,macro}) & (10) \\ & \text{Flow through macropores} \\ & + (\theta_{meso}^2/(1/D_{AB} + 1/D_{A,K,meso})) \\ & \text{Flow through mesopores} \\ & + (\theta_{micro}^2 (1 + 3\theta_{macro})/(1 - \theta_{macro}) / (1 - (1 + N_B/N_A)\gamma_A/D_{AB} + 1/D_{A,K,micro})) \\ & \text{Flow through micropores + macro/micro series} \end{aligned}$$

The micro-meso cutoff is 15 A and macro meso cutoff is 12.5 nm.

The multicomponent diffusivity was assumed to be the same as the binary diffusivities in the vapor phase with the predominant process being bulk and viscous diffusion. The Knudsen diffusion is accounted for by the collisions with the container walls. The collision integral for diffusion is a function of the Lennard Jones interaction potential parameter and is a simple arithmetic average of the pure component values. The temperature is a strong parameter for the bulk binary diffusion values and the molecular weight is key contributor.

Acknowledgments

Kal R. Sharma Ph.D. PE acknowledges Victoria F. Haynes Ph.D., Group Vice President and Chief Technical Officer, BF Goodrich, Brecksville, OH his mentor in industrial research, Richard Turton, Professor, Chemical Engineering, West Virginia University, Morgantown, WV his mentor in academic research, Prof. Nithiam T. Sivaneri, Professor and Associate Chair, Mechanical and Aerospace Engineering, West Virginia University, Morgantown, WV, Prof. Edward J. Wegman, Chair and Director, Center for Computational Statistics, George Mason University, Fairfax, VA, Prof. Eva Marand, Chemical Engineering at the Virginia Polytechnic and State University, Blacksburg, VA, Susan Meek, at the Virginia's Center for Innovative Technology, Hemdon, VA, Dr. Richard Shuford, Branch Chief, Polymers Research Branch at the Army Research Laboratory, Aberdeen Proving Ground, MD and his associates at Independent Institute of Technology.

THE APPLICATION OF A HYDROGEN RISK ASSESSMENT METHOD

Dr. Michael R. Swain
Eric S. Grilliot
University of Miami

Dr. Matthew N. Swain
Analytical Technologies, Inc.

ABSTRACT

A comparison of the predicted results from a calibrated CFD model with experimentally measured hydrogen data was made to verify the calibrated CFD model. The experimental data showed the method predicted the spatial and temporal hydrogen distribution in the garage very well. A comparison is then made of the risks incurred from a leaking hydrogen-fueled vehicle and a leaking LPG-fueled vehicle.

INTRODUCTION

The following is brief description of using a Hydrogen Risk Assessment Method (HRAM) to analyze the risk associated with hydrogen leakage in a residential garage. The four-step method is as follows:

1. Simulation of an accident scenario with leaking helium.
2. Calibration of a CFD model, of the accident scenario, using helium data.
3. Prediction of the spatial and temporal distribution of leaking hydrogen using the calibrated CFD model.
4. Determination of the risk incurred by hydrogen compared to a currently used fuel.

EXPERIMENTAL

Steps 1 and 2 were performed for a home refueling station, installed in a residential garage, to test the ability of the CFD model to predict hydrogen concentrations in a single car residential garage. The work was conducted utilizing a half scale model of the garage. The garage employed a vented garage door. The door was designed to provide adequate ventilation for a vehicle parked in the garage leaking hydrogen at a rate of 7200 liters/hr (at full scale). The garage geometry is depicted in Figure 1.

Figure 2 shows the general flow pattern created by the leaking low density gas (either helium or hydrogen). The gases rise over the leak, travel diagonally across the ceiling toward the garage door, exiting through the upper garage door vent. The loss of gases out of the upper vent draws fresh air into the lower vent. These gases flow across the floor toward the rear of the garage.

Experiments were conducted at three gas leakage rates; 900 l/hr, 1800 l/hr, and 2700 l/hr, using both helium and hydrogen. The predictions of the model and the experimental data were in good agreement. Figure 3 shows an example of the comparison of experimental data and computer model results. The data shown is for a hydrogen leakage rate of 2700 l/hr. Sensor location 7 was chosen because that location recorded the highest concentration of hydrogen during the test. The other sensor locations showed similar correlation between experimental and calculated data.

RESULTS

The model was used to compare gas leakage from vehicles stored in residential garages. Leakage from a LPG fueled vehicle was compared to leakage from a hydrogen-fueled vehicle. The comparison was based on a Ford Taurus sized vehicle stored in a single car garage of slightly different dimension, than the home refueling station test, but with the same vented garage door.

The computer model representation of the ventilated garage was run to predict the behavior of a LPG fueled vehicle. The leakage rates chosen for the LPG fueled vehicle were 848.2 liters/hr and 4334 liters/hr. These represent upper and lower bounds on the leakage rate of propane from a fuel line fracture that produced a 7200 liter/hr hydrogen leakage rate. The 848.2 liter/hr flow rate would occur if laminar flow was assumed in the hydrogen and propane leaks being compared. The 4334 liter/hr flow rate would occur if turbulent flow was assumed in the hydrogen and

propane leaks being compared. Due to differences in density and viscosity the volumetric leakage rate of propane was lower than that of hydrogen which was 7200 l/hr.

Figures 4-6 show the results after 2 hours of leakage. The figures show surfaces of constant gas concentration that represents the lean limit of combustion. Figure 4 is a plot of the surface of constant 4.1% hydrogen concentration at by volume. 4.1% hydrogen in air is the upward propagating lean limit of combustion for hydrogen-air mixtures (Coward 1961, Hansel 1993, Lewis 1961, and Ordin 1997). This is the lowest concentration of hydrogen considered combustible. The cloud under the front of the vehicle in Figure 4 represents the volume of burnable gas after 2 hours of leakage at 7200 liters/hr. Figure 5 is a plot of the surface of constant 2.1% propane concentration at by volume. 2.1% propane in air is the upward propagating lean limit of combustion for propane-air mixtures (Coward 1961, Hansel 1993, Lewis 1961, and Ordin 1997). This is the lowest concentration of propane considered combustible. The cloud covering almost the entire floor of the garage represents the volume of burnable gas after 30 minutes of leakage at 848 liters/hr. Figure 6 is a plot of the surface of constant 2.1% propane concentration at by volume. The cloud covering the entire floor of the garage represents the volume of burnable gas after 30 minutes of leakage at 4334 liters/hr.

CONCLUSIONS

It can be seen that the volume of combustible gas created by the hydrogen-fueled vehicle is much smaller than the volume created by the LPG fueled vehicle. This was true regardless of which of the two propane flow rates was assumed. It should be noted that the combustible cloud produced by the LPG fueled vehicle was continuing to grow. The volume of combustible gases produced by the hydrogen fueled vehicle had reached steady state after 1 hour as seen in Figure 7. Figure 7 shows the surface of constant 4.1% hydrogen concentration, which is the lean limit of combustion for hydrogen.

ACKNOWLEDGEMENTS

The authors would like to thank the Department of Energy and Sandia National Labs, without whose support this work would not have been possible.

REFERENCES

- Coward, H.F., and G.W. Jones. 1952. Limits of Flammability of Gases and Vapors, Bureau of Mines Bulletin 503
- Hansel, J.G., G.W. Mattem, and R.N. Miller. 1993. "Safety Considerations in the design of Hydrogen Powered Vehicles", *Int. J. Hydrogen Energy*, Vol. 18, No. 9, pp 790
- Lewis, B. and G. VonElbe. 1961. *Combustion, Flames and Explosions of Gases*, 2nd Edition New York: Academic Press
- Ordin, P.M. 1997. *Safety Standards for Hydrogen and Hydrogen Systems*, National Aeronautics and Space Administration, NSS 1740.16, Office of Safety and Mission Assurance, Washington D.C.

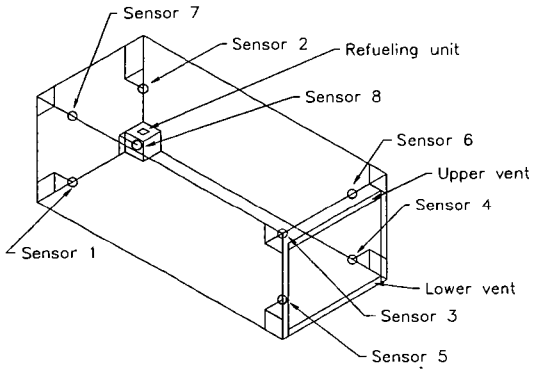


Figure 1 - Half-scale garage geometry

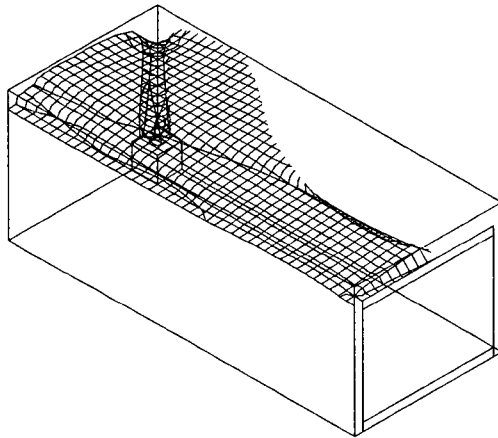


Figure 2 - General flow pattern

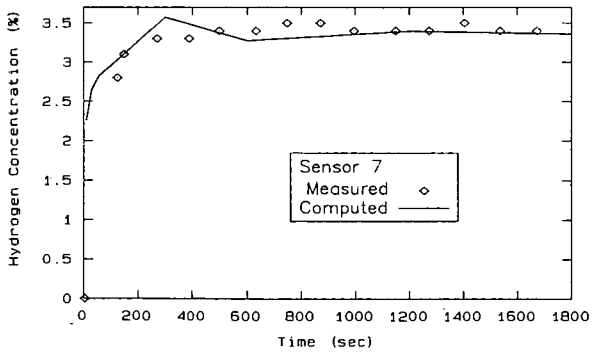


Figure 3 - Hydrogen results comparison (Sensor 7)

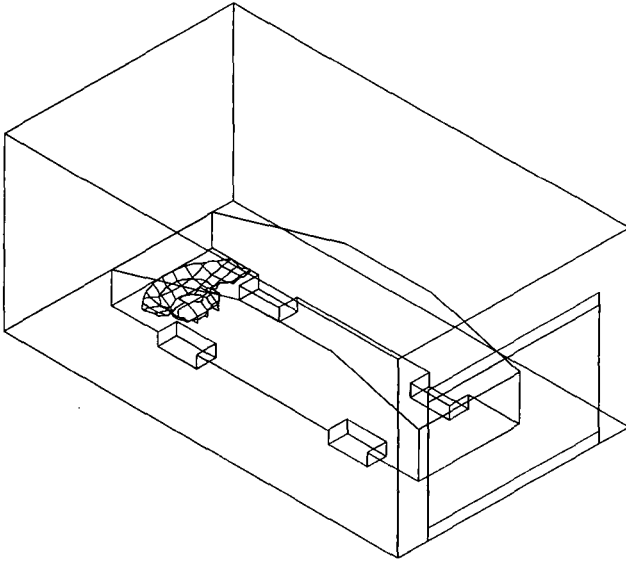


Figure 4 - Surface of constant 4.1% hydrogen concentration after 2 hours of leakage at 7200 liters/hr

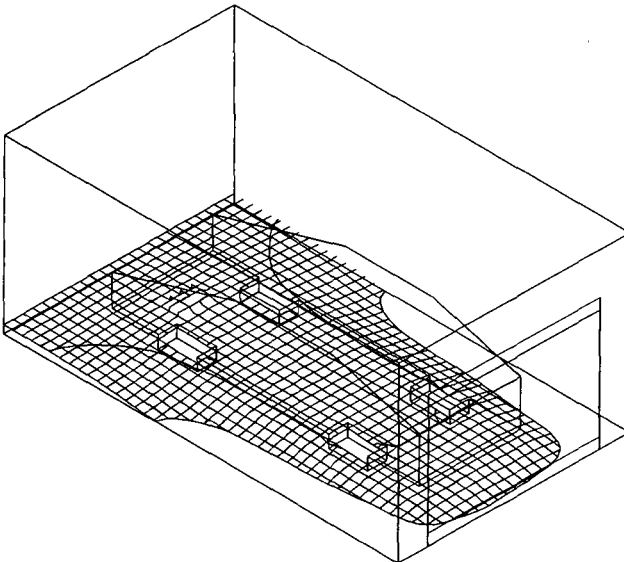


Figure 5 - Surface of constant 2.1% propane concentration after 2 hours of leakage at 848.2 liters/hr

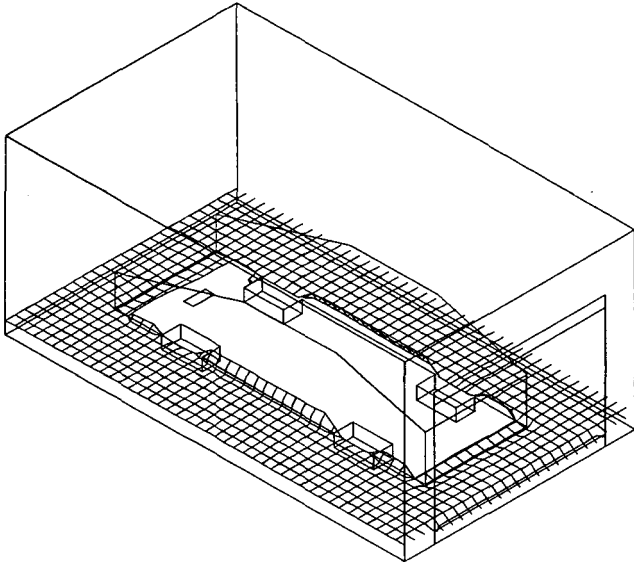


Figure 6 - Surface of constant 2.1% propane concentration after 2 hours of leakage at 4334 liters/hr

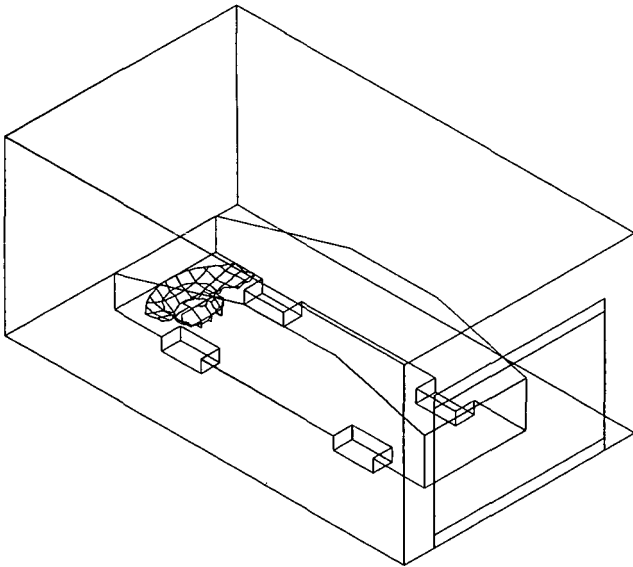


Figure 7 - Surface of constant 4.1% hydrogen concentration at 1 hour

LOW COST HYDROGEN SENSORS FOR HYDROGEN FUEL SAFETY

Mark Daughtery, Dave Haberman, Carlton Salter
DCH Technology, Inc.
Valencia, California

David Benson
National Renewable Energy Laboratory
Golden, Colorado

Barbara Hoffheins
Oak Ridge National Laboratory
Oak Ridge, Tennessee

Use of hydrogen as an energy carrier is increasing. Production and handling of hydrogen in industry is not new, but there are many new applications as a commercial fuel that bring its use into the public domain. Adequate safety monitoring equipment must parallel the advent of this technology. DCH Technology, in conjunction with the National Renewable Energy Laboratory (NREL) and Oak Ridge National Laboratory (ORNL), is developing and commercializing solid-state hydrogen sensors. They are designed to be inexpensive, small, and chemically inert. The NREL Fiber Optics sensor requires no electrical power at the sensing point and is ideal for high electromagnetic environments. The ORNL thick film sensor is versatile and can operate from a small battery. Data from combinations of multiple sensors can be fed into a central processing unit via fiber optics or telemetry to provide hydrogen situational awareness for small and large areas. These sensor technologies, functional attributes, and applications are presented below.

THICK FILM HYDROGEN SENSOR (TFHS)

The sensing mechanism of the ORNL sensor relies on the reversible absorption of atomic hydrogen into and out of palladium metal in proportion to the ambient partial pressure of hydrogen gas. Changes in hydrogen concentration in the palladium matrix lead to corresponding changes in the electrical resistance of the palladium that are easily measured. The sensor consists of four palladium resistors (or legs) that are arranged in a Wheatstone bridge configuration. Figure 1 depicts the sensor and its schematic representation. The current prototype sensor chip is 2.5 cm x 2.5 cm x 0.06 cm. Two of the legs serve as reference resistors and are passivated with a thick-film resistor encapsulant to prevent entrance of hydrogen into the underlying palladium layer; thus, changes in the resistance of the palladium caused by temperature variation are compensated.

The sensor concept was successfully demonstrated using prototypes fabricated with thin film techniques. Then the sensor was designed for thick film fabrication for a variety of reasons. Effective passivations, difficult to achieve with thin films, can be made more impermeable using glass-based, thick-film compositions. Glass frit, an important component of most thick-film compositions, is formulated to provide maximum adhesion, chemical resistance, and stability over a wide range of operating conditions. A thick-film sensor is also inherently simpler, more rugged, and much less expensive to manufacture in quantity. These ideas were incorporated in the hydrogen sensor designs patented in 1994 (Lauf 1994) and 1995 (Hoffheins 1995). The palladium resistor material used in fabricating sensor samples was developed and patented by DuPont Electronics (Felten 1994).

Theoretically, the diffusion of hydrogen into a thin layer of palladium occurs on the order of milliseconds. In laboratory tests, however, the time constant of the test setup can prevent direct observation of the actual response time of the sensor. Figure 2 shows the response of a sensor to increasing concentrations of hydrogen from 0 to 2% in air. The sensor was placed in a small test chamber (50 cm³). Hydrogen was added to air in 0.1% increments, while flow was maintained at a constant rate. Each step was 60 seconds. The sensor began to respond at the level of 0.2% H₂ in air. For each successive increment of hydrogen, sensor output increased and leveled off in 9 seconds. This time includes the time constant of the test chamber of about 2 seconds. The response in the range between 0 and 2% hydrogen is linear, so calibration is easily accomplished.

Currently the sensor is being tested to a list of specifications of interest for several commercial applications. Materials are being optimized for conditions that will typically never go above 2% H₂ in air. The temperature range is -40°C to +60°C. The sensor has been successfully tested between 20°C and 200°C [Hoffheins 1998]. In general, the response is faster at the higher temperatures, but the magnitude of the response is lower because of reduced hydrogen solubility

in the palladium. An acceptable response time for the intended commercial applications is 3 seconds. The raw output from current prototypes does not meet that requirement; however, methods to use the rate of response and the dc output with external circuitry to predict the hydrogen concentration are being examined. Another very important performance objective is that the sensor is insensitive to the following compounds: CO, CO₂, CH₄, NH₃, propane, butane, and acetylene. In preliminary tests, sensors were exposed to carbon monoxide, propane, and methane. The response indicated little or no effect on the sensor. The sensor appears to be insensitive to these compounds. More tests will be conducted with the above and other compounds to verify this performance.

APPLICATIONS FOR THE TFHS

DCH Technology is commercializing the TFHS. This device is most applicable as a low cost alarm sensor. The principal applications currently being addressed are for hydrogen powered automobiles, personal safety badges, and remote area monitoring.

The safety badge application has been chosen for initial market penetration because the environmental requirements match current knowledge of the performance of the sensor. DCH has built a prototype badge that is approximately the size of a standard business card and roughly one-quarter of an inch thick. DCH is undertaking a more detailed market analysis to determine customers and distribution partners, additional functional benefits (such as activating a vibrator to signal hydrogen), specific sensor technical requirements, and cost targets. A product specification will be developed from this data and an initial product will be built and distributed for alpha testing. In parallel with the product definition effort, DCH and ORNL will complete the technical bounding of the sensor operational characteristics, including response time, cross-sensitivity, and applicable firmware.

Sensors for automotive applications are being developed now. There are three general areas of interest: Low level alarms to sense leaks from hydrogen storage and delivery lines; sensors for high concentrations of hydrogen that exist in the output of reformers or inputs to fuel cells; and medium level sensors that are needed in the exhaust stream of an internal combustion engine running on hydrogen. The sensors considered in this paper are for the low level alarm application.

The automotive requirements for the device are low cost (one to four dollars per sensing point), rapid response, rugged and repeatable operation in the automotive environment, and a unit life of ten years. In addition, there cannot be any false positives, and the size of the sensor must be small enough to fit into critical areas.

The automotive requirements are considerably more stringent than those for the safety badge. The operating temperature range is very broad, from -40°C to over 60°C. While the TFHS is thermally self compensating by design, the sensor response speed decreases with decreasing temperature and the sensitivity decreases with increasing temperature. ORNL and DCH are currently investigating the sensor response under these conditions. Software methodologies are being investigated to provide interpretive decision making based on sensor output to both speed up response speed and to activate hierarchical responses to decreasing, continuing or increasing hydrogen concentrations.

The automotive operating environment can expose a sensor to a multitude of gases and vapors. The sensor must have no cross sensitivity and not be poisoned by such chemicals. To address these requirements, DCH and ORNL are testing the sensor against other gasses, such as CO₂, CH₄, NH₃, O₂ variations, water vapor, acetylene, and chemical vapors to which the sensor could be exposed. Additional considerations under evaluation are susceptibility of the sensor and associated wiring and electronics to electromagnetic interference. Also, sensor ruggedness and durability are being characterized. Finally, after all these technical considerations are put to rest, the sensor must meet the cost goals of the automotive industry.

All of these parameters are being addressed in cooperation with major automotive manufacturers. Publicly sold fuel cell powered cars are on the horizon and the need for low cost hydrogen sensors that meet the needs of the automotive environment is now.

The final application area being addressed for the TFHS is for monitoring of large industrial areas, both indoor and outdoor, which have risks of hydrogen leakage. DCH is aware of industrial disasters that were prevented because the company involved discovered the leak using a portable sensor. DCH intends to make hydrogen sensing simple and cost effective so

companies can easily install the protection they need. In particular, DCH is developing a wireless transmission capability to attach to the TFHS for remote and/or large area monitoring. A receiver unit will collect transmitted signals from multiple sensors. This unit can then be hard wired into control electronics or its output signal transmitted to remote control stations. The receiver could be one of many a large area network. DCH is presently evaluating transmitter suppliers as well as looking at making the transmitter in-house. In parallel, DCH is developing the market analysis to determine operating and cost specifications. In a few months, DCH will finalize the specifications and make the make/buy decision. This action will be followed by development of a prototype, obtaining FCC approval, and alpha testing.

FIBER OPTICS HYDROGEN SENSOR (FOHS)

The use of a fiber-optic, hydrogen-gas-leak detector has advantages of inherent safety (no electrical power in the vicinity of the sensor), reduced electromagnetic interference, lightness of weight, and low cost. Most if not all of the needed electro-optic components could be integrated into a single application-specific integrated circuit (ASIC) for economical mass production. An analysis of the probable manufacturing costs has shown that it should be possible to mass-produce similar detectors for about \$5 each (not including the cost of the optical fiber).

In this design, a thin-film coating at the end of a polymer optical fiber senses the presence of hydrogen in air (Benson, et al 1998). When the coating reacts reversibly with the hydrogen, its optical properties are changed. Light from a central electro-optic control unit is projected down the optical fiber where it is reflected from the sensor coating back to central optical detectors. A change in the reflected intensity indicates the presence of hydrogen. The fiber-optic detector offers inherent safety by removing all electrical power from the sensor sites and reduces signal-processing problems by minimizing electromagnetic interference. Critical detector performance requirements include high selectivity, response speed, and durability as well as potential for low-cost production.

Preliminary experiments were conducted with simple sensors. The end of a polymer optical fiber was coated with 500-nm WO_3 and a superficial layer of 10-nm palladium. Figure 3 shows a calibration curve obtained from such a sensor in air with various concentrations of hydrogen. The reflected signal at 850 nm is attenuated by the optical absorption in the WO_3 in proportion to the reaction with hydrogen, which in turn is proportional to the hydrogen concentration. The sensitivity is adequate for detection of the hydrogen well below the lower explosion limit of 4% in air.

A self-contained, hand-held portable fiber-optic hydrogen sensor was designed and built. The light source is a high-brightness, broad-spectrum "white" (phosphor-enhanced) LED. The light from the LED is projected into the proximal end of a 1-mm-diameter polymer optical fiber and transmitted through a 1 x 2 coupler to an exit port on the instrument. The optical-fiber sensor is plugged into that port with a standard fiber-optic ST connector. Light reflected from the sensor coating on the distal end of the fiber is returned to the instrument, and half of its power is directed through one of the coupler legs to a dichroic mirror. The dichroic mirror splits the return light beam into long- and short-wavelength portions that fall separately on two different photo-diode amplifiers. The voltage signals from the two photo-diodes are divided one by the other in an analog divide circuit. Figure 4 shows a schematic illustration of the detector's design features.

APPLICATIONS FOR THE FIBER OPTIC HYDROGEN SENSOR

Initially the FOHS was developed for automotive use because it will not inject any electrical circuitry into the sensed area and the signal transmission is over the fiber, which is insensitive to electromagnetic interference. However, this sensor needs further development work to accelerate the response time, especially at the low temperatures required by the automotive specifications. In the mean time, there are two applications for which the sensor, in its current state of development, can be used. The first is as a weld quality sensor. A sensor can be attached to the weld within hours after the weld is completed and used to measure the rate of hydrogen out gassing, which indicates the concentration of dissolved hydrogen in the welded steel. Using this process, the weld condition can be read in minutes. The current methods for measuring the concentration of dissolved hydrogen in welded steel require approximately a day to read and must use witness samples. The fiber optic sensor could be used, as a secondary standard, in conjunction with the existing method. As the faster method becomes proven, standards for its use as a primary weld quality sensor could be established.

The second application is in monitoring battery rooms. Again, multiple fibers would be easily distributed throughout the room and monitored at a central location. In this application, the fiber optic approach displays its inherent advantages of multi-point sensing and installation versatility.

INTEGRATED APPLICATIONS

DCH plans to mix and match these two technologies, along with the DCH Robust Hydrogen Sensor monitor, to provide optimal situation awareness in complex hydrogen use environments. To do this cost effectively, DCH is planning to develop common electronic packages which include easily modifiable software inputs to not only tailor the sensors to the customers unique application, but moreover, to give the user the tools to modify and expand their hydrogen sensing capabilities.

SUMMARY

DCH Technology is commercializing state of the art hydrogen sensors developed by Oak Ridge National Laboratory and the National Renewable Energy Laboratory. This blend takes the scientific knowledge resident in these laboratories and creates applicable, timely, and meaningful commercial products that assist the development of the hydrogen fuel economy. These sensors are necessary to help carry this development into the public domain.

Key Words: Hydrogen, Sensors, Safety

References

Benson, D. K., C. E. Tracy, and D. S. Bechinger, 1998. "Fiber Optic Device for Sensing the Presence of a Gas. U. S. Patent No. 5,708,735.

Felten, J.J. 1994. "Palladium Thick Film Conductor." U.S. Patent No. 5,338,708.

Hoffheins, B.S. and R.J. Lauf. 1995. "Thick Film Hydrogen Sensor." U.S. Patent No. 5,451,920.

Hoffheins, B.S., R.J. Lauf, T.E. McKnight, and R.R. Smith, 1998. "Design and Testing of Hydrogen Sensors for Industrial Applications," *Polymers in Sensors, Theory and Practice*, ACS Symposium Series 690, N. Akmal and A.M. Usmani, pp. 90-101.

Lauf, R.J., B.S. Hoffheins, and P.H. Fleming. 1994. "Thin-Film Hydrogen Sensor." U.S. Patent No. 5,367,283.

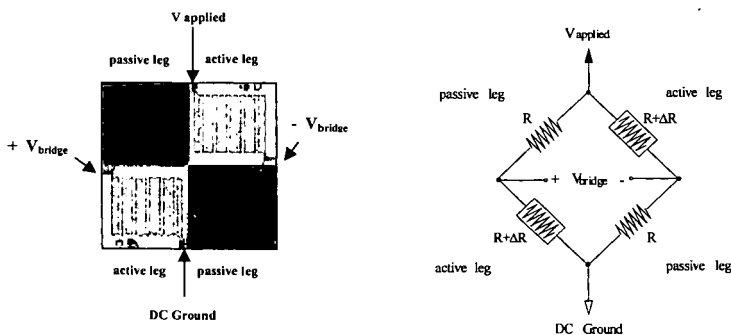


Figure 1. Thick Film Hydrogen Sensor Chip and Schematic Representation

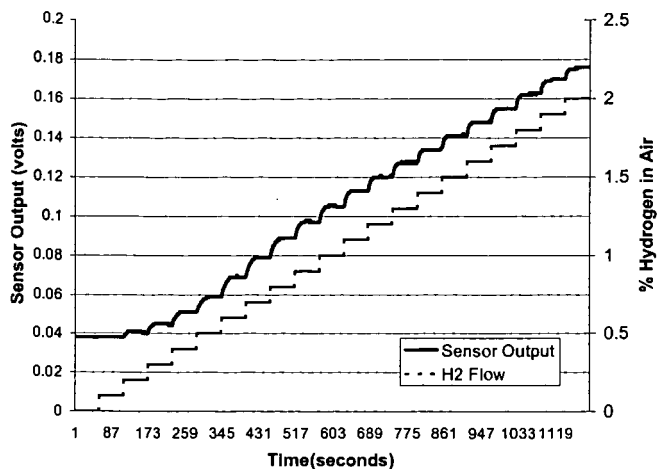


Figure 2. Sensor response to increasing concentrations of hydrogen in air

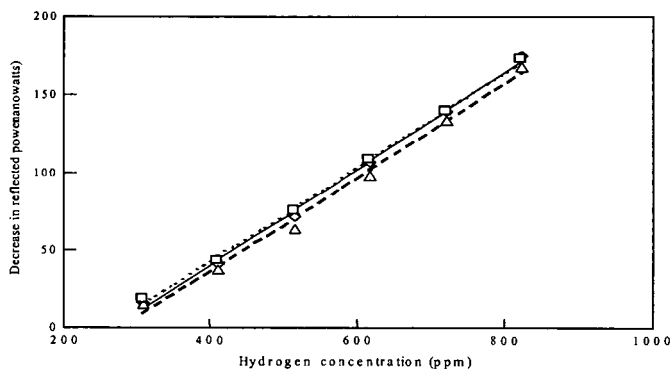


Figure 3. Calibration curves for a simple reflective WO_3/Pd -coated F-O sensor.

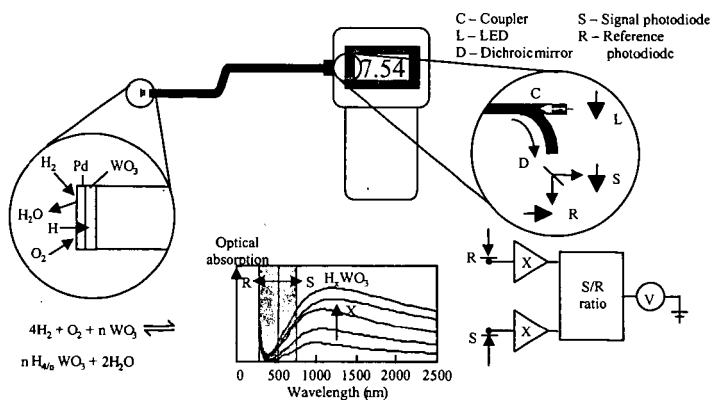


Figure 4. Schematic diagram of the prototype portable fiber-optic, hydrogen-gas-leak detector showing selected design features.

THE INTERNATIONAL ENERGY AGENCY'S HYDROGEN RESEARCH AND DEVELOPMENT ACTIVITIES

Carolyn C. Elam and Catherine E. Gregoire Padró,
National Renewable Energy Laboratory, Golden, CO, USA
Gary Sandrock, SunaTech, Inc., Ringwood, NJ, USA
Bjorn Gaudernack, Institute for Energy Technology, Kjeller, Norway
Neil P. Rossmeissl, U.S. Department of Energy, Washington, D.C., USA

Keywords: Hydrogen, International Energy Agency, Integrated Systems

INTRODUCTION

Today, hydrogen is primarily used as a chemical feedstock in the petrochemical, food, electronics, and metallurgical processing industries, but is rapidly emerging as a major component of clean sustainable energy systems. It is relevant to all of the energy sectors - transportation, buildings, utilities, and industry. Hydrogen can provide storage options for baseload (geothermal), seasonal (hydroelectric) and intermittent (PV and wind) renewable resources, and, when combined with emerging decarbonization technologies, can reduce the climate impacts of continued fossil fuel utilization. Hydrogen is truly the flexible energy carrier for our sustainable energy future.

International Energy Agency

The International Energy Agency (IEA) was established in 1974, following the first oil crisis and is managed within the framework of the Organization for Economic Cooperation and Development (OECD). The mission of the IEA is to facilitate collaborations for the economic development, energy security, environmental protection and well-being of its members and of the world as a whole. As part of this effort, the IEA launched the Production and Utilization of Hydrogen Program, known as the Hydrogen Agreement, in 1977 to advance hydrogen production, storage and end-use technologies and to accelerate hydrogen's acceptance and widespread utilization.

The use of hydrogen as an energy carrier is considered a mid- to long-term goal. This is due to infrastructure barriers, particularly in the storage area. Likewise, safety issues, both real and perceived, are concerns for acceptance of hydrogen by the general population. Finally, hydrogen production from renewables will likely not be cost-competitive with fossil-based production, at least in the near-term. Thus, the Hydrogen Agreement is focused on pursuing technologies that will help overcome some of the infrastructure barriers and/or result in the reduced cost of hydrogen systems.

- On-board storage in vehicles is one of the major barriers to the acceptance of hydrogen powered vehicles. Metal hydrides and similar storage medium, like carbon, are thought to have the greatest potential for the safe, on-board storage of hydrogen. However, work-to-date has not proven cost effective due to the inability of current hydride technology to meet the hydrogen storage percentages required for maintaining vehicle weights within a reasonable range.
- To achieve the advantages of a "hydrogen future," namely a reduction in carbon emissions, hydrogen must be able to be cost-effectively produced from renewables. Thus, the Hydrogen Agreement has been pursuing R&D in the solar production area, both biological and electrochemical. The electrochemical approach is, of course, hindered by the fact that photovoltaic technology is not yet cost-effective. Thus, it cannot compete with existing technology, except possibly in small niche markets. Much must still be learned about photobiological processes before we are able to understand the economic potential of this production technology.
- Achieving the vast potential benefits of a hydrogen system requires careful integration of production, storage and end-use components with minimized cost and maximized efficiency, and a strong understanding of environmental impacts and opportunities. System models combined with detailed life cycle assessments provide the platform for standardized comparisons of energy systems for specific applications. Individual component models form the framework by which these system designs can be formulated and evaluated.

- The use of hydrogen in the metals, chemicals, glass, food, electronics, fertilizer, petroleum and space industries is well established. The range of uses has been increasing as has the consumption by specific application. Historically, hydrogen has had an excellent safety record. The many studies, R&D efforts, and experience base have contributed to the publication of regulations, standards, industrial data sheets and technical reports. Hydrogen safety is an issue of every aspect from production to utilization and continues to be of the utmost importance; not only to those researching, designing and working with it; but to the general public, local authorities, insurance agents, etc., as well.

TECHNOLOGY ACTIVITIES

Integrated Systems

Through the IEA Integrated Systems activities, twenty-four component models were developed to model hydrogen production, storage, distribution and utilization (see Table 1). Guidelines for a standardized modeling platform were defined to ensure that the component models could be linked to simulate fully integrated systems. Using the component models, two integrated systems were evaluated for grid-independent remote village applications: PV-electrolysis-metal hydride-PEM fuel cell system and wind-electrolysis-compressed gas-internal combustion engine generator set. Using resource data for the region and a demand profile for a similar-sized village, the system components were designed to provide constant power to the villagers. For the location used in this study, the PV system required about 1/6th of the storage of the wind system, even though the PV resource exhibited significant seasonal variation compared to the wind resource. Similarly, a comparative study of hydrogen storage technologies for a remote renewable energy system examined relative costs of compressed hydrogen gas, low-temperature metal hydride and high temperature metal hydride storage systems for a grid-independent system supporting a village of 100 homes in Central America. The analysis showed that, while the compressed gas storage system had the lowest capital cost, the low-temperature metal hydride system was the easiest to operate and maintain, and was therefore the overall lowest cost system. [1-8]

In support of the Integrated Systems activities, fourteen international hydrogen demonstration projects were critically evaluated and compared, with system performance measurement as the central focus. Safety and regulatory issues were also considered. Representatives of these demonstration projects provided technical data and participated in the review workshops. Additionally, the international participants were able to visit a number of the demonstration sites to see the facilities and meet with the project engineers. The list of the projects that were reviewed is shown in Table 2.

Photoproduction of Hydrogen

As part of the IEA activities, the concept of using solar energy to drive the conversion of water into hydrogen and oxygen has been examined from the standpoints of potential and ideal efficiencies, measurement of solar hydrogen production efficiencies, surveys of the state-of-the-art, and technological assessments of various solar hydrogen options. The analysis demonstrated that the ideal limit of the conversion efficiency for 1 sun irradiance is ~31% for a single photosystem scheme and ~42% for a dual photosystem scheme. However, practical considerations indicate that real efficiencies will not likely exceed ~10% and ~16% for single and dual photosystem schemes, respectively. Four types of solar photochemical hydrogen systems were identified: photochemical systems, semiconductor systems, photobiological systems and hybrid and other systems. A survey of the state-of-the-art of these four types was performed and each system (and their respective subsystems) was examined as to efficiency, potential for improvement and long-term functionality. The following four solar hydrogen systems were identified as showing sufficient promise for further research and development: [10]

- Photovoltaic cells plus an electrolyzer
- Photoelectrochemical cells with one or more semiconductor electrodes
- Photobiological systems
- Photodegradation systems

Most photobiological systems use bacteria and green algae to produce hydrogen. These systems hold great promise for long term sustainable hydrogen production, but face two major barriers for meeting the cost limitations. These barriers are the fairly low solar conversion efficiencies of these systems of around 5-6%, and the fact that nearly

all enzymes that evolve hydrogen from water are inhibited in their hydrogen production by the presence of oxygen. Research efforts are focusing on overcoming this oxygen intolerance by developing strains of the green algae, *Chlamydomonas*, which contain oxygen-evolving enzymes, and thus can produce oxygen and hydrogen simultaneously. Genetic alterations of *Chlamydomonas* are being investigated in attempts to improve the solar conversion efficiencies. These new genetic forms are predicted to reach efficiencies on the order of 10%.

Photoelectrochemical production uses semiconductor technology in a one-step process of splitting water directly upon sunlight illumination by combining a photovoltaic cell and electrolysis into a single device. Research efforts are being focused on identifying structures and materials that will meet the high voltage requirements to dissociate water, not be susceptible to the corrosiveness of the aqueous electrolytes used in the electrolytic process, and are cost-effective. Amorphous silicon devices are one of the types most favored, due to their lower cost. These photovoltaic devices have achieved efficiencies of 7-8%. Photovoltaic devices using more expensive materials, have demonstrated efficiencies of 12.4%. [9] Researchers are now working to combine the low cost materials and high conversion efficiency materials to achieve a practical application of this promising technology.

Metal Hydrides and Carbon for Hydrogen Storage

The use of hydrogen as a vehicle fuel requires a storage means that has inherent safety and both volumetric and gravimetric efficiency. Metal hydrides offer alternatives to the storage of hydrogen in gaseous and liquid form. They store hydrogen in an essentially solid form and offer the potential for volume efficiency, high safety, low pressure containment and ambient temperature operation. Unfortunately, most known hydrides are either heavy in comparison to the hydrogen they carry or require high temperature for hydrogen release. In the past few years, carbon adsorbent materials have also gained attention as a possible, cost-effective storage medium for hydrogen. Whereas carbon was once considered only as a cryo-adsorbent for hydrogen, there is growing belief it can be used at ambient temperature. However, much must still be learned about consistent and high-purity production of these materials and the nature and potential for hydrogen storage. [11]

Work has been progressing to develop a variety of hydride and carbon materials for on-board storage, working towards both improved gravimetric capacity (5 weight %) and lower temperature (100-150°C) release of hydrogen. Building on the advances reported by the Max Planck Institute, Germany, [12] several international collaborations have been established to further develop the catalyzed sodium aluminum hydrides for hydrogen storage. The joint efforts of the experts has led to the identification of a material capable of 5 weight percent reversible hydrogen storage at 150°C, the necessary target for economic on-board hydrogen storage for vehicles. [11] The experts are now working to meet the new target of 5 weight percent at 100°C.

RESEARCH AND DEVELOPMENT NEEDS/FUTURE ACTIVITIES

Many advances were made in the longer-term photoproduction area. This includes identification of a semi-conductor-based hydrogen production system capable of 12.4% solar efficiencies and the construction of a process development scale bioreactor. However, this work is still at the early development stage. A variety of materials and organisms remain under investigation. System design is also an area that still requires a great deal of effort.

Hydrogen use in non-energy processes, such as the chemical, metallurgical, and ceramics industries was also identified as an area where a concentrated research effort could facilitate the increased utilization of hydrogen. Annually, these industries account for nearly 50 percent of the world's 500 billion Nm³ hydrogen consumption. Process improvements and novel synthesis approaches could lead to overall efficiency improvements and reduced environmental impacts. Likewise, increased market share for hydrogen in these arenas should lead to expedited infrastructure development, a necessity for facilitating the advancement of the energy-related and renewable-based applications.

Approximately 95% of the hydrogen produced today comes from carbon containing raw material, primarily fossil in origin. The conventional processes convert the carbon to

carbon dioxide, the majority of which is discharged to the atmosphere. The growing awareness of the impact of greenhouse gas emissions on global climate change has necessitated a reassessment of the conventional approach. Integrating carbon dioxide sequestration with conventional steam reforming will go a long way towards achieving "clean" hydrogen production. Likewise, improving the robustness of pyrolytic cracking technologies for the conversion of hydrocarbons to hydrogen and pure carbon should not only improve the process economics, but also its applicability to a variety of feeds. Finally, the thermal processing of biomass can yield an economic and carbon neutral source of hydrogen.

SUMMARY

As we enter the new millennium, concerns about global climate change and energy security create the forum for mainstream market penetration of hydrogen. Ultimately, hydrogen and electricity, our two major energy carriers, will come from sustainable energy sources, although, fossil fuel will likely remain a significant and transitional resource for many decades. Our vision for a hydrogen future is one of clean sustainable energy supply of global proportions that plays a key role in all sectors of the economy. We will implement our vision with advanced technologies including direct solar production systems and low-temperature metal hydrides and room-temperature carbon nanostructures for storage. Hydrogen in the new millennium is synonymous with energy supply and security, climate stewardship, and sustainability.

REFERENCES

1. Bracht, M., A. De Groot, C.E. Gregoire Padró, T.H. Schucan, and E. Skolnik, 1998, "Evaluation Tool for Selection and Optimization of Hydrogen Demonstration Projects. Application to a Decentralized Renewable Hydrogen System," *Hydrogen Energy Progress XII*, J.C. Bolcich and T.N. Veziroglu, eds., 1243-1254.
2. de Groot, A., M. Bracht, C.E. Gregoire Padró, T.H. Schucan, and E. Skolnik, 1998, "Development of Guidelines for the Design of Integrated Hydrogen Systems," *Hydrogen Energy Progress XII*, J.C. Bolcich and T.N. Veziroglu, eds., 75-86.
3. Schucan, T.H., E. Skolnik, M. Bracht, and C.E. Gregoire Padró, 1998, "Development of Hydrogen Technology Component Models for Systems Integration," *Hydrogen Energy Progress XII*, J.C. Bolcich and T.N. Veziroglu, eds., 111-120.
4. Gregoire Padró, C.E., V. Putsche, and M. Fairlie, 1998, "Modeling of Hydrogen Energy Systems for Remote Applications," *Hydrogen Energy Progress XII*, J.C. Bolcich and T.N. Veziroglu, eds., 2247-2262.
5. Gregoire Padró, C.E., 1998, "International Cooperative Development of Design Methodology for Hydrogen Demonstrations," *Proceedings of the 9th Annual U.S. Hydrogen Meeting*, Vienna, VA, 187-194.
6. Putsche, V. and C.E. Gregoire Padró, 1998, "Systems Modeling of Renewable Hydrogen Production, Storage, and Electricity Generation using ASPEN Plus," *Proceedings of the Electrical Energy Storage Systems Applications and Technologies Meeting*, Chester, U.K., 95-102.
7. Gregoire Padró, C.E., 1998, "Renewable Hydrogen Energy Systems for Grid-Independent Energy Systems," *Proceedings of the 1998 Colorado Renewable Energy Conference*.
8. Gregoire Padró, C.E. and M.J. Fairlie, 1998, "Renewable Hydrogen for Rural Electrification," *Poster at the Village Power '98 Conference*.
9. Khaselev, Oscar and John A. Turner, 1998, "A Monolithic Photovoltaic-Photoelectrochemical Device for Hydrogen Production Via Water Splitting," *Science*, Vol. 280, 425.
10. Bolton, James R., 1996, "Solar Photoproduction of Hydrogen," *IEA Technical Report*, IEA/H2/TR-96.
11. Elam, Carolyn C. (ed.), 1998, "IEA Agreement on the Production and Utilization of Hydrogen: 1997 Annual Report."
12. B. Bogdanovic' and M. Schwickardi, 1977, "Ti- Doped Alkali Metal Aluminum Hydrides as Potential Novel Reversible Hydrogen Storage Materials," *J. Alloys and Compounds*, 253-254, 1-9.

Table 1. Component Models Developed for Production, Storage, Distribution and Utilization

Technology	Team Lead	Technology	Team Lead
Production		Distribution	
PV-Electrolysis	Spain	Transport Tanker	Japan
Wind-Electrolysis	USA	High Pressure Pipeline	USA
Grid-Electrolysis	USA	Low Pressure Pipeline	USA
Steam Methane Reforming	USA	Tank Truck	Japan
Biomass Gasification	USA	Methanol Transport	Netherlands
Biomass Pyrolysis	USA	Utilization	
Coal Gasification	Netherlands	PEM Fuel Cell	Canada
Storage		Phosphoric Acid Fuel Cell	Spain
Low/High Pressure Gas	Canada	Solid Oxide Fuel Cell	USA
Metal Hydrides	USA	Molten Carbonate Fuel Cell	USA
Liquefaction	Japan	Gas Turbine	USA
Chemical Storage	Netherlands	Internal Combustion Engine	USA
Chemical Hydrides	Switzerland	Refueling Station	USA

Table 2. Hydrogen Demonstration Projects

Project	Lead
Solar H ₂ Production Facility	Electrolyser
Demonstration Plant for H ₂ Production and Use in Fuel Cell	ATEL
Solar H ₂ Pilot Plant with 3 Storage Systems	INTA
Stand Alone PV-H ₂ Small Scale Power System (SAPHYS)	ENEA
Alkaline Bipolar Electrolyser	ENEA
Off Peak Storage System	Kogakuin University
CO ₂ Fixation and Utilization in Catalytic Hydrogenation Reactor	RITE
H ₂ Vehicle	Mazda
H ₂ Rotary Engine Cogeneration System	Mazda
H ₂ Production Utilizing Solar Energy	Kansai Electric Power Co., Mitsubishi
Development of Solar H ₂ Processes	Helsinki University of Technology
Solar H ₂ Fueled Truck Fleet and Refueling Station	Clean Air Now, Xerox
Genesis Ten Passenger PEMFC Vehicle	Energy Partners
Schatz Solar H ₂ Project	Humboldt State University
City of Palm Desert Renewable H ₂ Transportation	Humboldt State University

MODELING OF SUSTAINABLE HYDROGEN PRODUCTION / STORAGE ENERGY SYSTEMS FOR REMOTE APPLICATIONS

Eric Martin and Nazim Muradov
Florida Solar Energy Center,
1679 Clearlake Road, Cocoa, FL 32922

KEYWORDS: Modeling, Sustainable Hydrogen Production, Fuel Cell

ABSTRACT

The results from computer simulation of an integrated renewable hydrogen energy system with daily and seasonal energy storage are reported in this paper. The main components of the energy system are a photovoltaic array, PEM electrolyzer, PEM fuel cell, battery, pressurized hydrogen storage unit, controller, and electric load. The modeling was performed using modified TRNSYS simulation software. System size, performance, and cost trade-offs were analyzed by simulating two short-term energy storage scenarios: one with a large battery storage capacity (approximately one day) and one with a much smaller capacity (two hours). Results show that a system with a small battery storage capacity is more desirable in the interest of system renewability, however it is more capital cost intensive.

INTRODUCTION

The concept of stand-alone renewable energy systems that use hydrogen as an energy storage medium has attracted much attention recently. The main objective of this work is to develop an efficient tool to assist in the design and evaluation of integrated solar hydrogen production/storage energy systems (ISHES). We have conducted an extensive literature search on different ISHES demonstration projects and the existing computer simulation software packages (CSP) (for example, references [1-5]).

In the simulation of the ISHES, batteries are included for short-term storage of electricity generated by the photovoltaic (PV) array and the fuel cell. In the interest of keeping the ISHES system as renewable as possible, it is desirable to utilize as few batteries as possible in the system design. Batteries tend to have a much shorter lifetime (5-10 years) compared to the renewable sources of electricity found in the system (20 years). However, as the amount of battery storage capacity decreases, the sizes of other system components, such as hydrogen storage capacity and size of the PV array, increase in order to compensate. In order to investigate this system trade-off, two simulation studies have been conducted on the proposed ISHES. Case 1 has a large battery storage capacity (approximately one day) and Case 2 has a much smaller capacity (two hours).

METHODS

We chose the TRNSYS simulation package, created by the Solar Energy Laboratory (SEL) at the University of Wisconsin-Madison, to be the main platform for the system integration and simulation [6]. TRNSYS is transient simulation software with source code written in FORTRAN. No models for the core components of the ISHES (fuel cell, electrolyzer, and hydrogen storage) are currently included with the standard version of the TRNSYS software. However, the SEL has collected many applicable component models, written by various users, and currently uses them to demonstrate the capabilities of the software.

The following paragraphs outline individual component specifications used in the simulation. These specifications have been optimized such that the renewable energy system can meet the load requirements with zero percent system downtime. The length of each simulation was one year, beginning in January and ending in December.

Location/Weather Conditions. Typical meteorological year (TMY) data which includes average values for solar insolation, ambient temperature, and humidity for Orlando, FL (28° N) has been used as a starting point for the simulation.

Load Profile. The peak load each day is 10 kW, which occurs in the early evening, and the daily average load is 2.5 kW. The daily, peak, and average loads that the ISHES system must supply also take into account losses encountered in AC/DC power inversion, DC/DC voltage conversion, and power requirements of various system components (i.e. controller).

Batteries. Case 1 includes a total of four deep cycle solar batteries. The batteries are connected in series, which maintains a battery bus voltage of 48 V. The battery string has a capacity of 125

Ah, which permits the batteries to store 2 hours of required system amperage based on a daily consumption of 58 kWh. Case 1 represents a situation where the batteries are only able to supply the system load when electricity production switches between the PV array and the fuel cell. No means of safety back-up power is provided in the event that the PV array and fuel cell become inoperable.

Case 2 include a total of 12 batteries arranged in an array of three parallel strings of four batteries each. In this case, each parallel string has a capacity of 635 Ah. With 1905 Ah total storage capacity, the battery array has the ability to solely power the load for 1.25 days, based on 58 kWh daily consumption. This scenario provides some back up power in the event that system interruptions are encountered with the PV array or fuel cell. Also, in this case, the size of the battery array prevents the need for the fuel cell to be solely responsible for powering the load every evening, when the PV array is inactive. Instead, the fuel cell is only required to supply power when the battery state-of-charge drops below a certain "safe" limit, caused by consecutive days of low solar insolation.

Photovoltaic Array. For case 1, a total of 588 individual modules are used in the simulation, and the array is configured with 147 parallel strings of 4 modules each. Each module is assumed to be rated at 100 W at standard test conditions (irradiance = 1000 W/m², cell temperature = 25 °C), therefore the peak power output of the array is expected to be 58.8 kW. The panels are tilted at an angle of 45° (28° + 17°), which optimizes electricity production during the winter months, due to the sun's wintertime position in the sky.

For case 2, a total of 256 of the same modules are used, and the array is configured with 64 parallel strings of 4 modules each. The panels are also tilted at an angle of 45°, and the peak output of the array at standard test conditions is expected to be 25.6 kW.

Electrolyzer. For these simulations, data for a high pressure (1000 psi) PEM type electrolyzer has been used in place of the alkaline data that was provided along with the TRNSYS subroutine. The PEM electrolyzer has a total of 25 cells and each cell is assumed to have an area of 279 cm². The electrolyzer operates at an efficiency of approximately 75%, producing approximately 0.48 kg/h (90 slpm) of hydrogen at 500 A.

Hydrogen Storage. A pressurized tank is included in these simulations that stores hydrogen as it is produced by the electrolyzer. The maximum pressure of the tank is 1000 psi. For case 1, an optimized storage volume of 20 m³ is used in the simulation, allowing a maximum of 90 kg of hydrogen to be stored at ambient (25 °C) temperatures. For case 2, an optimized storage volume of 10 m³ is used, allowing a maximum of 45 kg of hydrogen to be stored at 25 °C.

Fuel Cell. The PEM fuel cell used in these simulations operates on hydrogen and air and contains a total of 50 cells. Each cell has an area of 300 cm². The stack produces a total of 11.6 kW of DC power at 32 V and 363 A. The stack operates at an efficiency of 44% consuming 0.683 kg/h (127 slpm) of hydrogen.

Power Conditioning. In the ISHES simulation, four power conditioning devices are included. A maximum power point tracker (MPPT) maintains optimum performance of the PV panels by ensuring that the array operates at the maximum power point on its I-V curve. A DC to DC converter upgrades the fuel cell output voltage to the battery bus voltage. A diode prevents the back flow of current from the battery array and fuel cell to the electrolyzer. This ensures that the only source of power for the electrolyzer is the PV array. Finally, a DC to AC inverter is included to invert the DC power supplied by the battery array to AC power required by the electric consumer. The efficiency of all power conditioning devices is assumed to be approximately 90%.

Controller. A single controller device oversees total system operation in the ISHES simulation. By assessing the requirements and/or output available of every system component, including the electric load, the controller makes appropriate decisions to optimize system performance. These decisions include whether to connect or disconnect individual components to/from the system and whether power generated by the PV array is sent to the electrolyzer, for hydrogen generation, or to the battery array, for use by the electric consumer. The controller also decides whether the battery array contains sufficient charge to power the load under dark conditions, or whether the fuel cell should be activated to power the load and recharge the battery.

RESULTS AND DISCUSSION

Figures 1 and 2 show simulation results for case 1 and 2 respectively. In these graphs, the dark solid line shows seasonal variations (shown on the top axis) of the amount of hydrogen stored in

the pressurized tank. This amount is expressed as a fraction of the total storage capacity of the tank (shown on the left axis). All remaining plots on these graphs were created using the bottom axis to show daily variations.

The power required by the load and the power produced by the PV array are shown as dashed lines on these graphs. This data has been plotted for a simulated first week of February, occurring during the simulation year. The month of February represents a "worst case" scenario, for it is expected to be the month with the lowest average solar insolation. The values are read off of the right hand axis in units of watts (please note that the power produced by the PV array in case 1 has been divided by a factor of 2 such that it can be plotted on the same graph as the load).

Finally, the battery state of charge (SOC) is shown on these graphs as a dotted line. Similar to fractional hydrogen storage, battery SOC is expressed as a fraction of the total battery storage capacity. This plot has also been created for the first week of February, and its value is read off of the left axis.

Along with the design of each individual ISHES component, total system operation plays a major role in system performance, size, and cost. Each of the individual components are intimately linked together in some way, therefore changing the size or operational parameters of one component has the potential to disturb the balance of the entire system. Simulations of the proposed ISHES have been conducted with the intent of optimizing system performance, rather than cost, however it is expected that an optimized system will also be the most cost effective. The primary parameter that is intended to be the basis for optimization is the value for hydrogen storage. Other mandatory system criteria included use of a PEM type fuel cell and electrolyzer, maximizing battery lifetime, and maintaining zero percent system downtime.

As seen in Figure 1 and 2, fluctuations in battery SOC occur according to the relative size of the battery array. With a small battery array, as in case 1, SOC decreases rapidly under dark conditions. Upon reaching a lower limit, chosen to prevent excessive battery discharge, the fuel cell is activated to recharge the battery as well as power the load. With a larger battery array, as in case 2, the fuel cell is activated less often under dark conditions, due to the slower rate of battery array discharge.

Optimizing the PV array for wintertime performance maximizes the use of the fuel cell, which represents mainly a capital expense. By also requiring fuel cell activation during the summer months, when solar insolation is the greatest and the fuel cell ordinarily may not be needed depending on the battery array capacity, this expensive piece of equipment is used to its fullest extent rather than allowing it to lie dormant for several months.

The same fuel cell has been simulated in both case 1 and 2, and the frequency of its activation affects overall system cost. As seen by the results of simulations for case 1 and case 2, a system trade-off exists among battery array storage capacity, hydrogen tank storage capacity, and the size of the PV array. As previously discussed, the fuel cell is activated more often in case 1 due to the smaller battery array storage capacity. This case utilizes more hydrogen over the course of the year and subsequently requires a hydrogen storage tank that is twice the size of the tank in case 2 (see METHODS section). This is due to the fact that with a smaller battery array, less energy can be stored in that short-term medium. Since the same amount of energy is required in each case, more energy must be stored in the form of hydrogen. Since the values of solar insolation are identical in both cases, case 1 also requires a larger PV array (see METHODS section) to support the increased hydrogen production requirement. It is expected that case 1 will be more capital cost intensive than case 2, due to the fact that a larger hydrogen storage tank and larger PV array would cost more to implement than the added battery storage capacity.

Depending on what time of year the start-up of the ISHES system occurs, the hydrogen tank should be initially charged with the amount of hydrogen found in Figures 1 or 2 that corresponds to that particular time of year. The optimized storage tank values of maximum pressure and storage volume ensure that the tank is never completely empty, and rarely completely full to account for expected variation in weather conditions. Starting up the ISHES with a different value than what is found in Figure 1 or 2 will perturb this balance. Starting with more hydrogen than necessary will not cause system downtime, however the system will be overdesigned and will not utilize the full potential of each system component. Starting with less hydrogen than depicted will eventually cause system downtime during the winter season.

In principle, other methods of hydrogen storage (i.e. in the form of metal hydrides) could be used in ISHES and potentially lower the cost of the storage component. It is evident that the relative amount of hydrogen stored will essentially remain the same, therefore, for the purpose of system

performance optimization, the method of hydrogen storage is not essential. This issue will become important during cost optimization of the ISHES. The same holds true for an addition of an oxygen storage sub-system to the ISHES. Storing oxygen produced by the electrolyzer for use in the fuel cell (rather than ambient air) could potentially increase the overall cost of the system. However, since the use of oxygen affects the efficiency, and consequently size and cost of the fuel cell, the added cost of oxygen storage will have to be weighed against the reduced cost of the fuel cell.

CONCLUSIONS

TRNSYS was chosen as a viable platform for performing simulations on the proposed ISHES. The main components of the energy system are a photovoltaic array, PEM electrolyzer, PEM fuel cell, battery, pressurized hydrogen storage unit, controller, and electric load. The simulation code was customized in order to model the specific characteristics of proposed system components. A realistic load profile was chosen as an example application for the renewable energy produced by the ISHES system, and system components have been designed and optimized to meet this load with zero percent system downtime. Results from simulations of two cases, one with four batteries and one with twelve batteries, show that a system with fewer batteries and, therefore one that is more renewable, requires a larger PV array to supply necessary power, and may be more costly. The details of this cost analysis, along with the potential to store oxygen produced by the electrolyzer and the use of metal hydrides to store hydrogen, have been left until a system cost optimization is conducted.

ACKNOWLEDGEMENTS

Authors would like to acknowledge the financial support provided by U.S. Department of Energy, Energy Partners, Inc., Caribbean Marine Research Center, and the Florida Solar Energy Center, and the technical support provided by Solar Energy Laboratory/ University of Wisconsin-Madison.

REFERENCES

1. C. Gregoire Padro, V. Putche, M. Fairlie, *Proc. XII World Hydrogen Energy Conference*, Buenos Aires, Argentina, 1998, 2247.
2. J. Vanhanen, P. Lund, *Int. J. Hydrogen Energy*, v.20, 575, 1995.
3. H. Barthels, W. Brocke, K. Bonhoff, et al. *Int. J. Hydrogen Energy*, v.23, 295, 1998.
4. P. Lehman, C. Chamberlin, *Int. J. Hydrogen Energy*, v.16, 349, 199.
5. S. Galli, G. De Paoli, A. Ciancia, *Proc. X World Hydrogen Energy Conference*, Cocoa Beach, Florida, USA, 1994, 439.
6. S. Klein, W. Beckman, et al. TRNSYS A transient system simulation program. Solar Energy Laboratory, University of Wisconsin-Madison, WI 53706, 1992.

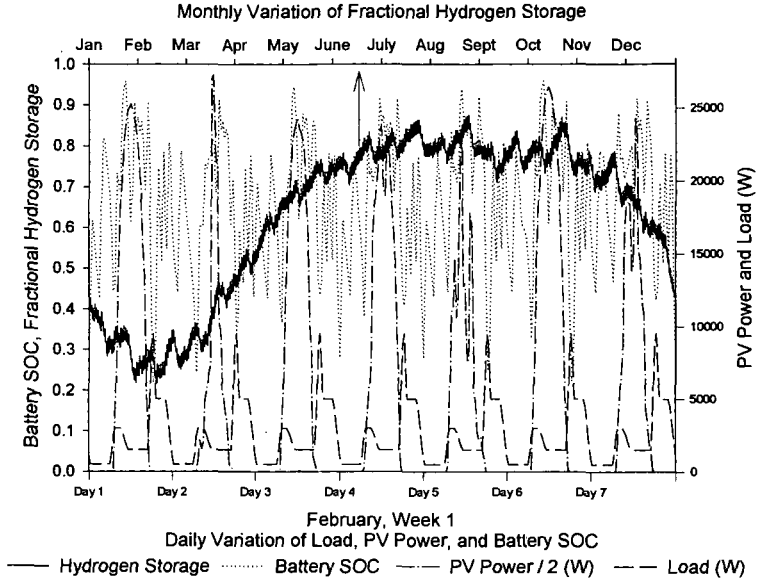


Figure 1: Case 1 Simulation Results

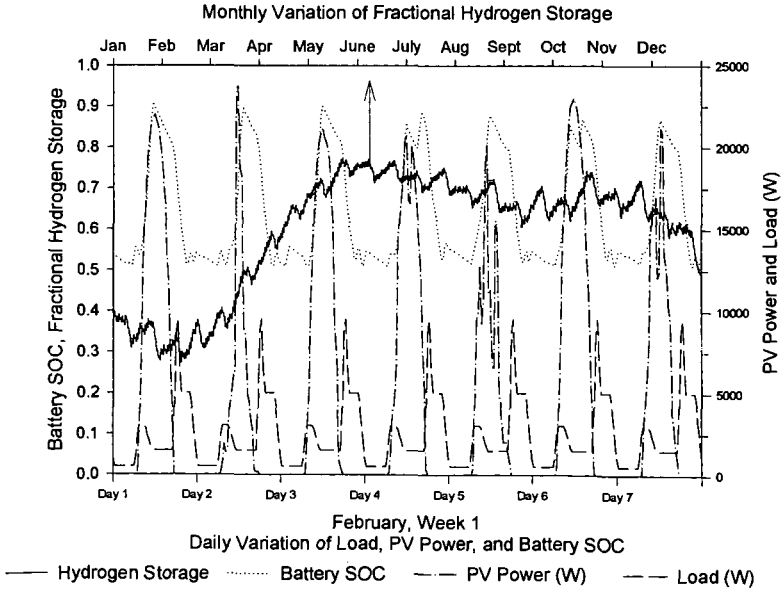


Figure 2: Case 2 Simulation Results

Hydrogen For A PEM Fuel Cell Vehicle Using A Chemical-Hydride Slurry

Ronald W. Breault, Christopher Larson, Jonathan Rolfe
Thermo Power Corporation

INTRODUCTION

Because of the inherent advantages of high efficiency, environmental acceptability, and high modularity, fuel cells are potentially attractive power suppliers. Worldwide concerns over clean environments have revitalized research efforts on developing fuel cell vehicles (FCVs). As a result of intensive research efforts, most of the subsystem technologies for FCVs are currently well established. These include: high power density PEM fuel cells, control systems, thermal management technology, and secondary power sources for hybrid operation. For mobile applications, however, supply of hydrogen or fuel for fuel cell operation poses a significant logistic problem.

A great many technologies have been investigated as candidates for the onboard storage of pure hydrogen for FCVs. These technologies include: 1) compressed hydrogen, 2) liquefied hydrogen, 3) rechargeable metal hydride, 4) carbon adsorption and hybrid systems, and 5) liquid hydrides and other chemical hydrides. However, the volume and/or weight energy densities of these onboard hydrogen storage technologies are significantly lower than those of internal combustion engines or the DOE hydrogen plan. Therefore, development of a high energy density subsystem to supply hydrogen for fuel cell operation is an urgently needed technology for the successful development of FCVs.

To supply high-purity hydrogen for FCV operation, Thermo Power Corporation (THP) has developed an advanced hydrogen storage technology. In this approach, a chemical (light metal) hydride/organic slurry is used as the hydrogen carrier and storage media. At the point of use, high purity hydrogen will be produced by reacting the hydride/organic slurry with water. The fluid-like nature of the hydride/organic slurry will provide us a unique opportunity for pumping, transporting, and storing these materials. In addition, the spent hydride can relatively easily be collected at the pumping station and regenerated utilizing renewable sources, such as biomass, natural gas, or coal at the central processing plants. Therefore, the entire process will be economically favorable and environmentally friendly. The final product of the program is a user-friendly and relatively high energy storage density hydrogen supply system for fuel cell operation.

BACKGROUND AND TECHNICAL APPROACH

Pros and cons of the currently available and advanced hydrogen storage technologies, along with expected performance of the proposed technology, are summarized in Table 1. A plot showing how chemically-reacting hydrides compare with other fuels is shown in Figure 1.

An essential feature of the THP approach is to develop a relatively high energy storage density hydrogen supply system based on exothermic chemical reactions between metal hydrides and water. Hydrogen production via metal hydride and water reactions is a well-established industrial process. In fact, several groups of researchers have investigated the metal hydride/water reaction process to supply hydrogen for fuel cells for mobile power generations. In this research, it has been identified that reaction rate control, frequent on/off operation, and safety of the operation could be significant problems for high energy density operations.

One of the key technical challenges in the program is, therefore, to precisely control the metal hydride and water reaction. In our approach, the continuous organic slurry media will act as a path for dissipating heat that is generated from the hydride/water reaction. Furthermore, by controlling surface chemistry of the organic media, the water/metal hydride reaction rate can easily be controlled. This concept is shown in Figure 2. In Figure 2a, a sketch is shown of two hydride particles, one surrounded by oil and one not. The oil layer inhibits the water access to the hydride and thereby controls the rate of reaction, which would otherwise be explosive. In Figure 2b, the hydride suspension is shown to exemplify how the dispersant acts to hold the particle in suspension within the oil and further inhibit the reaction with water.

Because of the reaction rate control afforded by the organic media, the hydrogen reactor can be a simple device. Water and hydride slurry are metered into the reactor, where they are thoroughly mixed to ensure complete reaction. This reaction goes to completion quickly, leaving a powdery waste. Hydrogen production rate is controlled by the injection rate of water and hydride. Heat

released by the reaction can be absorbed by the evaporation of water. No complicated control systems are needed to ensure proper and safe operation of the hydrogen reactor.

The water required for thermal control and hydrogen reaction is provided by condensed vapor from the hydrogen fuel cell. Only a small reservoir of water is required for startup, makeup, and surge demand. Thus, the required water does not significantly affect the volumetric and gravimetric energy storage densities.

The slurry form of hydride has other benefits beyond reaction control. The hydride fuel can be handled as a liquid, simplifying transportation, storage, and delivery. Use of a slurry permits refueling similar to current gasoline filling stations, allowing the tank to be easily topped-off at any time. The hydroxide waste products produced by the hydrogen system can be washed from the onboard storage tank during the slurry filling operation. Both the hydride fuel and hydroxide waste product can be easily transported between the distribution centers and a central recycling plant.

The used reactant slurry containing LiOH is returned to a central processing plant where the LiOH is recycled to LiH in a large-scale chemical process. The LiH is remixed with the slurry fluid and transported back to refueling stations scattered over a large area as needed. The basic energy input to the system is provided at the central plant and can be from a variety of energy sources, including fuels like coal, biomass, natural gas, and petroleum oil. All environmental emissions occur at the central processing plant. The vehicle is zero emission, with no hydrocarbon, CO, or CO₂ emissions. The central plant can include more sophisticated emission cleanup processes than would be possible for an onboard processing system.

An important concept feature that needs to be pointed out is the recovery and recycle of the spent hydride at centralized processing plants using a low cost fuel, such as coal or biomass. Regeneration process analysis has indicated that recycling can be performed utilizing a carbothermal process with minimum energy input and at a low cost. Compared to current hydrogen costs of about \$9.00 to \$25.00 per million Btu, this concept should enable hydrogen costs as low as \$3.00 per million Btu to be realized for a LiH system^(1&2). Also, because the hydride reaction will liberate only pure hydrogen, fuel cell catalyst life should be maximized, resulting in high system performance and reliability.

PROTOTYPE DEVELOPMENT

The major objectives of this hydrogen generation development effort are twofold. The first is to use a laboratory-scale system to determine optimum materials and hydrogen generation process conditions to achieve high specific energy for hydrogen supply. The second objective is the design and fabrication of a prototype hydrogen generation system capable of supplying 3.0 kg/hr of high purity hydrogen for fuel cells.

Although there are numerous metal hydrides and organic carrier candidate materials, only a limited number of metal hydrides and organic carrier materials can be used to satisfy DOE's goals of specific weight and volume. One of the essential considerations for the metal hydride is its hydrogen generation efficiency, which includes reaction chemistry between metal hydride and water to complete hydrolysis reactions in a safe and controlled manner. The organic carriers should be chemically inert toward metal hydrides and spent hydrides for storing and transporting, and during hydrolysis reaction. These materials also should be easily separated from spent hydrides, either thermally or mechanically, and be recycled for reuse. Although regeneration of the spent hydrides is not part of the technical effort of this program, it is an important issue for economical and commercial development of the technology.

In the initial effort, we thoroughly analyzed, both theoretically and experimentally, the reaction chemistry of a variety of metal hydrides and water, and the chemical stability of the organic carriers in contact with metal hydrides and spent hydrides. Since detailed hydrolysis reaction kinetics of the metal hydride/organic carrier slurry were not known, we conducted experiments using a high-pressure (2000 psi) and high-temperature (232°C) vessel with temperature, pressure, and magnetic stirrer control capabilities (500 cm³ internal volume). For this investigation, we selected the candidate materials based on the guidelines listed in Table 2.

In the development of a hydride/water activation system, several ideas were considered. These are:

- Single Tank Reactor
- Slurry Atomization Reactor
- Water Bathed Reactor
- Auger-aided Water Vaporizing Reactor

The single tank reactor, shown in Figure 4, is the simplest system. However, several problems exist for this system. The heat exchanger allows hot spots, increasing hydrocarbon contamination. It will also have a slow response to H₂ demand. Furthermore, it is likely that not all hydride will react, leaving a hazardous waste product, and a large volume containing pressurized hydrogen.

The atomized slurry reactor, shown in Figure 5, was conceptualized to remove heat from 15µm droplets by direct hydrogen heat transfer. This system is complicated and has a wear-prone slurry atomization system. The ½ m³/sec H₂ flow rates needed for cooling are quite high. In addition, the heat exchanger may be fouled by dust. There is also the likelihood of poor hydride/water mixing reducing generation efficiency, and a large pressurized hydrogen volume is required.

In the water-bathed reactor configuration, shown in Figure 6, heat is removed by the recirculated flow of water. Excess water assures low reaction temperature and complete reaction in a relatively small water to air heat exchanger. Problems, such as the water soaked LiOH waste product and the weight of wasted water, push this concept outside the system goals. The water could be separated by a filter or a filter press, but neither a filter or filter press system allows the concept to reach the weight goals. Also, unfiltered particles will wear the recirculation pump.

In the auger-aided reactor, shown in Figure 7, reactants are pumped to a mixing auger. At 300 rpm, the auger mixes, crushes particles, and eliminates foaming within the hydrogen generation reactor. The waste product contains 10% by mass of water and is a dry, free-flowing powder. About three times the stoichiometric water is added and vaporized by the heat of reaction to control the temperature.

The hydrogen water vapor content in the auger-aided reactor depends on the heat exchanger outlet temperature. Vapor condensation is slowed by the presence of hydrogen, increasing the size of the heat exchanger. The water vapor content could also be reduced by using hydride as a desiccant. This hydrogen production system device achieves the weight and volume goals.

Based on the preliminary analysis and testing of the various concepts discussed above, a prototype system to produce up to 3 kg/hr of hydrogen was designed. This system is shown in Figure 8. To produce the hydrogen, 0.5 l/min 60% LiH slurry flows into the auger reactor, along with 1.4 l/min water for reaction and vapor cooling. The system produces up to .75 kg hydrogen per run. A 1.6 gallon reservoir of 60% LiH slurry, a 5.5 gallon water reservoir, and a 12 gallon hydroxide container make up the reactant and product volumes. A computer controls the hydride and water pumps. Data acquisition of pertinent pressures, temperatures, hydrogen flow, hydrocarbon, and water vapor content are recorded. The system is self-contained on a rolling cart.

A valveless ceramic piston pump is used for the LiH slurry and a gear pump is used for water flow. Three heat exchanger cores with 8-10" fans are used to condense the water from the hydrogen. Table 3 summarizes the energy, mass, and volumetric densities for the system, assuming storage of 15 kg H₂. To meet the design goals of 3355 Whr/kg and 929 Whr/l, our system must weigh less than 179.9 kg and must have a volume of less than 649.6 l. Table 3 shows that the system designed will meet the weight goal and exceed the volume goal.

SUMMARY

In summary, the following can be stated:

- A hydride/water activation process (the hydrogen generation reactor) has been developed.
- Thermal management design for prototype system has been established.
- A chemical hydride slurry can be used to generate hydrogen for transportation vehicle applications.
- The system has the potential to be safe and easy to use.
- Chemical hydride-based systems can achieve DOE's energy density goals.

REFERENCES

1. Breault, Ronald, "Advanced Chemical Hydride Hydrogen Generation/Storage System for PEM uel Cell Vehicles," to be published in the DOE Office of Advanced Automotive Technology FY 1999 Annual Progress Report.

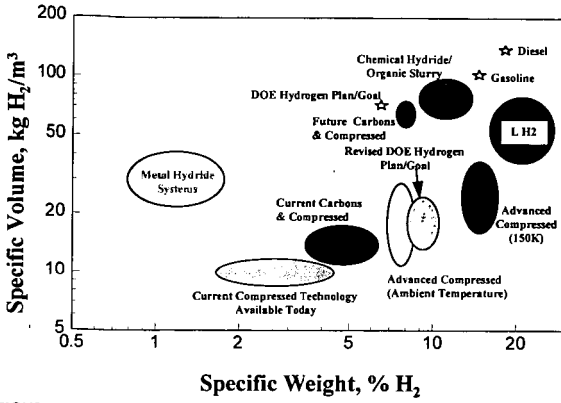


FIGURE 1. Summary of Current and Future Hydrogen Storage Systems

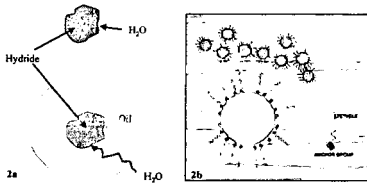


FIGURE 2. Hydride-Water Reaction Concept

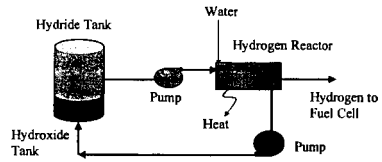


FIGURE 3. Hydrogen - Hydride Concept

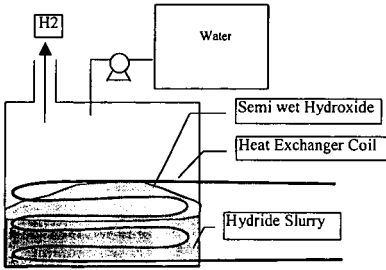


FIGURE 4. Simple One Tank Concept

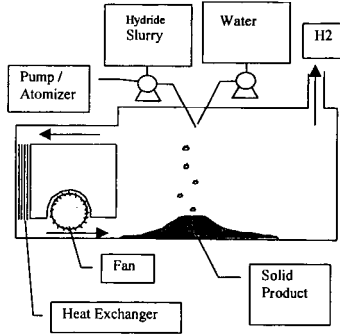


FIGURE 5. Atomized Slurry Reactor Concept

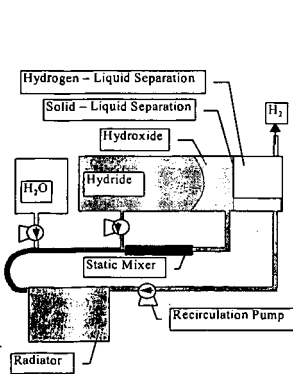


FIGURE 6. Water Bathed Reactor Concept

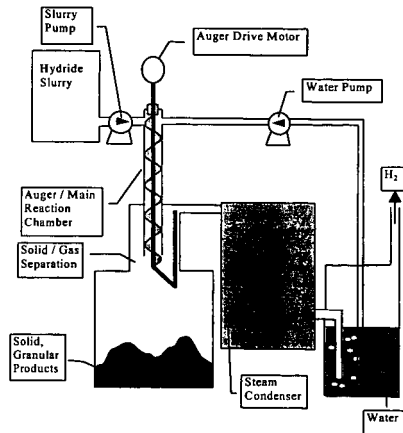


FIGURE 7. Auger-Aided Reactor Concept

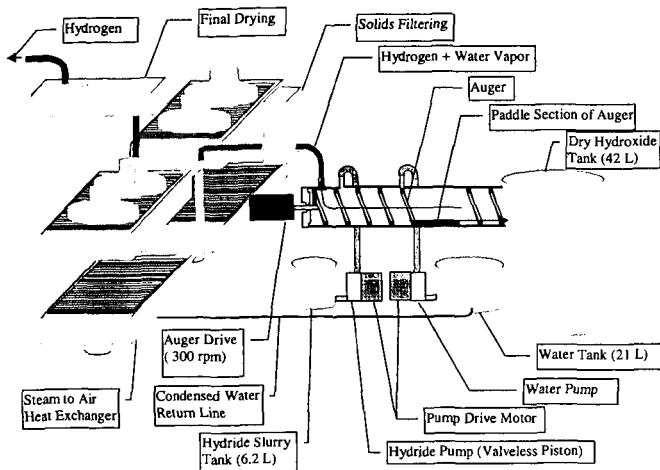


FIGURE 8. Auger-Aided Reactor System Being Built

TABLE 1. Hydrogen Storage Technology Status

Storage Technology	Specific Weight (HHV)		Specific Volume (HHV)		Remarks
	Wh/kg	%H ₂	Wh/L	kg H ₂ /m ³	
DOE Goal • Liquid/Gas	3963/5323	9.9/13.4	1100/828	28/21	-DE-RA02-97EE50443
Liquid H₂ • Cryogenic	6350	16.1	1250	32	-Not including boil-off loss
Gaseous H₂ • 5000 psia	2630	6.7	780	20	-Could be better with new high-pressure tanks
Carbon Adsorption • 794 psi at 78°K	2858	7.2	1535	39	-New materials with better capacities
Liquid Hydride • Methylcyclohexane	2070	5.9	1618	46	-Need more fundamental research
Proposed Chemical Hydride Slurry • CaH ₂ • LiH	2670 5050	6.8 12.8	2430 2430	62 62	-Includes weight and volume of the container, and ancillary components -Does not include reactant water, which is assumed to be provided partially from exhaust gas
• NaBH ₄	4760	12.1	2570	65	
• LiBH ₄	6350	16.1	2640	67	

TABLE 2. Considerations for Selecting Metal Hydrides and Organic Carriers

Metal Hydrides	Organic Carriers
<ul style="list-style-type: none"> • High specific energy density • High hydrogen generation efficiency • Relatively inert during storage before and after reaction with water • Ease of regeneration • Low costs 	<ul style="list-style-type: none"> • Non-reactive with metal hydrides and spent hydrides • Low molecular weight • Easy to recycle (easy to separate from spent hydride and water, and to collect for reuse)

TABLE 3. System Mass and Volumetric Design Summary

	Wt (kg)	Vol (L)
65% Lithium Hydride Slurry Hydroxide	95.5	
Heat Exchanger	31.38	82.5
Hydride Tank	20	120
Hydroxide Tank	12	310
Hydride Metering Pump	6.8	4
Water Metering Pump	3	2.5
Auger Drive Motor	4	2.3
Auger Construction	5	10
Total	177.7	531.3
System Goals (kg, l)	179.9	649.6
System Values (watt-hr/kg, watt-hr/liter)	3397	1136
Goals (watt-hr/kg, watt-hr/liter)	3355	929

ELECTROCHEMICAL INVESTIGATION OF
 $Y_xZr_{1-x}Mn_mFe_nCo_pV_oCr_q(m+n+o+p+q=2)$
ELECTRODE FOR Ni-MH BATTERY APPLICATION

N.Rajalakshmi, K.S.Dhathathreyan
Centre for Electrochemical and Energy Research
SPIC Science Foundation
111, Mount Road
Guindy, Chennai 600 032, INDIA
&
Sundara Ramaprabhu
Magnetism and Magnetic Materials Laboratory
Department of Physics
Indian Institute of Technology
Chennai 600 036, INDIA

ABSTRACT:

The AB₂ type Laves phase hydrogen absorbing alloys are being investigated as suitable electrode materials for Ni-MH batteries, because of their higher electrochemical capacity. The electrochemical properties like electrode potential, reversible electrochemical capacity and diffusion coefficient as a function of state of charge in the Y_xZr_{1-x}Mn_mFe_nCo_pV_oCr_q(m+n+o+p+q=2) electrodes were investigated in an alkaline solution. The reversible electrochemical capacity of the electrode was found to be in excess of 450 mAh/g and hydrogen concentration was estimated as 3.5 hydrogens/formula unit. The process that occur in the electrode during charge and discharge, has been studied by Cyclic Voltammogram(CV) experiments, carried out at different sweep rates. It was found that at low sweep rates, the hydrogen concentration on the surface increases due to longer polarisation and the hydrogen concentration approaches a value which favours a metal hydride formation. The diffusion coefficients were also evaluated with respect to state of charge. The results will be presented in the paper.

INTRODUCTION:

AB₂ hydrogen storage alloys are promising for negative electrodes in Ni-MH batteries for their higher discharge capacities and better resistance to oxidation than those of AB₅ alloys [1,2]. As AB₂ type multiphase hydrogen storage alloys are mainly composed of C14, C15 Laves phase, and some solid solutions with bcc structure, there exist abundant boundaries, with enriched electrochemically catalytic elements as active reaction sites and diffusion pipes for transporting reactants and products. However, the activation and electro-catalytic activity of the alloy electrode is still inferior to that of the MnNi₅ based alloy [3]. The main reasons for the slow activation and low electro-catalytic activity are: an oxide layer is formed on the surface of the alloy grains, and this oxide layer is a bad electrical conductor, hence impedes the diffusion of hydrogen and absence of Ni content layer on these AB₂ alloy surface results in a lower surface activity for hydrogen absorption/desorption [4].

The hydrogen storage properties of the alloys, whether as an electrode or as a storage medium, are initially related to their composition and vary widely with small changes in the type and the amount of substituent elements [5]. Thus, depending on the battery use, it is possible to design the electrode characteristics by changing the alloy compositions. The choice of the material is based on the desirable metal-hydrogen bond strength for use as electrodes in aqueous media and an appreciable hydrogen storage capacity/partial substitution for both the A and B sites, dramatically improves the cycle lifetime and the electrochemical discharge capacity has been optimized by substituting various metals as partial constituents, and by moving the composition ratio from stoichiometry. This has resulted in the preparation of four or five component Laves phase hydrogen storage alloys with discharge capacities over 400 mAh/g [6]. Knosp et al [7] has studied the Laves phase alloys of composition (Zr,Ti)(Ni,Mn,M)_x where M= Cr,V₂Co,Al and x= 1.9 to 2.1 with hexagonal C14 or cubic C15 structure in order to select the most suitable AB₂ alloys as an active material for Ni-MH batteries. Kim et al [8] studied the hydrogen storage performance and electrochemical properties of ZrMn_{1-x}V_xNi_{1.4+y} (x= 0.5,0.7; y =

0.0 to 0.6) and found that the major factor controlling the electrode properties was the specific reaction surface area and the exchange current density depending upon the composition. The maximum electrochemical capacity experimentally observed was found to be 338 mAh/g for $ZrMn_{0.5}V_{0.5}Ni_{1.4}$, and the discharge efficiency was found to be 85%. Hence fundamental studies on the charge/discharge characteristics are required for improving the performance of a Ni-MH battery [9,10]. The present work focuses on elucidating the electrochemical properties like charge/discharge characteristics, diffusion coefficient etc., or an AB_2 compound with the composition $Y_xZr_{1-x}Mn_mFe_nCo_pV_oCr_q(m+n+o+p+q=2)$ and the processes that occur during charge and discharge were also evaluated.

EXPERIMENTAL:

Hydrogen storage alloys of composition $Y_xZr_{1-x}Mn_mFe_nCo_pV_oCr_q(m+n+o+p+q=2)$ were prepared by arc melting in an argon atmosphere. The buttons were turned upside down and remelted 5 to 6 times in order to get good homogeneity and the alloy buttons were annealed at 900 K for about 3 days. The intermetallics were pulverized mechanically into powders in an agate mortar. Structure and phase density of the sample was characterized by X-ray diffraction (XRD). The samples prepared had an overall AB_2 phase.

For the electrochemical measurements, the electrodes were prepared by grinding the alloy into 75 μ size and mixing it with copper powder in the ratio of 1:3 with a PTFE binder. The putty form of the mixture was mechanically pressed onto a current collector (Ni mesh) at RT. Then the electrode was sintered at 300°C for about 3 hrs under vacuum. The geometric area of the electrode was about 2 cm^2 . The counter electrode was Pt, has a much larger geometric area than the WE. The electrolyte 31% KOH, which is the same as that used in the alkaline batteries, were prepared from reagent grade KOH and deionised water. The electrodes were tested for their charge-discharge characteristics, initial capacity, cycle life and diffusion coefficient. The electrochemical measurements were carried out in a flooded electrolyte condition in open cells. Potentials were monitored using a saturated calomel as reference electrode. The electrochemical measurements include the diffusion coefficient as a function of state of charge and also the electrochemical processes that occur during charge/discharge. These measurements were carried out using a EG & G galvanostat/potentiostat Model 273, with the available techniques like chronopotentiometry, cyclic voltammetry and constant potential coulometry.

RESULTS AND DISCUSSION:

The electrochemical capacity of a hydride electrode depends on the amount of reversibly absorbed hydrogen in the hydriding material. Fig. 1 shows the charge/discharge curves of the electrode after 30 cycles. The electrode showed the highest electrochemical charging capacity of 470 mAh/g, which corresponds to a hydrogen concentration of 3.5 hydrogens/formula unit. Hydrogen evolution was found to occur around -1.35V. This shows that the metal-hydrogen bond is not weak, and hence hydrogen can react with the alloy for hydride formation. However, if the bond is very strong, the metal hydride electrode is extensively oxidised, and cannot store hydrogen reversibly. The coulombic efficiency was found to be 85%, the charging potential and the discharging potential was around -0.9 and -0.5V respectively. The electrochemical charging capacity was found to be slightly lower when the electrode is charged at the 2C rate (80 mA) compared to the 1C rate (40 mA) as shown in Fig 2. As already mentioned, the highest electrochemical capacity was observed only after 30 cycles and then the capacity remained constant for almost 100 cycles, as shown in Fig.3, which clearly reveals that degradation of the electrode material is very slow.

To estimate the diffusion coefficient parameter D/a^2 , the following procedure was carried out. The alloy was fully activated by charging and discharging the electrode for about 30 cycles. Then the electrodes with different states of charge were equilibrated until an equilibrium potential was reached. Initially, the activated electrode was discharged at constant potential at three different states of charge. In order to secure a zero concentration of hydrogen at the surface of each individual particle, the electrode was

discharged at a constant anodic potential of $-0.56\text{V}(\text{SCE})$. Discharge curves obtained for seven different charged states are given in Fig. 4. For large times in Fig.4, an approximately a linear relationship exists between $\log(i)$ and t , which is consistent with the equation

$$\log(i) = \log\{(6FD(C_0 - C_s)/da^2) - (\pi^2/2.303(D/a^2)t)\} \quad (1)$$

Where C_0 is the concentration in the bulk of the alloy and a constant surface concentration C_s , \pm sign indicates the charge (-) and discharge (+) process [11]. From the slope of the linear portion of the corresponding curves in Fig.4, the ratios of D/a^2 were estimated.

The diffusion coefficient may also be determined from the amount of charge transferred [12]. Assuming that the hydride alloy particles are in spherical form, the diffusion equation is,

$$\partial(rc)/\partial t = D \partial^2(rc)/\partial r^2 \quad (2)$$

where c is the concentration of hydrogen in the alloy, t is the time, D is an average(or integral) diffusion coefficient of hydrogen over a defined concentration range, and r is a distance from the centre of the sphere. Since the discharge process was carried out under a constant current condition, it is reasonable to assume that a constant flux of the species at the surface and uniform initial concentration of hydrogen in the bulk of the alloy. Thus, the value of D/a^2 may be evaluated for large transition times, τ ,

$$D/a^2 = 1/[15\{Q_0/I - \tau\}] \quad (3)$$

Where Q_0 is the initial specific capacity (c/g), I is the current density (A/g) and τ is the transient time (s), i.e the time required for the hydrogen surface concentration to become zero. The ratio Q_0/I corresponds to the discharge time necessary to discharge completely the electrode under hypothetical conditions, when the process proceeds without the interference of diffusion. Thus D/a^2 were calculated using the above equation for different states of charge and are given in Fig.5. As shown in Fig.5, the ratio of D/a^2 is almost independent of the state of charge with an average value of $0.37 \times 10^{-5} \text{ s}^{-1}$. Assuming that the average particle radius is $15 \mu\text{m}$, the effective diffusion coefficient of hydrogen through the $\text{Y}_x\text{Zr}_{1-x}\text{Mn}_m\text{Fe}_n\text{Co}_p\text{V}_o\text{Cr}_q(m+n+o+p+q=2)$ electrode was estimated to be $8.32 \times 10^{-12} \text{ cm}^2/\text{s}$. This value is in consistent with the diffusion coefficient of hydrogen in Nickel alloys, which are in the range 20×10^{-12} to $56 \times 10^{-12} \text{ cm}^2/\text{s}$ estimated using a permeation technique[13-15]. Fig 6 shows the cyclic voltammogram(CV) of an activated sample of the alloy after 5 cycles ranging from -0.6 to -1.4 v vs SCE at various scanning rates. The definite peaks at potentials ranging from -0.9 to -1.2 v were observed and these adsorption peaks indicate that there are H atoms adsorbed on the surface due to the formation of the hydride. The counterparts responsible for the desorption of hydrogen from the alloys were also observed and are shown in Fig 7 in the range -0.1 to -0.6 . At low sweep rates, the hydrogen concentration on the surface increases due to longer polarisation and the hydrogen concentration approaches a value for the hydride formation.

ACKNOWLEDGEMENTS:

The authors are thankful to the Management, SPIC Science Foundation, for the financial assistance and for the facilities provided to carry out this work.

REFERENCES:

1. S.R.Ovshinsky, M.A.Fetcenko, J.Ross, Science, 260(91)(1990), 176
2. X.L.Wang, S.Suda,S.Wakao, Z.Phys.Chem 183(1994), 297
3. H.Sawa,S.Wakao, Mater.Trans JIM, 31 (1990)487
4. A.Zuttel, F.Meli and L.Schlapbach, J Alloys and Compounds 231(1995) 645
5. T.Sakai,K.Oguro,H.Miyamura,N.Kuriyama,A.Kato,H.Ishikawa and K.Iwakura, J Less Common Metals 231(1995) 645
6. H.Nakano, I.Wada and S.Wakao, Denki Kagaku, 672 (1994) 953
7. B.Knosp, C.Jordy,Ph.Blanchard and T.Berlureau, J Electrochem soc 145, (1998) 1478
8. Dong-Myung Kim, Sang-Min Lee, Jae-Han Jung, Kuk-Jin Jang and Jai-Young Lee, J Electrochem Soc 145(1998) 93
9. H.Inoue, K.Yamataka,Y.Fukumoto and C.Iwakura, J Electrochem Soc 143(1996) 2527
10. M.P.Sridhar Kumar, W.Zhang,K.Petrov, A.A. Rostami and S.Srinivasan, J Electrochem soc 142 (1995) 3424
11. G.Zheng, B.N.Popov and R.E White, J.Electrochem Soc 142(1995) 2695
12. G.Zheng, B.N.Popov and R.E White, J.Electrochem Soc 143(1996) 834
13. W.M.Robertson, Metall Trans., 8A, (1977) 1709
14. R.M.Latanision and M.Kurkela, Corrosion, 39,1(1983),174
15. W.M.Robertson, Metall Trans., 10A, (1979) 489

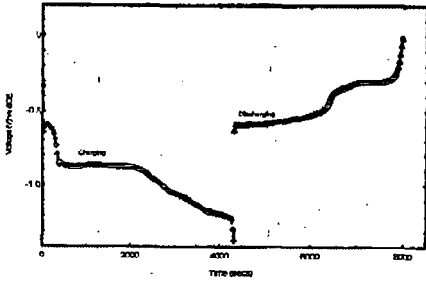


Fig. 1. Charge-Discharge characteristics of the electrode at 1C rate

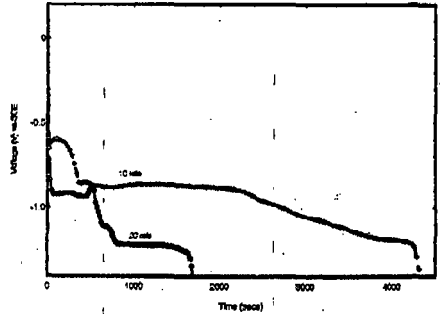


Fig. 2. Capacity dependence with different charging rates

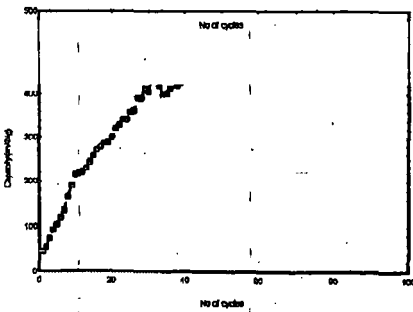


Fig. 3. Capacity variation with Cycle Number

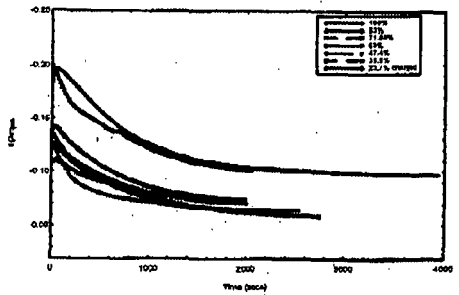


Fig. 4. Constant potential discharge curves at different states of charge

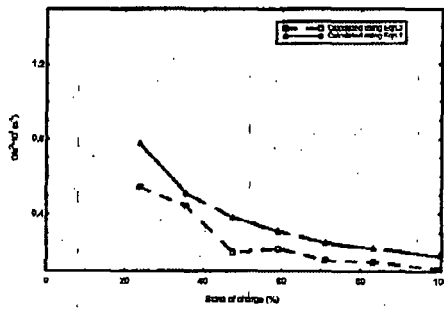


Fig. 5 Dependence of Diffusion coefficient with state of charge

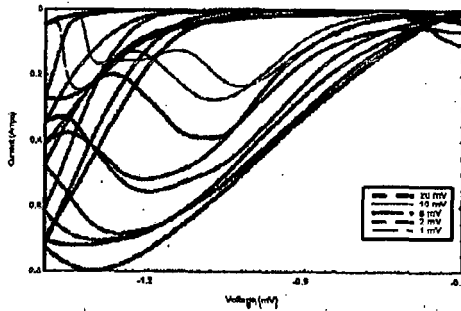


Fig. 6 Cyclic Voltammogram(CV) of the electrode for absorption at various sweep rates

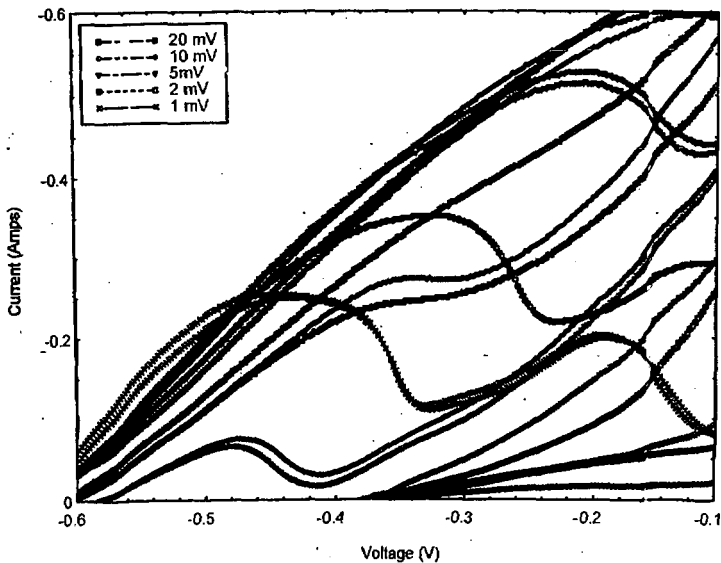


Fig. 7 Cyclic Voltammogram(CV) of the electrode for desorption at various sweep rates

INTERACTION OF HYDROGEN WITH NANOPOROUS CARBON MATERIALS

T. D. Jarvi, J. Sun, L. F. Conopask, and S. Satyapal

United Technologies Research Center
Energy Systems, MS 129-90
411 Silver Lane
East Hartford CT 06108

KEYWORDS: Carbon nanotubes, carbon nanofibers, hydrogen adsorption

INTRODUCTION

High-density hydrogen storage represents a key enabling technology to the widespread implementation of portable, hydrogen-based, fuel cell systems. In the long term, portable fuel cells will use stored hydrogen fuel due to power density and systems simplification issues. Although automotive applications remain the primary industry focus at the present moment, we may expect that small portable systems will eventually become extremely important as well. Moreover, effective hydrogen storage may enable fuel cell power for a wide array of applications not presently considered viable. Clearly, fuel cell systems of any size can benefit from improved hydrogen storage technologies, therefore success in this area will have lasting societal impact.

Hydrogen's low molecular weight makes storage as a compressed gas less effective than for other fuel gases, such as methane. This fact drives compressed hydrogen storage pressures to very high values, thus requiring expensive storage systems to reach reasonable gravimetric capacities. Volumetric capacities for compressed hydrogen storage are well below the target values at pressures as high as 60 MPa. Other hydrogen storage systems have been developed including storage as a cryogenic liquid, in metal hydrides, physisorption on carbon or other sorbents, and chemical hydrides (such as dehydrogenation of organic molecules). While progress has been made, no hydrogen storage technology meets the stringent requirements that are imposed by an automotive fuel cell system [1,2].

Recently several reports have suggested that hydrogen storage in carbon nanomaterials, such as carbon nanotubes and nanofibers may exhibit storage capacity that meets (or perhaps exceeds) DOE goals for automotive fuel cell applications [1,3,4]. At first glance these suggestions appeared counter-intuitive since surface science studies of hydrogen adsorption on graphite, for example, were necessarily conducted at very low temperature in order to stabilize the adsorbate [5]. It seems clear that if the reports of high capacity are correct that these new materials must exhibit interactions with carbon that exceed those of more typical carbon materials, like activated carbon. In this study, we set out to determine if the interactions between carbon nanomaterials and hydrogen were greater than between prototypical activated carbon and hydrogen to understand these storage results.

Hydrogen storage technologies can be compared on the basis of gravimetric and volumetric storage capacities. Both of these capacities must meet certain targets in order for a hydrogen storage system to reach viability [1,2]. The storage capacity requirements for a hydrogen-fueled fuel cell vehicle derive from requiring fuel cell vehicles to exhibit comparable range and gas storage system weight and volume to conventional automobiles. To achieve a 500 km range, the hydrogen storage system must exhibit a volumetric capacity of 60 kg H₂/m³ and a gravimetric capacity of 6.2 wt. % H₂ for an installed system [1,2]. It is important to consider both gravimetric and volumetric storage capacities as weight and volume are both important in the automotive application. Another factor of prime importance is the energy penalty associated with the storage method. For example, liquifaction of hydrogen consumes about 1/3 of the lower heating value of the hydrogen. Ideal hydrogen storage systems would store hydrogen at high-density using relatively low pressure and ambient temperature.

Figure 1 compares various hydrogen storage technologies with the DOE goal [1]. Compressed gas storage is clearly the most developed technology and it shows good gravimetric capacity but low volumetric capacity at suitably high pressure. In contrast, metal hydrides show moderately good volumetric capacity, and poor gravimetric capacity. Some metal hydrides exhibit better capacities than the range indicated on Fig. 1, e.g. magnesium hydride. Generally, however, these materials suffer other problems; in the case of magnesium hydride, the dissociation temperature is very high and the material undergoes decrepitation following cycling. Newer (or perhaps resurgent) technologies for the storage of hydrogen include chemical hydrides and cryogenic adsorption on activated carbon.

Carbon nanofibers have been reported to store from 30-300% hydrogen by weight at about 112 atm [3,4]. By comparison, methane, the most compact organic arrangement of carbon and hydrogen, is 25% hydrogen by weight [6]. Despite the counter-intuitive nature of these results, because of the potential societal impact of high-density hydrogen storage, attempts were made to reproduce these results. To the best of our knowledge, other such attempts have failed [7,8].

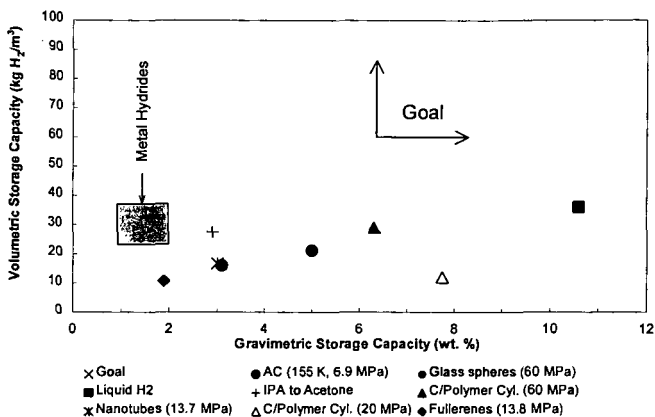


Figure 1: Comparison of gravimetric and volumetric storage capacity of various hydrogen storage technologies [1].

Recent careful studies reported that carbon nanotubes stored hydrogen at 5-10 wt% [1,9]. These later reports suggested to us that increased interactions with hydrogen arise in carbon nanotubes. Enhanced interactions were clearly required to explain the data, because typical carbon materials (activated carbon) show very low capacity at near-ambient temperature [10]. While less dramatic than the nanofiber claims, these results were very significant, in the context of Fig. 1. Especially important in these later experiments was the fact that high pressure was not required in order to store hydrogen at high density.

In general, the experimental procedures followed in the study of hydrogen storage within carbon nanomaterials have been inconsistent. This makes a systematic comparison of the various experiments impossible to perform. Nevertheless, it is useful to tabulate the results of some of these experiments. Table 1 summarizes some of the data reported in the literature for hydrogen storage in new carbon structures. Notice that the data cover a range of storage conditions and show highly variable capacity. The variety of conditions encountered in the data in Table 1 precludes a separation of the effects of storage condition from material structure (e.g. nanotube vs. nanofiber). Therefore the purpose of this study was to perform well-controlled adsorption of hydrogen on various carbon nanostructures to determine the relative interaction of hydrogen with these materials.

Sample	T / K	P / atm	$x_{wt} / \%$	Ref.
Nanofibers	298	112	35	3,4
Nanotubes	~133	~1	5-10	1,9
Nanotubes	340	136	4	11
Fullerenes	673	101	2.4	12

EXPERIMENTAL

We used the following carbon materials in this study: single walled carbon nanotubes from Rice University [13] and the University of Kentucky [14], activated carbon (BPL from Calgon Carbon Corporation), and carbon nanofibers synthesized in our laboratory. Single-walled carbon nanotubes from Rice University were estimated to be 90% pure with a diameter of 1.2 nm [13,15]. Nanotubes from the University of Kentucky were estimated as 50-70% pure SWNT by volume [14]. Carbon nanotubes were formed into "nanopipes" by processing the Rice University nanotubes [16]. A sample was placed in a mixture of concentrated sulfuric and nitric acids (3:1 by volume) and the solution was sonicated for about 24 hours at 30-40 °C. This procedure had a yield of about 50%. We synthesized carbon nanofibers by catalytic decomposition of ethylene over various catalysts in the temperature range of 500-700 °C [17]. Scanning electron microscopy and transmission electron microscopy were used to characterize the synthetic nanofibers. Calorimetry experiments made use of an isothermal flow

microcalorimeter (CSC, model 4400) at atmospheric pressure and 25 °C. Hydrogen was delivered as a pure gas at a flow rate of 10 cc/min. Degassing samples above 100 °C under vacuum overnight minimized surface contamination by residual water.

RESULTS AND DISCUSSION

Among structural questions, the nature of the synthetic nanofibers was of the greatest interest. Other researchers have characterized carbon nanotubes extensively by SEM, TEM, XRD, and Raman spectroscopy, so we did not further characterize those samples. The synthetic nanofiber sample that we were most interested in was synthesized on ceramic pellets. Insulating ceramic pellets were placed in the entrance region of the reactor in an attempt to improve the uniformity of the reactant temperature distribution. These insulating pellets were estimated to reach a temperature of ca. 500 °C during reactor operation and over several syntheses produced a large quantity of nanofiber (ca. ¼ kg) material. All of our nanofibers were synthesized using smooth surfaces.

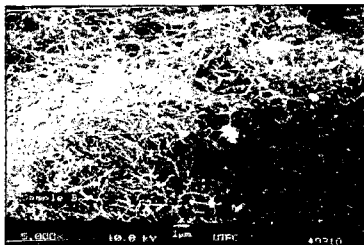


Figure 2: SEM image of carbon nanofibers synthesized by ethylene decomposition over a mixed oxide surface at ca. 500 °C.

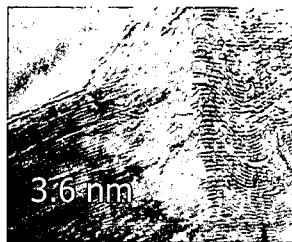


Figure 3: High resolution TEM image of carbon nanofibers synthesized by ethylene decomposition over a mixed oxide surface at ca. 500 °C.

Figure 2 shows a SEM micrograph of nanofibers synthesized on the oxide surface. In general, the structure is fibrous and few large clumps of amorphous carbon were observed in this sample. The question of the microstructure of the material could only be answered by high-resolution TEM imaging. One question was whether the structure of this material was similar to the material that Rodriguez et. al. have claimed store large quantities of hydrogen [3,4]. Figure 3 shows a high resolution TEM image of a carbon fiber synthesized on the oxide pellets. Graphite-like plane spacing is observed in this sample (ca. 0.36 nm). This measurement cannot be made to a high degree of precision without a standard specimen installed in the TEM during imaging. Therefore, this value is indistinguishable from that of graphite (0.34 nm). The plane spacing runs parallel to the fiber axis along most of its length, Fig. 3. There are some regions where the fiber axis bends and in these areas the plane spacing appears at an angle to the fiber axis. This result shows that the material we have synthesized is different than the GNF materials used in other studies [17].

Isothermal flow microcalorimetry reveals the degree of interaction of the adsorbate (hydrogen) with the sorbent. This method is sensitive to both the total heat of adsorption ΔH_{ads}^{total} , and the mass storage capacity, x_{wt} , as shown in eq. 1.

$$Q/m = \frac{1}{M_{H_2}} \Delta H_{ads}^{total} x_{wt} \quad (1)$$

Rather than measuring isosteric heats of adsorption as a function of coverage, here ΔH_{ads}^{total} refers to the total heat released in going from the clean surface to the equilibrium coverage, per mole of hydrogen adsorbed. In essence, eq. 1 translates the heat of adsorption from an adsorbate basis to a sorbent basis. The point of this relationship is to show that the measured quantity (Q/m) will track changes in both the mass capacity and the heat of adsorption. Therefore, this technique should reveal differences among various carbon sorbents if such differences are significant.

Figures 4-7 show the calorimetry data for hydrogen adsorption on various carbon materials. All of the heat data are normalized to the initial mass of the sorbent. In these experiments mass change following adsorption is difficult to detect. Figure 4 shows the calorimetry data for BPL, a typical activated carbon used for natural gas storage [18]. The significance of the structure observed in the calorimetric curves is presently under investigation. Peak heights and areas in Figs. 4-7 are much smaller than those observed in typical chemisorption experiments [19].

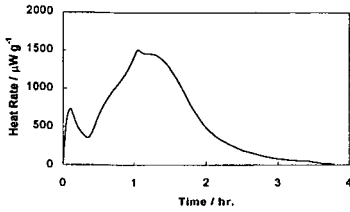


Figure 4: Hydrogen adsorption calorimetry data for BPL; hydrogen flow rate, 10 cc/min, 25 °C.

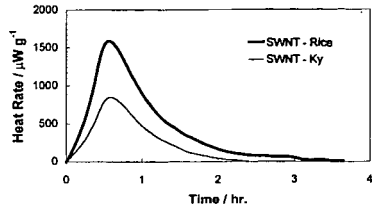


Figure 5: Hydrogen adsorption calorimetry data for carbon nanotubes; hydrogen flow rate, 10 cc/min, 25 °C.

Figure 5 shows the calorimetry data for hydrogen adsorption on the carbon nanotube samples. The Rice University sample displays a higher peak height and area than the University of Kentucky sample. This result can be rationalized either by a higher fraction of nanotubes or more active residual soot in the Rice sample. While the differences between these samples may be significant, as we will see later the total heat released is comparable to that when activated carbon is exposed to hydrogen (Fig. 4, Table 2).

One concern with the nanotube samples was whether hydrogen could access the interior of the tubes. If the tube interiors were not accessible, we might expect a lower measured heat due to a lower heat of adsorption on the tube exterior, as well as a lower mass capacity [6]. Figure 6 compares the hydrogen adsorption calorimetry for the Rice sample in both nanotube and “nanopipe” form. Processing the nanotubes to make pipes increases the degree of interaction of the hydrogen with the nanotube sample. While the effect of cutting the tubes is not extremely large, it is the most significant change observed in this study. Several possible explanations for this behavior exist. The processing step could: 1) increase surface area through opening the tube ends, 2) increase the heat of adsorption due to allowing access to more energetic surface sites, 3) increase adsorption capacity. We cannot rule out any of these possibilities at the present time. The initial rate of heat release is also significantly higher for the cut sample, which may indicate a different mechanism of adsorption or increased availability to sites with a higher adsorption potential.

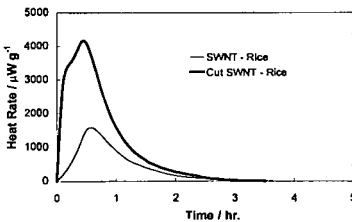


Figure 6: Hydrogen adsorption calorimetry data on carbon nanotubes; hydrogen flow rate, 10 cc/min, 25 °C.

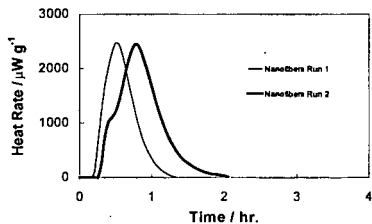


Figure 7: Hydrogen adsorption calorimetry data on synthetic carbon nanofibers; hydrogen flow rate, 10 cc/min, 25 °C.

Figure 7 shows the hydrogen adsorption calorimetry data for our nanofibers. This plot shows two different runs on the same sample. Following the first run the sample was placed in a vacuum oven at ~100 °C overnight and the experiment was repeated under identical conditions. The apparent shift in the peak maximum toward longer times is not significant because the zero on the time axis is arbitrary. Qualitatively the peak shape and height appear consistent from these two runs. The reasonable agreement between runs demonstrates the reproducibility of the technique.

The total heat released in the adsorption process (eq. 1) can be obtained simply by integrating the calorimetric signal over the period of the experiment. Table 2 shows the *semi-quantitative* results of these measurements. Since the statistical certainty on these measurements is not clear, we prefer to discuss these data qualitatively. The BPL sample shows one of the largest heat

releases obtained, consistent with the fact that this sample has a high micropore volume of 0.5 cm³/g making it a good sorbent for adsorbed natural gas storage [18]. The nanotube samples show somewhat decreased interaction with hydrogen relative to BPL. However, the "cut" nanotubes show the largest heat released of all samples, demonstrating either an increased heat of adsorption or an improved adsorption capacity. The nanofiber sample shows a total heat release that is somewhat less than that of BPL. The run-to-run variability can be judged qualitatively by comparing the two nanofiber runs. The results can be reproduced within about 27%. For the low-level signals observed in these experiments, we consider this degree of reproducibility very good.

Table 2: Semi-quantitative calorimetry results

Sample	Q/m (J/g)
BPL	7.8
U Ky Nanotubes	2.6
Rice University Nanotubes	5.5
"Cut" Rice University Nanotubes	13.9
Nanofibers, Run 1	4.3
Nanofibers, Run 2	5.9

The primary purpose of the calorimetry measurements was to look for extremely strong interactions between carbon nanotubes or nanofibers and hydrogen. The basis of comparison was a high quality activated carbon, BPL. From the measurements obtained we can say that the interactions of these materials are comparable to the interactions of activated carbon and hydrogen. Of course, the possibility exists for offsetting changes in the heat of adsorption and capacity (eq. 1), e.g. an increase in $\Delta H_{\text{ads}}^{\text{total}}$ and a decrease in x_{wt} . However, we interpret the data as suggesting a relative constancy of both quantities. Therefore, our initial question of some fundamentally different interactions between carbon nanotubes or nanofibers and hydrogen has been answered for conditions of atmospheric pressure and ambient temperature.

During the course of this experimental study, the computational chemistry community has been very active [6,20-25]. Several papers have sought to answer the same questions addressed here. These studies have made use of well-known interaction potentials for both C-H₂ and H₂-H₂ interactions. In one instance the carbon-hydrogen interaction potential (well depth) has been used as an adjustable parameter in an attempt to fit the experimental data of Rodriguez et. al. [3,4]. The conclusion from these studies is that the interaction potentials must be adjusted beyond physically reasonable limits in order to fit the data [21]. As a feasibility study, these computational studies are extremely valuable since years of materials optimization can be conducted in short order using adjustable computer models [6].

CONCLUSIONS

Hydrogen storage in new carbon nanostructures like carbon nanotubes and nanofibers appeared in the literature rather recently. Early experiments were conducted using different materials under different conditions leaving little conclusive evidence for good storage capacity. In this study we have characterized the interaction of hydrogen using isothermal flow microcalorimetry under constant conditions with high purity materials. Our data shows that the interaction of hydrogen with carbon nanotubes and nanofibers is comparable to the interaction of hydrogen with activated carbon. In view of our results, the results of attempts by other groups to reproduce the reported high storage capacities, and recent computational work, we conclude that carbon nanotubes and carbon nanofibers are not suitable as high-capacity hydrogen storage materials.

ACKNOWLEDGEMENTS

We acknowledge funding and permission to publish from Michael Winter and Jim Irish at UTRC. We enjoyed discussions of this work with Harvey Michels and Margaret Steinbugler of UTRC, Bryan Murach, Les Van Dine, and Tim Bekkedahl of International Fuel Cells, Sanjeev Mukerjee of Northeastern University, and Bob Bowman of the Jet Propulsion Laboratory.

REFERENCES

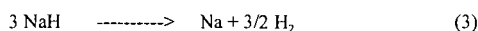
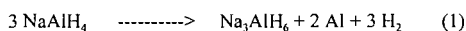
1. A.C. Dillon, K.M. Jones, T.A. Bekkedahl, C.H. Kiang, D.S. Bethune, and M. J. Heben, *Nature*, 386 (1997) 377.
2. M.A. DeLuchi, *Int. J. Hydrogen Energy*, 14 (1989) 81.
3. A. Chambers, C. Park, R.T.K. Baker, and N.M. Rodriguez, *J. Phys. Chem. B*, 102 (1998) 4253.

4. S. Hill, "Green Cars go Further with Graphite," *New Scientist*, December 28, 1996.
5. W. Liu and S.C. Fain, Jr., *Phys. Rev. B*, 47 (1993) 15965.
6. Q. Wang and J.K. Johnson, *J. Phys. Chem. B*, In press (1999).
7. C.C. Ahn, Y. Ye, B.V. Ratnakumar, C. Witham, R. C. Bowman, and B. Fultz, *Appl. Phys. Lett.*, 73 (1998) 3378.
8. Y. Ye et al., *Appl. Phys. Lett.* 74 (1999) 2307.
9. A.C. Dillon, T.A. Bekkedahl, A.F. Cahill, K.M. Jones, and M.J. Heben, In: *Proceedings of the 1995 DOE Hydrogen Program Review*, Vol. II, p. 521, NREL/CP-430-20036.
10. D. P. Valenzuela, and A. L. Myers, In: *Adsorption Equilibrium Data Handbook*, Prentice Hall, 1989.
11. T. Yildirim, Presented at the MRS Symposium, Boston MA, Paper S1.4, December 1998.
12. E. Brosha, Presented at the MRS Symposium, Boston MA, Paper S2.9, December 1998.
13. cnst.rice.edu/tubes/index.shtml
14. www.carbolex.com
15. A. Thess et. al., *Science*, 273 (1996) 483.
16. J. Liu et. al., *Science*, 280 (1998) 1253.
17. N.M. Rodriguez, *J. Mater. Res.*, 8 (1993) 3233.
18. J. Sun, S. Chen, M.J. Rood, and M. Rostam-Abadi, *Energy and Fuel* 12 (1998) 1071.
19. S. Satyapal, T. Filburn, J. Trela, J. Strange, "Novel Amine Sorbents for Separation of Carbon Dioxide", Submitted to: *Industrial and Engineering Chemistry Research*, 1998.
20. Q. Wang and J.K. Johnson, *J. Chem. Phys.*, 110 (1999) 577.
21. Q. Wang and J.K. Johnson, *J. Phys. Chem. B*, 103 (1999) 277.
22. Q.Y. Wang and J.K. Johnson, *Molecular Physics*, 95 (1998) 299.
23. Q.Y. Wang and J.K. Johnson, *Int. J. Thermophysics*, 19 (1998) 835-844.
24. F. Darkrim and D. Levesque, *J. Chem. Phys.*, 109 (1998) 4981.
25. M. Rzepka, P. Lamp, M.A. de la Casa-Lillo, *J. Phys. Chem. B*, 102 (1998) 10894.

Catalytically Enhanced Sodium Aluminum Hydride as a Hydrogen Storage Material. Craig M. Jensen, Kevin Magnuson, Ragaay A. Zidan, Satoshi Takara, Allan G. Hee, Nathan Mariels, and Chrystel Hagen, Department of Chemistry, University of Hawaii, Honolulu, HI 96822.

For decades, hydrogen has been targeted as the utopian fuel of the future due to its abundance and environmental friendliness. A major difficulty in the utilization of hydrogen as a fuel is the problem of onboard hydrogen storage. High pressure and cryogenic hydrogen storage systems are impractical for vehicular applications due to safety concerns and volumetric constraints. This has prompted an extensive effort to develop solid hydrogen storage systems for vehicular application. Metallic hydrides [1,2] activated charcoal [3,4] and carbon nanotubes [5] have been investigated as hydrogen carriers. Unfortunately, despite decades of extensive effort, especially in the area of metal hydrides, no material has been found which has the combination of a high gravimetric hydrogen density, adequate hydrogen dissociation energetics, and low cost required for commercial vehicular application [6].

The dissociation of hydrogen from sodium aluminum hydride, NaAlH₄, is not a single concerted process. It has been found to occur by the series of discrete reactions seen in equations 1, 2, and 3 [7-9]. Their independence is verified by the observation of a series



of equilibrium plateau pressures. The first two of these reactions are thermodynamically favorable at moderate temperatures and liberate 1.8 and 3.6 weight percent, wt %, hydrogen. However, NaAlH₄ has generally been discounted from consideration as a potential hydrogen storage material due to slow dehydriding kinetics [9] and the severe conditions required for its rehydriding [10]. Thus this material has not been developed as a rechargeable hydrogen carrier despite its high gravimetric hydrogen density and favorable dehydriding thermodynamics at moderate temperatures.

In 1996, Bogdanovic reported [11,12] that doping of NaAlH₄ with a few mole percent of titanium significantly enhanced the kinetics of the dehydriding and rehydriding processes. The temperature required for rapid dehydriding of NaAlH₄ was found to be

lowered from 200 °C to 150 °C. The conditions required for rehydriding were also dramatically reduced to 170 °C and 150 atm. It was also noted that these materials showed the application-relevant properties of no hysteresis on cycling and negligible plateau slopes. Unfortunately, the hydrogen capacities of the materials produced by Bogdanovic quickly diminish upon cycling. Following the initial dehydriding of the titanium doped material, only 4.2 of the lost 5.6 wt % could be restored under the moderate conditions employed in these studies. The hydrogen capacity is further diminished to 3.8 wt % after the second dehydriding cycle and reduced to only 3.1 weight percent after 31 cycles. This lack of stability along with the still unacceptably high (150 °C) temperature required for their rapid dehydriding, precludes them from consideration as viable onboard hydrogen carriers. This work, however, suggested that sodium aluminum hydride might be adapted for application as a practical hydrogen storage material.

The Bogdanovic materials were prepared by evaporation of suspensions of NaAlH_4 in solutions of titanium precursors. We recently found that titanium doping of NaAlH_4 also occurs upon mechanically mixing the liquid catalyst precursor, titanium tetra-*n*-butoxide, $\text{Ti}(\text{O}i\text{Bu})_4$, with the aluminum hydride host [13]. The resulting purple materials are visually very distinct from the brown powders obtained through Bogdanovic's procedure. While our homogenization technique is equivalent to ball milling of the material, there is compelling evidence that a chemical reaction also transpires in the process.

The materials resulting from our homogenization process have kinetic and cycling properties that are much closer to those required for a practical hydrogen storage medium [13]. The material undergoes rapid dehydriding at 120 °C and proceeds at an appreciable rate even at 80 °C. The temperature required for rapid kinetics in the first dehydriding is further lowered to 100 °C after the preliminary dehydriding-rehydriding cycle. The cyclable hydrogen capacity is also improved in the advanced titanium doped material. Over 4.0 wt % hydrogen can be evolved through 10 dehydriding-rehydriding cycles.

We have found that the dehydriding of NaAlH_4 is also kinetically enhanced upon doping with zirconium through our procedure [14]. The zirconium doped material has a further improved, 4.5 wt % cyclable hydrogen capacity. In contrast to the titanium doped material, the catalytic effect is most pronounced for the second rather than the first dehydriding process and inferior kinetics are observed for the first dehydriding reaction.

We have found that titanium and zirconium can act in concert to optimize dehydrogenating/rehydrogenating kinetics while achieving a 4.5 wt % cyclable hydrogen capacity.

The chain of advancement in the development of metal catalyzed NaAlH_4 is illustrated by comparison of the thermal programmed desorption spectra of the third dehydrogenating cycle of the various doped materials. As seen in Fig 1, hydride that was doped with titanium through the method of Bogdanovic has a cyclable hydrogen capacity of 3.2 wt % and dehydrogenating behavior that is markedly improved over undoped NaAlH_4 . Titanium doping through our homogenization technique further enhances the kinetics of the first dehydrogenating reaction and improves the cyclable hydrogen capacity to over 4.0 wt %. The zirconium doped material shows improved kinetics for the second dehydrogenating process and a cyclable

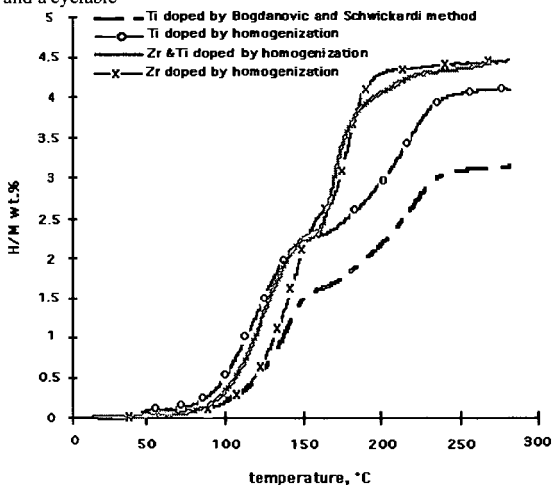


Fig. 1. Thermal programmed desorption (2 C min^{-1}) of hydrogen from various doped samples NaAlH_4 after 3 cycles of dehydrogenating/rehydrogenating.

hydrogen capacity of 4.5 wt %. Finally the titanium/zirconium doped material exhibits dehydrogenating behavior that is a virtual superpositioning of the behavior of homogenized titanium doped material for the first dehydrogenating process and the zirconium doped material for the second dehydrogenating process while maintaining a cyclable hydrogen capacity of 4.5 wt %. The finding of rapid dehydrogenating at 100 °C in conjunction with a stable, hydrogen cycling capacity of 4.5 wt % suggests the application of these materials as hydrogen carriers for onboard fuel cells.

References

1. G. Sandrock, S. Suda, and L. Schlapbach, in L. Schlapbach (ed.), *Hydrogen in Intermetallic Compounds II, Topics in Applied Physics*, Vol. 67, Springer-Verlag, 1992, Chap. 5, p. 197.
2. G. Sandrock, in Y. Yurum (ed.), *Hydrogen Energy Systems: Production and Utilization of Hydrogen and Future Aspects*, NATO ASI Series, Kluwer Academic Publishers, 1994 p 253.
3. C. Carpetis, and W. Peshka, *Int. J. Hydrogen Energy*, 5 (1980) 539.
4. R.K. Agarwal, J.S. Noh, J. Schwarz, and R. Davini, *Carbon*, 25 (1987) 219.
5. A.C. Dillion, K.M. Jones, T.A. Bekkedahl, C.H. Kiang, D.S. Bethune, M. Heben, *Nature*, 386 (1997) 377.
6. S. Suda, and G. Sandrock, *Z. Phys. Chem.*, 183 (1994) 149.
7. W.E. Garner and E.W. Haycock, *Proc. Roy. Soc. (London)*, A211 (1952) 335.
8. E.C. Ashby and P. Kobetz, *Inorg. Chem*, 5 (1966) 1615.
9. T.N. Dymova, Y.M. Dergachev, V.A. Sokolov, and N.A. Grechanaya, *Dokl. Akad. Nauk SSSR*, 224 (1975) 591, Engl. ed (1976) 556.
10. T.N. Dymova, N.G. Eliseeva, S.I. Bakum, and Y.M. Dergachev, *Dokl. Akad. Nauk USSR*, 215 (1974) 1369.
11. B. Bogdanovic and M. Schwickardi, International Symposium on Metal-Hydrogen Systems, August 25-30, 1996, Les Diablerets, Switzerland.
12. B. Bogdanovic and M. Schwickardi, *J. Alloys and Compounds*, 1-9 (1997) 253
13. C.M. Jensen, R. Zidan, N. Mariels, A. Hee, and C.Hagen, *Int. J. Hydrogen Energy*, 23 (1999) in press.
14. R.A. Zidan, S. Takara, A.G. Hee, and C.M. Jensen, *J. Alloys and Compounds* (1999) in press.
15. R. Ehrlich, A.R. Young, D.D. Perry, *Inorg. Chem*, 4 (1965) 758.